

NASA Contractor Report 165859

(NASA-CR-165859) WATER TUNNEL FLOW
VISUALIZATION AND WIND TUNNEL DATA ANALYSIS
OF THE F/A-18 (Northrop Corp.) 268 p
HC A12/AF A01

N82-25215

CSCI 01A

Jacobs

G3/J2 28019

Water Tunnel Flow Visualization and Wind Tunnel Data Analysis of the F/A-18

ORIGINAL CONTENTS

COLOR ILLUSTRATIONS

Gary E. Erickson

Northrop Corporation, Aircraft Division
Hawthorne, CA 90250

Contract NAS1-16617
May 1982



NASA

National Aeronautics and
Space Administration

Langley Research Center
Hampton, Virginia 23565

NASA Contractor Report 165859

**Water Tunnel Flow
Visualization and Wind
Tunnel Data Analysis
of the F/A-18**

Gary E. Erickson

**Northrop Corporation, Aircraft Division
Hawthorne, CA 90250**

**Contract NAS1-16617
May 1982**

NASA

National Aeronautics and
Space Administration

Langley Research Center
Hampton, Virginia 23665

ORIGINAL PAGE
COLOR PHOTOGRAPH

WATER TUNNEL FLOW VISUALIZATION AND WIND TUNNEL DATA ANALYSIS
OF THE F/A-18



PRECEDING PAGE BLANK, NOT FILMED

ORIGINAL PAGE
COLOR PHOTOGRAPH

PRECEDING PAGE BLANK NOT FILMED

CONTENTS

	Page
SUMMARY	1
BACKGROUND	6
INTRODUCTION	21
SYMBOLS	26
EXPERIMENTAL METHODS	27
Water Tunnel Facility	27
Test Procedure	27
MODEL DESCRIPTION	28
DISCUSSION OF RESULTS	35
Water Tunnel Flow Visualization of the F/A-18	35
Baseline ($\delta_n/\delta_f = 35^\circ/0^\circ$; $\delta_n = -12^\circ$).	35
Double-Width Forward LEX Slots (LEX 12).	64
Double-Width, Extended Length Forward LEX Slots (LEX 12A)	85
LEX Lower Surface Fence - Oblique (Fence "B")	86
LEX Lower Surface Fence - Streamwise (Fence "A").	101

ORIGINAL PAGE IS
OF POOR QUALITY

CONTENTS (Continued)

	Page
Closure of Forward LEX Bleed Slots	102
Closure of All LEX Bleed Slots	102
Forebody Strakes (Radial Position: +40°)	113
Forebody Strakes (Radial Position: 0°)	130
Forebody Strakes (Radial Position: -45°)	131
Flight Test Nose Boom	131
Wing Leading-Edge Snag and Upper Surface Fence	132
Wing Leading-Edge Extensions (LEXS) Off	132
Reinstallation of Wing Leading-Edge Extensions	145
 Correlation of Water Tunnel Flow Visualization Results with 0.16-Scale F/A-18 Wind Tunnel Data Trends	
Baseline Configurations ($\delta_n/\delta_f=25^\circ/0^\circ$; $\delta_n/\delta_f=35^\circ/0^\circ$; $\delta_h=-12^\circ$)	149
Double-Width Forward LEX Slots (LEX 12).	157
Double-Width, Increased Length Forward LEX Slots (LEX 12A)	163
LEX Lower Surface Fence (Fence "B").	168
LEX Lower Surface Fence (Fence "A").	170
LEX Planform Modifications	170
Wing Leading-Edge Snag and Upper Surface Fence	179
Forward LEX Slots Closed	182
Forebody Strakes (Radial Location: +40°).	186
Forebody Strakes (Radial Location: +60°).	194
Forebody Strakes (Radial Location: +30°).	194
Forebody Strakes (Radial Location: 0°)	199

CONTENTS (Continued)

	Page
Forebody Strakes (Radial Locations: -15° and -30°) . . .	199
Forebody Strakes (Radial Location: -45°)	202
Flight Test Nose Boom	204
Flight Test Nose Boom and Forebody Strakes ($\phi=+40^\circ$) . . .	204
"Wing Rock" Phenomena.	207
Analysis of Scale-Model F/A-18	
Wind Tunnel Data	207
Baseline Configurations - Longitudinal	
Characteristics	208
Baseline Configurations - Lateral/	
Directional Characteristics	208
Vertical Tail Effects	224
Wing Leading-Edge Extension (LEX)	
Effects	226
Forebody Effects	233
Forebody Strake Effects	240
CONCLUSIONS	248
RECOMMENDATIONS FOR FUTURE WIND TUNNEL TESTS	256
REFERENCES	260

SUMMARY

The Navy/McDonnell Douglas/Northrop F/A-18 operating at high angles of attack (α) is characterized by significant amounts of flow separation from the fuselage forebody and leading-edge extension (LEX)-wing surfaces. Sheets of distributed vorticity are shed from the slender forebody and LEXs, which roll up into concentrated vortices. Due to the size of the LEXs and their proximity to the forebody, a strong interaction can occur at high α 's between the forebody and LEX vortices. A consequence of the coupling of the forebody and LEX flow fields is that LEX and/or forebody geometry changes can promote large changes in the vortex interactive behavior. Particularly, small disturbances to the forebody flow development near the nose can be amplified downstream by the more powerful LEX vortical motions. As a result, small perturbations to the forebody vortex behavior can, under certain conditions, dictate the wing stall and, hence, lateral stability characteristics near stall angle of attack. Similarly, subtle differences in the flow behavior on different F/A-18 test models can be responsible for large differences in lateral stability levels determined in wind tunnel tests at high angles of attack.

A detailed study has been made of the sensitivity of the F/A-18 vortex flow field behavior and low-speed wind tunnel data trends to LEX-wing and forebody geometry modifications. Flow field surveys in the Northrop 16x24-inch Diagnostic Water Tunnel of a 0.025-scale F/A-18 model and analyses of 0.06-, 0.07-, and 0.16-scale F/A-18 wind tunnel model data obtained in the NASA Langley Research Center 30x60-foot facility were made to assess the effects of (1) increased forward LEX boundary layer bleed slot width and length, (2) forward LEX slot closure, (3) closure of all LEX slots, (4) LEX lower surface fences located forward of the production break, (5) wing snag and fence combination, (6) forebody strakes at several radial positions, (7) flight test nose boom, and removal of (8) LEXs, (9) twin vertical tails, and (10) forebody. Emphasis was placed on variations of forebody and LEX vortex interactions and lateral-directional characteristics at low subsonic speeds with sideslip angle at angles of attack from 30 to 40 degrees. Note is made that the water tunnel and wind tunnel Reynolds numbers based on maximum body width were all within the laminar regime.

The qualitative results obtained in the water tunnel correlated reasonably well with 0.16-scale F/A-18 wind tunnel model data trends. Wing stall patterns and the flow behavior about the forebody and twin vertical tails at high α 's were consistent with baseline (all LEX slots open; $\delta_n/\delta_f=35^\circ/0^\circ$; $\delta_h=12^\circ$) longitudinal and lateral-directional aerodynamic data trends. The F/A-18 baseline water tunnel model developed a highly-asymmetric forebody vortex system in sideslip. The leeward body vortex was strongly entrained into the leeward LEX vortex whereas the windward body vortex "sheared" away from the fuselage with no apparent influence on the downstream flow behavior.

The flow field effects of increased forward LEX slot width and length and LEX lower surface fences, when considered in conjunction with the low-speed wind tunnel data, indicated that such modifications reduced the "effective" generating length of the leading-edge extensions. The LEX modifications limited the amount of shed vorticity at the leading-edge available for feeding into the primary vortex, rendering the forward portion of the LEX ineffective as a vortex generator. The earlier wing stall and reduction of LEX vortex breakdown asymmetry in sideslip at high α 's were in qualitative agreement with reduced $C_{L_{MAX}}$ (and angle of attack for $C_{L_{MAX}}$) and increased levels of lateral stability near stall angle of attack, respectively, determined in wind tunnel tests.

Open LEX boundary layer bleed slots promoted the formation of two primary vortices on each LEX due primarily to forward slot flow entrainment which caused a significant local reduction in vorticity shed at the LEX leading edge near the production break. Forward LEX slot closure and closure of all slots resulted in a single concentrated LEX vortex. The interactive behavior of the forebody and LEX vortices at high α 's was similar, however, regardless of whether the slots were open or closed.

A wing leading-edge snag and upper surface fence combination promoted nearly-symmetric bursting of the LEX vortices in sideslip at high angles of attack which appeared to contribute in large part to the improved lateral stability characteristics obtained in wind tunnel tests.

The sensitivity of the LEX-wing flow field behavior to changes in the forebody geometry was vividly demonstrated in water tunnel studies of nose strake effects. Depending on the radome strake radial position, enhancement or disruption of the forebody vortices occurred, with a corresponding change in the body vortex interactions with the wing flow field. Nose strakes located 40 degrees above the maximum half-breadth (MHB) were nearly coincident with the primary boundary layer separation lines along the radome and were immersed in a region of relatively low local angle of attack due to body vortex-induced downwash. Strakes located in this manner were observed to promote symmetric boundary layer separation lines within a limited range of sideslip and to shed discrete vortices up to very high angles of attack which fed directly into the body primary vortex system. As a consequence, the forebody vortices were highly resistant to asymmetric orientation in sideslip and, furthermore, were strongly coupled such that powerful induced sidewash effects on the windward wing panel occurred. Wing stall was thus delayed to higher angles of attack. The body vortex behavior observed by colored dye emissions in the water tunnel was slightly oscillatory with nose strakes installed due to an apparent "hydrodynamic instability" phenomenon. The strake effects on forebody vortex behavior, including the vortex oscillations, were also observed in smoke flow visualization studies of the 0.16-scale F/A-18 model in the Langley wind tunnel. The improved wing stall characteristics and the unsteady body vortex behavior were reflected, respectively, in improved lateral stability and modest wing rock at high α 's on the 0.16-scale model and full-scale flight tests of the F/A-18.

Nose strakes at 45 degrees below the MHB promoted flow field changes similar to, but much less pronounced than, strakes at 40 degrees above the MHB. Location of strakes along the MHB was found in the water tunnel studies to completely disrupt the forebody primary vortices at high α 's due to a low-energy wake shed by the strakes and to a discontinuity in the vortex sheets emanating from the forebody sides.

Installation of a flight test nose boom weakened the forebody primary vortex system due to the wake shed by the boom. The fundamental structure of the vortices was similar, however, whether the boom was on or off.

Due to minor changes in the forebody and LEX geometries incurred during model changes, a small variation in the baseline F/A-18 water tunnel model forebody vortex orientation in sideslip occurred. This effect was magnified downstream, however, such that the wing stall patterns in sideslip were markedly different relative to previous baseline runs. A highly-favorable forebody vortex-induced effect on the windward wing panel was evident.

To confirm that the latter effect emanated from the nose region, the forebody was removed from the water tunnel model. The vortex-induced effects on the wing panel with forebody on were noticeably absent with forebody off.

Large differences in lateral stability levels near stall angle of attack were revealed in wind tunnel studies of 0.06-, 0.07-, and 0.16-scale F/A-18 models when tested in the Langley 30x60-foot facility at the same or different Reynolds numbers. These trends were repeatable. Furthermore, a comparison of wind tunnel data obtained at the NASA Ames Research Center 12-foot facility and in the Langley facility on the 0.06-scale F/A-18 revealed excellent agreement between the respective lateral stability levels. Inspection of the models failed to reveal discernible differences in LEX geometry, position, and incidence, horizontal and vertical tail positions, and forebody contours, for example, although the forebody contours were not inspected to the degree that now appears warranted based on the present results. Furthermore, test data obtained in the Langley facility indicated that model support interference had only a secondary effect on the wind-tunnel data trends. Water tunnel flow field observations of the 0.025-scale F/A-18 and analyses of 0.06-, 0.07-, and 0.16-scale F/A-18 wind tunnel data suggested that the apparent "model-scale" effect was associated with subtle differences in the forebody contours which promoted markedly different forebody-LEX vortex interactive behavior at high α 's. Assessment of the relative effects of removal of the LEXs and twin vertical tails led in an indirect manner to the conclusion that the 0.16-scale F/A-18 model developed a more severe and persistent LEX vortex breakdown asymmetry in sideslip. The latter phenomenon appeared attributable to forebody flow field differences, for a comparison of small- and large-scale model data obtained with forebody off revealed excellent high- α data agreement.

Additional evidence of different forebody vortex behavior on the sub-scale baseline F/A-18 models was provided by data obtained with nose strakes mounted 40 degrees above the maximum half-breadth. Strakes positioned in this manner on the 0.07-scale model were destabilizing in roll whereas the opposite was true for the 0.16-scale model.

An excellent match of lateral-directional characteristics was obtained for the 0.06- and 0.16-scale models with nose strakes mounted at the MHB. These results appeared attributable to the disruption of the forebody vortices with strakes installed and, consequently, alleviation of the differences in body vortex orientations and interactive behavior with the wings that were evident on the baseline models.

The results of this study indicated that, for high angle-of-attack testing of F-18-type aircraft featuring strongly-coupled forebody and LEX vortex flows, model tolerances may have to be reduced to ensure sub-scale wind tunnel model data correlation. However, until experiments are conducted in a systematic way, one cannot define what a reasonable tolerance level is.

It has long been established in wind tunnel tests of slender bodies that free-stream turbulence, model support rigidity, model contour variations, Reynolds number, Mach number, etc. can all contribute to changes in body vortex behavior at high angles of attack. Accordingly, a wind tunnel test program has been proposed for the NASA Langley Research Center VSTOL facility using the 0.06-, 0.07-, and 0.16-scale F/A-18 models. The proposed test program would provide force and moment results with which to compare the existing Langley data. The flow visualization capabilities available in the VSTOL tunnel would enable an assessment of the flow behavior in the forebody and wing regions of each model. The sensitivity of high angle-of-attack lateral stability to artificial turbulence induced by upstream screens, downstream obstacles, model support rigidity, slight misalignment of the fuselage forebody or small forebody contour variations, etc. could be addressed in this facility. The National Transonic Facility (NTF) was suggested as a suitable facility for longer-term studies to assess Reynolds number and Mach number effects on highly-coupled forebody-wing vortex flows in the extended angle-of-attack regime.

BACKGROUND

Current and future aircraft designs are characterized by expanded flight envelopes within which complex flow interactions are frequently encountered. Significant increases in the maximum lift coefficient and reductions in drag at high lift can result from the separation-induced vortex flows shed from slender fuselage forebodies, wings, canards, and wing leading-edge extensions (LEXs). Concurrent with these longitudinal benefits, however, is susceptibility to highly nonlinear lateral-directional characteristics at high angles of attack.

The LEX vortex on the F/A-18 is illustrated in the flight photograph in Figure 1 (from Reference 1) and in the water tunnel photograph in Figure 2. The vortex flow was made visible in flight and in the water tunnel by natural condensation and dye injection, respectively.

The thrust of the present study pertains to forebody and LEX vortex interactions at high angles of attack on a "hybrid" fighter aircraft configuration. The latter terminology applies to configurations such as the Northrop F-5G and the Navy/McDonnell Douglas/Northrop F/A-18 which feature slender forebodies and highly-swept wing leading-edge extensions. Distinctions must be made, however, between F-5 and F-18-type aircraft in that the degree of interaction between the forebody and LEX vortices at high angles of attack differs considerably.

The water tunnel photograph in Figure 3(a) illustrates the flow about an F-5 model near stall angle of attack. Although the relatively strong forebody vortices do influence the wing flow field to some extent, the body and LEX vortices are essentially uncoupled. One reason for this is that the F-5 LEX vortex cannot persist to very high angles of attack due to the low ratio of LEX exposed area-to-wing area (~ 0.06). The dominant vortex flow on the F-5 at stall and post-stall angles of attack is, therefore, developed along the fuselage forebody. The body vortex flow can also shed asymmetrically at zero sideslip as shown in Figure 3(b). Furthermore, the LEX surface is not in proximity to the forebody and the wing is in a low position, both factors contributing to the relative absence of forebody and LEX vortex interaction.



FIGURE 1. LEADING-EDGE EXTENSION (LEX) VORTEX ON THE F/A-18 IN FLIGHT

ORIGINAL PAGE

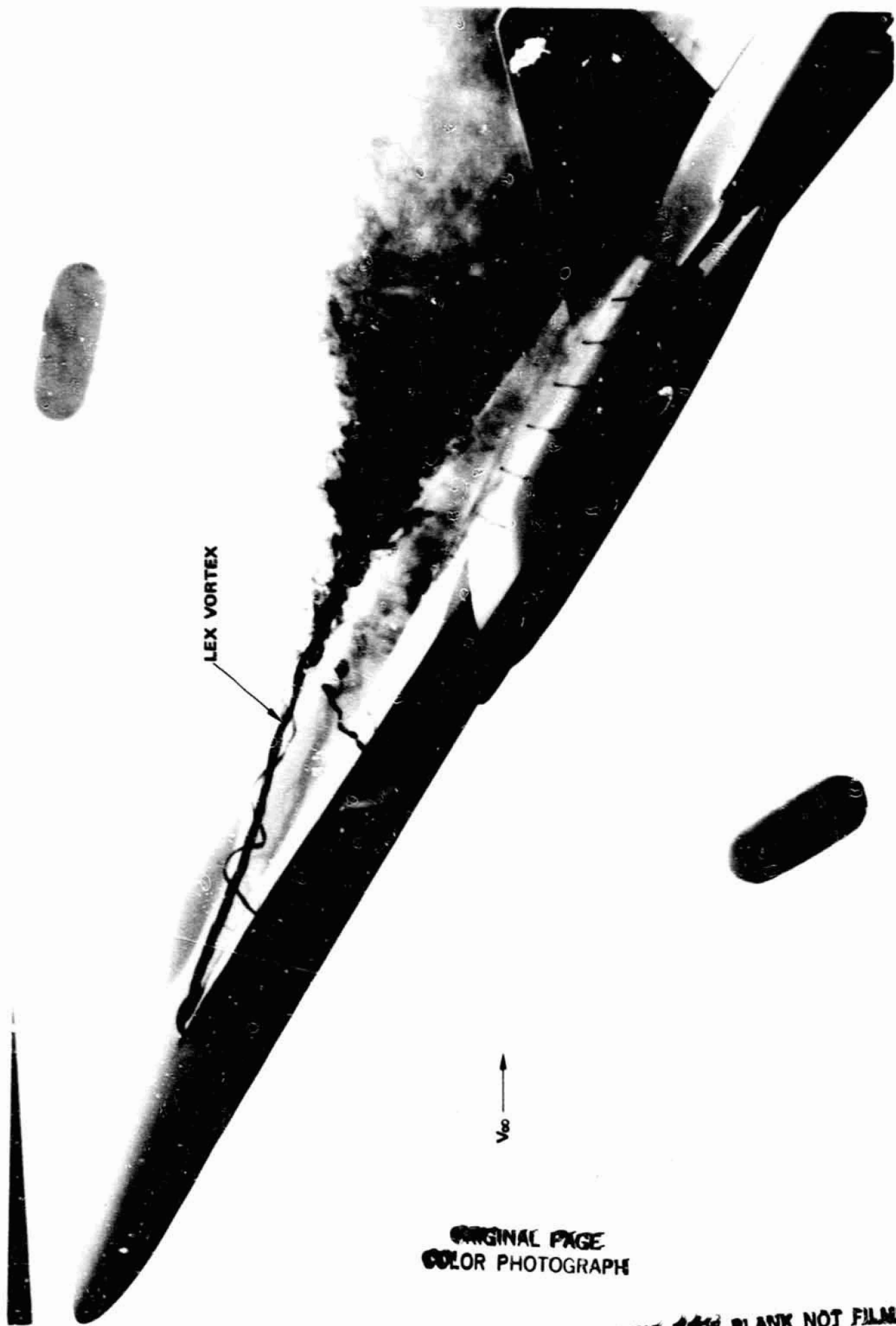


FIGURE 2. WATER TUNNEL FLOW VISUALIZATION OF A LEADING-EDGE
EXTENSION (LEX) VORTEX ON AN F-18 MODEL; $\alpha = 32^\circ$; $\beta = 0^\circ$; ALL LEX
SLOTS CLOSED

ORIGINAL PAGE
COLOR PHOTOGRAPH

PRECEDING PAGE BLANK NOT FILMED

ORIGINAL PAGE
COLOR PHOTOGRAPH

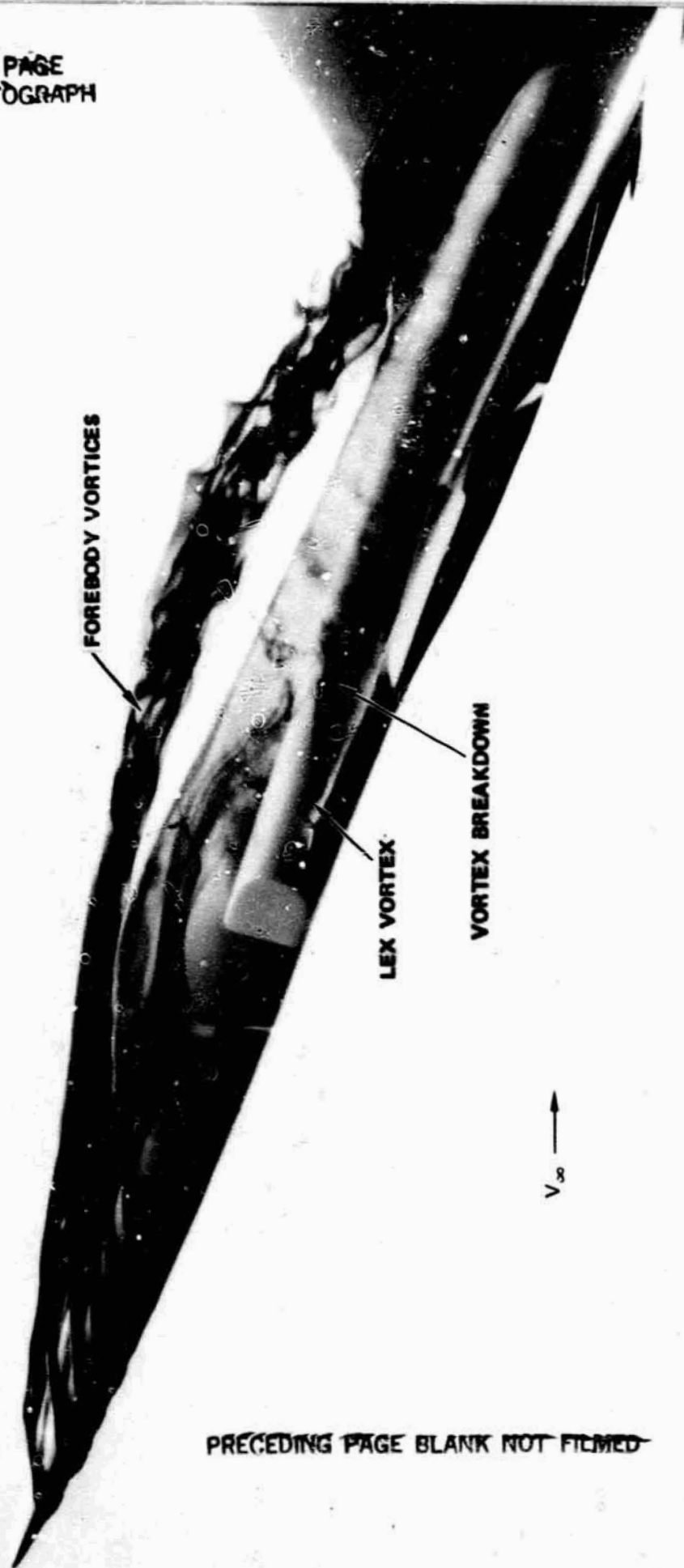


FIGURE 3A. WATER TUNNEL PHOTOGRAPH OF FOREBODY AND LEX VORTICES
ON A 0.025-SCALE F-5 MODEL NEAR STALL ANGLE OF ATTACK; $\beta = 0^\circ$

~~PRECEDING PAGE BLANK NOT FILMED~~

ORIGINAL PAGE
COLOR PHOTOGRAPH

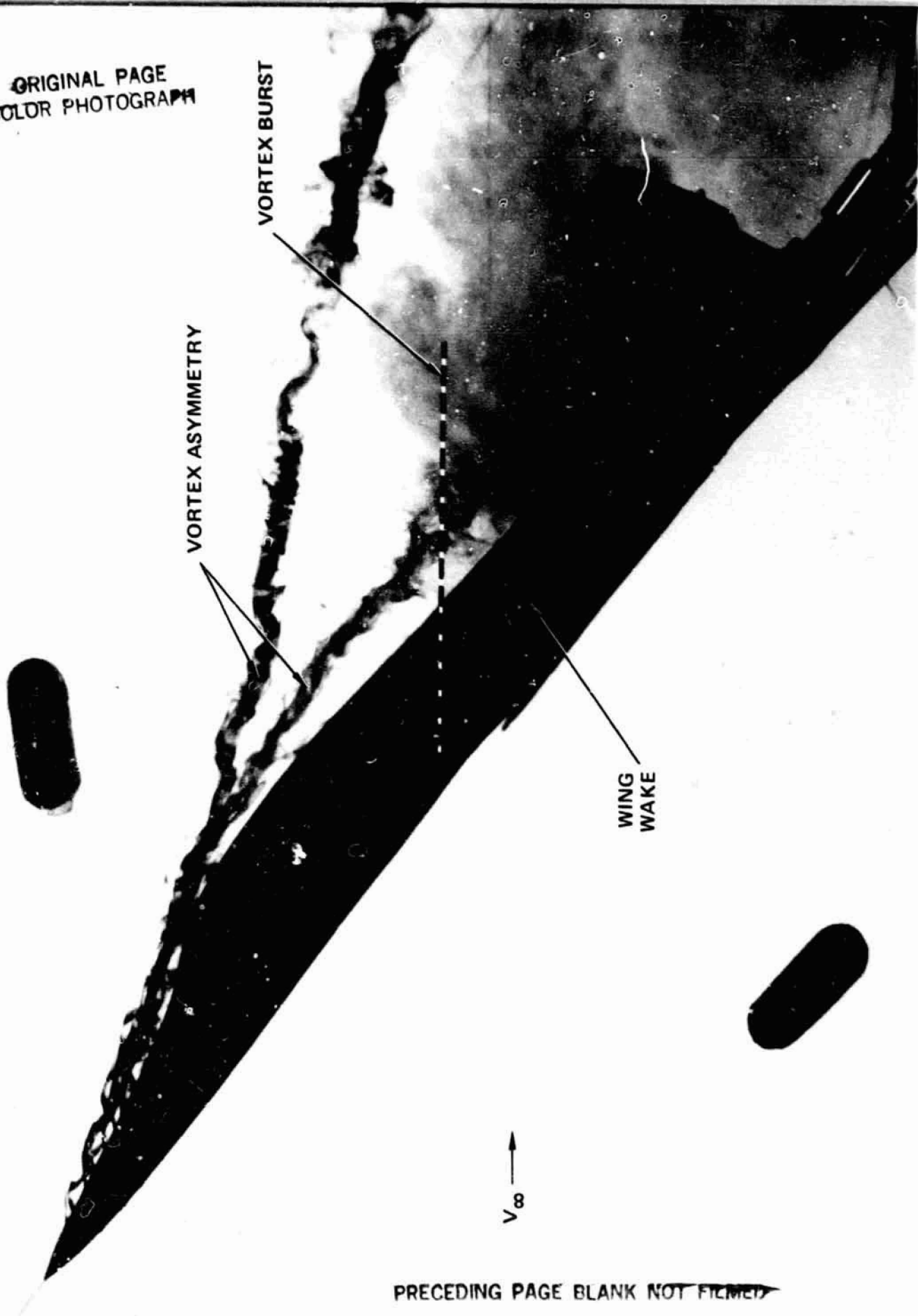


FIGURE 3B. ASYMMETRIC FOREBODY VORTEX SHEDDING AT ZERO SIDESLIP

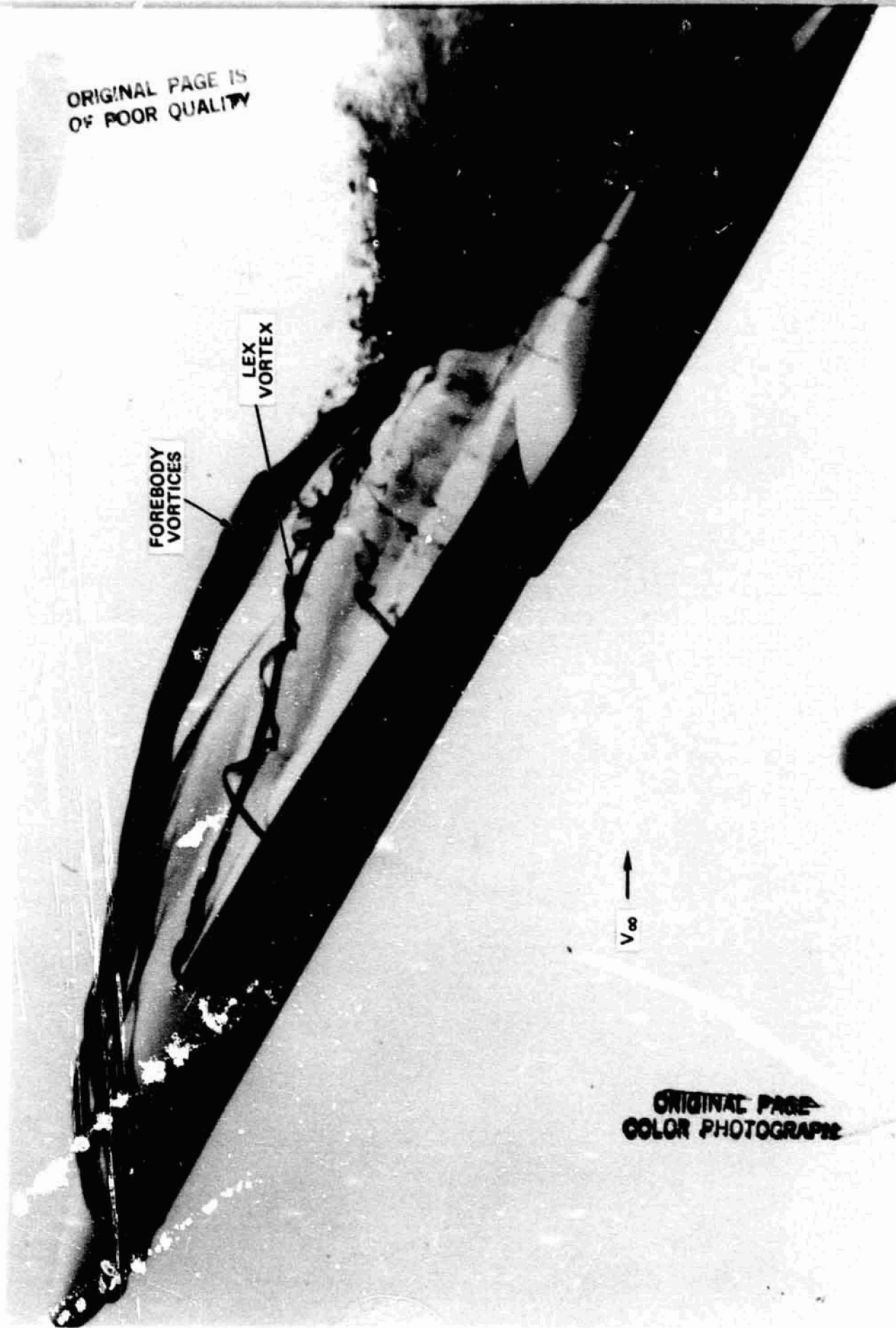
PRECEDING PAGE BLANK NOT FILMED

Consequently, forebody geometry changes will influence, primarily, the high- α static directional stability with higher-order influence on static lateral stability, the major contributor to the latter being the wings. Conversely, wing geometry changes will be reflected in the lateral stability characteristics at stall/post-stall angles of attack with second-order effects on directional stability.

This is not the case for the F-18, however. Due to the relatively large ratio of LEX exposed area-to-wing area (~ 0.14), the slight positive incidence angle of the LEXs, and the proximity of the LEX surfaces to the forebody, the LEX vortices persist to very high angles of attack and interact in a significant manner with the forebody vortices. This flow phenomenon is illustrated in the water tunnel photograph in Figure 4(a). The forebody vortices shed in a symmetric manner at zero sideslip. Due to the powerful vortex interactions, however, the vortices assume a highly asymmetric orientation at small sideslip angles, as depicted in Figure 4(b). The forebody and LEX vortices are strongly-coupled and, as a result, so are the lateral-directional characteristics at high α 's. The F-18 flow field is characterized, then, by multiple vortex interaction and vortex breakdown, both of which can occur in a symmetric or asymmetric manner depending on the angles of attack and/or sideslip, and highly-nonlinear lateral-directional characteristics. It is this class of vortex flow interactions that is of primary concern in the present investigation.

PRECEDING PAGE BLANK NOT FILMED

ORIGINAL PAGE IS
OF POOR QUALITY



ORIGINAL PAGE
COLOR PHOTOGRAPH

FIGURE 4(A). NORTHROP WATER TUNNEL FLOW VISUALIZATION PHOTOGRAPH OF FOREBODY
VORTEX - LEX VORTEX FLOW INTERACTION; $\alpha = 32^\circ$; $\beta = 0^\circ$

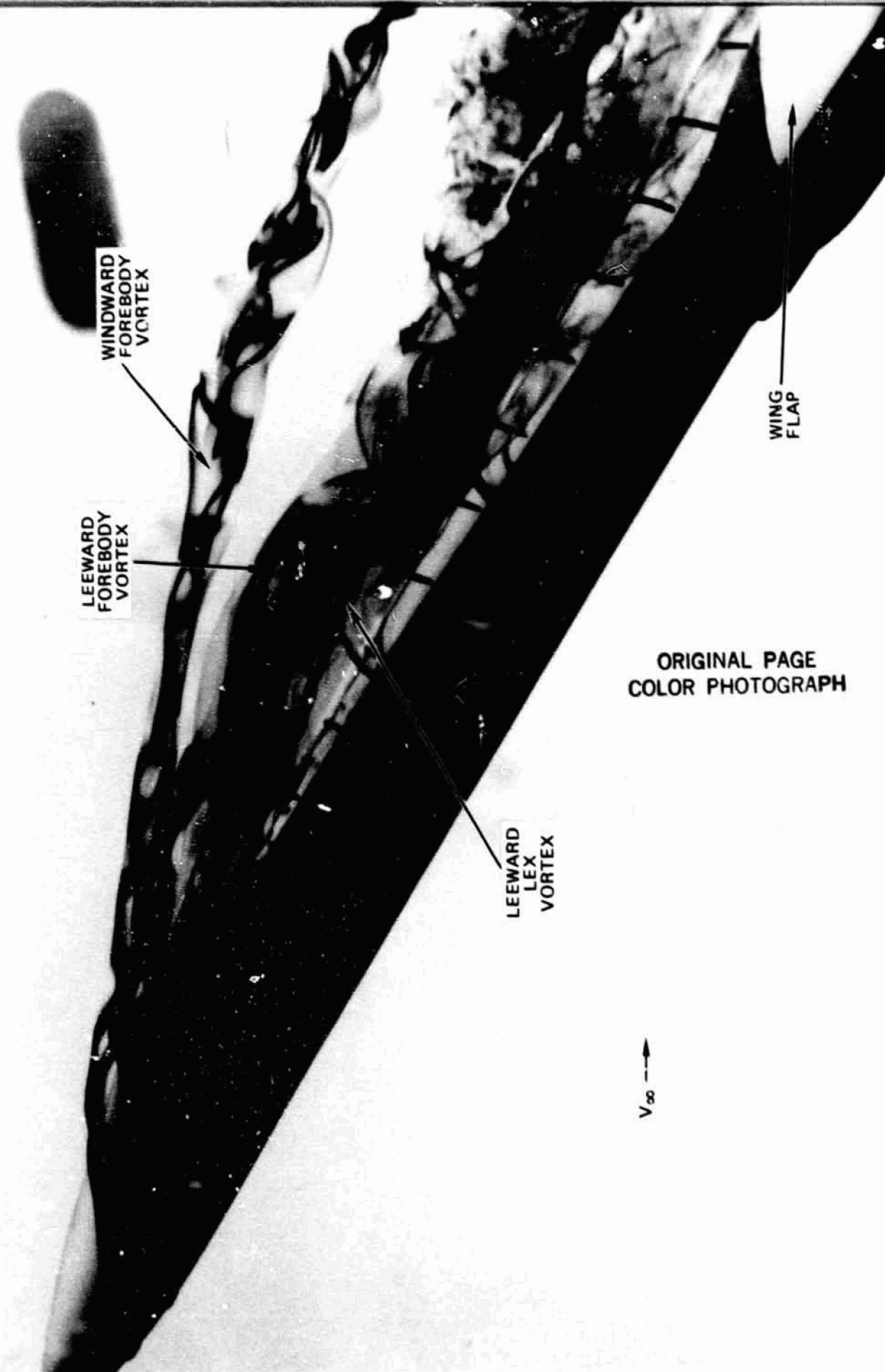


FIGURE 4(B). NORTHROP WATER TUNNEL FLOW VISUALIZATION OF THE STRONG COUPLING BETWEEN THE FOREBODY AND WING-LEX VORTEX FLOW FIELDS AT SMALL ANGLE OF SIDESLIP

PRECEDING PAGE BLANK NOT FILMED

PRECEDING PAGE BLANK NOT FILMED

INTRODUCTION

On December 21, 1978 the No. 1 F/A-18 aircraft on Flight 16 experienced a mild yaw departure. The aircraft achieved an angle-of-attack in excess of 30 degrees and a sideslip angle of 15 degrees at M 0.7 while attempting a wind-up turn at M 0.9 at 40,000 feet to achieve 4.5 g's (Mil power throughout). An unbalanced rolling moment of approximately 1400 ft-lb due to a right wing fuel imbalance of some 200 pounds may have contributed to the initial sideslip motion.

Six-degree-of-freedom studies were utilized to extract a band of yawing and rolling moment coefficients from the flight records. These were compared with 0.06-scale model data obtained in the Arnold Engineering Development Center (AEDC) 16T wind tunnel facility. The results, shown in Figure 5, indicate the flight test yawing moment data exhibit an improvement over the wind tunnel data to near-neutral stability and a significant reduction in lateral stability (again to a near-neutral level). These data are consistent with the flight test results since the motion was characterized by a relatively slow departure. Flight tests in November 1980 repeated the slow yaw departure at M 0.3.

Only NASA Langley 0.16-scale model wind tunnel data showed levels of lateral stability similar to the flight test results, as shown in Figure 6. Accordingly, geometric modifications were investigated commencing in April 1979 on the 0.16-scale model in the NASA Langley Research Center 30x60-foot wind tunnel to improve high-angle-of-attack ($\alpha=30-40$ deg) lateral stability. Modifications tested included increased leading-edge flap deflection to 35° (from 25°); incorporation of nose strakes; widening of the forward LEX boundary layer bleed slot; and incorporation of a LEX lower surface fence.

In addition to the lateral sensitivity, a "model-scale" effect was evident which precluded model data correlation. Prior to the first flight test incident, initial exploratory static force and moment tests in the Langley 30x60-foot wind tunnel using the 0.16-scale F/A-18 model revealed anomalies in the high-angle-of-attack lateral stability characteristics when

the results were compared with 0.06-scale model data obtained at the NASA Ames Research Center 12-foot transonic pressure tunnel. The directional stability results obtained on the Langley 0.16-scale model were in agreement with the Ames 0.06-scale results. However, disagreement was evident in the lateral stability data near $C_{L\text{MAX}}$, that is, at $\alpha = 35^\circ$ to 40° , the 0.16-scale results indicating a lateral sensitivity.

A review of available literature on configurations similar both in size and geometry to the 0.16-scale model (e.g., the Northrop YF-17) revealed comparable levels of lateral stability.

The 0.06-scale high-Reynolds-number model was brought to Langley and tested in the 30x60-foot wind tunnel at (1) the same chordal Reynolds number as the 0.16-scale model, (2) the same Reynolds number as tested in the Ames 12-foot tunnel, and (3) the same free-stream dynamic pressure as the 0.16-scale model. The lateral-directional stability results obtained on the 0.06-scale model in the Langley facility were found to agree with the data obtained at Ames.

A 0.07-scale F/A-18 model was subsequently fabricated by Langley for tests at the Virginia Polytechnic Institute (VPI) 6x6-foot curved flow wind tunnel and in the Langley 30x60-foot facility. Results obtained on this model were in agreement with the 0.06-scale data, that is, these results reveal vastly different lateral stability levels relative to the 0.16-scale model, as can be seen in Figure 7.

The closely-coupled forebody/wing/LEX arrangement on the F/A-18 is conducive to powerful interactions between the vortices shed from the forebody and LEXs. In an effort to determine an explanation for the differences between small- and large-scale model data, tests were conducted in Langley's 30x60-foot wind tunnel using the 0.07- and 0.16-scale models. Geometric parameters influencing the forebody/wing/LEX vortex development, interaction, and stability were investigated. Among these parameters were forebody on/off, LEXs on/off, LEX boundary layer bleed slots open/closed, and radome strakes on/off.

The complex vortex interactions were not well-understood during the wind tunnel tests due to a lack of adequate flow visualization capability. The

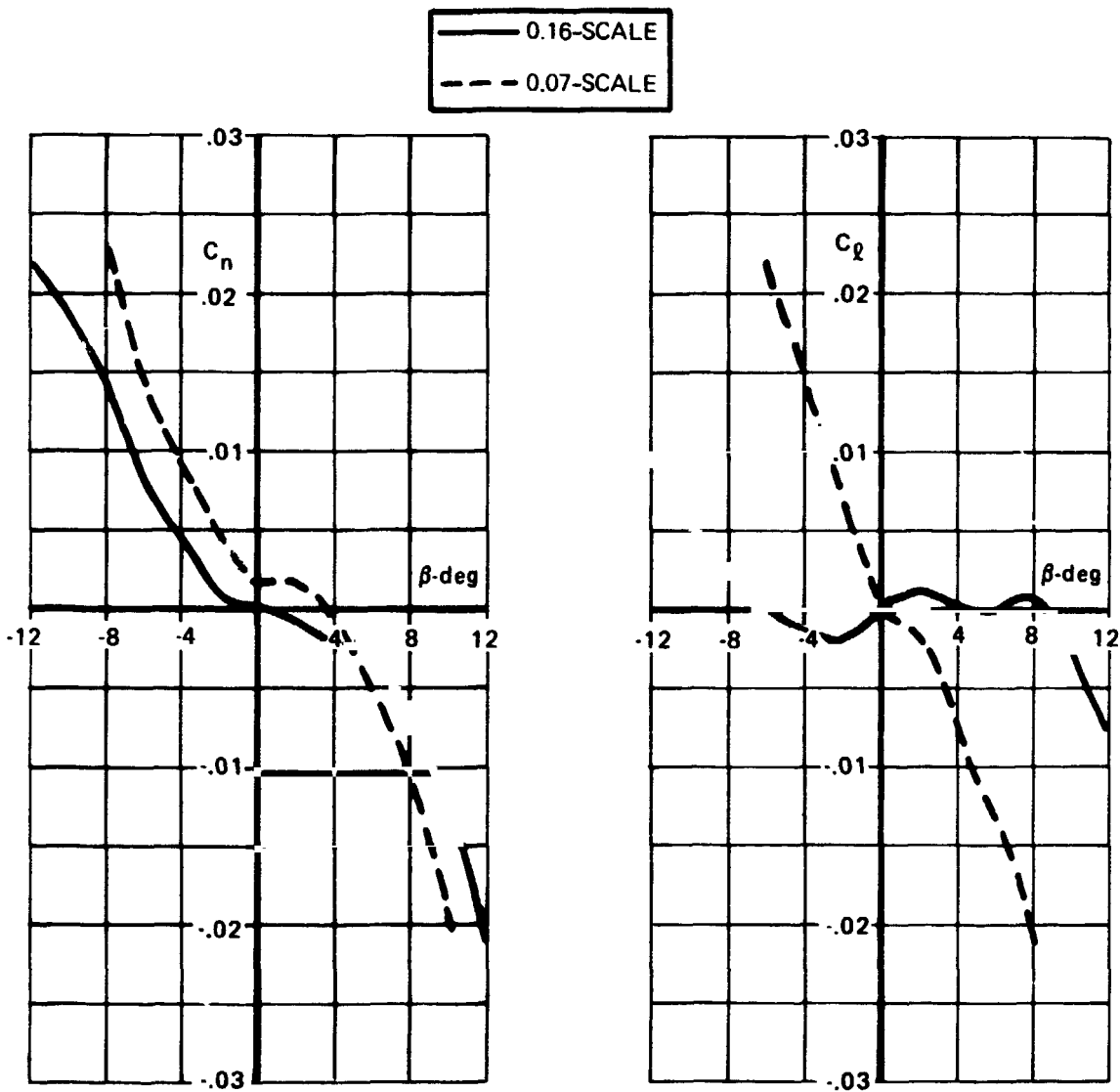


FIGURE 7. YAWING MOMENT AND ROLLING MOMENT VARIATIONS WITH SIDESLIP AT $\alpha = 35^\circ$ ON 0.07 AND 0.16-SCALE F/A-18 MODELS TESTED IN THE NASA LANGLEY 30 X 60 FOOT WIND TUNNEL.

difficulty in visualizing in a vivid manner highly-three-dimensional vortical motions is typical of low-speed wind tunnels at the present time. Consequently, the Northrop water tunnel facility was chosen to provide detailed flow visualization of the F-18 vortex flow field. At the angles of attack of primary interest ($\alpha=30-40$ degrees), significant regions of separated flow exist on the forebody, LEX, and wing surfaces regardless of the value of Reynolds number. Consequently, the fundamental structure of the vortices will be similar whether the flow is developed at low Reynolds number in a low-speed water tunnel or at higher Reynolds number in a wind tunnel (References 2 and 3). In this manner, the results obtained in the water tunnel can be applied to obtain a qualitative understanding of the low-speed wind tunnel data trends.

SYMBOLS

\bar{c}	mean aerodynamic chord
C_{ℓ}	rolling moment coefficient
C_L	lift coefficient
C_M	pitching moment coefficient
C_n	yawing moment coefficient
C_N	normal force coefficient
$C_{\ell\beta}$	lateral stability parameter
$C_{n\beta}$	directional stability parameter
C_R	wing root chord measured along wing-fuselage junction
C_S	section suction coefficient
D	maximum body width
M_∞	free-stream Mach number
Re_c	Reynolds number based on mean aerodynamic chord
Re_D	Reynolds number based on maximum body width
X	chordwise distance of vortex burst position measured from wing trailing edge
V_∞	free-stream speed
q_∞	free-stream dynamic pressure
α	angle of attack
β	angle of sideslip
δ_h	horizontal tail deflection angle
δ_n	leading-edge flap deflection
δ_f	trailing-edge flap deflection
Λ	leading-edge sweep angle
ϕ	forebody strake radial position
η	dimensionless span station

EXPERIMENTAL METHODS

Water Tunnel Facility

The Northrop water tunnel is a closed return tunnel used for high quality flow visualization of complex three-dimensional flow fields. The water tunnel is shown in Figure 8. The test section is 16 in. by 24 in. by 720 in. long and has walls made of transparent Plexiglas. The test section is oriented in the vertical direction, which permits the model to be viewed from any angle. A model is shown installed in the test section in Figure 9. The model is accessed through the top of the tunnel by means of suspension cables connected to the model support system.

The model support system consists of a sting and auto pitch and yaw mechanisms which are capable of pitch angles from -10° to concurrent with sideslip range of -15° to 15° .

Test Procedure

The flow visualization in the water tunnel is obtained by injecting colored food dyes having the same density as water. The density of water is 800 times that of air, which gives the dye excellent light reflecting characteristics relative to using smoke in air. The dye is introduced into the flow field through small orifices and dye tubes distributed at selected positions on the model as shown in Figure 9. The dye can also be introduced through a dye probe, which can be accurately positioned at any point in the test section by means of a traversing mechanism. This mechanism is utilized for the sole purpose of determining proper dye port positions on models for which the latter are not readily evident. Use of this external dye probe apparatus necessitates removal of the honeycomb flow straightener which is positioned directly above the vertical test section. Absence of the honeycomb promotes undesirable flow characteristics in the test section. Consequently, it has become standard procedure to fully-instrument the test models for best flow visualization.

Inlet flows are simulated in the water tunnel by applying suction to tubes connected to the rear of the model's exhaust nozzles. The tubes are run

to a water flow meter outside the tunnel. Flow meters are used to accurately measure and set the inlet flow rate and any jet blowing rates. The water tunnel is operated at a test section velocity of 0.25 foot/second which has been found to produce desirable flow visualization results. This velocity corresponds to a Reynolds number of 3×10^4 /foot. The Reynolds number based on mean aerodynamic chord for the 0.025-scale F/A-18 model is approximately 8700.

MODEL DESCRIPTION

The general layout of the F/A-18 is depicted in Figure 10. A planview photograph of the F/A-18 in flight is shown in Figure 10(a) which vividly depicts the primary airframe components. A 0.025-scale F/A-18 model was used for flow visualization tests in the water tunnel. The model was fully-instrumented with internal and external dye injection orifices. For example, the fuselage forebody featured 24 internal dye ports: 4 longitudinal rows of 6 ports each with 2 rows on the top and bottom surfaces (the rows were positioned on either side of the model centerline). Additional ports (6) internal to the fuselage were installed along the left side below the leading-edge extension (LEX). The left LEX was instrumented with 18 internal dye release holes: 2 chordwise rows of 6 each on the upper surface and a single row of 6 ports on the lower surface. Both left and right LEXs featured external dye lines consisting of small stainless steel tubes extending up to the LEX apex and the LEX planform break. The LEX planform break is depicted in Figure 10(b). The left wing featured 24 upper surface dye orifices: 6 chordwise ports at each of the 4 span stations. With the model instrumented in this fashion, it was possible to provide detailed visualization of the forebody, LEX and wing surface flows and the forebody and LEX vortices throughout the ranges of angle of attack and sideslip ($0^\circ \leq \alpha \leq 40^\circ$; $-12^\circ \leq \beta \leq 12^\circ$). A pair of suction tubes was inserted in the exhaust nozzles to provide inlet suction to simulate a realistic inlet mass flow ratio.

The baseline model featured all LEX slots open (see Figures 10(a) and 10(b)), leading-edge flaps deflected 35° , trailing-edge flaps undeflected, horizontal tails deflected full trailing-edge up (-12°). Leading-edge flap deflection angle of 25° was not assessed since the associated flow field changes in the water tunnel, operating at low Reynolds number, are virtually undetectable on a wing of such low sweep angle.

ORIGINAL PAGE
COLOR PHOTOGRAPH

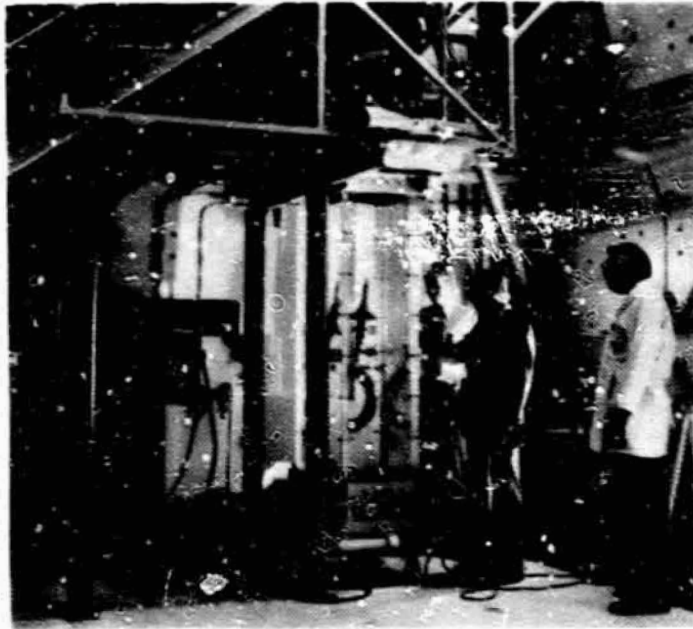


FIGURE 8. NORTHROP 16 X 24-INCH DIAGNOSTIC WATER TUNNEL FACILITY

ORIGINAL PAGE
COLOR PHOTOGRAPH

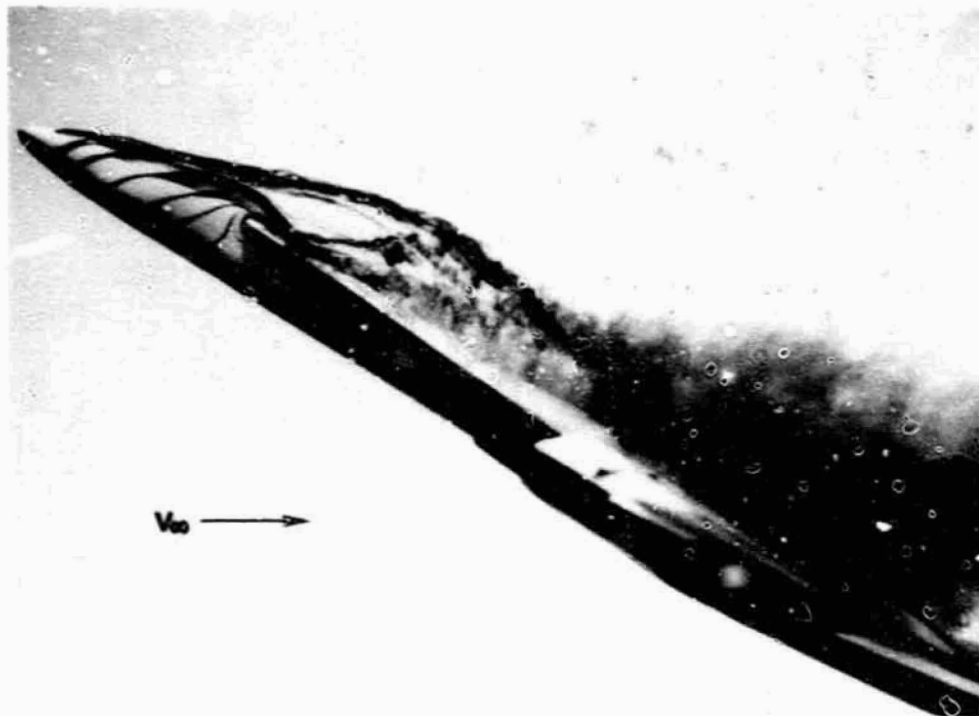
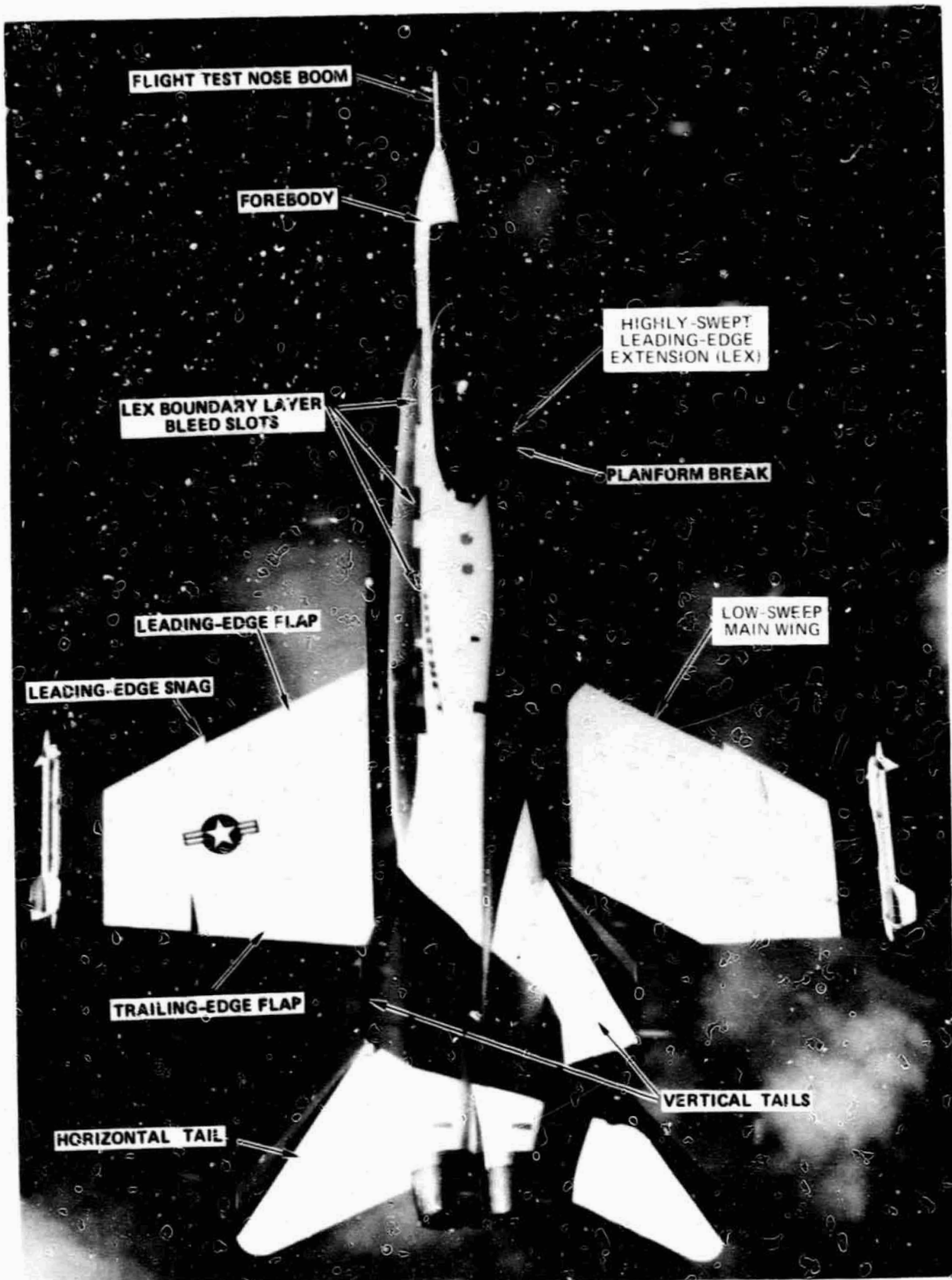


FIGURE 9. ADVANCED FIGHTER MODEL INSTALLED IN THE WATER TUNNEL
(DYE INJECTION THROUGH INTERNAL AND EXTERNAL PORTS)

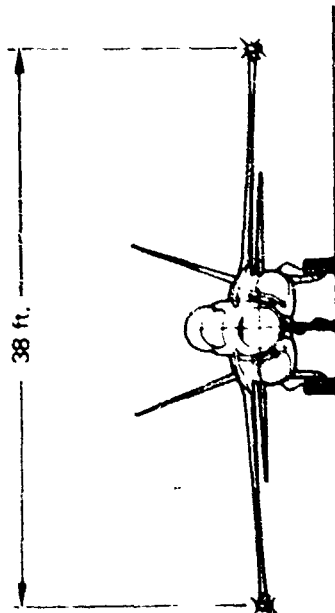
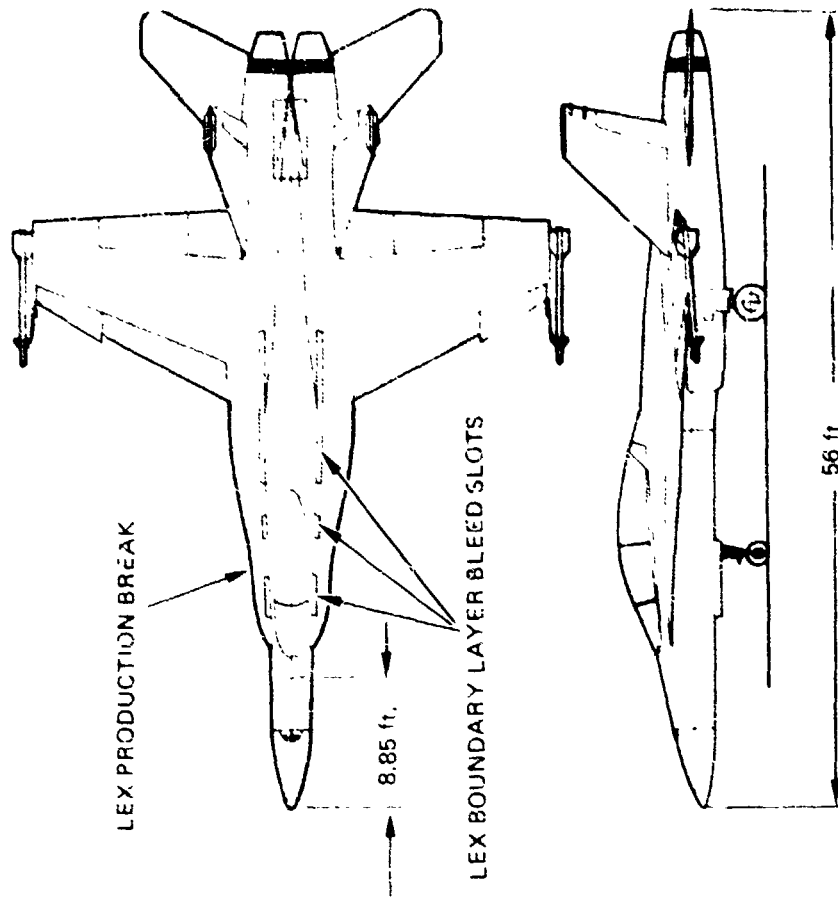


(A) F/A-18 IN FLIGHT

FIGURE 10. F/A-18 DESCRIPTION

PRECEDING PAGE BLANK NOT FILMED

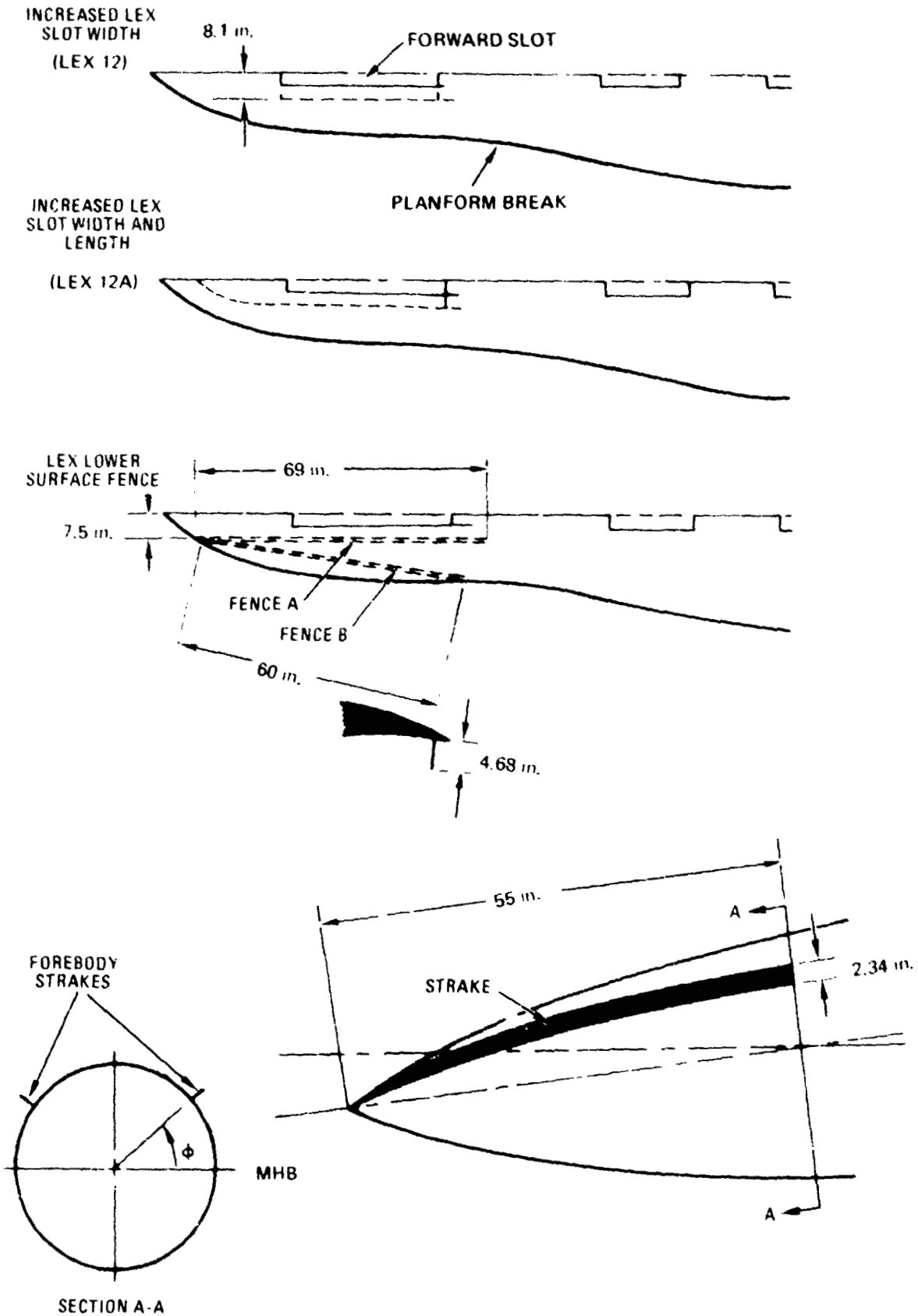
ORIGINAL PAGE
 COLOR PHOTOGRAPH



(B) 3-VIEW DRAWING (ALL DIMENSIONS ARE FULL-SCALE).

FIGURE 10. F/A-18 DESCRIPTION (CONTINUED)

ORIGINAL PAGE IS
OF POOR QUALITY



(C) LEX AND FOREBODY MODIFICATIONS (ALL DIMENSIONS ARE FULL-SCALE).

FIGURE 10. CONCLUDED.

Several of the water tunnel model geometry changes investigated in the water tunnel test program are illustrated in Figure 10(c). The model changes include: double-width forward LEX bleed slots (LEX 12); double-width, increased length forward slots (LEX 12A); LEX lower surface fences oriented in a streamwise and oblique manner (Fence "A" and Fence "B", respectively); and forebody strakes mounted at radial positions of $\phi = +40^\circ$, 0° , and -45° .

Additional model variations included: flight test nose boom; wing snag and fence combination; removal of the LEXs; and removal of the forebody. The point at which the forebody was removed is indicated in Figure 10(b). A length of 8.85 ft. (full-scale) was removed and replaced with a hemispherical cap.

DISCUSSION OF RESULTS

WATER TUNNEL FLOW VISUALIZATION OF THE F/A-18

Baseline ($\delta_n/\delta_f=35^\circ/0^\circ$; $\delta_h=-12^\circ$)

The significance of the leading-edge extension (LEX) slot flow is revealed in Figure 11, which depicts the strong curvature of the 0.025-scale model fuselage surface flow near the LEX struts and slots at $\alpha=0^\circ$ and $\beta=0^\circ$. The entrainment of the boundary layer fluid into the slots is evident. The water tunnel photographs in Figure 11 provide a pictorial description of the purpose of the slots: to prevent ingestion of low-energy boundary layer fluid into the side-mounted engine inlets.

It has been established in Northrop water tunnel flow visualization studies and in smoke flow visualization tests at NASA Langley Research Center's 30x60-foot wind tunnel that the F/A-18 LEX planform with slots open generates a dual leading-edge vortex system: one primary vortex originating at the LEX apex and another near the production break (or inflection point) in the LEX planform. This flow phenomenon is sketched in Figure 12. With bleed slots closed, however, only one primary vortex, originating at the LEX apex, is evident, as sketched in Figure 12. As a consequence of the slot flow, which rolls up into a vortex on the LEX upper surface and rotates in a sense opposite to the leading-edge vortices (see Figure 12), less lower surface flow is available for feeding into the primary leading-edge vortex. Due to slot entrainment effects, the angle and velocity at which the lower surface flow

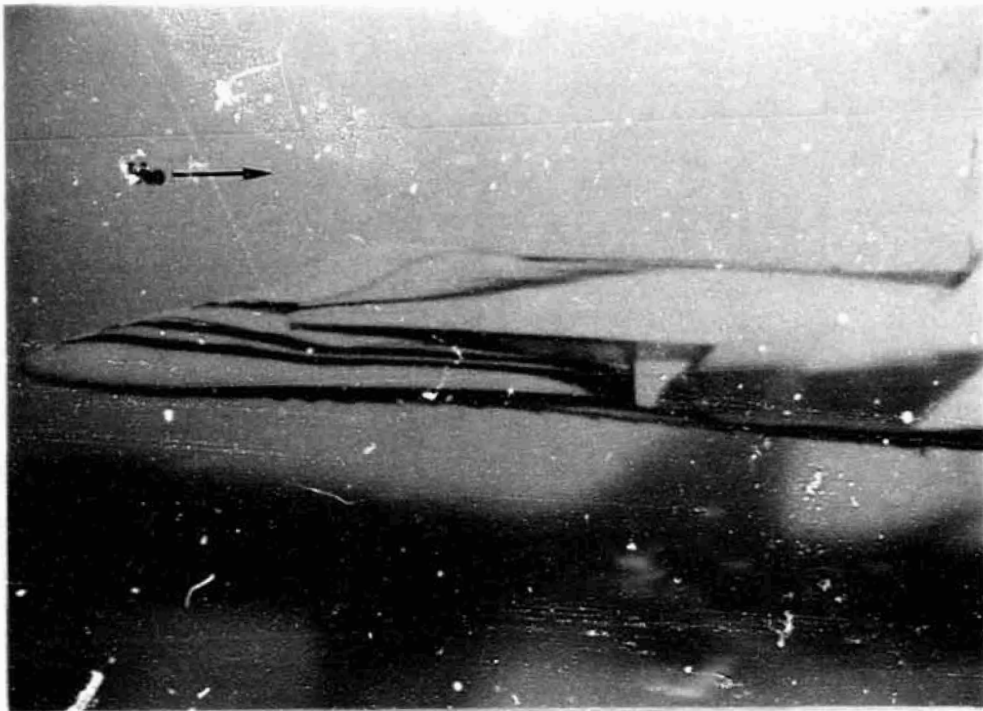
departs the leading edge are reduced, as depicted in Figure 12. The strength of the leading edge vortex is dependent on the difference between the velocities at the outer edge of the lower and upper surface boundary layers. The greater the velocity difference, the greater is the vortex strength, and vice versa. Consequently, in the vicinity of the forward LEX slot, the difference in upper and lower velocity components at a typical LEX cross-section is reduced, with a corresponding reduction in apex primary vortex strength in this region.

An F/A-18-type LEX planform is characterized by a section suction distribution (see Reference 4) as sketched in Figure 13. A distinct break is evident in this qualitative suction distribution near the inflection point. If the suction peak near the inflection point is sufficiently strong, the generation of a vortex at the inflection point may result (in the absence of a bleed slot). Water tunnel studies at Northrop have confirmed a tendency of such planforms to develop a second primary vortex. In the extreme, a double delta wing is characterized by a two-vortex system.

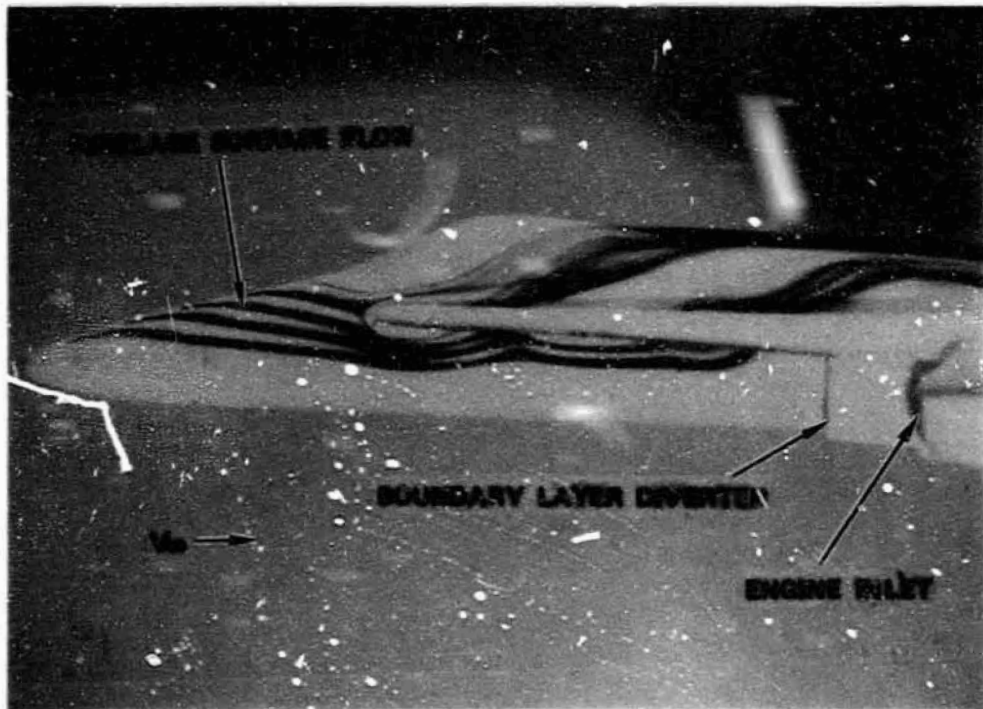
Consideration of the two factors just discussed, (1) reduced lower surface flow near the forward LEX slot available for feeding into the leading-edge vortex and (2) inflection point suction peak, leads to the following conclusions:

The proximity of the forward LEX slot to the planform inflection point (in terms of both longitudinal and lateral spacing) promotes the formation of two primary vortices. Closure of the slot results in only one primary vortex, since the F/A-18 LEX local sweep angle variation is insufficient by itself to promote a second vortex (see Figure 2, for example).

LEX vortex behavior is expected to be sensitive to bleed slot geometry (which determines slot entrainment effects), LEX planform variations, and the relative location of the slot to the LEX leading edge. It can be seen, then, that any modification of the forward LEX slot geometry or LEX planform, or more generally, any means by which the vorticity-feeding mechanism is altered in this region, will influence the F/A-18 LEX vortex system behavior.



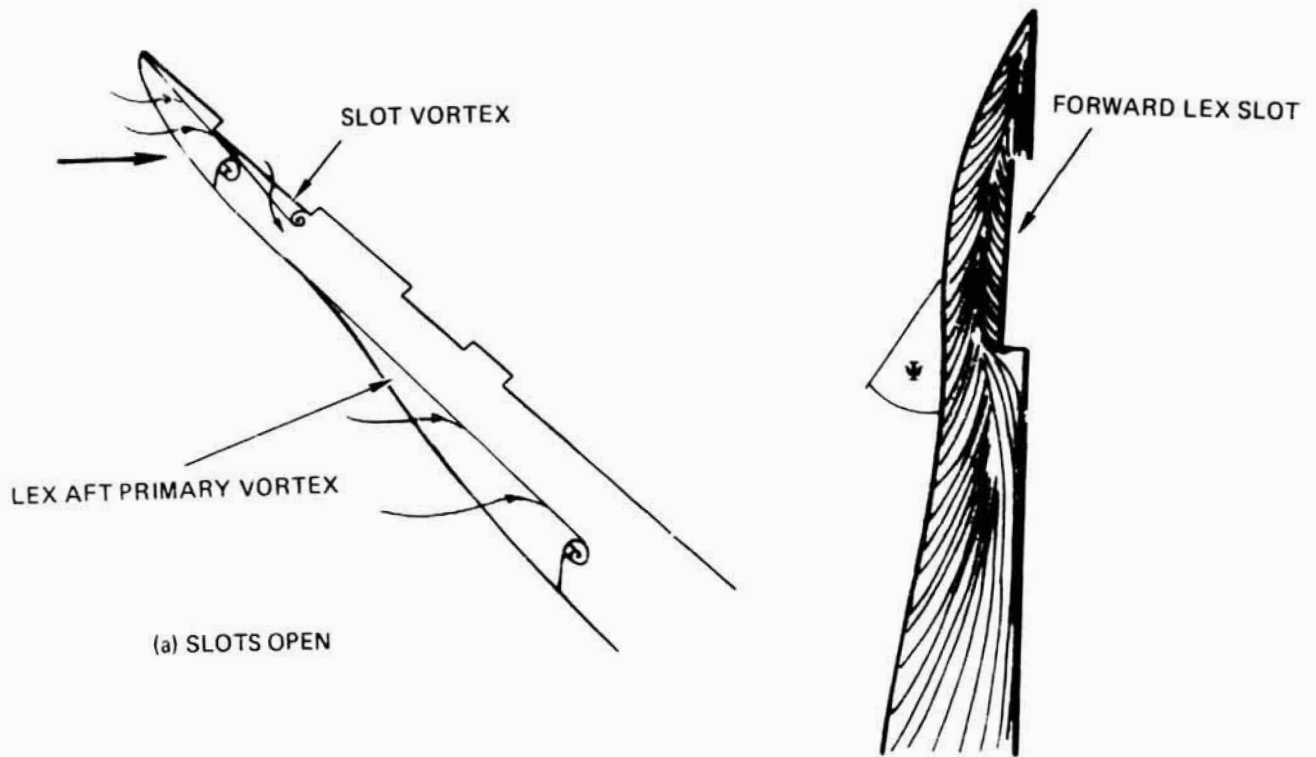
(A) LEX SLOTS CLOSED



(B) LEX SLOTS OPEN

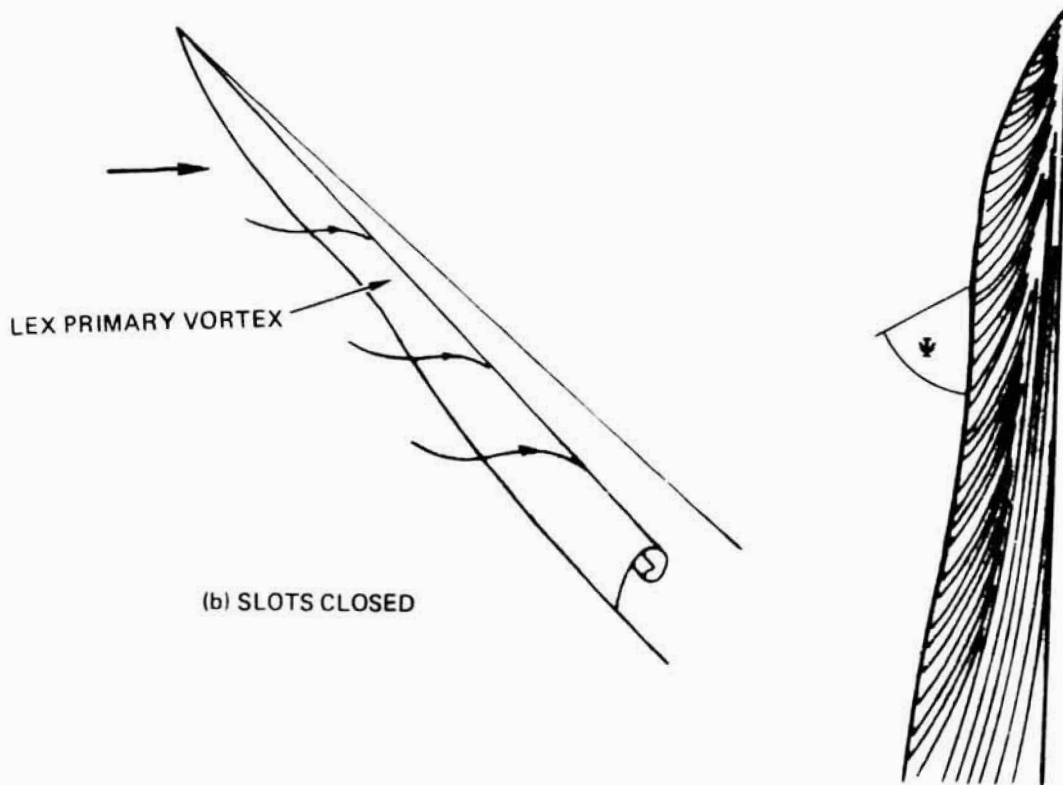
ORIGINAL PAGE
COLOR PHOTOGRAPH

FIGURE 11. FUSELAGE SURFACE FLOW PATTERNS AT $\alpha = \beta = 0^\circ$



(a) SLOTS OPEN

ORIGINAL PAGE IS
OF POOR QUALITY



(b) SLOTS CLOSED

FIGURE 12. SKETCHES OF LEX LOWER SURFACE FLOW PATTERNS.

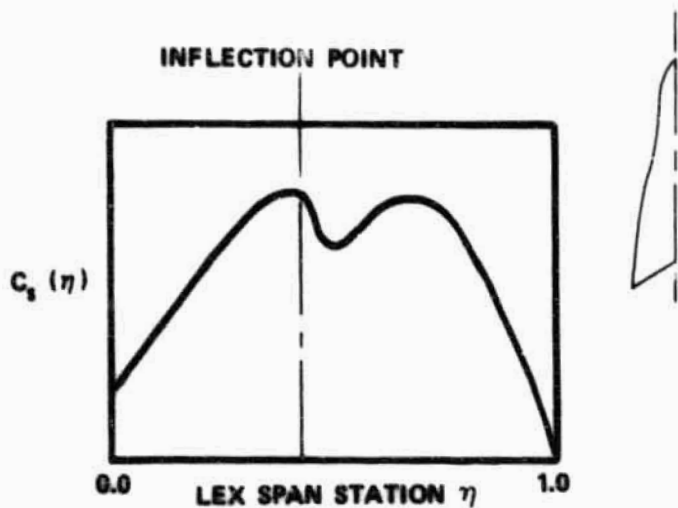


FIGURE 13. SKETCH OF SECTION SUCTION DISTRIBUTION ON F/A-18-TYPE LEX PLANFORM

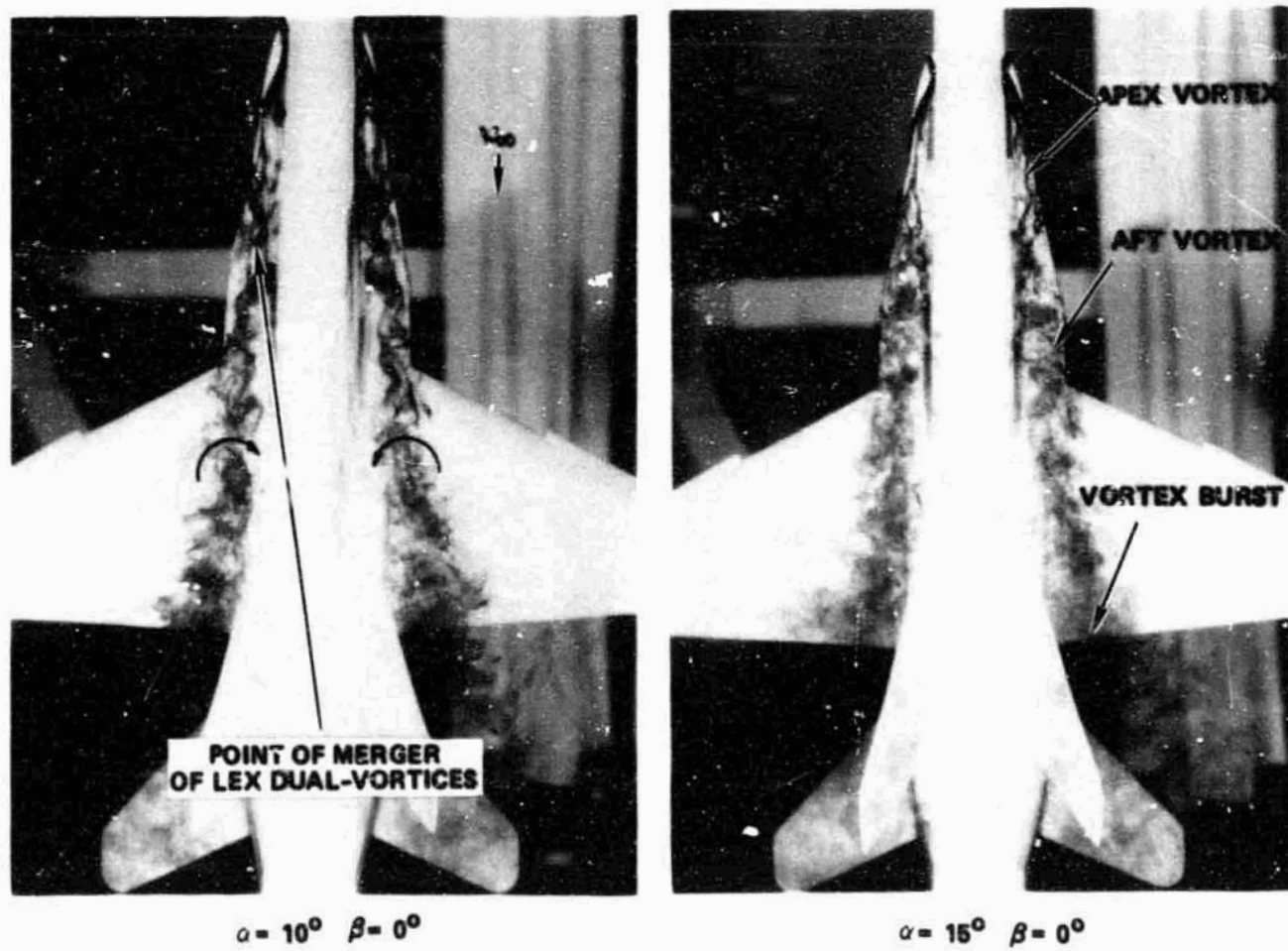


FIGURE 14. WATER TUNNEL PHOTOGRAPHS OF 0.025-SCALE F/A-18 BASELINE; $\delta_n/\delta_f = 35^\circ/0^\circ$; $\delta_h = -12^\circ$

The LEX vortices at $\alpha=10^\circ$ and 15° ($\beta = 0^\circ$) are depicted in the flow visualization photographs in Figure 14. The first point of interest is that the vortices appear diffuse, with no distinct core being depicted. The vortices are energetic but, due to the two-vortex system on the F/A-18 LEX, the rotational flow is somewhat difficult to define in a vivid manner. At these angles of attack, the two primary vortices merge a short distance downstream of the planform inflection point. Vortex bursting at the wing trailing edge occurred at $\alpha \approx 15^\circ$, although this angle of attack is considered low relative to the expected value at higher Reynolds numbers in air. Laminar boundary layer separation at the low Reynolds number conditions in the water tunnel promoted a larger region of wing flow separation and, hence, premature bursting of the LEX vortices. Review of NASA videotapes of smoke flow visualization on the 0.16-scale F/A-18 indicates vortex bursting at the wing trailing edge at $\alpha = 20^\circ$. In sideslip, $\beta = 4^\circ$ and 8° , for example, vortex breakdown asymmetry was evident (photographs not shown), with the windward vortex breaking down near the windward vertical tail leading edge and no evidence of leeward vortex breakdown over the leeward wing panel. There was also a noticeable inboard and outboard displacement of the windward and leeward LEX vortices, respectively.

The flow photograph (planview) in Figure 15 shows the LEX vortex at $\alpha=20^\circ$, $\beta=0^\circ$, where vortex bursting is observed at approximately $X/C_R = 0.3$. Here, X is defined as the dimensional distance of the burst point measured from the wing trailing edge and C_R is the wing chord measured along the wing-fuselage junction extending from the trailing edge to the wing leading edge projected to the fuselage. The determination of the vortex burst point is highly subject to the individual observer's interpretation. Breakdown in this report is defined as the point at which the first noticeable region of stagnated and reversed flow along the vortex axis was observed.

The two primary vortices on the LEX are apparent in the sideview photograph in Figure 15. The point of origin of the second LEX primary vortex is difficult to determine precisely but is, approximately, slightly forward of the planform inflection point.

PRECEDING PAGE BLANK NOT FILMED

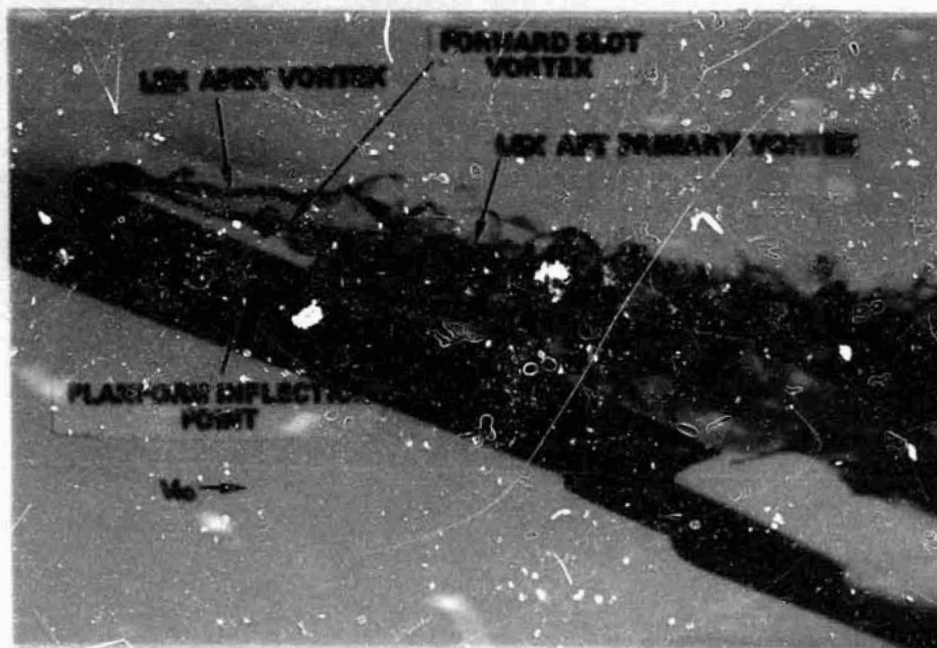
Note is made that the photographs in this report are inadequate in providing a complete description of the nature of the vortex flows. For example, the aft primary vortex on the LEX in Figure 15 appears a diffuse, ill-organized mass of dye. Observation of this vortex in situ, however, provides the full three-dimensional nature of the flow and an appreciation for the significant rotation of the LEX vortex which greatly influences the wing flow.

The results in Figure 16 show that at $\alpha=20^\circ$ the LEX vortices do not exhibit a large difference in burst positions in sideslip, although the leeward vortex does burst farther aft. This may be due, in part, to the presence of the twin vertical tails. The twin verticals act as downstream obstacles which impose an adverse pressure field on the LEX vortices, thereby reducing the potential for large asymmetry in burst positions. A second reason is related to viscous effects. At $\alpha=20^\circ$, the LEX vortices are not yet of sufficient strength to dominate the flow field at the low-Reynolds-number conditions in the water tunnel. Consequently, laminar flow separation on the cambered wing upper surface may tend to reduce vortex breakdown asymmetry. The primary differences in the LEX vortex characteristics lie in the core positions and the rotational energy of the respective vortices. The leeward LEX vortex appeared more energetic (this assessment is based on the "tightness" of the helicoidal pattern depicted by the dye tracers) and was displaced outboard. The flow photograph in Figure 16 shows that at higher sideslip angle ($\beta=8^\circ$) there is a greater difference in burst positions relative to the $\beta=4^\circ$ result due to the displacement of the leeward LEX vortex from the leeward vertical tail surface and/or reduced leeward wing flow separation due to the higher sideslip angle. Strong vortex-induced sweeping action is observed on the leeward wing panel. The outer extent of the dye tracers entrained into the vortex defines, approximately, the spanwise extent of this sweeping action. In contrast, the windward wing surface exhibits significant flow separation without reattachment (no photograph available). (Note: Surface flows will be discussed quite frequently. It is recognized that surface flow characteristics at the low Reynolds number in the water tunnel ($Re_c \approx 8700$) are not representative of the flow behavior at higher Reynolds numbers. The trends observed in water, however, are insightful and, as a result, will be utilized where appropriate.)

ORIGINAL PAGE
COLOR PHOTOGRAPH



PLANVIEW; $\alpha = 20^\circ$ $\beta = 0^\circ$



SIDEVIEW; $\alpha = 20^\circ$ $\beta = 0^\circ$

FIGURE 15. WATER TUNNEL PHOTOGRAPHS OF 0.025-SCALE BASELINE
F/A-18 DUAL LEX VORTEX SYSTEM

ORIGINAL PAGE IS
OF POOR QUALITY

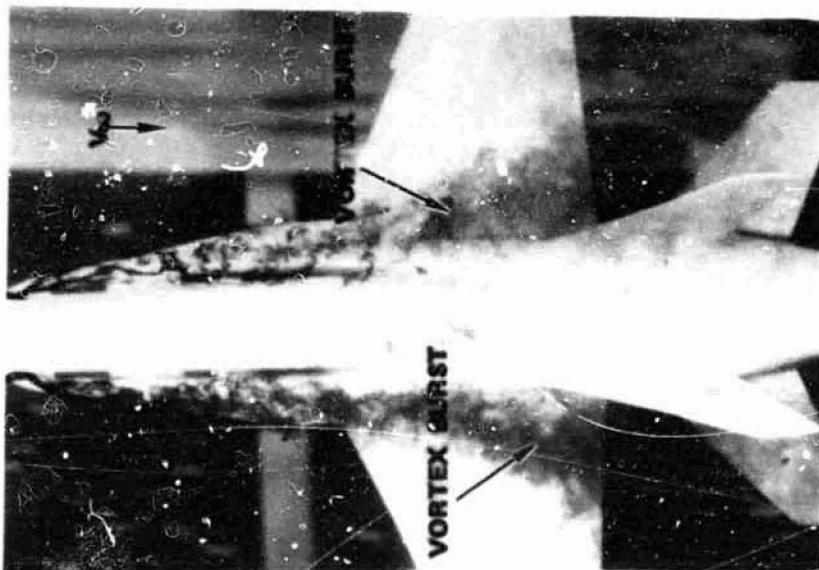
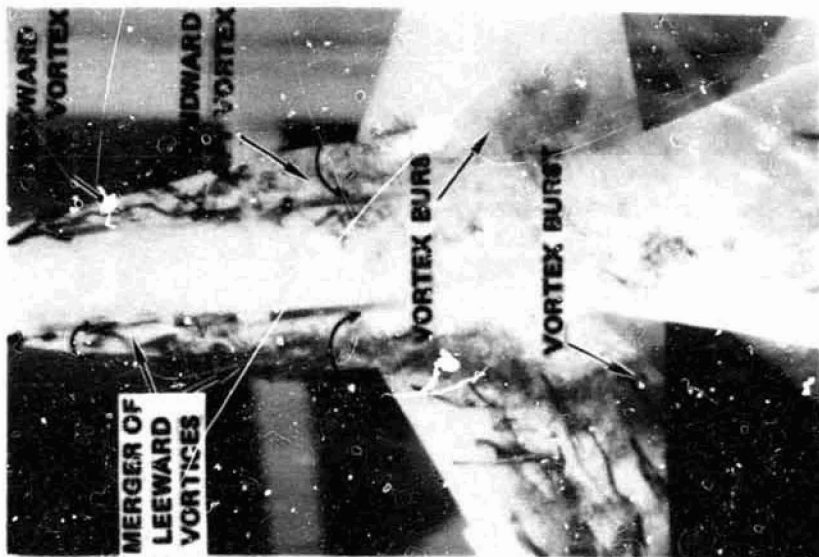
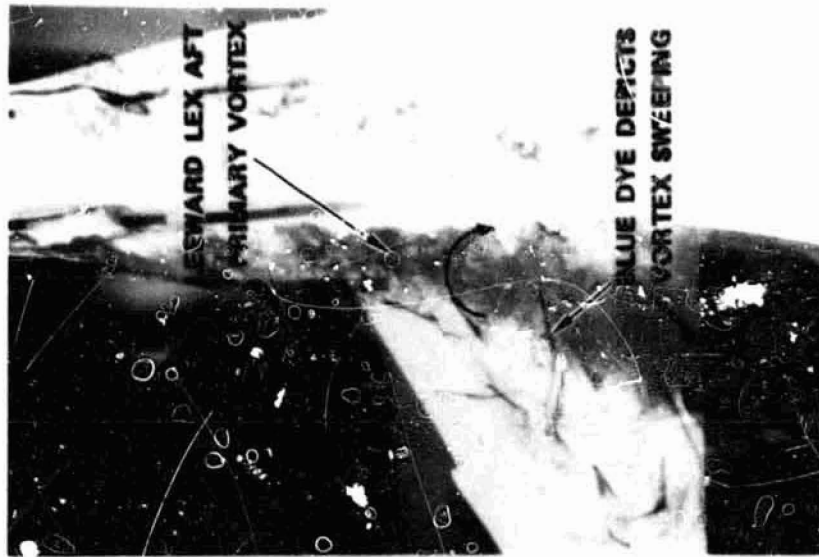


FIGURE 16. FLOW VISUALIZATION PHOTOGRAPHS OF BASELINE F/A-18 IN
SIDESLIP AT $\alpha = 20^\circ$

ORIGINAL PAGE IS
OF POOR QUALITY

PRECEDING PAGE BLANK NOT FILMED

PRECEDING PAGE BLANK NOT FILMED

In sideslip, the leeward LEX primary vortices merge quite strongly as shown in Figure 16 (the apex vortex exhibits a helical pattern about the second primary vortex), whereas the windward LEX vortices tend to become independent. A wing vortex is also developed (not discernible in Figure 16), emanating from the leading-edge flap hingeline region. This vortex was particularly evident on the leeward panel due to the "effective" sweep increase associated with sideslip.

Figure 17 presents photographs taken at $\alpha=25^\circ$, $\beta=0^\circ$ where vortex breakdown occurred at approximately $X/C_R=0.5$. As vortex strength increased with angle of attack, the breakdown position was somewhat more discernible. Of note is that the LEX apex vortex exhibits less tendency for merger with the second primary vortex and breakdown of the apex vortex occurs. This is depicted in the photographs in Figure 17. The primary differences in vortex behavior at nonzero sideslip appear to be the vortex strength and core positions. The LEX vortex behavior observed in smoke flow visualization of a 0.16-scale F/A-18 model in the Langley 30x60-foot wind tunnel was quite similar to the water tunnel results. Examination of NASA videotapes revealed reasonable trend agreement of LEX vortex burst progression and vortex positions with the low-Reynolds-number hydrodynamic flow visualization.

A comparison of upper surface flow characteristics in sideslip at $\alpha=25^\circ$ is provided in Figure 18. The leeward wing exhibits greater vortex sweeping action, indicated by the spanwise orientation of the surface dye, relative to the windward wing.

The forebody vortex patterns at $\alpha=25^\circ$ are shown in Figure 19. The vortices appear not to be a major factor in the flow field at this angle of attack. The vortices are weak (no "tight" helicoidal pattern) and, upon traversing the canopy, the vortical motions in sideslip exhibit a marked instability. The relative strength of a vortex is assessed in a highly qualitative fashion in the water tunnel by observing the number of turns per unit distance along the vortex. The vortex motion in the water tunnel is so slow ($V_\infty \approx .25$ ft/sec) that the path of a dye element can be tracked along the vortex. The angles of attack of primary interest, however, in this study

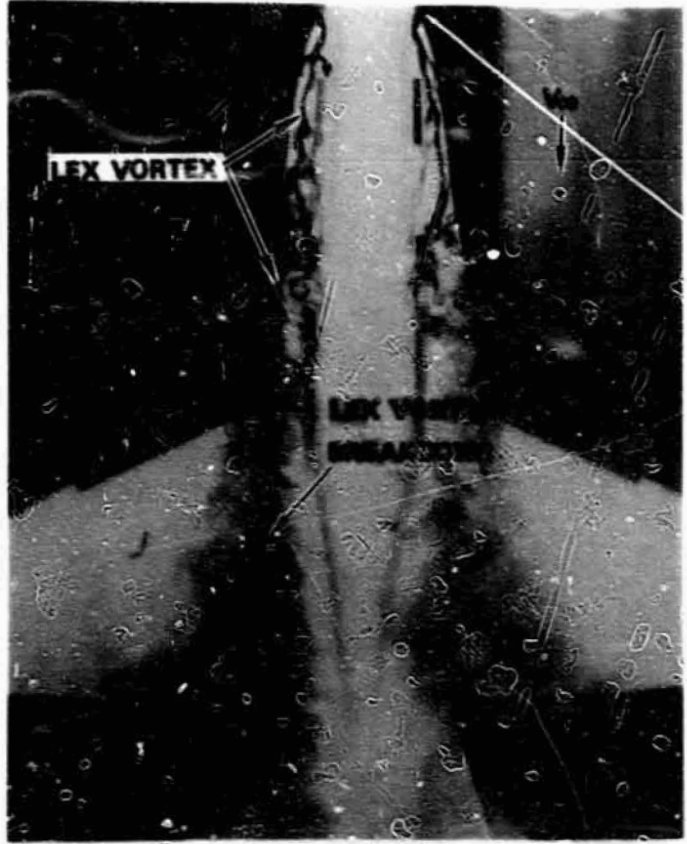
of F/A-18 vortex behavior are $\alpha=30^\circ$ to 40° , inclusive. At these angles of attack potentially significant forebody-wing-LEX flow interactions can arise.

At $\alpha=30^\circ$, $\beta=0^\circ$, LEX vortex breakdown occurred at approximately the leading-edge flap hingeline as shown in Figure 20. The results in Figure 20 indicate that differences still exist in the leeward and windward wing surface flow characteristics in sideslip. The LEX apex vortex was observed to break down shortly downstream of the second primary vortex point of origination, as depicted in Figure 21. The forward slot vortex is also illustrated in the photograph in Figure 21.

Qualitative observations indicate that the body vortices at $\alpha=30^\circ$, shown in Figure 22, are of increased strength relative to the results obtained at $\alpha=25^\circ$ (see Figure 19). The body vortices are fed by vorticity generated within the fuselage forebody boundary layer up to the point of intersection of the LEX and fuselage. The line of separation of the fuselage primary boundary layer is denoted in Figure 22. Thereafter, the body vortices exhibit essentially constant spacing between turns of the dye tracers, indicative of approximately constant vortex strength. The LEX vortices remain dominant and the forebody vortices at zero sideslip are entrained into the wing flow as shown in Figure 22. The point of entrainment of the body vortices in Figure 22 is at approximately $X/C_R = 0.5$ where the body vortices pass underneath the LEX vortices and exhibit a rapid diffusion as they enter the wing pressure field.

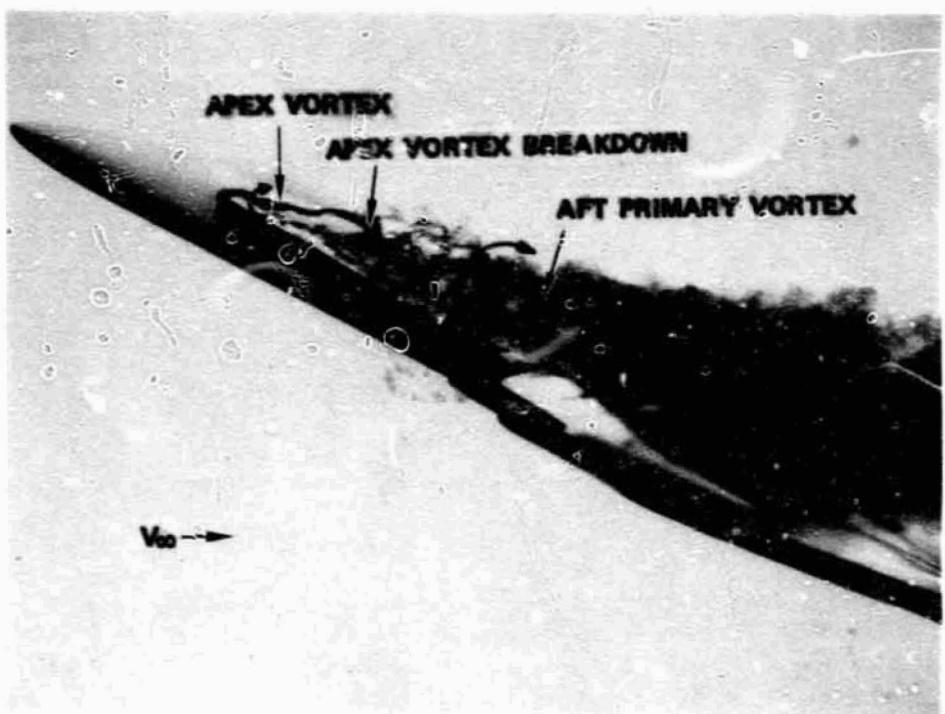
In a sideslip condition, the body vortices exhibit a strongly asymmetric orientation. Figure 23 is presented for illustrative purposes only which shows the leeward body vortex entrainment into the leeward LEX-wing flow and the windward body vortex displacement upward and away from the windward wing flow. This flow situation arises from such factors as the close coupling of the LEX and forebody and the forebody cross-sectional shape (and, consequently, the manner in which the forebody primary boundary layers separate along the fuselage sides). There is a significant rotation of the forebody primary separation lines due to sideslip, the leeward separation line rotating downward while the windward separation line rotates upward. Consequently, the body vortex trajectories will rotate so that the leeward body vortex is

ORIGINAL PAGE
COLOR PHOTOGRAPH



$\alpha = 25^\circ, \beta = 0^\circ$

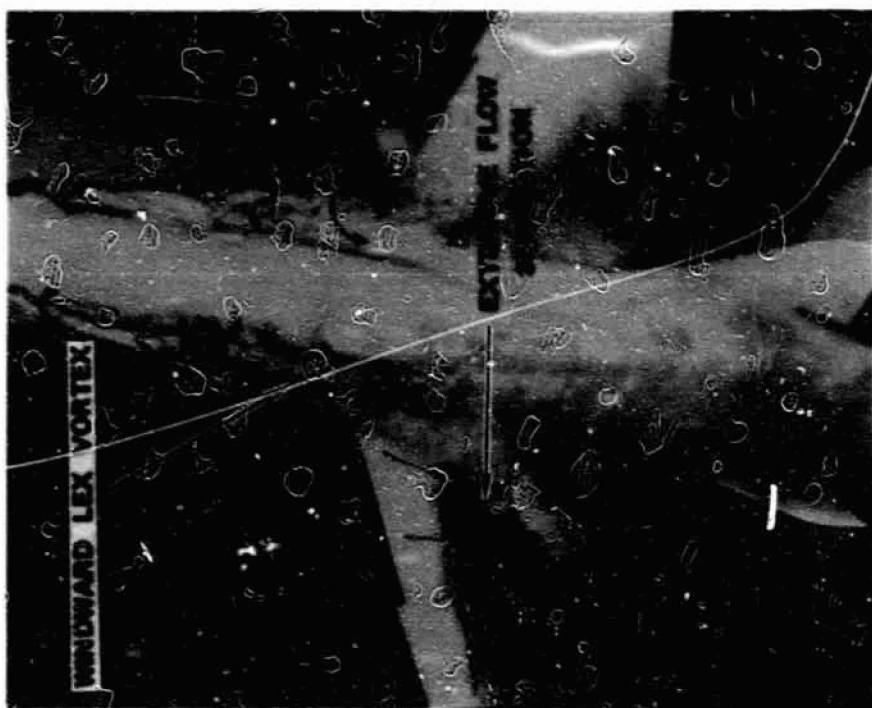
ORIGINAL PAGE
COLOR PHOTOGRAPH



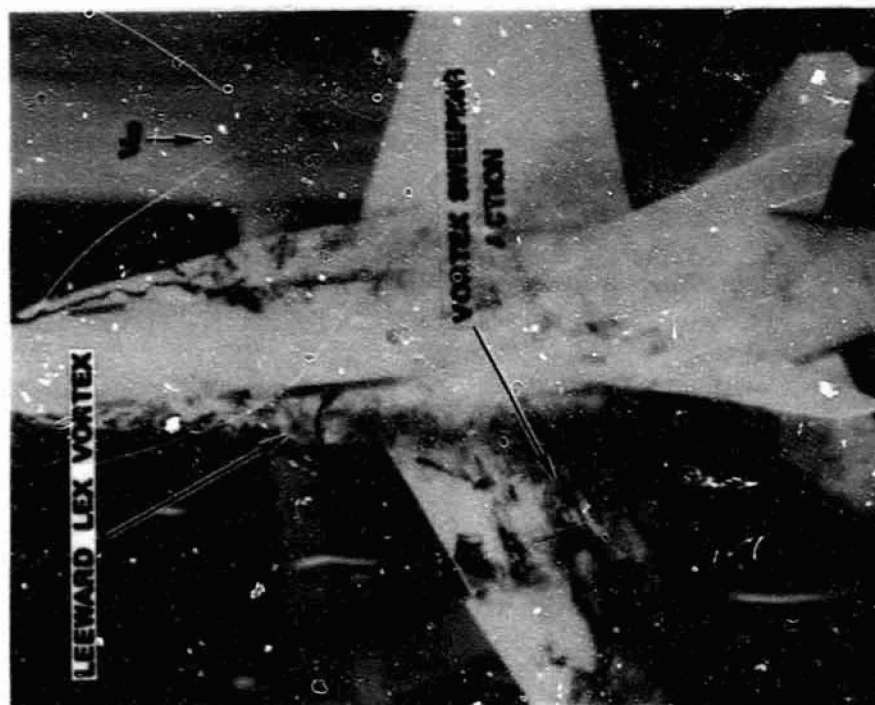
$\alpha = 25^\circ, \beta = 0^\circ$

FIGURE 17. LEX VORTEX FLOW ON BASELINE F/A-18

ORIGINAL PAGE
COLOR PHOTOGRAPH



$\beta = 0^\circ$



$\beta = 0^\circ$

FIGURE 18. FLOW VISUALIZATION PHOTOGRAPHS OF BASELINE
F/A-18 IN SIDESLIP AT $\alpha = 25^\circ$.

PRECEDING PAGE BLANK NOT FILMED

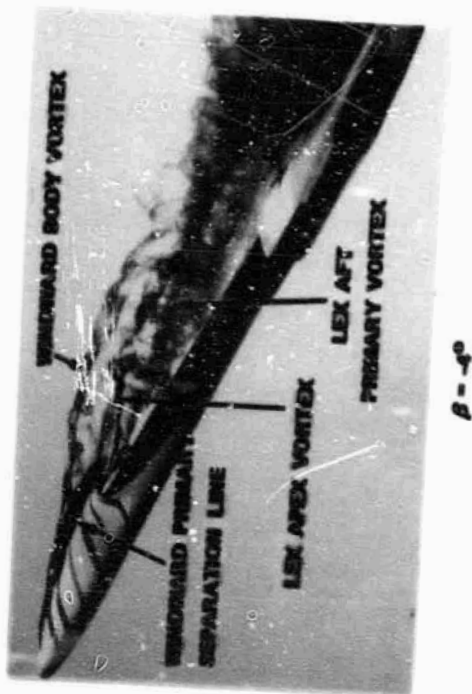
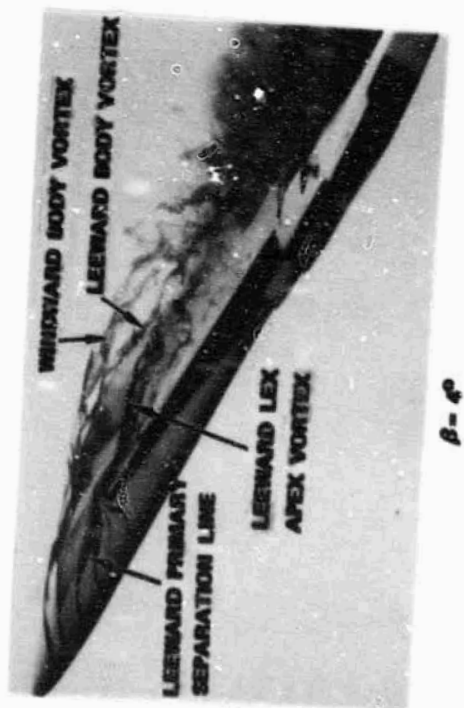
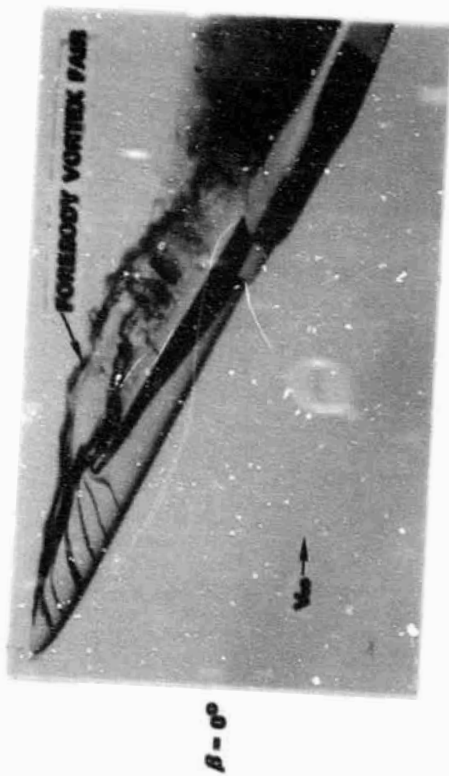


FIGURE 19. FLOW VISUALIZATION OF FOREBODY VORTICES ON BASELINE
F/A-18 AT $\alpha = 25^\circ$

ORIGINAL PAGE
COLOR PHOTOGRAPH



$\beta = 0^\circ$



$\beta = 0^\circ$



$\beta = -5^\circ$

PRECEDING PAGE BLANK NOT FILMED

FIGURE 20. WATER TUNNEL PHOTOGRAPHS OF BASELINE F/A-18 FLOW
FIELD AT $\alpha = 30^\circ$

ORIGINAL PAGE
COLOR PHOTOGRAPH

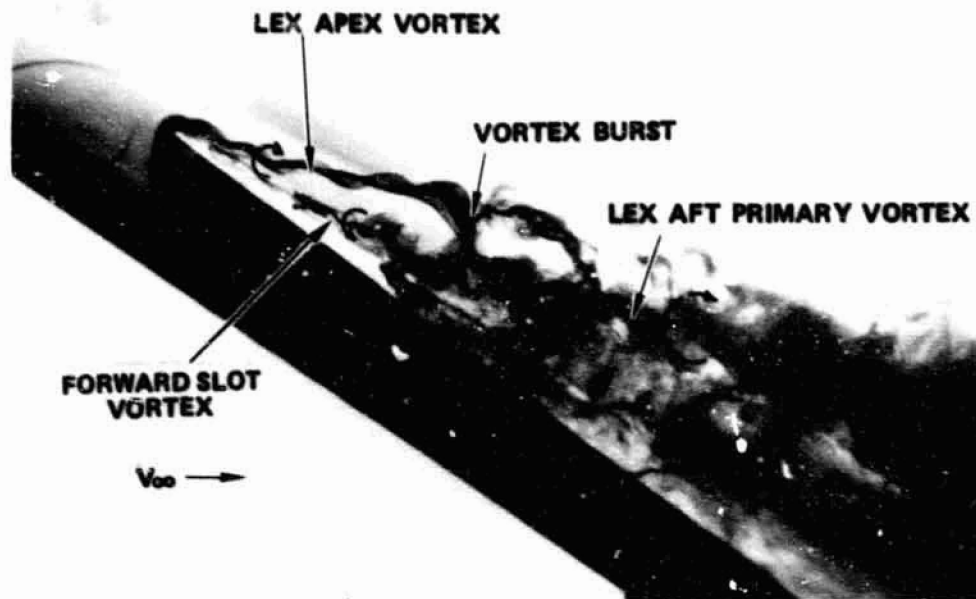


FIGURE 21. DUAL LEX VORTEX SYSTEM AT $\alpha = 30^\circ$; $\beta = 0^\circ$

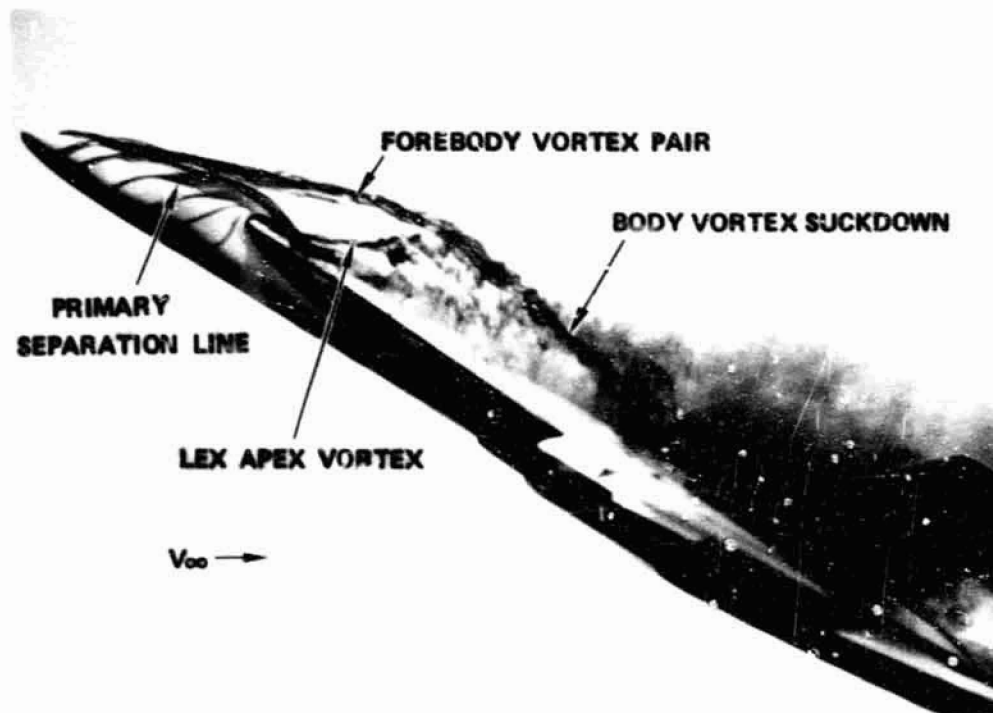
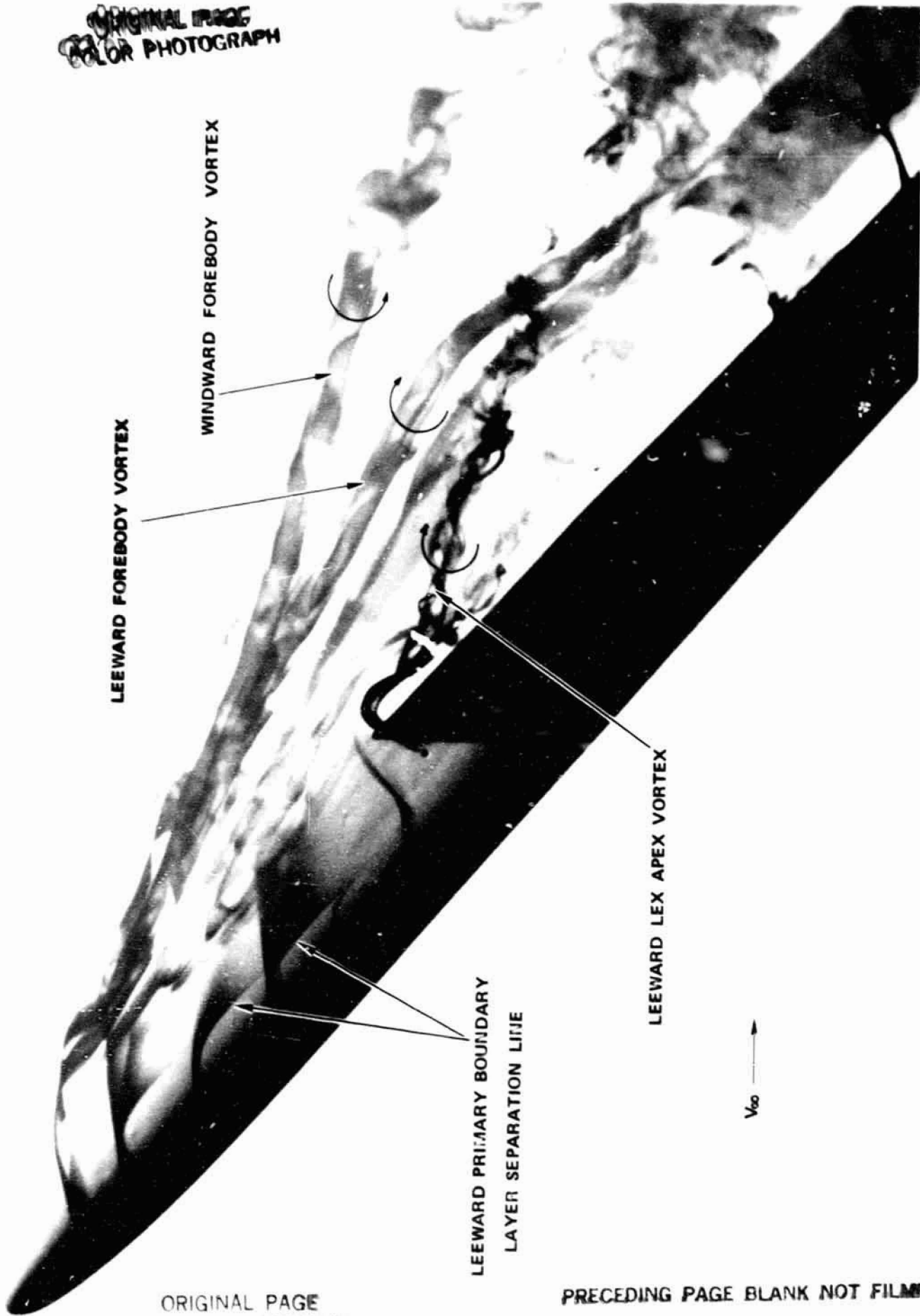


FIGURE 22. FOREBODY VORTEX PATTERN AT $\alpha = 30^\circ$, $\beta = 0^\circ$

ORIGINAL PAGE
COLOR PHOTOGRAPH



ORIGINAL PAGE
COLOR PHOTOGRAPH

PRECEDING PAGE BLANK NOT FILMED

FIGURE 23. BASELINE F/A-18 FOREBODY VORTEX ORIENTATION IN
SIDESLIP; $\alpha = 40^\circ$; $\beta = 8^\circ$

closer to the fuselage and, hence, subject to stronger interaction with the leeward LEX vortex. In contrast, the windward body vortex-LEX vortex interaction is reduced since the former is displaced away from the windward LEX and wing.

At $\alpha=33^\circ$, the windward and leeward wing stall patterns are quite similar (see Figure 24). Small sideslip changes produced no marked alteration of the LEX vortex burst positions, which were observed near the LEX-wing junction.

The qualitative observations in the water tunnel reveal no apparent influence of the forebody vortices on the wing flow field. The sideview and planview photographs at $\alpha=33^\circ$ in Figure 25 show that at $\beta=0^\circ$ the body vortex entrainment point is near the LEX-wing junction. In sideslip, the leeward body vortex is entrained forward of this point into the LEX vortex and dissipates rapidly. The windward body vortices in Figure 25 are shifted so far off the body that any induced effects on the windward wing are considered small. Figure 25 also reveals the rotation of the primary separation lines due to sideslip.

Qualitative assessment of the twin vertical tail region indicates that the dynamic pressure at the tails is reduced relative to the free-stream value. This can be inferred from the photographs in Figure 25 which reveal the low energy wing wake which "blankets" the tails.

At $\alpha=35^\circ$ and 40° , the leeward wing exhibited a massive stall. This may be due to the large angle of attack normal to the leeward LEX resulting from the combination of high sweep-back, angle of attack, and sideslip. The surface flow patterns in Figure 26 show at $\alpha=35^\circ$, $\beta=+6^\circ$ that the windward wing stall is somewhat less pronounced than the leeward panel.

Representative photographs of the baseline forebody vortices at $\alpha=40^\circ$ are presented in Figure 27. Flow field observations suggest that the leeward body vortex effect on the downstream flow behavior is small, since it bursts abruptly upon entering the leeward LEX wing flow field. The windward body vortex may provide small beneficial effects on the windward wing. Dye entrained aft of the canopy into the windward body vortex was observed to flow downwards towards the fuselage and then spanwise over the windward wing. This

PRECEDING PAGE BLANK NOT FILMED

effect was not pronounced, however. Because of the increased displacement of the windward body vortex away from the fuselage with increased angles of attack and sideslip, this effect is expected to diminish accordingly.

Double-Width Forward LEX Slots (LEX 12)

The effects of the increased forward slot width are vividly illustrated in Figure 28 at $\alpha=20^\circ$. The double-width slot tends to decouple the LEX apex and aft primary vortices, particularly at the higher sideslip angles in Figure 28. Also, the aft primary vortices are quite well-defined and appear more concentrated relative to the baseline. A comparison of baseline and LEX 12 flows is provided in Figure 28.

The LEX lower surface flow patterns near the forward slot (photographs not available) reflect the increased slot flow entrainment with LEX 12 and, in addition, suggest a flow situation similar to that developed on a LEX of reduced generating length. By a purely qualitative argument, the changes in the leading-edge suction coefficient distribution are shown in Figure 29 for a representative LEX planform. Increased forward slot flow entrainment produces a more marked break in the suction distribution. Sufficient widening of the slot results in a suction distribution similar to the variation of section suction with LEX span exhibited by a smaller LEX. Due to the smaller "effective" generating length, it is expected that the LEX vortex stability will be reduced at a given angle of attack.

Although photographs are not presented, the progression of LEX vortex breakdown was more rapid with angle of attack relative to the baseline. The dye tracers at $\alpha=30^\circ$ shown in Figure 30 reveal a more tightly-wrapped LEX aft primary vortex and no distinguishable asymmetry in burst positions in sideslip. These results are representative of the flow field effects at higher α 's. The decoupling of the LEX apex and aft primary vortices is evident in the sideview photographs in Figure 30.

ORIGINAL PAGE
COLOR PHOTOGRAPH

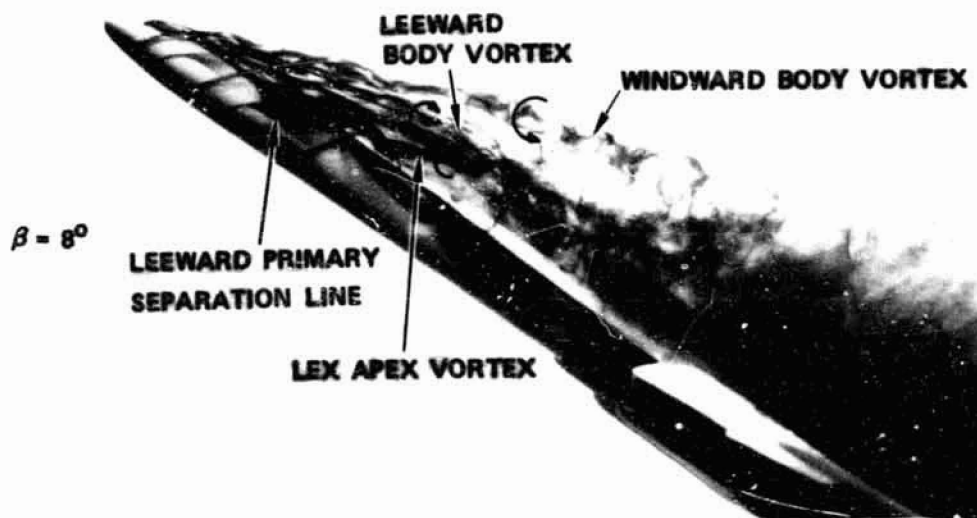
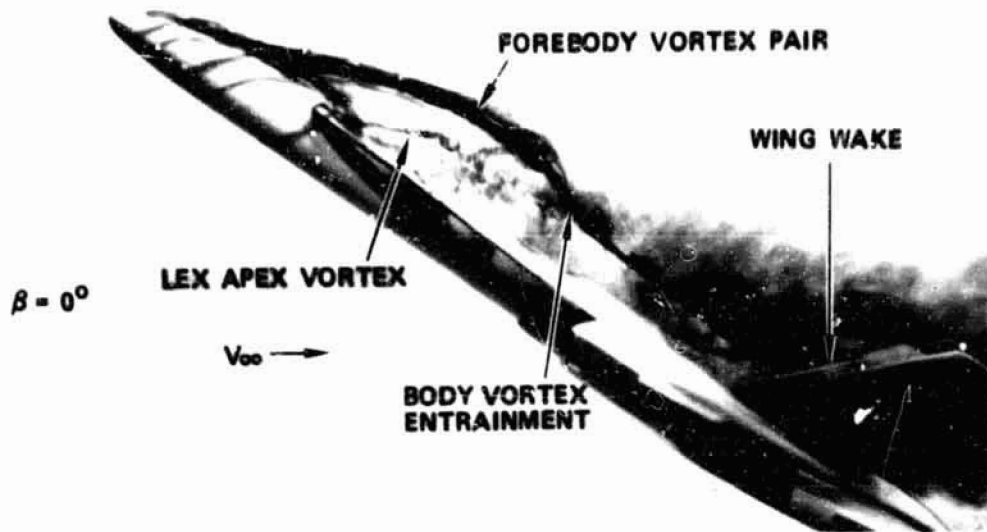


$\beta = -8^\circ$



$\beta = 8^\circ$

FIGURE 24. WING SURFACE FLOW PATTERNS IN SIDESLIP AT $\alpha = 33^\circ$



ORIGINAL PAGE
COLOR PHOTOGRAPH

(A) SIDEVIEW

PRECEDING PAGE BLANK NOT FILMED

FIGURE 25. FOREBODY AND LEX VORTEX FLOWS ON BASELINE F/A-18 AT $\alpha = 33^\circ$

ORIGINAL PAGE
COLOR PHOTOGRAPH

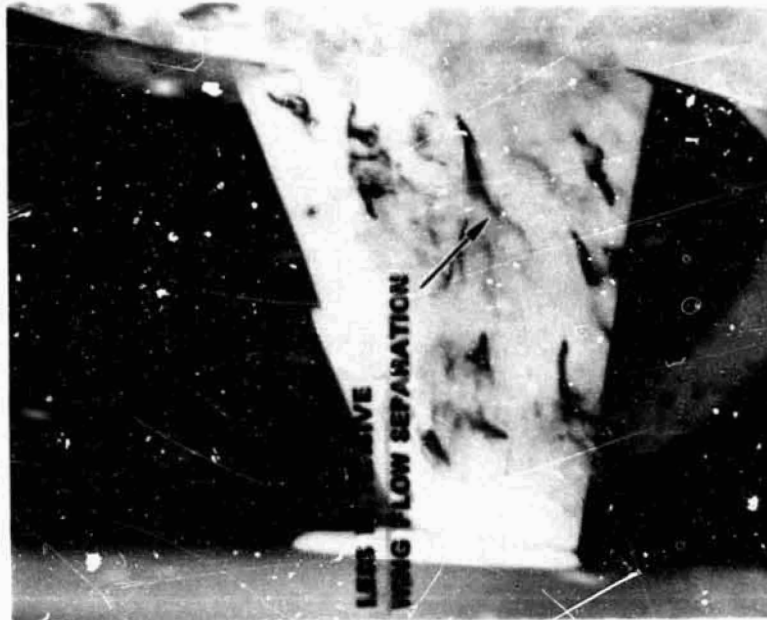


FIGURE 26. COMPARISON OF WING SURFACE FLOW PATTERNS IN SIDESLIP AT $\alpha = 35^\circ$

PRECEDING PAGE BLANK NOT FILMED

ORIGINAL PAGE
COLOR PHOTOGRAPH

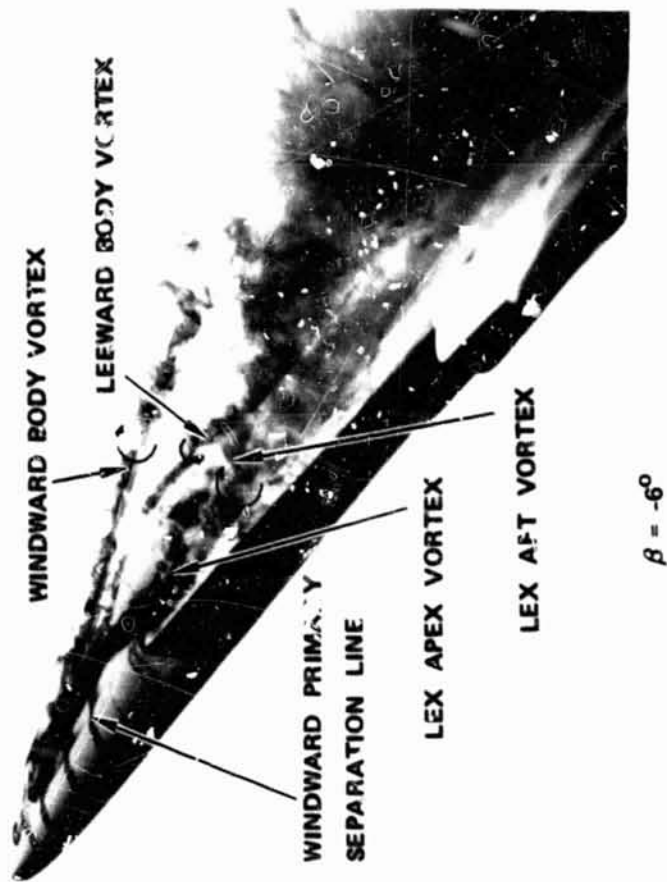
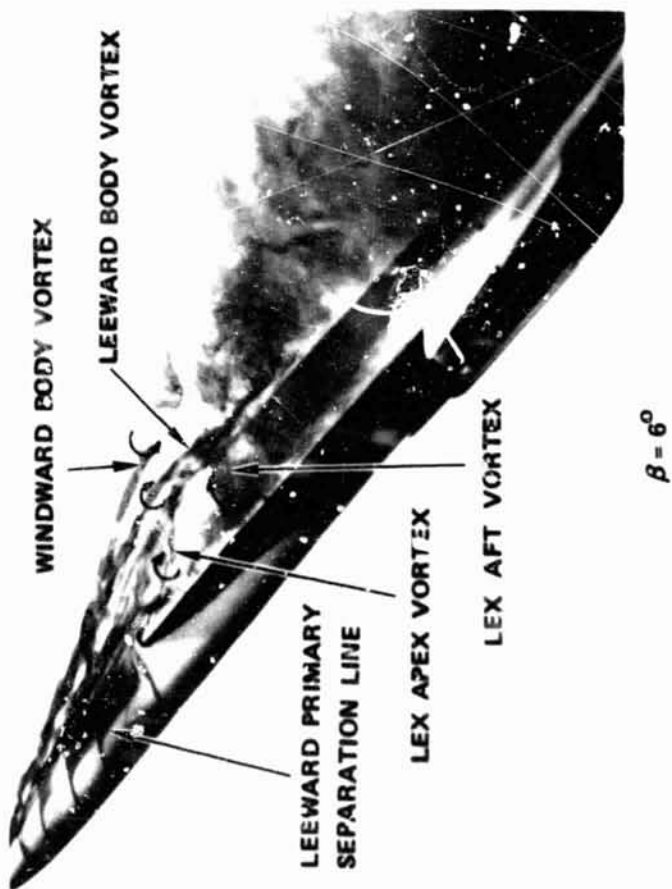
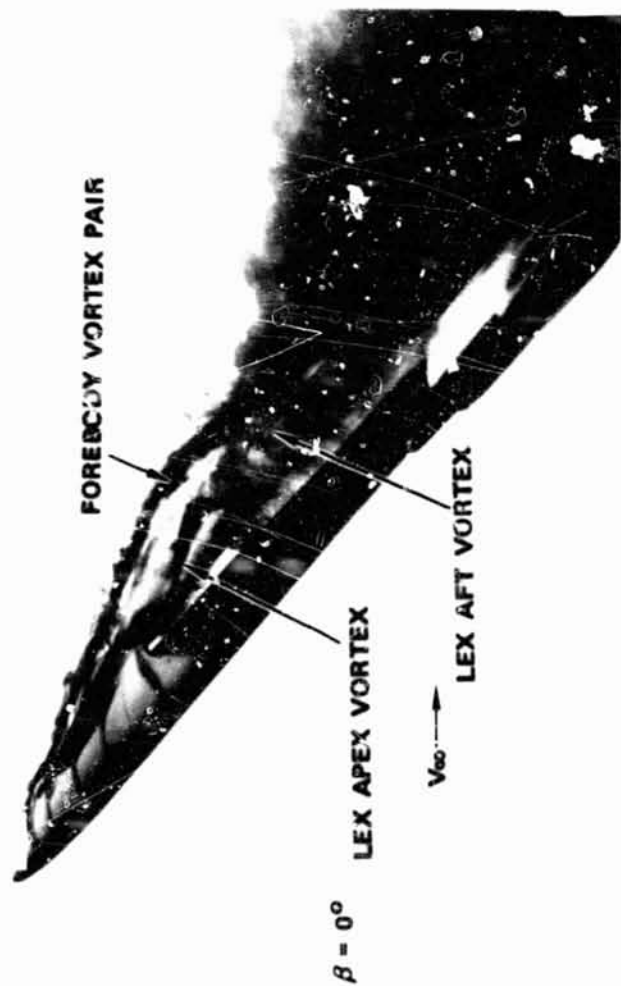


FIGURE 27. BASELINE F/A-18 FOREBODY AND LEX VORTEX PATTERNS IN SIDESLIP AT $\alpha = 40^\circ$

PRECEDING PAGE BLANK NOT FILMED

ORIGINAL TV,CC
COLOR PHOTOGRAPH

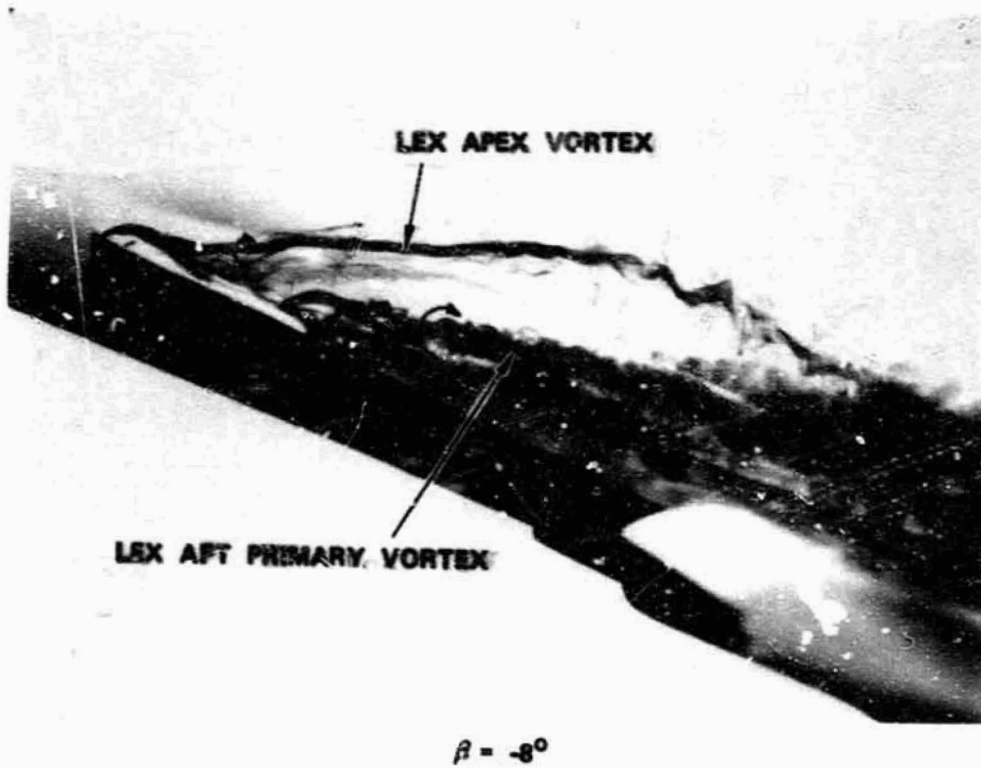
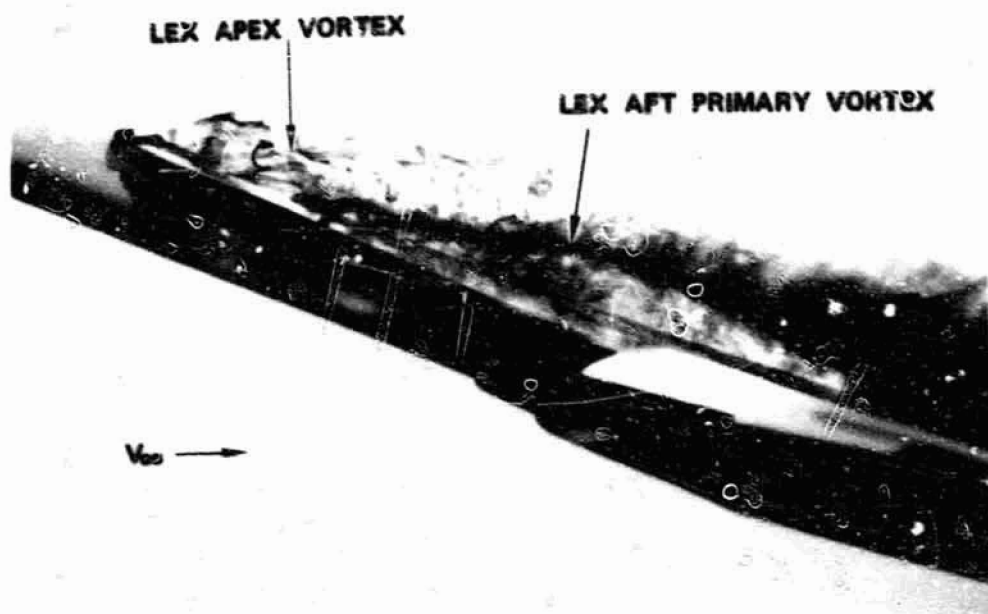
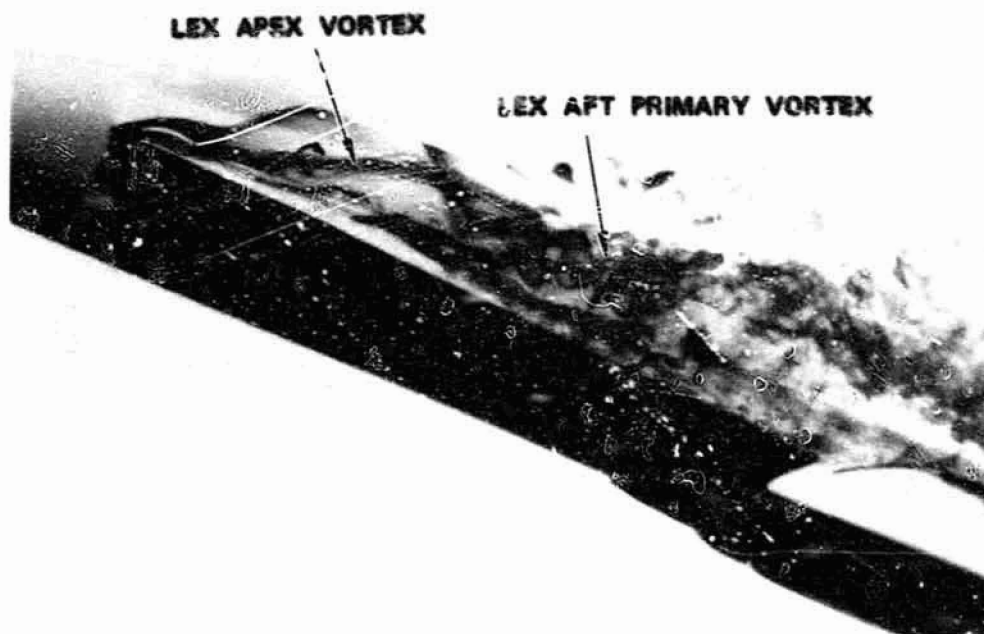


FIGURE 28. LEX VORTEX FLOW CHARACTERISTICS WITH LEX 12 AT $\alpha = 20^{\circ}$

ORIGINAL PAGE
OR PHOTOGRAPH



$\beta = 8^{\circ}$ (LEX 12)



$\beta = 8^{\circ}$ (BASELINE)

FIGURE 28. CONCLUDED.

PRECEDING PAGE BLANK NOT ~~FILMED~~

PRECEDING PAGE BLANK NOT FILMED

ORIGINAL PAGE IS
OF POOR QUALITY

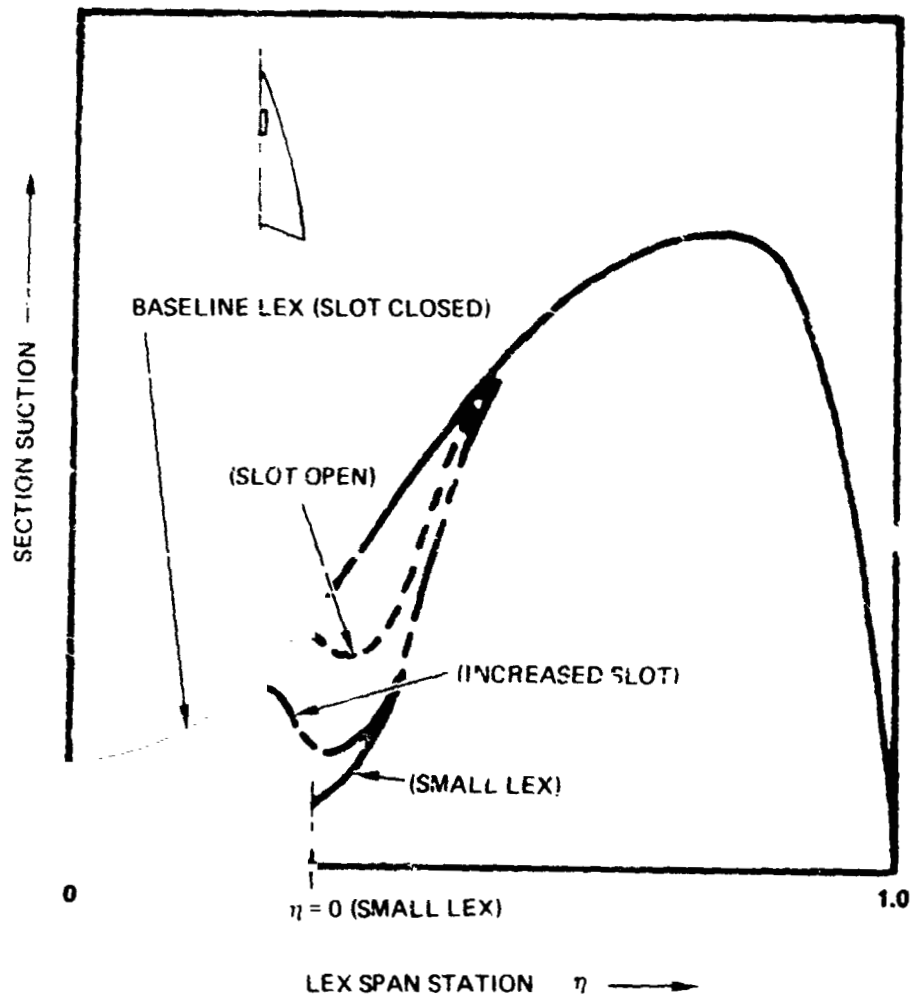
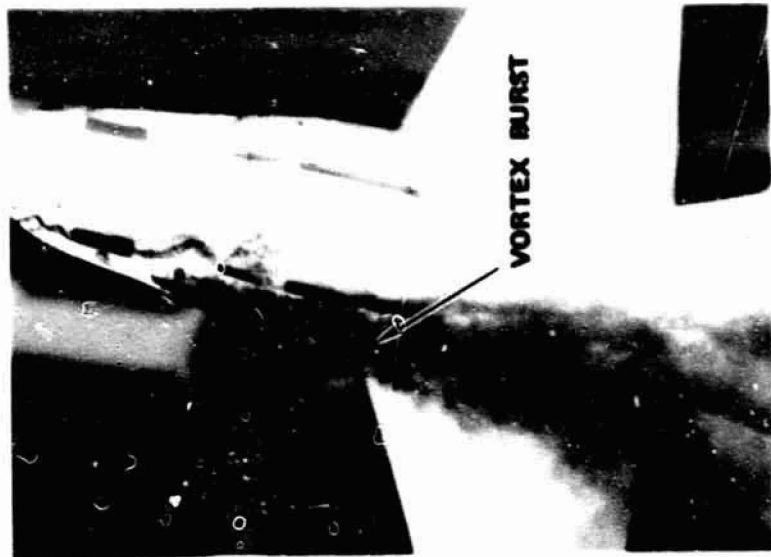


FIGURE 29. SKETCH OF LEX SLOT EFFECTS ON SECTION SUCTION DISTRIBUTION.



ORIGINAL PAGE
COLOR PHOTOGRAPH



(A) PLANVIEWS



FIGURE 30. LEX 12 VORTEX FLOW IN SIDESLIP AT $\alpha = 30^\circ$

ORIGINAL PAGE
COLOR PHOTOGRAPHS



(B) SIDEVIEWS

FIGURE 30. CONCLUDED.

The slot modification also alters the body vortex-LEX vortex interactions. The forward slot flow displaces the apex vortices upward, reduces the stability of the LEX vortex system, and thereby reduces the body vortex entrainment into the wing flow. The flow visualization results in Figure 31 at $\alpha=40^\circ$ indicate that the body vortex asymmetry in sideslip is reduced relative to the baseline results.

Double-Width, Extended Length, Forward LEX Slot (LEX 12A)

The effects of double-width, increased length forward LEX bleed slots (LEX 12A) are similar to LEX 12 but considerably more pronounced. For example, at $\alpha=25^\circ$ LEX vortex breakdown was observed at approximately the leading-edge flap hingeline, whereas breakdown at the same position on the baseline configuration did not occur until $\alpha\approx 30^\circ$. The forward slot modification, therefore, promotes earlier breakdown of the LEX vortex. Figure 32 presents representative results at $\alpha=40^\circ$ which reveal the disruption of the LEX apex vortex. The effective generating length of the LEX commences, essentially, at the production break.

LEX 12A promotes significant changes in the forebody vortex patterns and vortex interactions in sideslip. The planview and sideview results in Figure 33 indicate that the increased forward slot flow at $\alpha=40^\circ$ restricts the rotation of the body vortex paths in sideslip. The body vortices are highly-resistant to asymmetric orientation at $\beta=+4^\circ$. The forebody vortex patterns are remarkably similar to the $\beta=0^\circ$ case and strong evidence of body vortex-induced effects on the windward wing occurs (no photograph available). The leeward and windward body vortex positions and rotational sense are such as to provide strong spanwise flow toward the windward side, as sketched in Figure 34. The conjectured flow mechanism is such that the two vortices act together to induce strong sidewash on the windward wing. This effect diminishes at higher α values, since the asymmetric body vortex orientation, shown in Figure 33, becomes more pronounced.

The primary qualitative effects associated with LEX 12A are: (1) a decoupling of the LEX dual vortex system, (2) reduction of vortex stability at a given angle of attack, (3) decrease in vortex burst asymmetry due to side-

slip, and (4) resistance of body primary vortices to asymmetric orientations in sideslip. These results also provide preliminary indication of the potentially-strong coupling of the F/A-18 forebody and LEX vortex flows at high α 's.

LEX Lower Surface Fence-Oblique (Fence "B")

The effects of a fence installed on the lower surface of each LEX near the apex and oblique to the free-stream (Fence "B"), are very similar to the vortex flow field changes associated with LEX 12 and LEX 12A. This similarity is not fortuitous, since the corresponding flow mechanisms observed in the water tunnel reveal marked similarities, as discussed below.

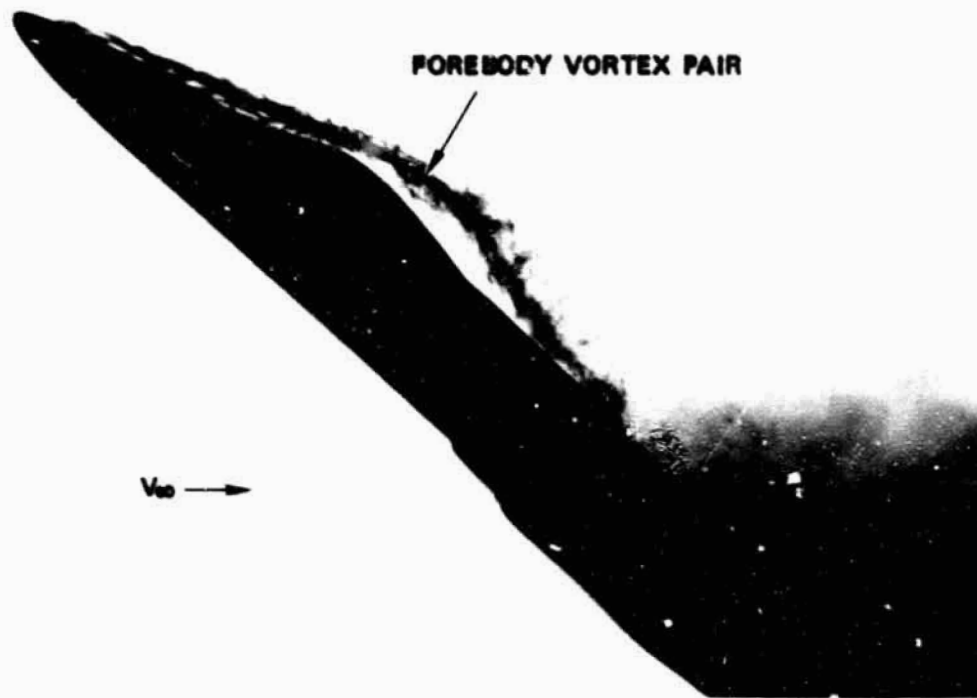
Relative to the baseline, the progression of LEX vortex burst position is slightly more rapid with LEX fences on, due to the reduced "effective" LEX generating length. At $\alpha=25^\circ$ and 30° , for example, vortex breakdown was observed at approximately $X/C_R = 0.7$ and 1.0 , respectively, as opposed to baseline results of $X/C_R = 0.5$ and 0.8 , respectively.

The photographs in Figure 35 reveal similar stall patterns on the windward and leeward wings at $\alpha=25^\circ$. This can be attributed to the nearly-symmetric LEX vortex burst positions in sideslip due to the lower surface fences. Note also in Figure 35 the better-delineated aft primary vortices.

At higher angles of attack ($\alpha=30^\circ-40^\circ$) the LEX apex vortex persists but, in general, interaction with the aft primary vortex is minimal. This is illustrated in Figure 36 at $\alpha=30^\circ$. The fences, in a manner similar to the effects due to LEX 12 and LEX 12A, promote a symmetry in LEX breakdown positions at high angles of attack, similar to the effects shown at $\alpha=25^\circ$ in Figure 35.

The flow fields associated with Fence "B", LEX 12, and LEX 12A are dissimilar in certain respects. The LEX apex vortex behavior with Fence "B" and LEX 12A at high angles of attack reveals a more concentrated apex vortex with the former. This can be attributed to the disproportionate amount of forward slot flow with LEX 12A which disrupts the apex vortex flow.

ORIGINAL PAGE
COLOR PHOTOGRAPH



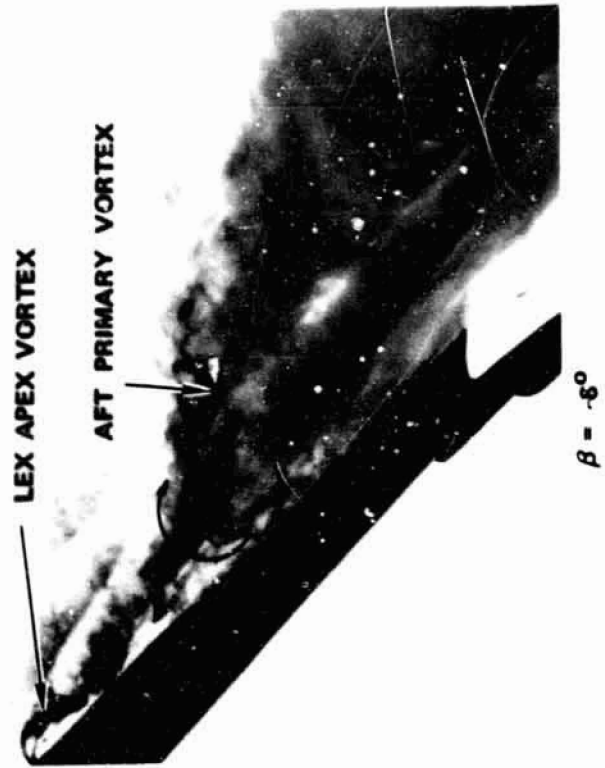
$\beta = 0^{\circ}$



$\beta = 4^{\circ}$

FIGURE 31. FOREBODY VORTEX PATTERNS IN SIDESLIP WITH LEX 12
AT $\alpha = 40^{\circ}$

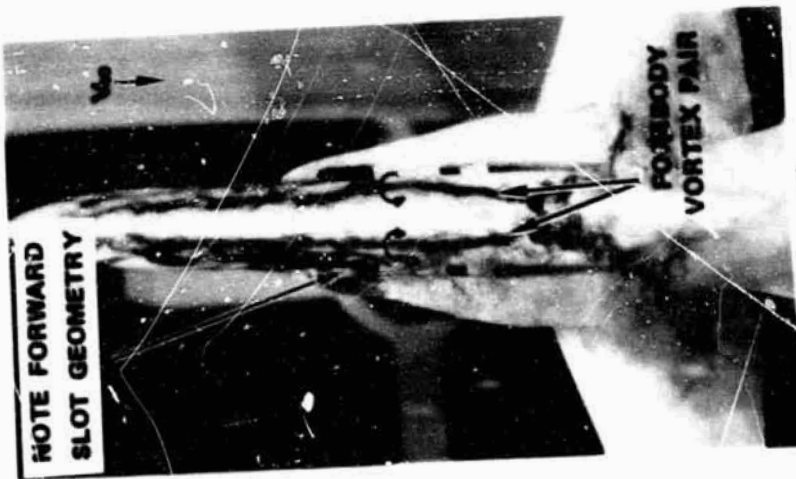
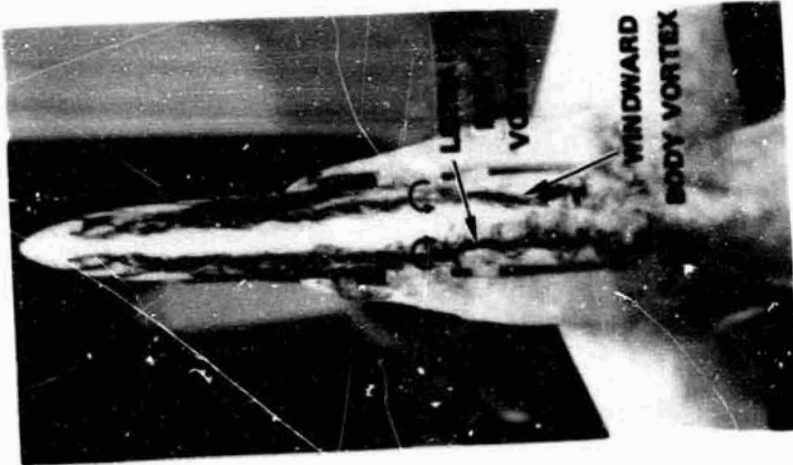
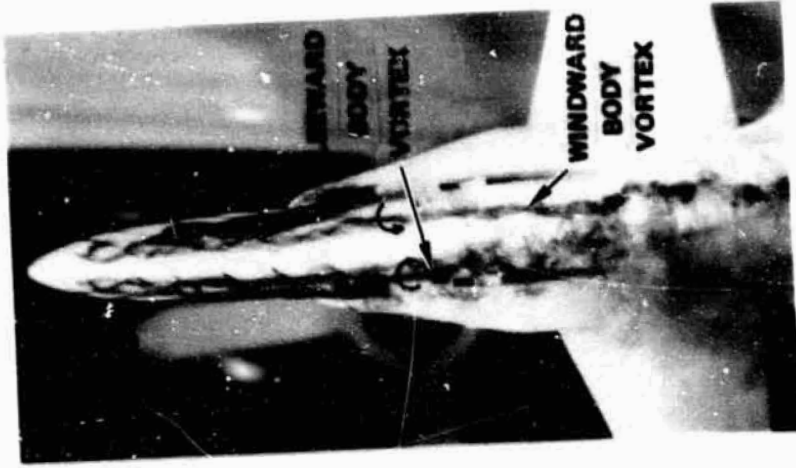
ORIGINAL ~~735~~
COLOR PHOTOGRAPH



PRECEDING PAGE BLANK NOT FILMED

FIGURE 32. LEX 12A VORTEX FLOW BEHAVIOR IN SIDESLIP AT $\alpha = 40^\circ$

ORIGINAL PAGE
COLOR PHOTOGRAPH

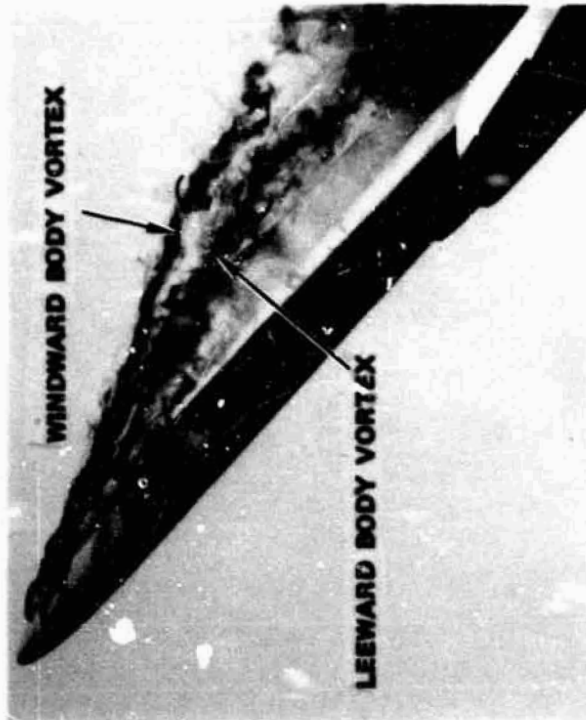


(A) PLANVIEW

FIGURE 33. FOREBODY VORTEX PATTERNS IN SIDESLIP WITH LEX 12A
AND $\alpha = 40^\circ$

PRECEDING PAGE BLANK NOT FILMED

ORIGINAL PAGE
COLOR PHOTOGRAPH



(B) SIDEVIEW

ORIGINAL PAGE
COLOR PHOTOGRAPH

PRECEDING PAGE BLANK NOT FILMED

FIGURE 33. CONCLUDED.

PRECEDING PAGE BLANK NOT FILMED

ORIGINAL PAGE IS
OF POOR QUALITY

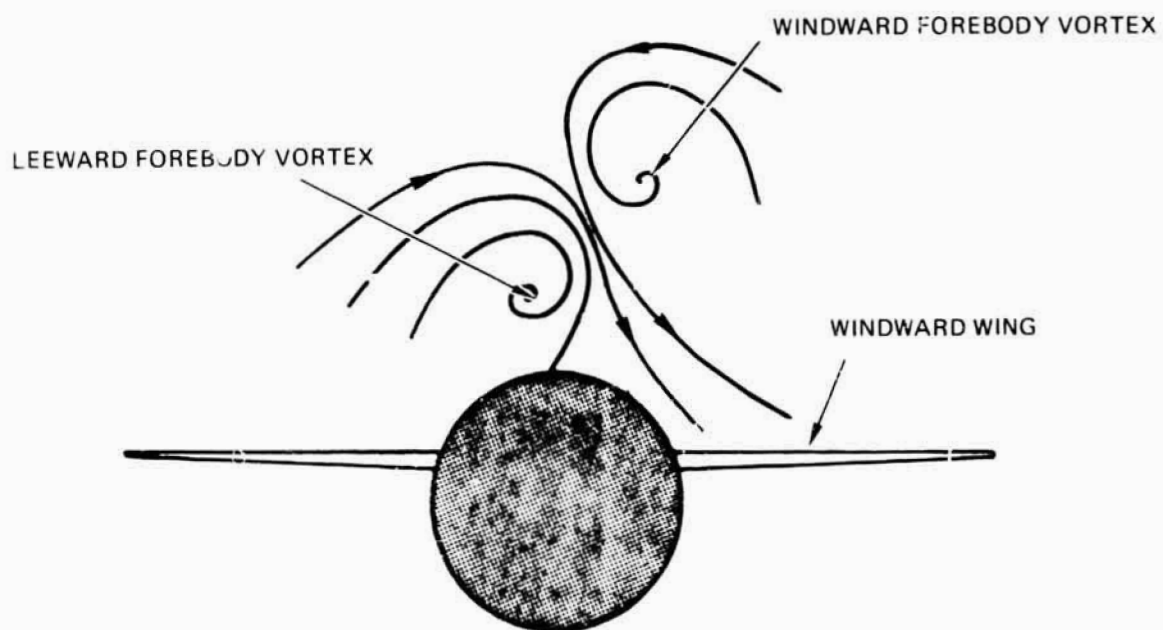


FIGURE 34. SKETCH OF FOREBODY VORTEX EFFECTS ON WINDWARD WING.

ORIGINAL PAGE
COLOR PHOTOGRAPH



$\beta = 0^\circ$



$\beta = 4^\circ$



$\beta = -4^\circ$

PRECEDING PAGE BLANK NOT FILMED

FIGURE 3E LEX VORTEX BEHAVIOR IN SIDESLIP WITH LEX FENCE "B"; $\alpha = 25^\circ$

ORIGINAL PAGE
COLOR PHOTOGRAPH

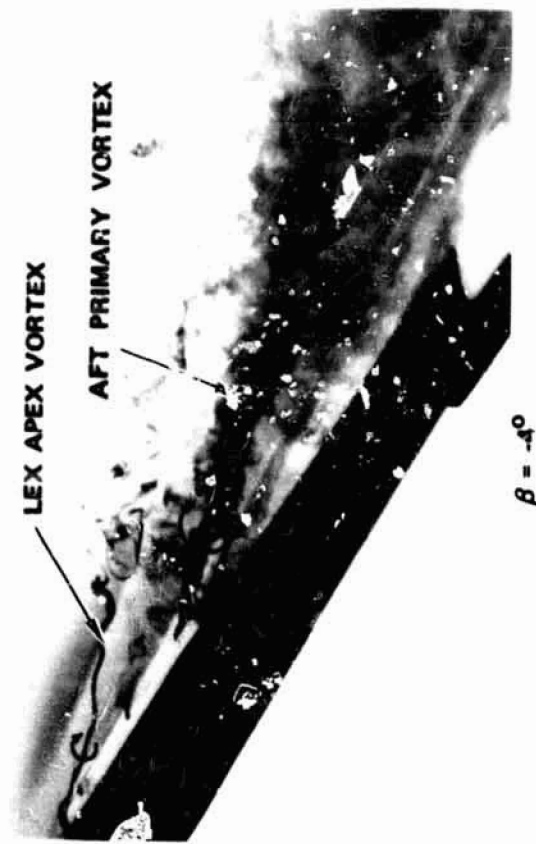
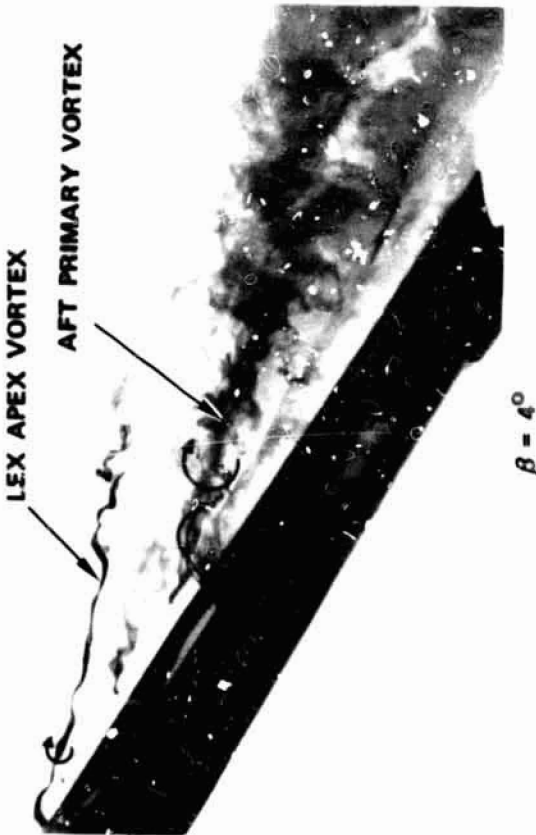
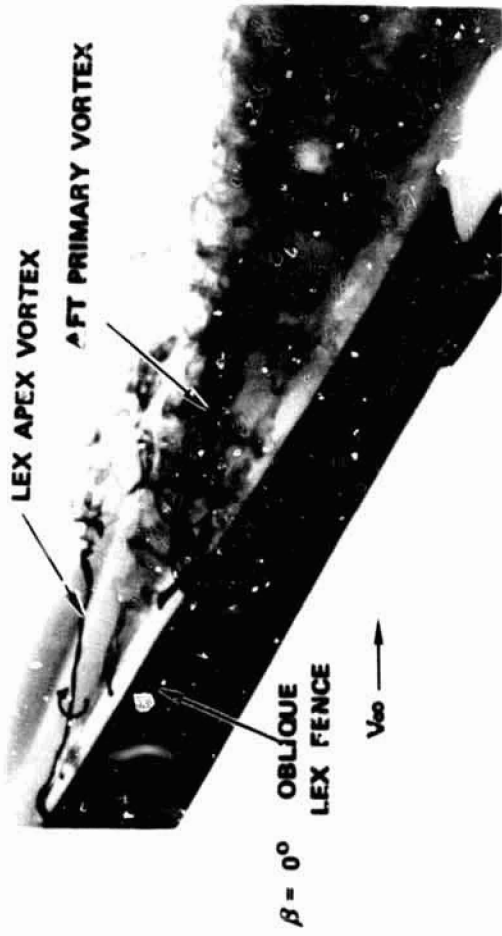


FIGURE 36. LEX VORTEX FLOW BEHAVIOR IN SIDESLIP WITH LEX FENCE "B"
AT $\alpha = 30^\circ$

PRECEDING PAGE BLANK NOT FILMED

PRECEDING PAGE BLANK NOT FILMED

Fence "B" slightly alters the body vortex-LEX vortex interactive behavior relative to the baseline vortex behavior. The rotation of the body vortex paths at small sideslip angles is restricted, as depicted in Figure 37 at $\alpha=35^\circ$. The effects are not as pronounced, however, as the results shown in Figure 33 with LEX 12A.

LEX Low r Surface Fence - Streamwise (Fence "A")

Flow field observations with LEX lower surface fences oriented in a streamwise manner (Fence "A") reveal the sensitivity of LEX fence effectiveness to relatively small position changes. Typical results from the water tunnel studies are shown in Figure 38 at $\alpha=30^\circ$. The streamwise LEX fence reduces the coupling of the LEX vortex system, in a manner similar to LEX Fence "B". However, marked differences do exist between the fence arrangements. With Fence "A", the point of origin of the aft primary vortex is difficult to ascertain in contrast to the fixed origin with Fence "B". Part of the lower surface flow which separates at the leading edge feeds into the LEX apex vortex while the remainder feeds into the aft vortex. Close examination of dye tracers in the water tunnel reveal this quite clearly. For example, dye emitted on the LEX lower surface near the leading edge splits at the leading edge, thereby delineating the flow which goes into each vortex. It was evident during the tests that LEX Fence "A" was less effective in isolating the LEX dual-vortex system. In general, the aft primary vortex was more concentrated relative to the baseline and vortex burst progression was slightly more rapid (similar to Fence "B" effects). However, the wing flow field in sideslip near stall angle of attack suggested that Fence "A" was less effective than Fence "B" in promoting more symmetric stall patterns.

The flow mechanisms associated with LEX 12, LEX 12A, Fence "B" and Fence "A" are similar. All modifications limit the amount of vorticity shed at the LEX leading edge in the region of the production break. LEX 12 and LEX 12A promote a "fluid fence" phenomenon, diverting LEX lower surface boundary layer fluid away from the leading edge in a manner similar to a solid fence.

Closure of Forward LEX Bleed Slots

Closure of the forward LEX bleed slots results in the development of a single concentrated leading-edge vortex on each LEX surface, as shown in Figure 39 at $\alpha=25^\circ$. Slot closure results in an increase in lower surface flow available for feeding into the leading-edge vortex. The flow field observations indicate, then, that the gradual planform inflection point on the F/A-18 LEX is insufficient to promote a dual-vortex system. Also shown in Figure 39 is an accumulation of dye on the lower surface of the LEX. The dye tracers are entrained into a vortex formed at the junction of the fuselage and LEX.

As far as can be determined in the water tunnel, the single-vortex system exhibits slightly greater vortex burst asymmetry in sideslip relative to the baseline. Recall, however, that it was difficult to determine precisely the burst position on the baseline configuration due to the diffuse nature of the dual-vortex system.

The manner in which the body vortices interact with the LEX vortex flows in sideslip is similar to the baseline results. The body vortex core trajectories depicted in Figure 40 at $\alpha=35^\circ$ exhibit similar characteristics to the slots-open case, although the leeward body vortex appeared somewhat better-defined at small β -values as it enters the wing flow field. This is consistent with the apparent increase in leeward LEX vortex stability due to forward slot closure. In addition, the point of entrainment of the leeward body vortex occurred somewhat farther downstream with slots closed.

Closure of All LEX Bleed Slots

Closure of all LEX boundary layer bleed slots results in no significant changes in the high- α vortex flow field relative to closure of the forward slots only. This appears reasonable since the forward slot, by virtue of its large width-to-local LEX span ratio, is in a position to most affect the LEX vortex behavior. Typical results with all slots closed are presented in Figure 41 at $\alpha=30^\circ$. Examination of the LEX lower surface flow patterns (photographs not available) near the aft slots reveal only small variations when the slots are closed. Furthermore, a qualitative assessment of the weak

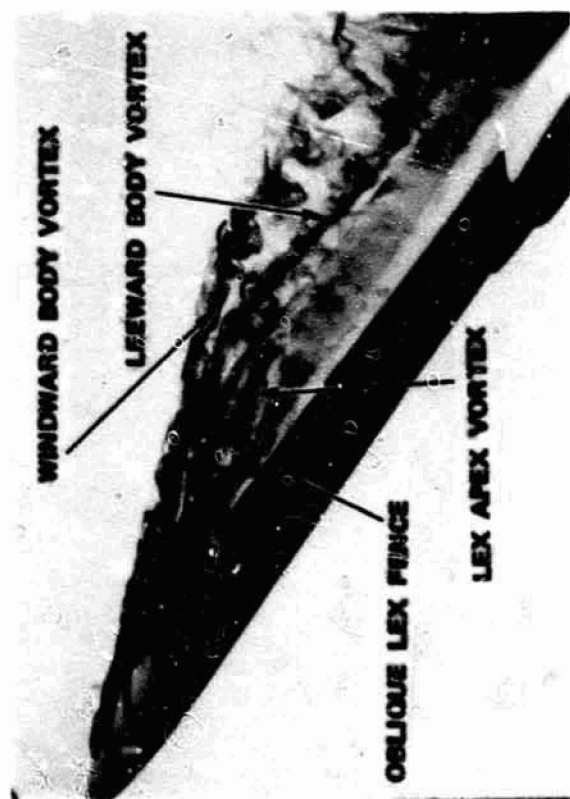
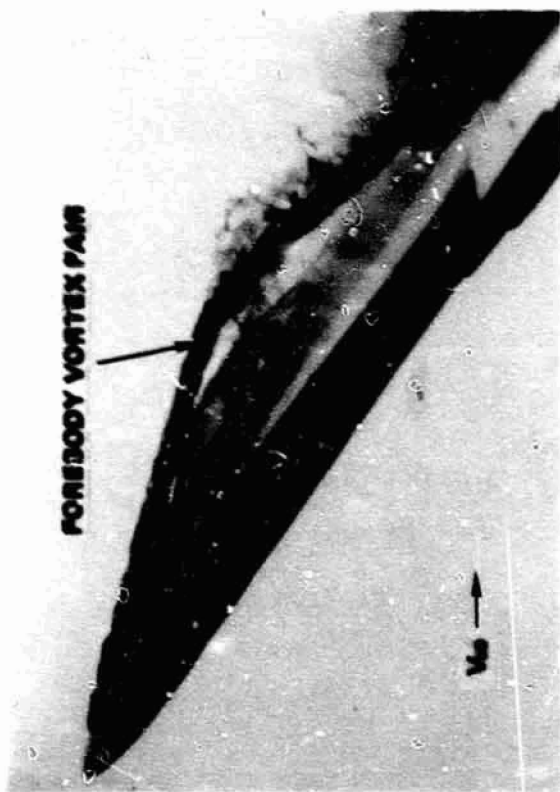


FIGURE 37. FOREBODY VORTEX BEHAVIOR IN SIDESLIP WITH LEX FENCE "B"
AT $\alpha = 35^\circ$

ORIGINAL PAGE
COLOR PHOTOGRAPH

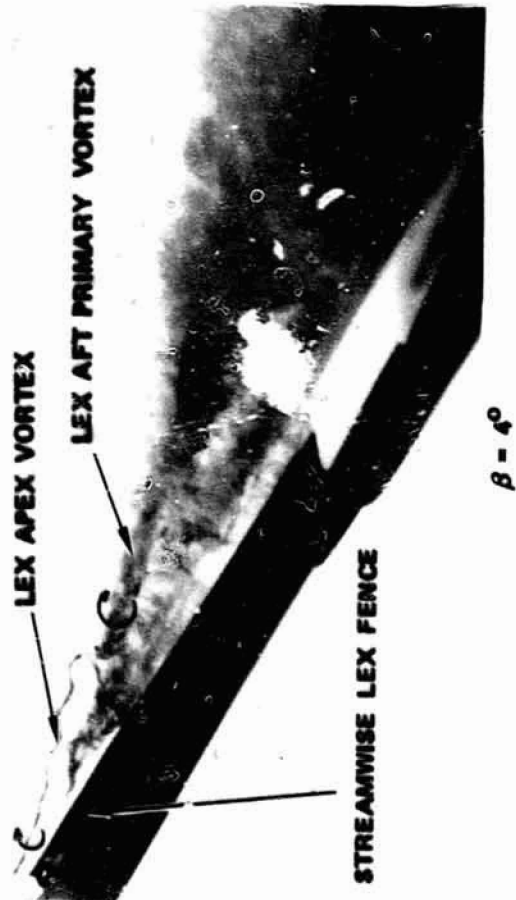


FIGURE 38. LEX VORTEX BEHAVIOR WITH LEX FENCE "A" AT $\alpha = 30^\circ$

PRECEDING PAGE BLANK NOT FILMED

ORIGINAL PAGE
OF POOR QUALITY

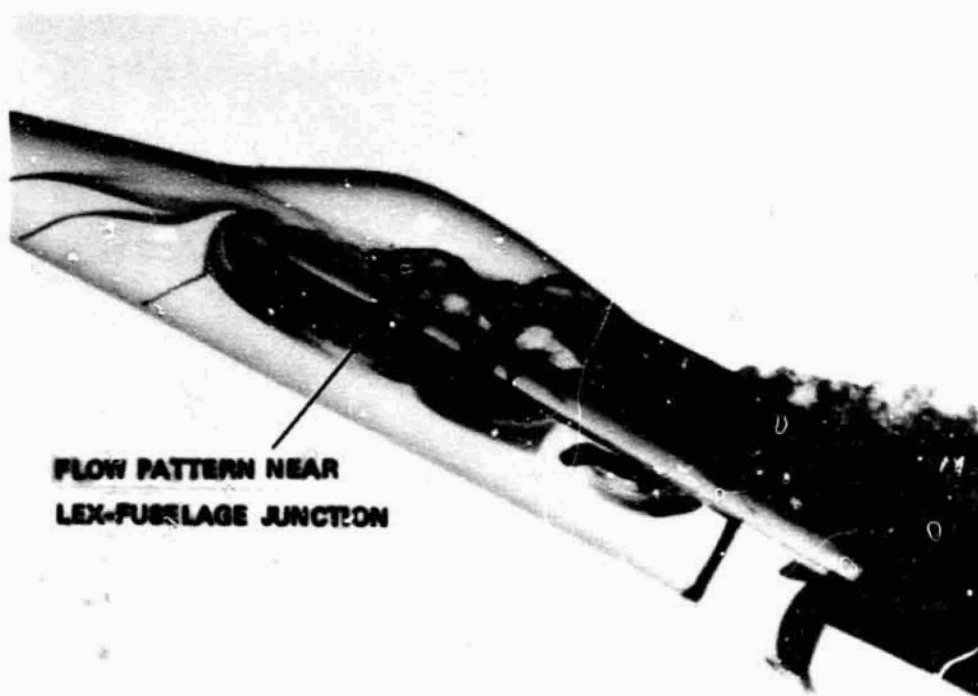


FIGURE 39. SINGLE LEX VORTEX SYSTEM AND LOWER SURFACE FLOW BEHAVIOR WITH FORWARD SLOTS CLOSED; $\alpha = 25^\circ$

ORIGINAL PAGE IS
OF POOR QUALITY

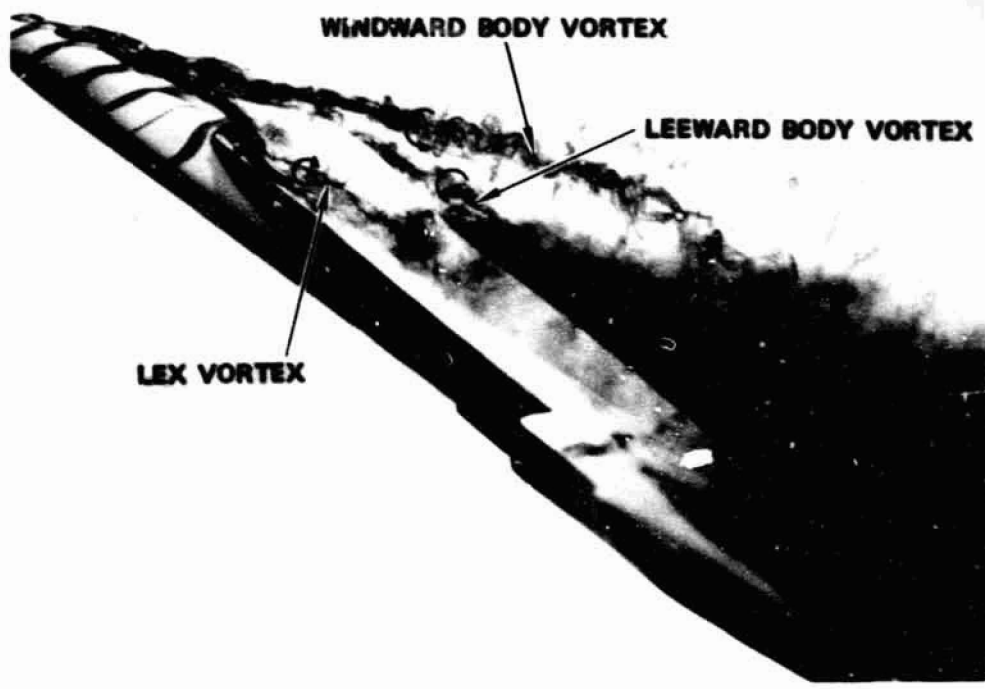
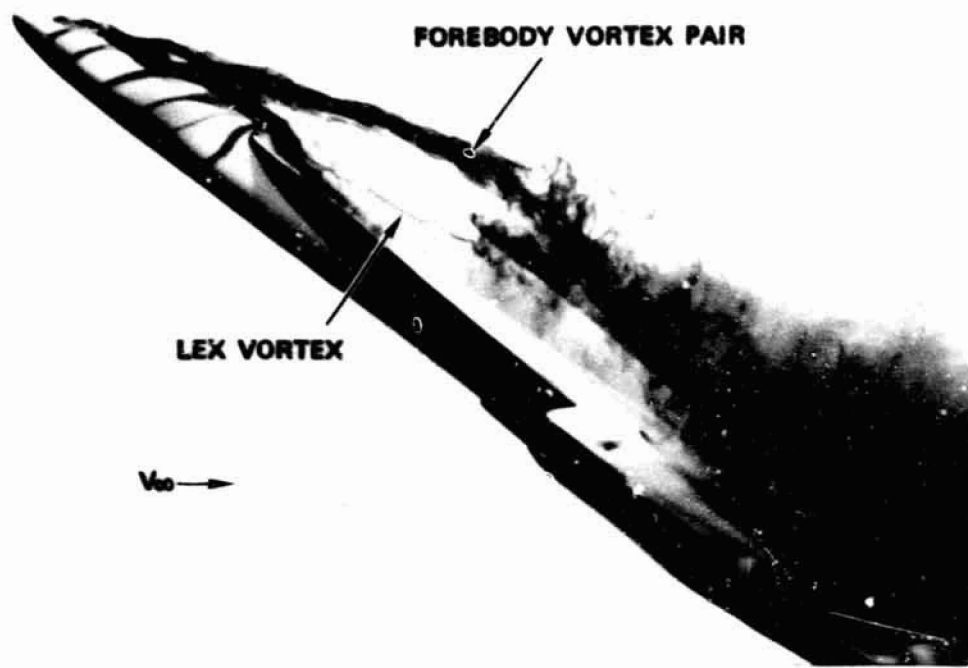
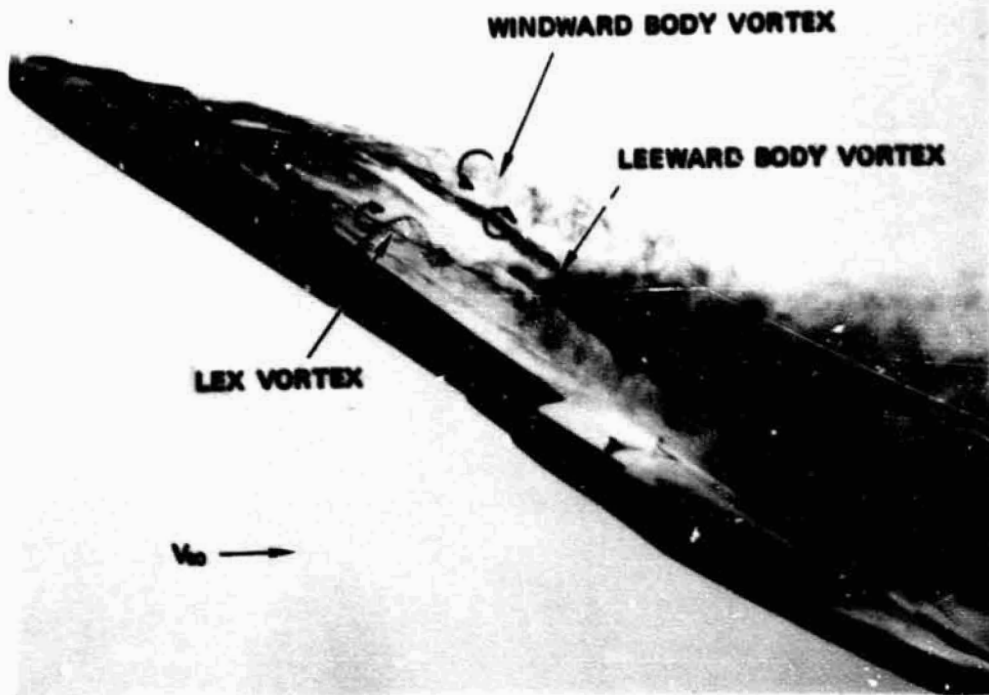


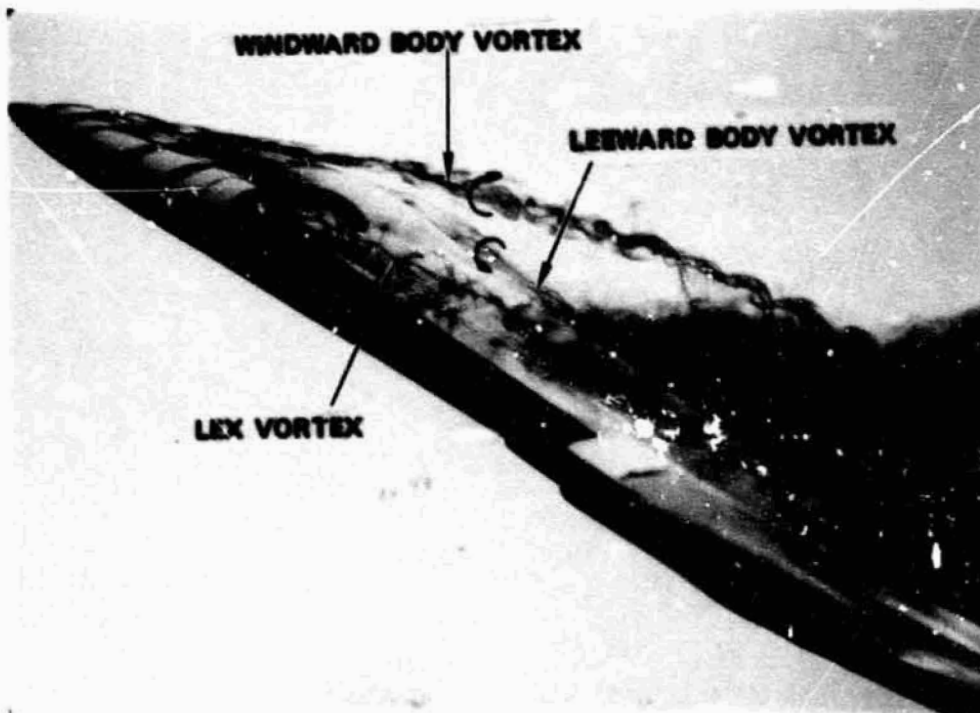
FIGURE 40. FOREBODY VORTEX FLOW BEHAVIOR IN SIDESLIP WITH FORWARD SLOTS CLOSED; $\alpha = 35^\circ$

PRECEDING PAGE BLANK NOT FILMED

ORIGINAL PAGE
COLOR PHOTOGRAPH



$\beta = 4^{\circ}$



$\beta = 4^{\circ}$

PRECEDING PAGE BLANK NOT FILLED

FIGURE 41. F/A-18 VORTEX FLOW FIELD BEHAVIOR IN SIDESLIP WITH ALL SLOTS CLOSED AT $\alpha = 30^{\circ}$

contra-rotating aft slot vortices which form on the LEX upper surface indicates that the slot flow has little effect on LEX vortex behavior and, also, body vortex-LEX vortex interactions. A qualitative perspective of the relative effects of the forward slot flow as opposed to the aft slot flows is as follows. The "size" of the forward slot flow and LEX vortex near the apex are of the same order of magnitude. Consequently, changes to the forward slot geometry are likely to promote large changes in LEX vortex behavior. Farther downstream, however, the LEX vortex strength and size have increased to the extent that the leading-edge vortex dominates the aft slot vortices. Therefore, flow perturbations emanating from the aft slots are less likely to have significant global effects.

Forebody Strakes (Radial Position: $+40^\circ$)

Water tunnel results discussed thus far have revealed significant flow field changes arising from modifications to, primarily, the LEX apex region. Due to the strong coupling of the F/A-18 forebody and LEX flow fields, however, it is evident that forebody geometry variations are a potential source of large global flow field perturbations. The following discussions will address the effects of forebody strakes on the high angle-of-attack vortex flow behavior. The results obtained in these flow visualization tests will be shown in later sections to figure prominently in the major conclusions of this study.

No significant flow changes are incurred with forebody strakes mounted at 40° above the maximum half breadth ($\phi = +40^\circ$) up to angles of attack of approximately 25° (photographs not shown). The forebody primary vortices are weak within this α -range and, consequently, nose strakes are not expected to have any global impact. The flow photographs in Figure 42 indicate that at $\alpha = 25^\circ$ the windward wing is stalled whereas the leeward wing exhibits strong vortex action. This trend is similar to the baseline flow field results.

Progression of LEX vortex breakdown position with angle of attack at $\beta = 0^\circ$ is essentially identical to that observed on the baseline configuration. For example, at $\alpha = 25^\circ$ and 30° , vortex burst occurred at approximately $X/C_R = 0.5$ and 0.8 , respectively.

The water tunnel flow surveys indicated that the strakes cause an outboard and downward displacement of the windward body vortex and a corresponding inboard and upward displacement of the leeward body vortex. This alteration of the body vortex paths in sideslip is of great import to the wing stall patterns, as will now be discussed.

The most dramatic strake effects were observed at $\alpha = 35^\circ$ and 40° . Utilizing the numerous internal dye ports, several regions on the model were progressively investigated. For example, the wing upper surface flow patterns indicate that the leeward wing is completely stalled whereas vortex action is present on the windward wing panel. This is illustrated in the water tunnel photographs in Figure 43 at $\alpha = 40^\circ$.

The flow visualization photographs (planviews) in Figure 44 indicate that the leeward LEX vortex breaks down at a more forward position on the LEX relative to the windward LEX vortex. A very interesting feature of the leeward flow field in Figure 44 is that dye originally entrained into the leeward LEX vortex is swept over the top of the fuselage and onto the windward wing.

The latter phenomenon strongly suggested the presence of a powerful flow mechanism emanating from the forebody. Observation of the forebody vortices, depicted in Figures 45 and 46 at $\alpha = 35^\circ$ and 40° , respectively, shows that the strakes promote a more symmetric shedding of the body vortices in sideslip and create a vortex pattern featuring strong coupling of the windward and leeward forebody vortex flows. At $\alpha = 35^\circ$ and 40° and $\beta = 4^\circ$, for example (see Figures 45 and 46), the forebody vortices in the sideviews remain symmetric. In the planviews in Figures 45 and 46, however, the windward and leeward body vortices are actually biased towards the windward side. The result of this coupling is strong vortex-induced sidewash on the windward wing, as sketched in Figure 47, and consequently improved windward LEX vortex behavior and reduction in wing flow separation. The body vortex-induced sidewash accounts for the flow phenomenon discussed in Figure 44. Note is made that strake effectiveness decreases at higher sideslip angles since an asymmetric body vortex pattern is once again evident (see Figures 45 and 46).

ORIGINAL PAGE
COLOR PHOTOGRAPH

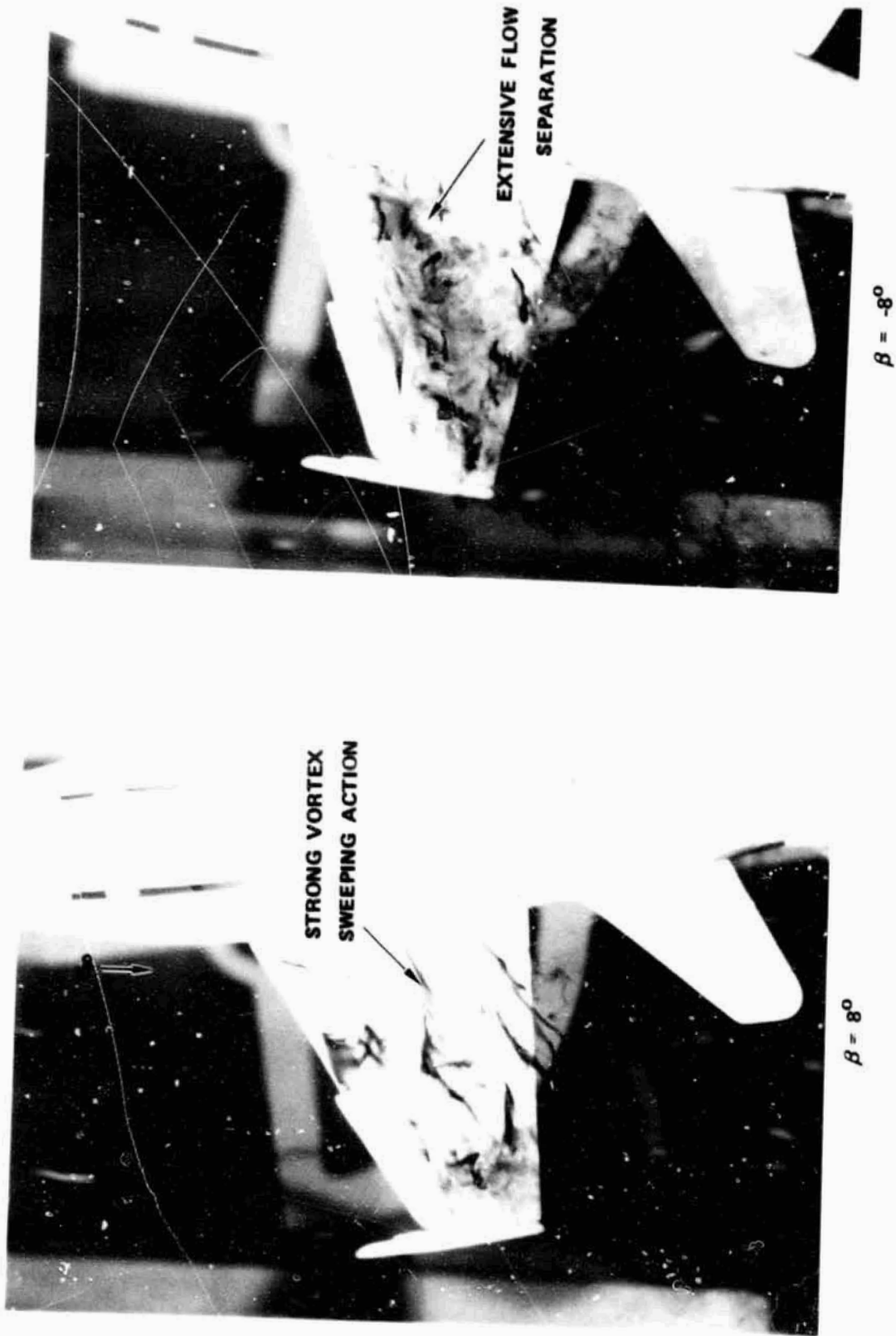


FIGURE 42. WING SURFACE FLOW PATTERNS WITH FOREBODY STRAKES
($\phi = 40^\circ$); $\alpha = 25^\circ$

ORIGINAL PAGE
COLOR PHOTOGRAPH



$\beta = -4^\circ$



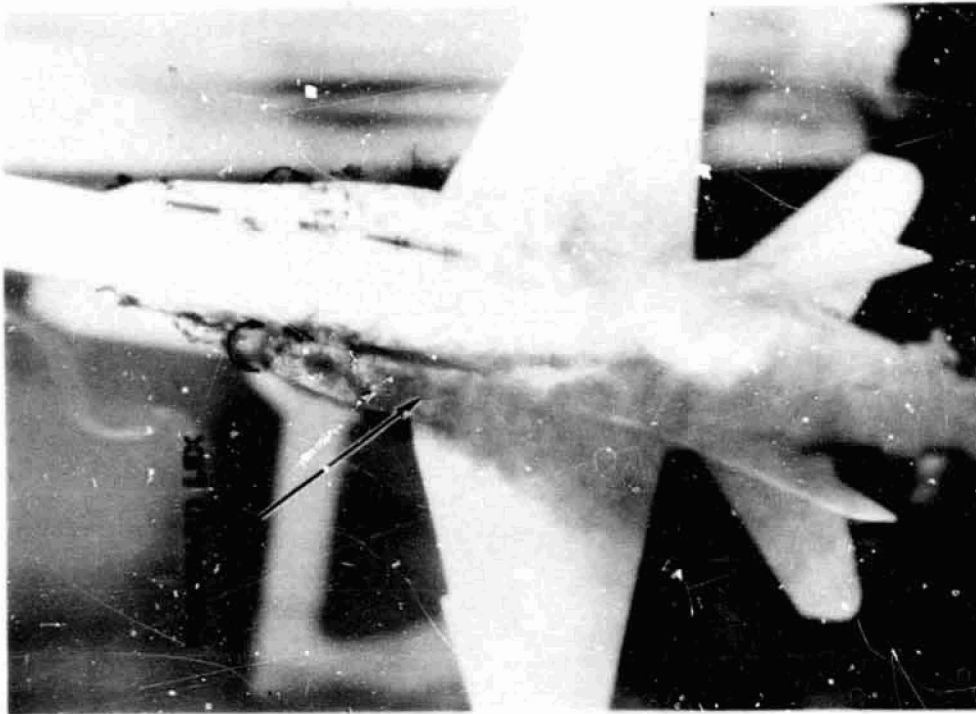
$\beta = 4^\circ$

FIGURE 43. WING SURFACE FLOW PATTERNS WITH FOREBODY STRAKES ($\alpha = 40^\circ$)
AT $\alpha = 40^\circ$

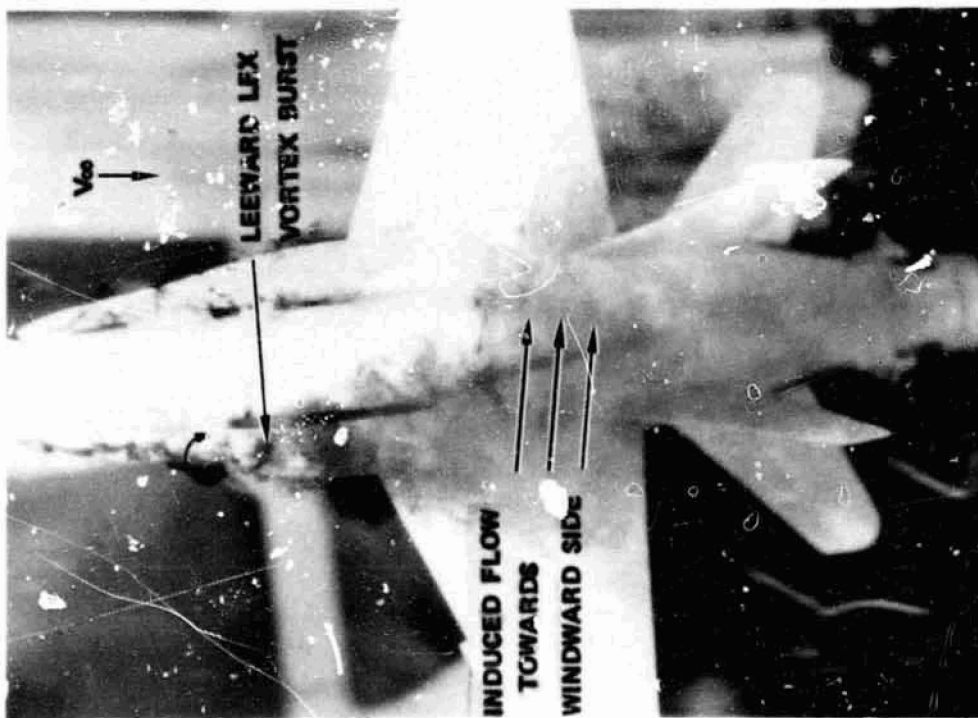
PRECEDING PAGE BLANK NOT FILMED

ORIGINAL PAGE
COLOR PHOTOGRAPH

ORIGINAL PAGE
COLOR PHOTOGRAPH



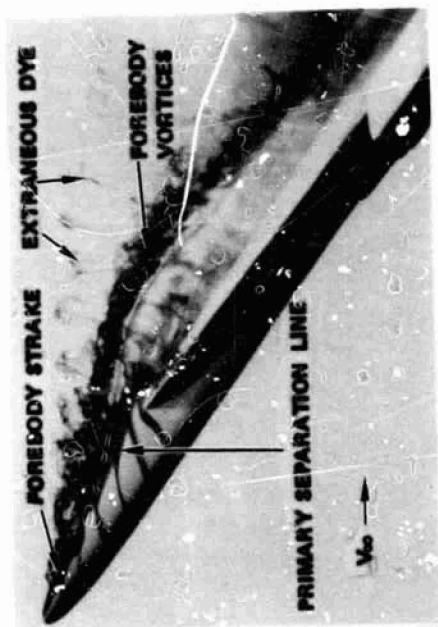
$\beta = -8^\circ$



$\beta = 8^\circ$

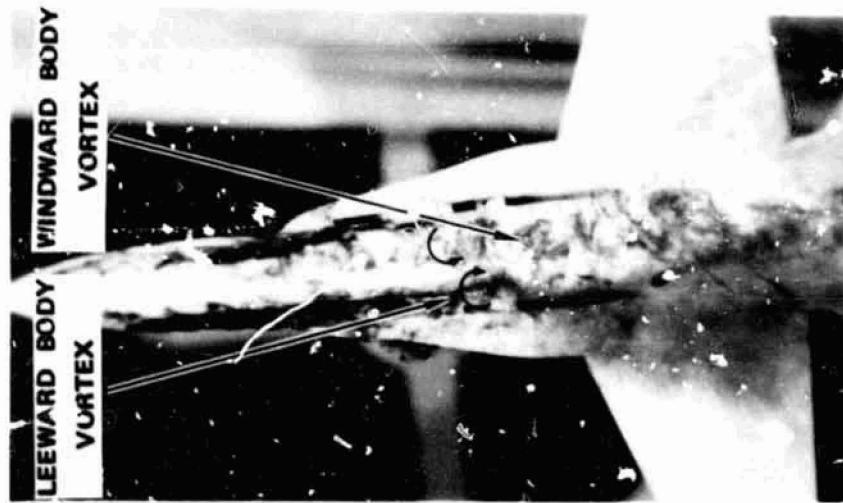
FIGURE 44. LEX VORTEX FLOW IN SIDESLIP AT $\alpha = 35^\circ$ WITH NOSE STRAKES ($\phi = 40^\circ$)

ORIGINAL PAGE
COLOR PHOTOGRAPH



(A) SIDEVIEW

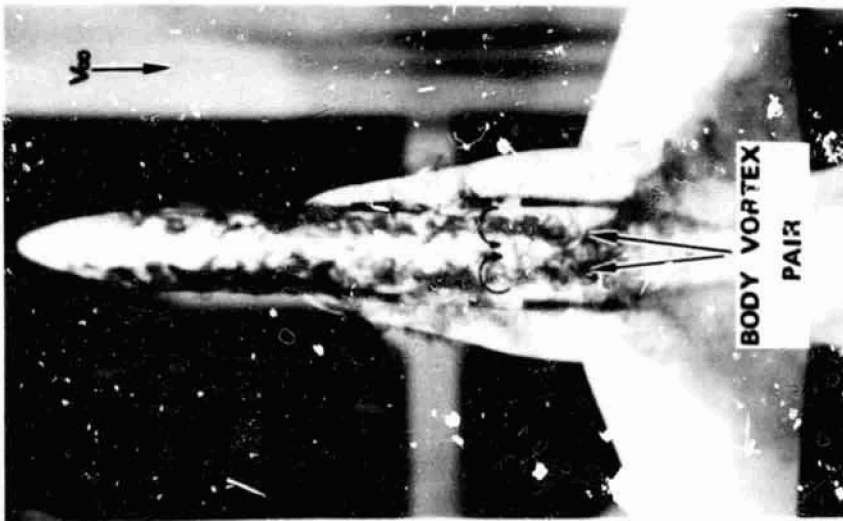
FIGURE 45. F/A-18 FOREBODY VORTEX BEHAVIOR WITH NOSE STRAKES
($\phi = 40^\circ$) AT $\alpha = 35^\circ$



$\beta = 8^\circ$



$\beta = 4^\circ$



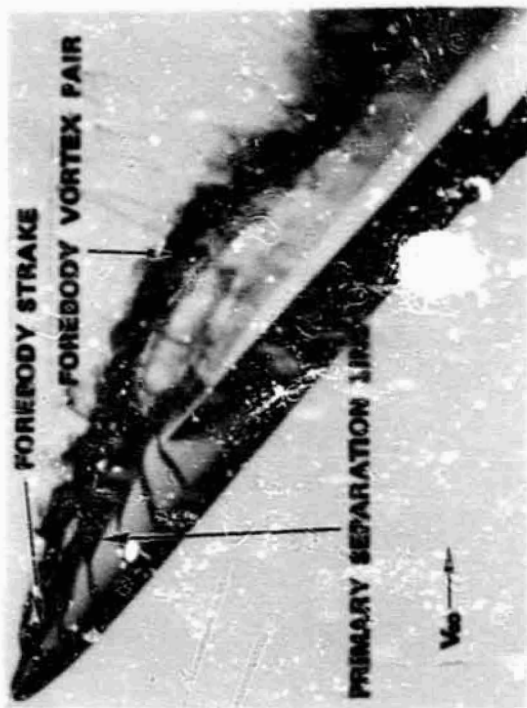
$\beta = 0^\circ$

(B) PLANVIEW

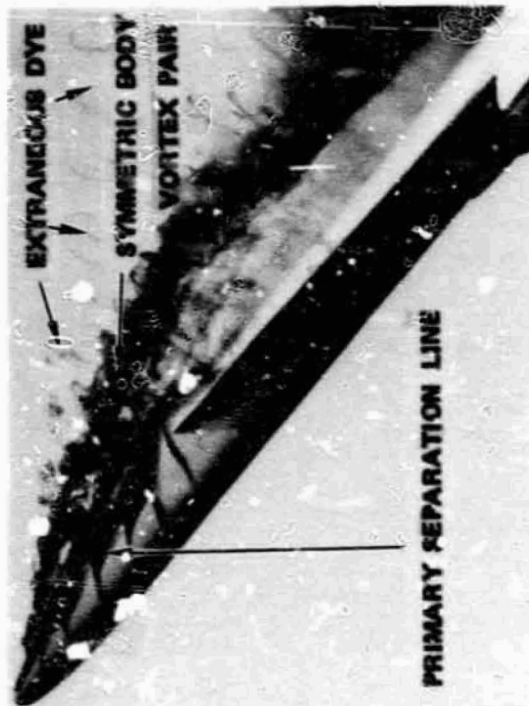
FIGURE 7 - CONCLUDED.

ORIGINAL PAGE
COLOR PHOTOGRAPH

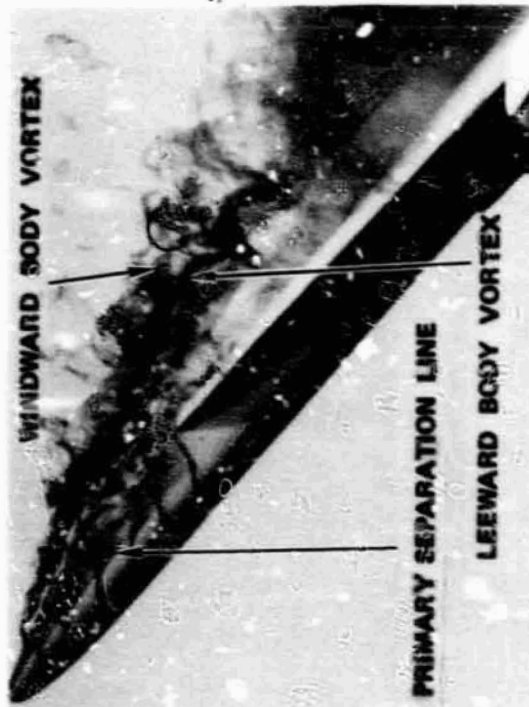
PRECEDING PAGE ~~BLANK NOT FILMED~~



$\beta = 0^\circ$



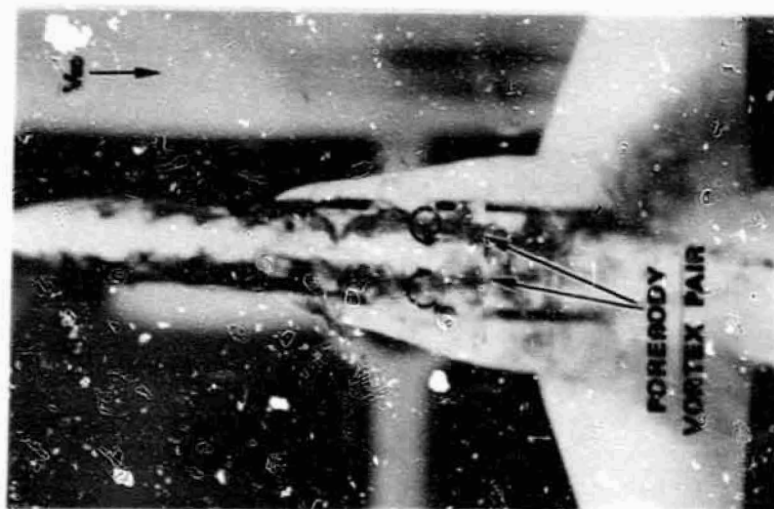
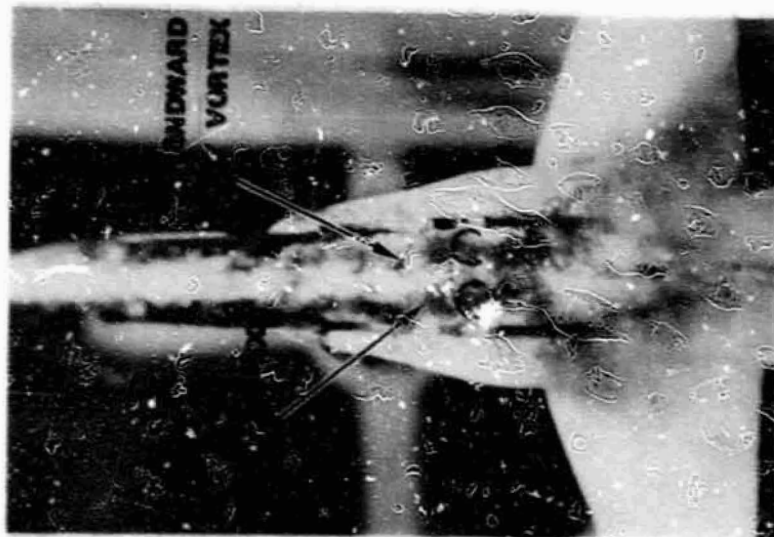
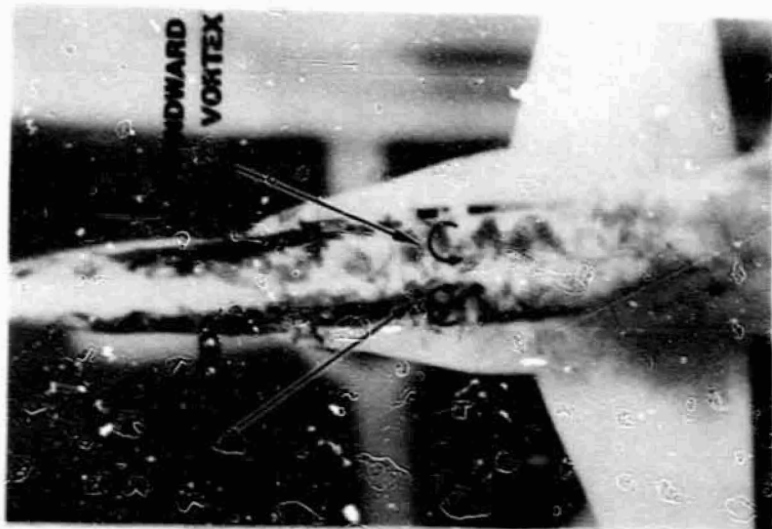
$\beta = 4^\circ$



$\beta = 3^\circ$

SIDEVIEW

FIGURE 46. F/A-18 FOREBODY VORTEX BEHAVIOR IN SIDESLIP WITH NOSE STRAKES ($\phi = 40^\circ$; $\alpha = 40^\circ$)



(B) PLANVIEW

FIGURE 46. CONCLUDED.

ORIGINAL PAGE
COLOR PHOTOGRAPH

PRECEDING PAGE BLANK NOT FILMED

ORIGINAL PAGE IS
OF POOR QUALITY

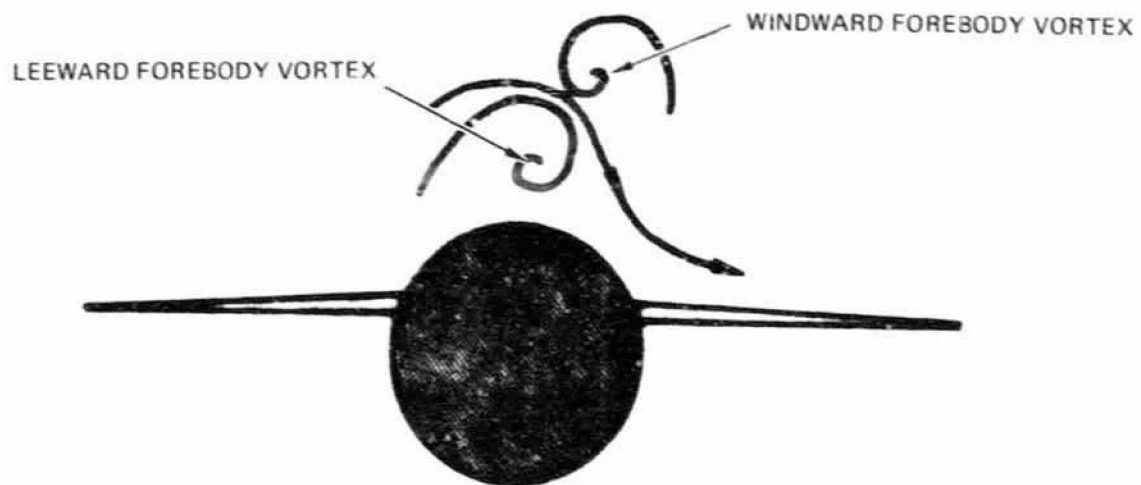


FIGURE 47. SKETCH OF WINDWARD AND LEEWARD FOREBODY VORTEX COUPLING.

The present results indicate that nose strakes at $\phi = +40^\circ$ promote a body vortex system which acts primarily to enhance the windward wing flow. The qualitative studies in the water tunnel indicate that under certain flow conditions the forebody vortices can be of great significance in influencing the wing stall characteristics at high angles of attack. Depending on the orientation of the body vortices relative to the LEX and wing surfaces, wing flow separation (without reattachment) or vortex-induced attached flow may prevail.

Low-speed smoke flow visualization studies made in the NASA Langley Research Center 30 x 60-foot wind tunnel of the 0.16-scale F/A-18 with strakes at $\phi = +40^\circ$ have yielded results in excellent qualitative agreement with the water tunnel observations. For example, observation of the smoke flow patterns from a position behind the 0.16-scale model revealed the strong coupling of the forebody primary vortices and the tendency of the leeward body vortex to pass below the windward vortex. The agreement between flow visualization results in water at low Reynolds number and in air at higher Reynolds number is due to the low local Reynolds number along the radome. The local cross-section is sufficiently small in this region that the local Reynolds numbers remain within the laminar range. Consequently, the boundary layer separation characteristics will be similar on the respective test models. Furthermore, the nose strake position is nearly coincident with the primary separation line and the strake vortex flows, which are reasonably insensitive to changes in Reynolds number, feed directly into the body primary vortices. Therefore, the flow field effects associated with the nose strakes at $\phi = +40^\circ$ are not strongly dependent on Reynolds number, within the range of test conditions considered.

Forebody Strakes (Radial Position: 0°)

Alternate strake radial positions were investigated to assess the relative effects on body vortex development, vortex trajectories, and interactions.

At $\alpha = 35^\circ$ and $\beta = 0^\circ$ the body flow field in the presence of nose strakes at the MHB ($\phi = 0^\circ$) is essentially an ill-organized wake-like flow, as shown

in Figure 48. Due to the high local angles of attack, the strakes at $\phi = 0^\circ$ generate more of a wake-like, rather than vortex, flow. This is in contrast to the $\phi = +40^\circ$ strake position where discrete vortices were observed even at very high angles of attack. The latter phenomenon can be attributed in large part to the body vortex-induced downwash which promotes lower local angles of attack in this region.

In general, at $\alpha = 35^\circ$ and 40° there is no qualitative evidence of favorable body vortex-induced effects on the wing stall behavior with strakes at $\phi = 0^\circ$.

Foreboom Strakes (Radial Position: -45°)

Typical results obtained with nose strakes mounted at 45° below the MHB ($\phi = -45^\circ$) are shown in Figure 49 at $\alpha = 35^\circ$. The strake vortices are of sufficient strength to induce flow reattachment above the strakes. As a result, a pair of body primary vortices form along the nose. These vortices are reasonably symmetric at small sideslip and, consequently, create a flow situation analogous to the $\phi = +40^\circ$ case. The effects are less pronounced, however, due to the weakened body vortex system. There is a slight bias at small β -values of the body vortex system towards the windward side which results in downstream flow effects similar to the $\phi = +40^\circ$ results. Due to an apparent transition of the leeward strake from a vortex-generator to a wake-generator at higher sideslip angles, as sketched in Figure 50, the effectiveness of the nose strakes diminishes.

Flight Test Nose Boom

Representative results from water tunnel studies of flight test nose boom effects are presented in Figure 51 at $\alpha = 35^\circ$. The wake shed by the constant-diameter nose boom disrupts the body vortices to a certain extent. Although the body vortices are weaker relative to the baseline, the vortex paths are very similar as depicted in Figure 51. At higher α 's (approximately 40°) the flow shed by the nose boom and forebody combination exhibits a slightly oscillatory behavior.

Wing Leading-Edge Snag and Upper Surface Fence

A 17-percent local wing chord extension, or snag, positioned at $\eta=0.5$ increased the wing camber near the leading edge and, as a result, delayed flow separation. In combination with an upper surface wing fence ($\eta=0.5$), the most significant effects observed during the flow studies were: (1) the upper surface fence on the leeward wing precluded LEX vortex-induced sweeping action at wing stations outboard of the fence (a weak wing vortex developed outboard of the fence, emanating from the leading-edge flap hingeline), (2) an inboard displacement of the leeward LEX vortex path occurred, and (3) the leeward LEX vortex stability appeared reduced. Representative results are presented in Figure 52 at $\alpha = 30^\circ$ which reveal comparable windward and leeward wing flow fields.

Wing Leading-Edge Extensions (LEXs) Off

The LEXs were removed in an effort to enhance the understanding of the qualitative effects of the LEX surfaces on the F/A-18 flow field.

At $\alpha = 15^\circ-20^\circ$ both wing panels are stalled in sideslip (no photographs available). The flow field with LEXs off is not vortex-dominated, hence the water tunnel results are highly-qualitative (the massive wing flow separation is unrealistic). The results with LEXs off do confirm, however, the significant effects associated with the leading-edge extensions, particularly sideslip. For example, at the same angles of attack with LEXs on, a large disparity in the wing stall patterns in sideslip exists due to asymmetries in LEX vortex breakdown position, vortex strength, and vortex core path.

Representative results at an angle of attack of 40° are shown in Figure 53 where body vortex asymmetry at $\beta = 0^\circ$ is apparent. A multiple asymmetric vortex system is shed along the body length. In an indirect manner, the photographs in Figure 53 provide an appreciation for the significant influence of the LEXs on the forebody vortex flow behavior.



$\beta = 0^\circ$



$\beta = 4^\circ$

FIGURE 48. F/A-18 FOREBODY VORTEX FLOW BEHAVIOR WITH NOSE STRAKES ($\phi = 0^\circ$) AT $\alpha = 35^\circ$

ORIGINAL PAGE
COLOR PHOTOGRAPH

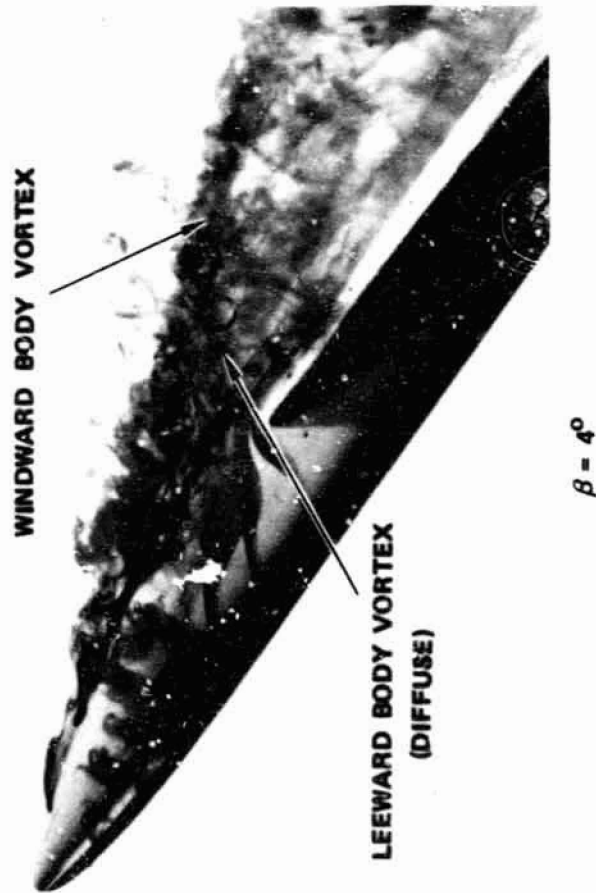
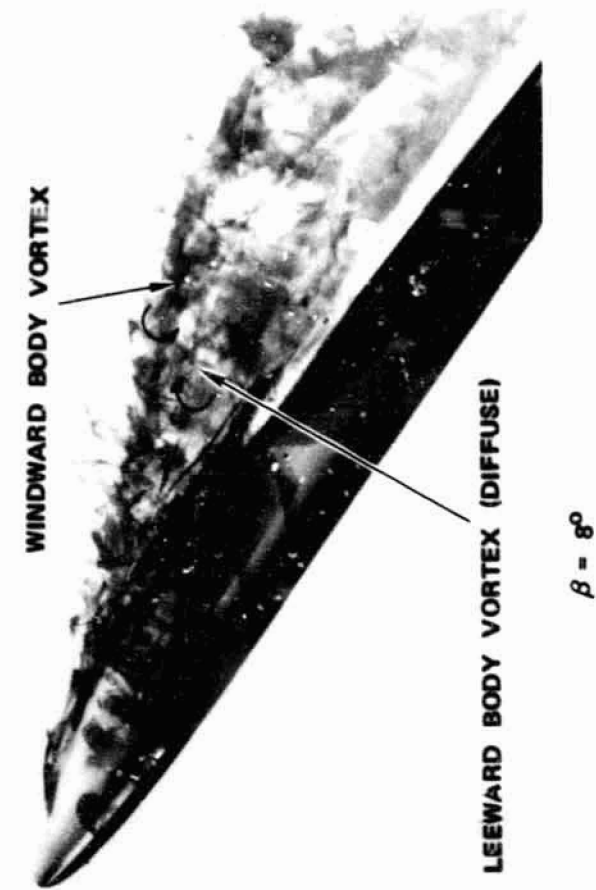
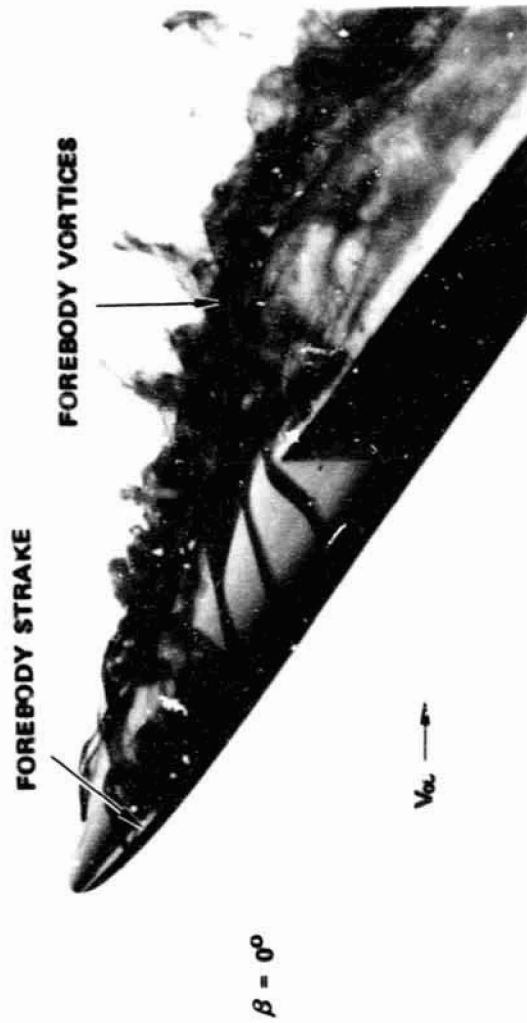
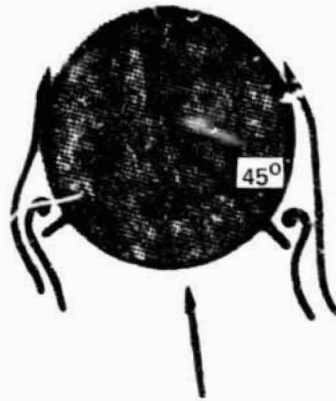


FIGURE 49. F/A-18 FOREBODY VORTEX FLOW BEHAVIOR WITH NOSE STRAKES
($\phi = -45^\circ$); $\alpha = 35^\circ$

PRECEDING PAGE BLANK NOT FILLED

PRECEDING PAGE BLANK NOT FILMED

ORIGINAL PAGE
COLOR PHOTOGRAPH



SMALL SIDESLIP



LARGE SIDESLIP

FIGURE 5C. SKETCH OF FOREBODY STRAKE FLOW AT HIGH ANGLE OF ATTACK.

ORIGINAL PAGE
COLOR PHOTOGRAPH

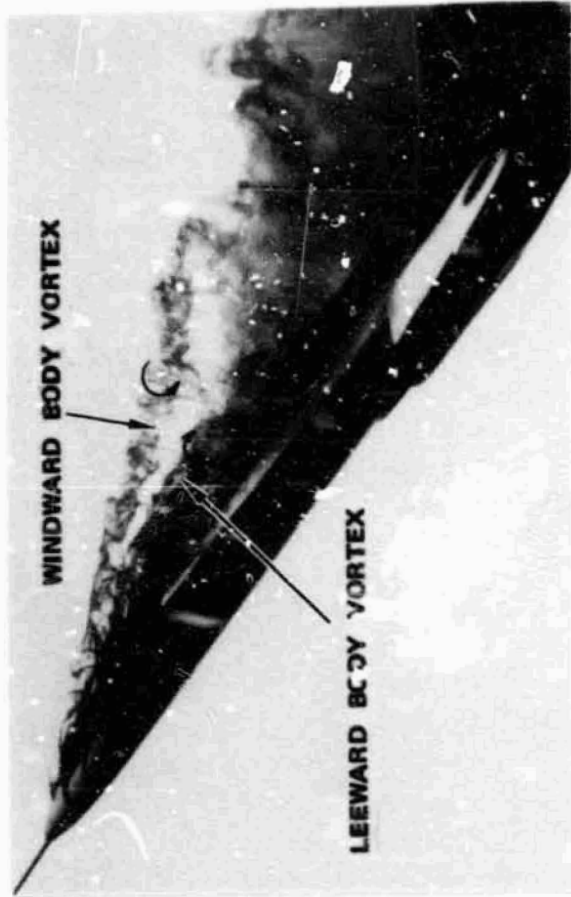
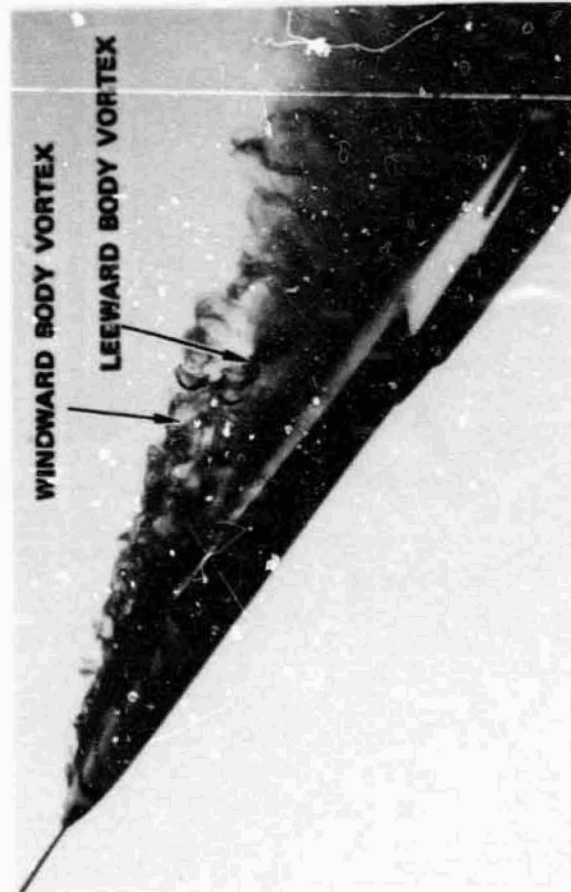
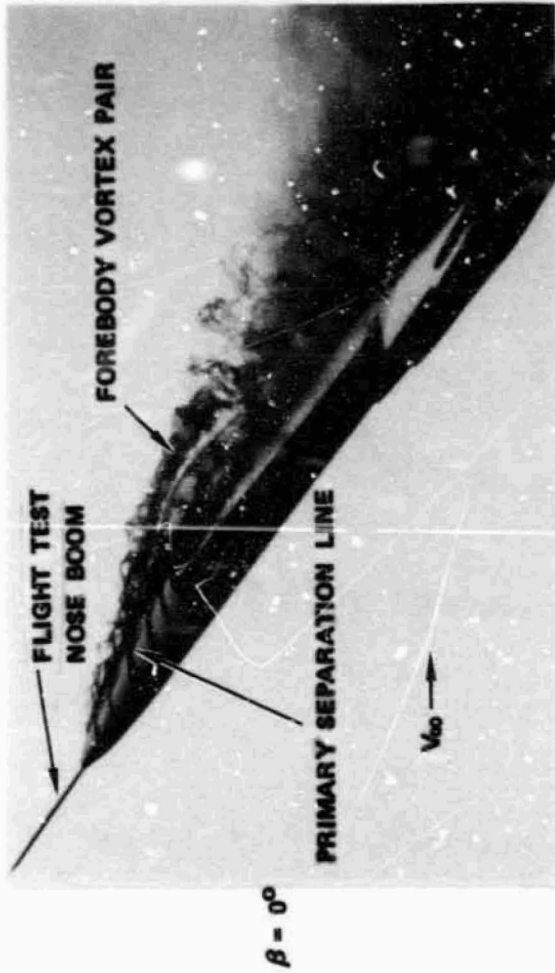
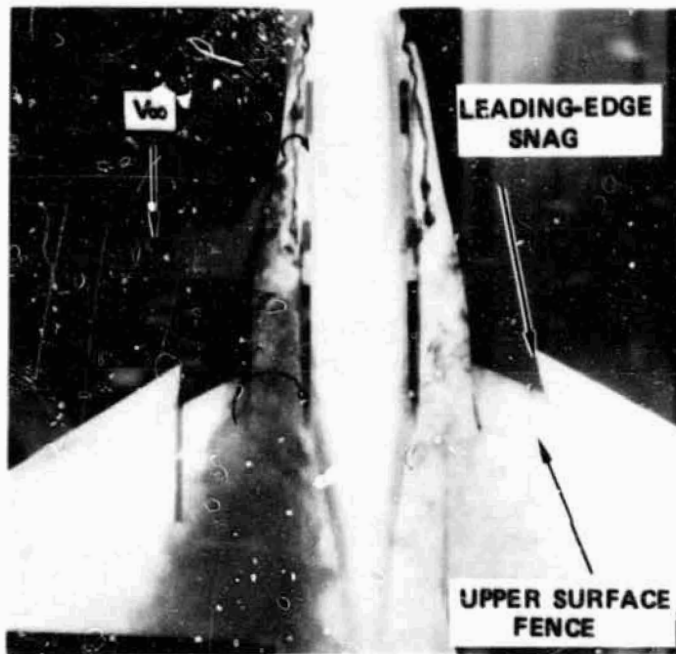
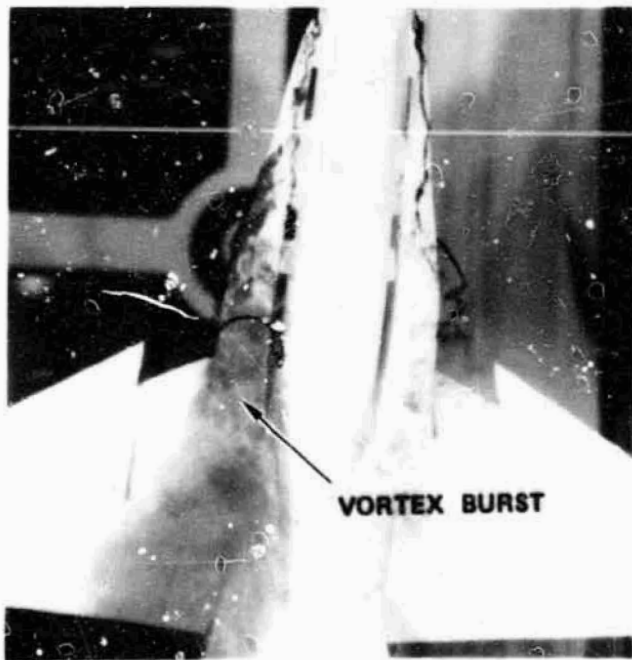


FIGURE 51. F/A-18 FOREBODY VORTEX CHARACTERISTICS WITH FLIGHT TEST
NOSE BOOM; $\alpha = 35^\circ$

PRECEDING PAGE BLANK NOT FILMED



$\beta = 0^\circ$



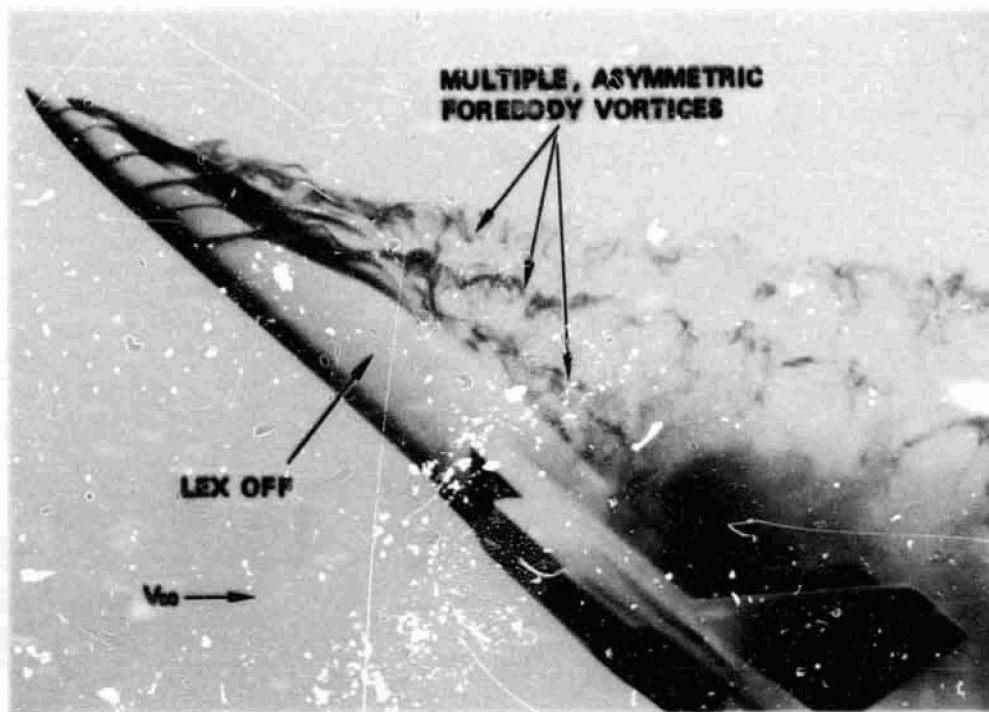
$\beta = -4^\circ$



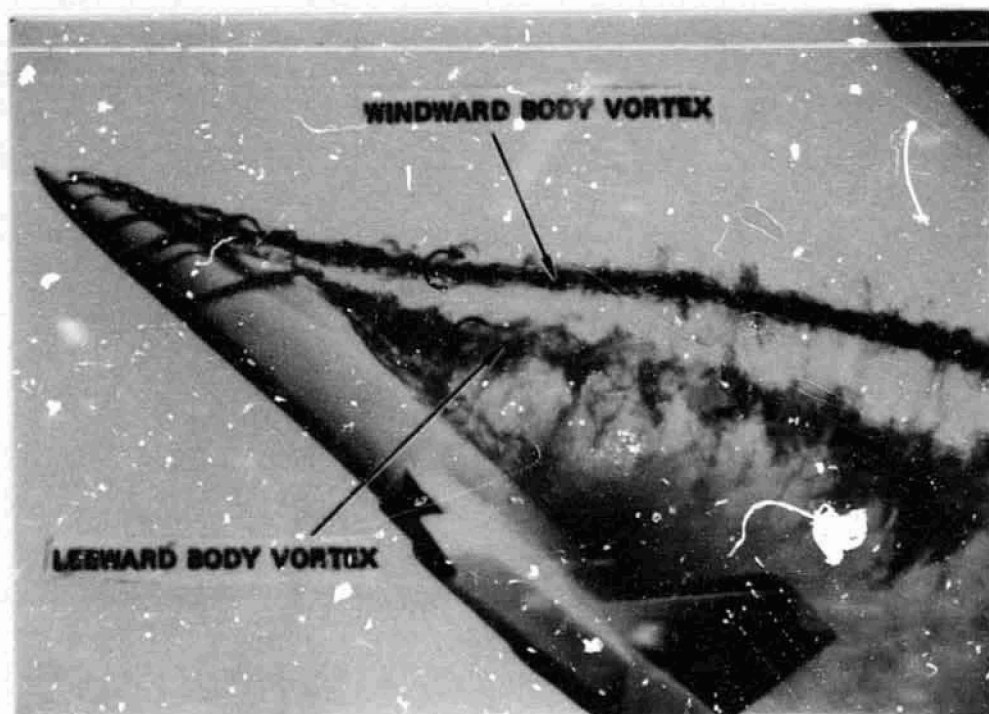
$\beta = 4^\circ$

PRECEDING PAGE BLANK NOT FILMED

FIGURE 52. F/A-18 LEX VORTEX FLOW BEHAVIOR WITH LEADING EDGE SNAG AND WING UPPER SURFACE FENCE; $\alpha = 30^\circ$



$\beta = 0^\circ$



$\beta = -8^\circ$

FIGURE 53. F/A-18 BODY VORTEX BEHAVIOR WITH LEXs REMOVED; $\alpha = 40^\circ$

Reinstallation of Wing Leading-Edge Extensions

Repeat runs were made of the baseline F/A-18 model (LEXs reinstalled) to assess any changes in the vortex flow field at high angles of attack.

The forebody-LEX vortex flow fields at $\alpha=40^\circ$ shown in Figure 54 exhibit differences relative to the initial baseline runs. The primary change is in the path of the windward body vortex: instead of shearing away from the fuselage forebody when the model is sideslipped, the vortex remains in proximity to the fuselage. As a consequence, the windward wing panel exhibits a surface flow pattern indicative of the presence of a vortical motion. This effect is of particular significance at $\alpha = 35^\circ - 40^\circ$ where the windward wing flow separation is less extensive when compared to the leeward panel.

The forebody vortex patterns prior to removal and reinstallation of the LEXs were very repeatable. The latter two model changes appeared to produce small model geometry variations near the LEX apex and along the fuselage forebody. Although the geometry changes were not significant in terms of absolute dimensions, a large response was, nevertheless, triggered in the vortex flow interactions.

The differences observed in the forebody vortex patterns in the two baseline runs will be utilized later in this report to provide a plausible explanation for the apparent F/A-18 "model-scale" effect.

These results serve to point out, in particular, the significance of the F/A-18 windward forebody vortex and its proximity to the fuselage and wing surfaces. Although the relative change in the windward body vortex path between the respective baselines was not large, the trajectory change is sufficient to trigger a large response in the overall flow field. That is, the windward body vortex was transformed from a decoupled vortical flow ("free" vortex) to a motion that is coupled to the F/A-18 multiple vortex system. This flow sensitivity is analogous to the sensitivity of a vortex to minor perturbations outside the core. Such perturbations are greatly magnified within the core because of the strong coupling of swirl and axial velocity components.

PRECEDING PAGE BLANK NOT FILMED

ORIGINAL PAGE
COLOR PHOTOGRAPH



FIGURE 54. F/A-18 FOREBODY VORTEX PATTERNS AT $\alpha = 40^\circ$ WITH
LEXs REINSTALLED (REPEAT BASELINE)

PRECEDING PAGE BLANK NOT FILMED

CORRELATION OF WATER TUNNEL FLOW VISUALIZATION RESULTS WITH 0.16-SCALE F/A-18
WIND TUNNEL DATA TRENDS

Baseline Configurations ($\delta_n / \delta_f = 25^\circ / 0^\circ$; $\delta_n / \delta_f = 35^\circ / 0^\circ$; $\delta_n = -12^\circ$)

Two baseline F/A-18 configurations will be discussed featuring leading-edge flap deflection angles of 25° and 35° . As a result, discussions of baseline data trends will also include effects of flap deflection angle.

Estimates of the angle of attack for LEX vortex breakdown at the wing trailing edge (α_{BD-TE}) are 16° and 20° , respectively, for $\delta_n = 25^\circ$ and 35° . These estimates are made from the initial local lift-curve slope reductions in Figure 55. In addition, estimates of angle of attack for vortex bursting near the LEX-wing junction (α_{BD-LWJ}) are 36° and 40° for $\delta_n = 25^\circ$ and 35° , respectively. Based on Northrop water tunnel correlations of thin, flat-plate, sharp-edged LEX-wing planforms with low-speed wind tunnel results (Reference 5), the angle of attack at which $C_{L_{MAX}}$ is attained appears a good approximation to α_{BD-LWJ} .

The current test model, however, departs from the thin, uncambered lifting surface assumed above. Water tunnel-determined values of α_{BD-TE} and α_{BD-LWJ} with $\delta_n = 35^\circ$ were, approximately, 15° and 35° . The results in the hydrodynamic facility, then, reveal vortex instability at a given wing chord position at approximately 5 degrees lower angle of attack relative to the wind tunnel estimates due to viscous effects.

A review of NASA videotapes of smoke flow visualization studies of the 0.16-scale F/A-18 model confirm the similarity of LEX vortex behavior in water and air but, also, reveal more stable vortices in the wind tunnel. These trends are consistent with previous comparisons of water-to-air results obtained on a LEX-wing planform with deflected leading- and trailing-edge flaps. The water tunnel consistently underpredicted the flap effects on LEX vortex stability, although the trends were the same (Reference 6).

C-2

ORIGINAL PAGE IS
OF POOR QUALITY

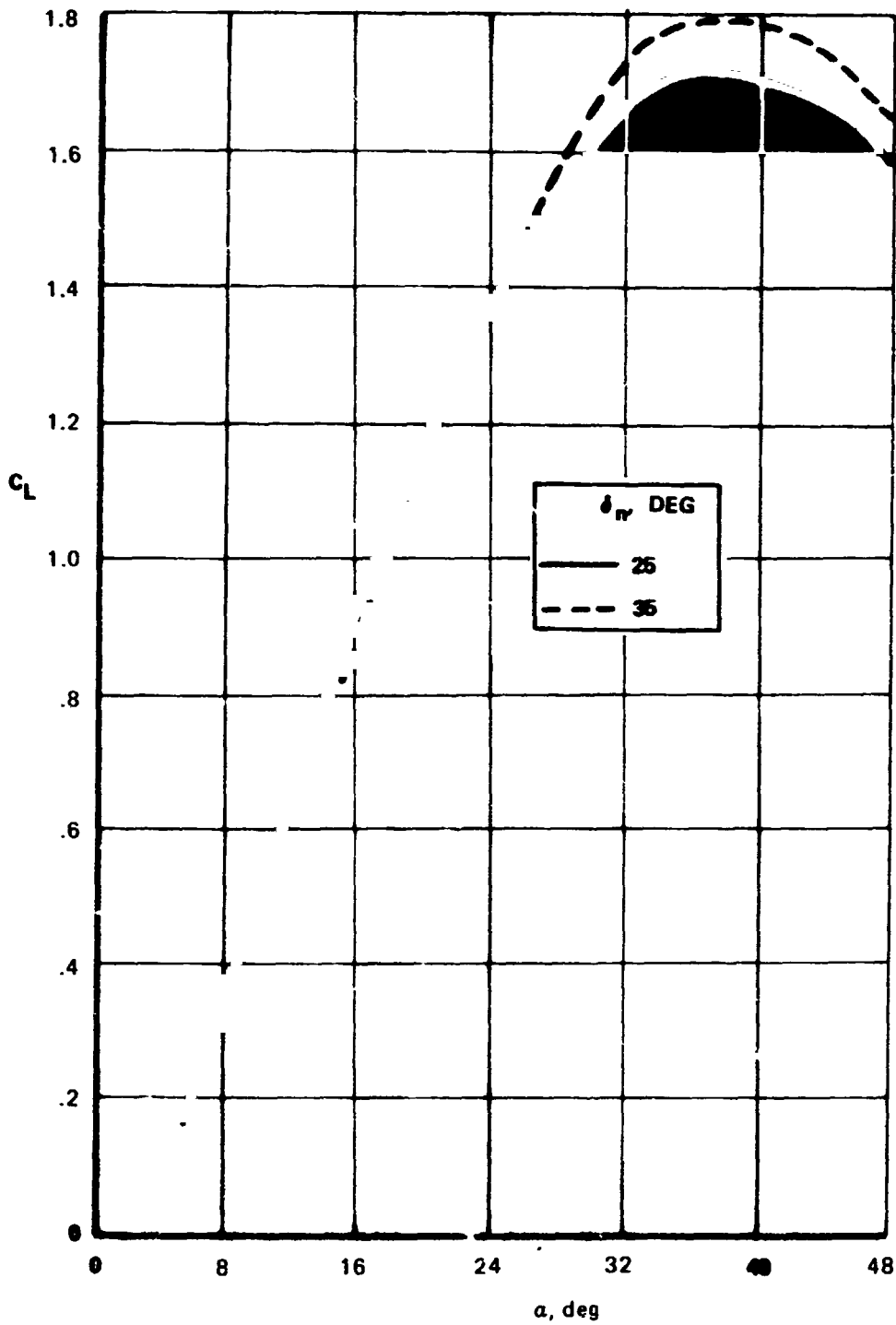


FIGURE 55. EFFECT OF INCREASED LEADING-EDGE FLAP DEFLECTION ON LIFT CHARACTERISTICS OF THE BASELINE 0.16-SCALE F/A-18; $\delta_h = -12^\circ$; $Re_c = 1.1 (10^6)$.



It is evident from these results that deflecting the leading-edge flaps to 35° increases the lift at higher angles of attack relative to the $\delta_n = 25^\circ$ case. This is due to delayed LEX vortex breakdown and improved wing flow separation characteristics. The reduction in positive pressure gradient near the wing leading edge enables the LEX vortex to penetrate somewhat farther into the wing flow field. Concurrent with increased flap angle, however, is a reduction in vortex strength at a given angle of attack.

Figure 56 presents variations of lift and pitching moment coefficients with sideslip at constant angle of attack. The data show little variation of C_L and C_m with β at all angles of attack. This is in contrast to results obtained on arrow-wing planforms in Reference 7, where, at high angles of attack, large variations in C_L occurred. The latter planforms are considerably more vortex-dominated, however, at high α 's relative to the F/A-18. The present 0.16-scale F/A-18 data suggest, then, that the integrated lift and pitching moments on the wing panels in sideslip are similar and relatively insensitive to sideslip variations.

The variations of rolling moment, yawing moment, and side force coefficients with angle of attack at $\beta = -4^\circ$ are presented in Figure 57. Rolling moment coefficient is increasingly stable up to $\alpha \approx 20^\circ$ after which occurs an unstable "break" in the C_l vs. α curve. The latter can be attributed to the appearance of LEX vortex breakdown over the wing panel. The flow visualization photograph in Figure 58 illustrates this effect at $\alpha = 20^\circ$ and $\beta = 10^\circ$ (all LEX slots are closed in this photograph). The unstable break in C_n vs. α is also the result of vortex bursting. However, this effect is evident at a lower angle of attack ($\alpha \approx 15^\circ$) since vortex burst occurs at the windward vertical tail prior to advancing forward over the wing panel (see Figure 58). A reduction in side force coefficient also reflects the decrease in tail effectiveness commencing at about $\alpha = 15^\circ$. Increasing vortex burst asymmetry promotes unstable variations of rolling moment and yawing moment up to $\alpha \approx 30^\circ$ and 25° , respectively. A further increase in angle of attack produces decreased vortex breakdown asymmetry and, consequently, stable variations of C_l and C_n with α . The stable increments in C_n and C_y commencing at $\alpha \approx 25^\circ$ may

ORIGINAL PAGE IS
OF POOR QUALITY

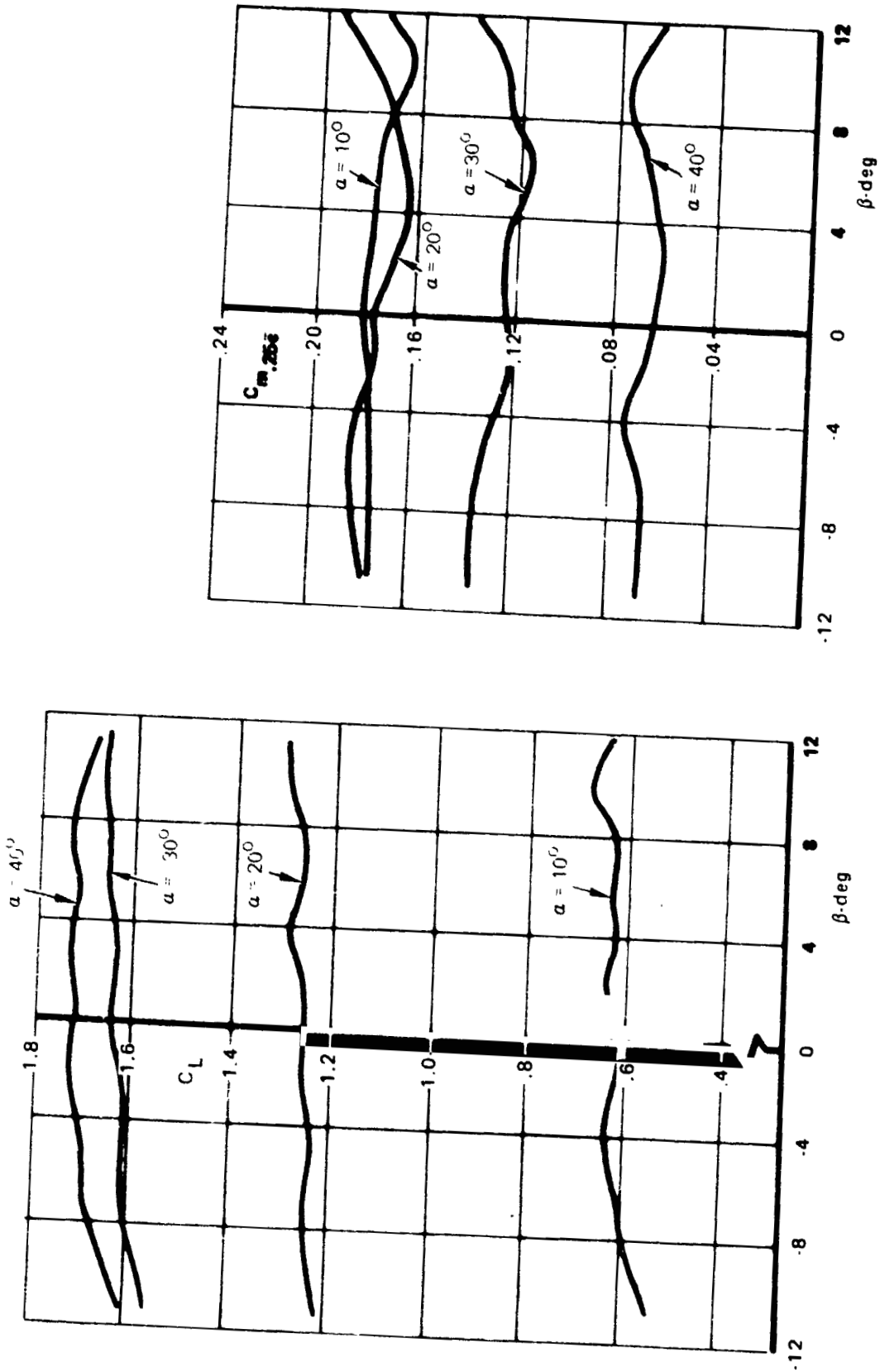


FIGURE 56. VARIATION OF LIFT COEFFICIENT AND PITCHING MOMENT COEFFICIENT WITH SIDESLIP; 0.16 -SCALE $F/A-18$; $\delta_h = -12^\circ$; $\delta_n = 25^\circ$; $Re_{\bar{c}} = 1.1 (10^6)$.

ORIGINAL PAGE IS
OF POOR QUALITY

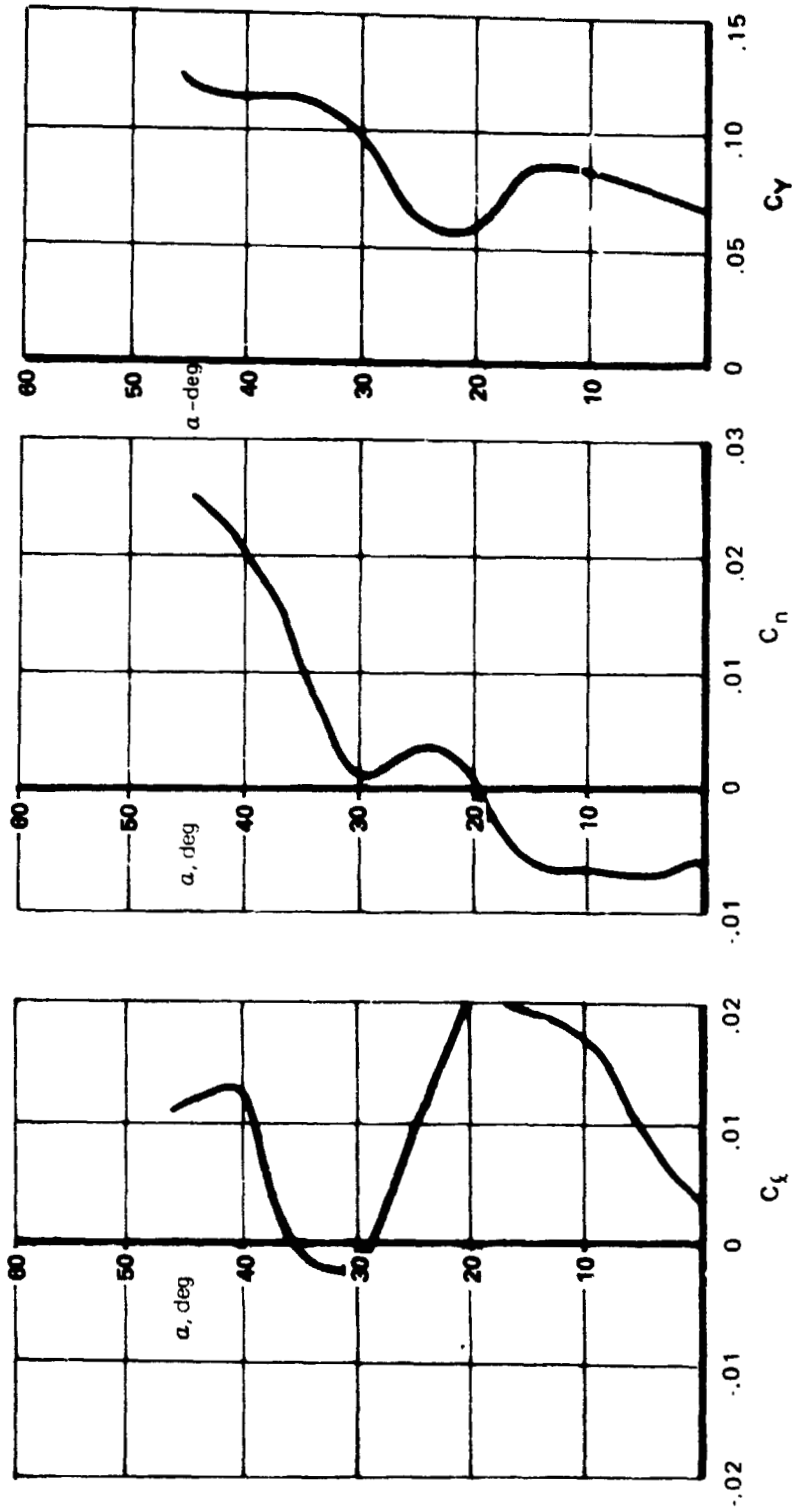


FIGURE 57. VARIATION OF ROLLING MOMENT, YAWING MOMENT, AND SIDE FORCE COEFFICIENTS WITH ANGLE OF ATTACK; 0.16-SCALE F/A-18; $\beta = -4^\circ$; $\delta_h = -12^\circ$; $\delta_n = 25^\circ$; $Re_c = 1.1 (10^6)$.

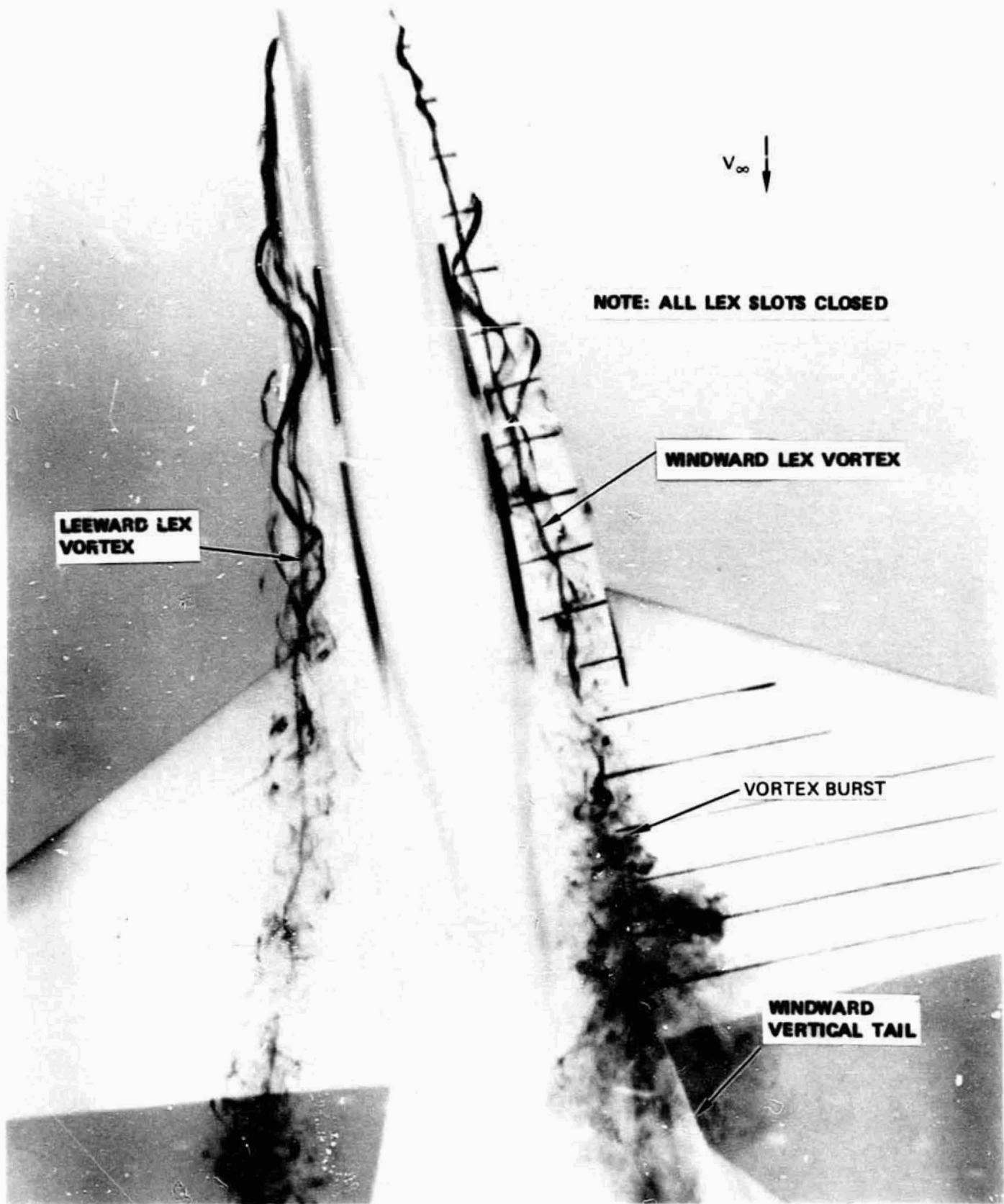


FIGURE 58. WINDWARD LEX VORTEX BREAKDOWN NEAR VERTICAL TAIL AT $\alpha = 20^\circ$, $\beta = 10^\circ$ (NORTHROP WATER TUNNEL)

be due to a reduction in adverse sidewash on the leeward vertical tail associated with a forward progression of leeward LEX vortex burst point. A second unstable break occurs in the yawing moment curve at $\alpha = 30^\circ$ which is apparently the result of immersion of the twin verticals in an increasingly larger wake as the wings approach stall. In general, the angles of attack at which large changes in the wind tunnel data arise are about 5° higher than the corresponding angles for major flow field changes in the water tunnel.

Figure 59 presents rolling moment variation with sideslip at $\alpha = 30^\circ$, 35° , and 40° for $\delta_n = 25^\circ$ and 35° . Increased deflection of the wing leading-edge flaps from $\delta_n = 25^\circ$ to $\delta_n = 35^\circ$ results in large stable rolling moment increments at $\alpha = 30^\circ$ and 35° as a result of delayed wing flow separation. Flap effects are negligible at $\alpha = 40^\circ$, however, since the angle of attack is too high to effectively alleviate flow separation near the flap hingeline.

Note is made in Figure 59 of the relative insensitivity of rolling moment coefficient to small variations about $\beta = 0^\circ$ at the higher angles of attack ($\alpha = 35^\circ$ and 40°). At these model attitudes LEX vortex breakdown occurs near the LEX-wing junction. In addition to the F/A-18 water tunnel observations, water tunnel tests of LEX-wing planforms, arrow wings, and delta wings have indicated that, near stall angle of attack, the vortices are resistant to changes in burst position due to small β - variations. These trends may be reflected in the 0.16-scale F/A-18 rolling moment invariance at $\alpha = 35^\circ$ and 40° between $\beta = \pm 6^\circ$. Further supportive evidence is available from Northrop water tunnel and wind tunnel tests (Reference 8) and NASA wind tunnel studies (Reference 7), which have shown that at angles of attack where LEX vortex breakdown occurs well forward on the wing panels, the burst positions are insensitive to variations in sideslip. At high- α conditions, extensive wing flow separation occurs and small sideslip perturbations do not alter the wing pressure field sufficiently to affect the stability of the LEX vortices.

Double-Width Forward LEX Slots (LEX 12)

LEX 12 reduces $C_{L_{MAX}}$ from about 1.79 to 1.77 and, in addition, lowers

PRECEDING PAGE BLANK NOT FILMED

ORIGINAL PAGE IS
OF POOR QUALITY

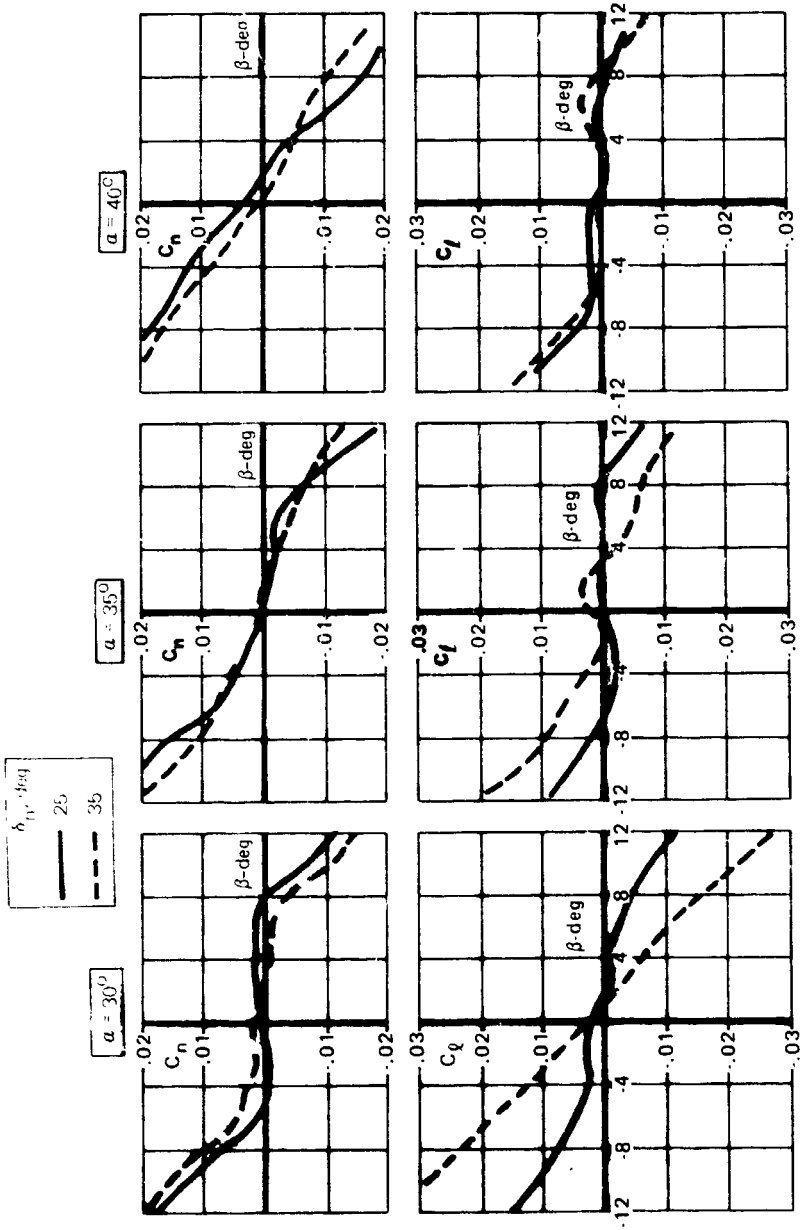


FIGURE 59. VARIATION OF ROLLING MOMENT COEFFICIENT WITH SIDESLIP;
0.16-SCALE F/A-18; $\delta_h = -12^{\circ}$; $Re_h = 1.1 (10^6)$.

the stall angle of attack from 40° to 38° , approximately, as shown in Figure 60. Water tunnel flow field observations suggest this effect is due to the increased forward slot flow entrainment which limits the amount of lower surface boundary layer flow available for feeding into the LEX vortex system. The result is a reduction in the effective LEX generating length, slightly faster progression of vortex breakdown, and earlier stall.

Figure 61 presents rolling moment and yawing moment variation with sideslip at $\alpha = 35^\circ$ and 40° . The slot modification induces, in general, stable rolling moment increments and unstable yawing moment coefficient increments. Based on water tunnel observations, the former effect can be attributed to a more symmetric breakdown of the LEX vortex in sideslip, whereas the latter effect is associated with a reduction in dynamic pressure at the vertical tails due to the larger wake shed from the wings. It is noted that, as was the case with the baseline data, the water tunnel results tend to reveal flow field changes due to the LEX mods at about 5 degrees lower angle of attack than the corresponding α 's at which effects are evident in the wind tunnel data.

It is interesting to observe that reducing the leading-edge flap deflection angle to 25° eliminates much of the favorable LEX 12 effects at $\alpha = 35^\circ$ and 40° , as shown in Figure 62. Extensive wing flow separation occurs at these angles of attack and the downstream influence of the LEX forward slot mod is correspondingly decreased. This situation is analogous to spanwise blowing effectiveness at high angles of attack. Blowing effectiveness requires leading-edge flow separation. However, if the degree of separation is too extensive, considerably higher blowing rates are required to achieve flow reattachment to the wing surface. Similar results have been provided in flow visualization tests of LEX vortex enhancement by blowing. At high angles of attack, a slight forward shift of the vortex burst point due, say, to decreased leading-edge flap deflection angle, requires disproportionately higher blowing rates to provide the same enhancement of the vortex achieved with a greater flap angle.

ORIGINAL PAGE IS
OF POOR QUALITY

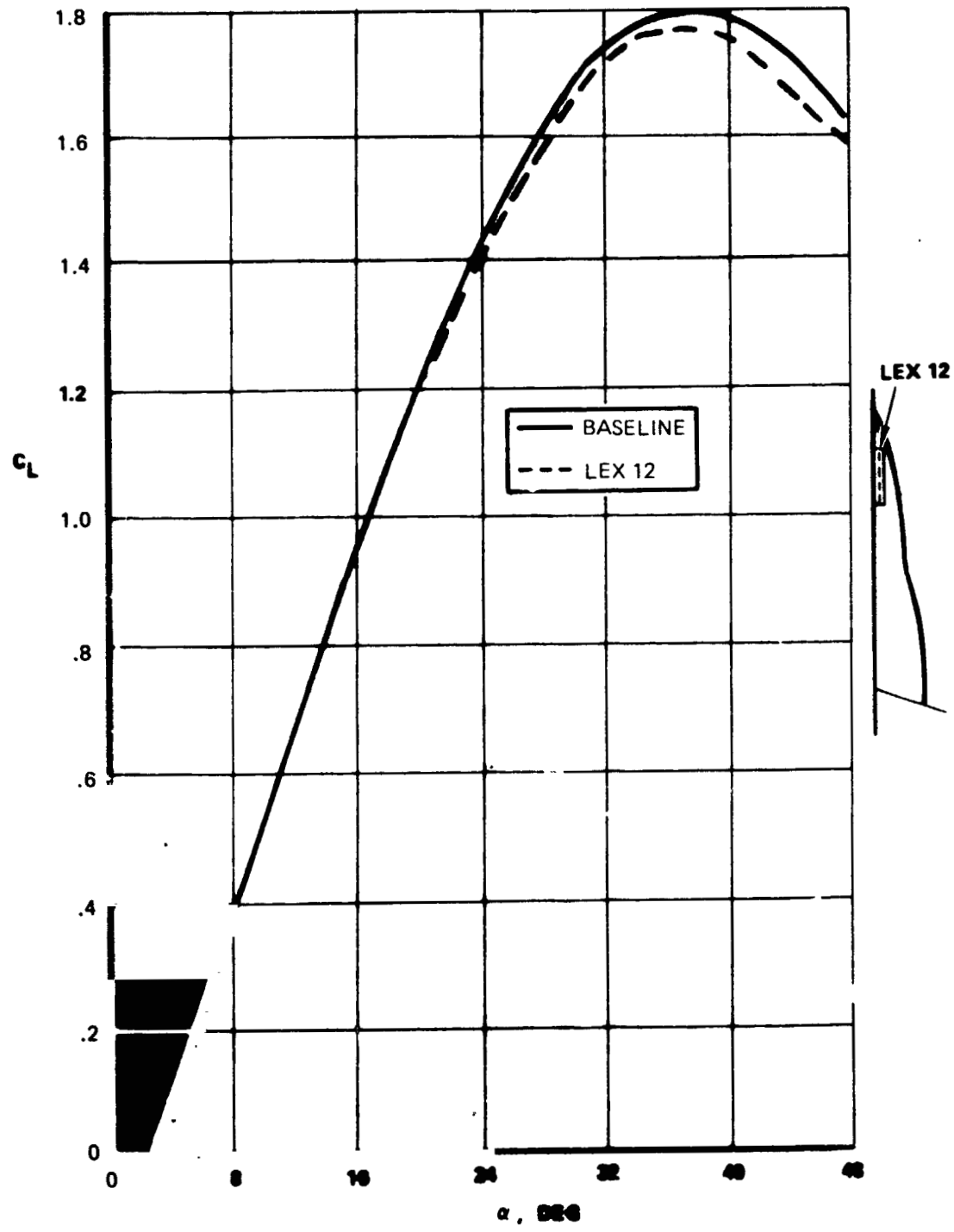


FIGURE 60. EFFECT OF LEX 12 ON LIFT COEFFICIENT; 0.16-SCALE F/A-18;
 $\delta_n = 35^\circ$; $\delta_h = -12^\circ$; $Re_c = 1.1 (10^6)$.

ORIGINAL PAGE IS
OF POOR QUALITY

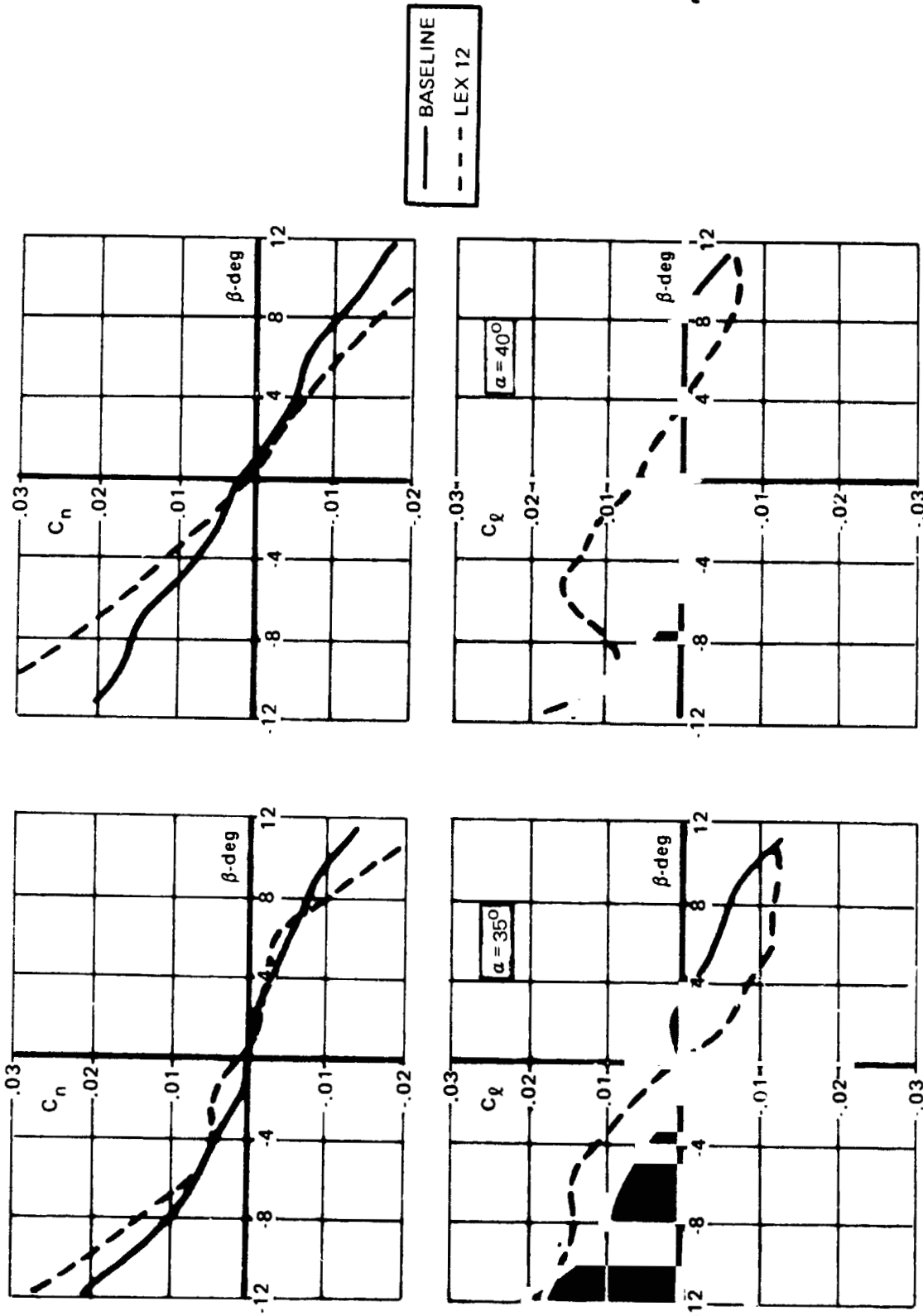


FIGURE 61. EFFECT OF LEX 12 ON VARIATION OF ROLLING MOMENT AND
YAWING MOMENT COEFFICIENTS WITH SIDESLIP; 0.16-SCALE F/A-15;
 $\delta_n = 35^\circ$; $\delta_h = -12^\circ$; $Re_c = 1.1 (10^6)$.

ORIGINAL PAGE IS
OF POOR QUALITY

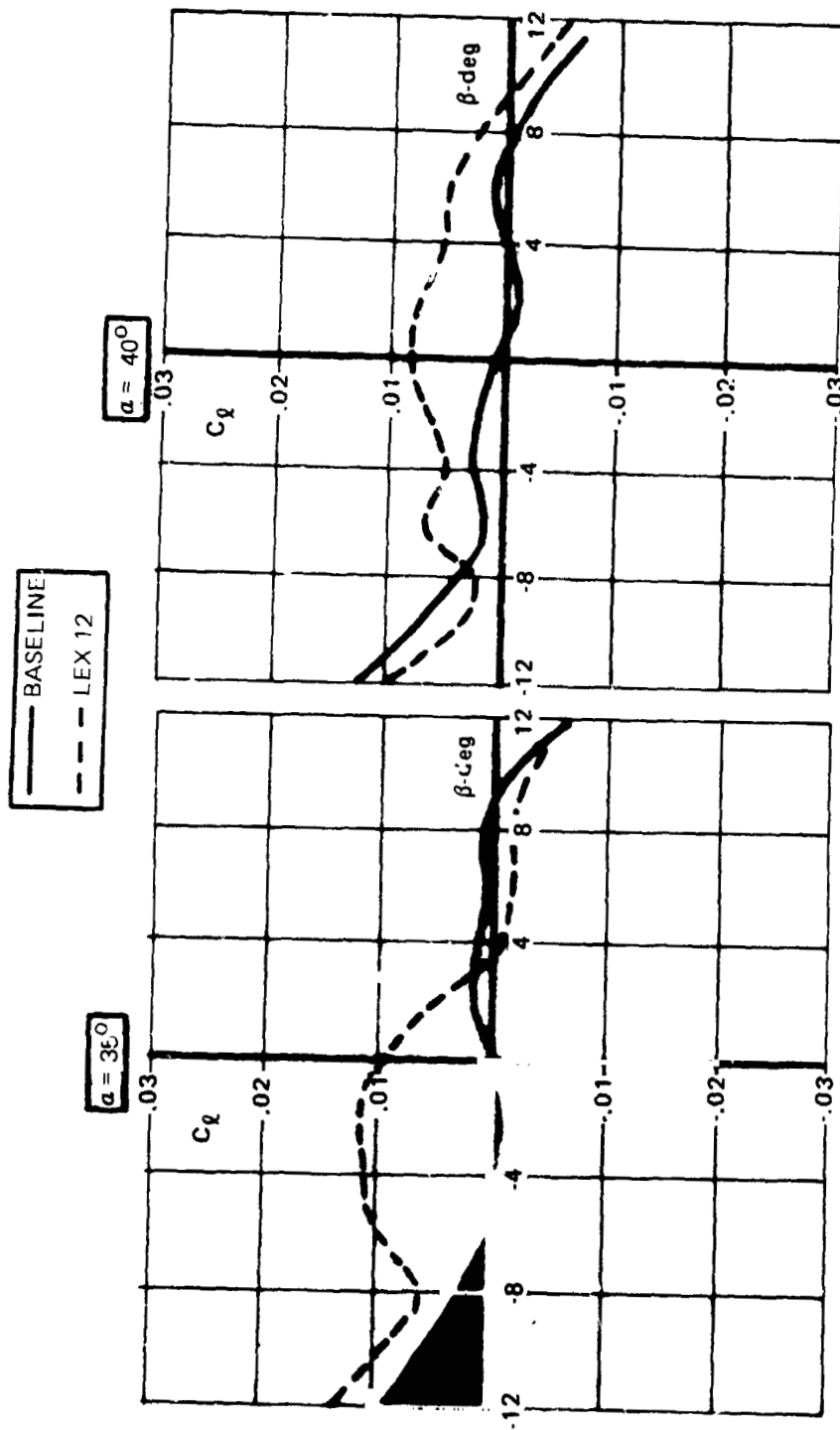


FIGURE 62. EFFECT OF LEX 12 ON ROLLING MOMENT VARIATION WITH SIDESLIP;
0.16-SCALE F/A-18; $\delta_n = 25^\circ$; $\delta_h = -12^\circ$; $Re_c = 1.1 (10^6)$.

Double-Width, Increased Length Forward LEX Slots (LEX 12A)

The effects of forward LEX slot modifications are more vividly illustrated with LEX 12A, or the double-width, increased length forward slots. The flow phenomena associated with LEX 12A are similar to the corresponding flow situation with LEX 12. However, the effects on longitudinal and lateral-directional characteristics are evident over a broader angle of attack range and to a greater degree.

Lift losses relative to the baseline data are apparent beginning at $\alpha \approx 20^\circ$ as shown in Figure 63. In addition, $C_{L\text{MAX}}$ (1.70 with LEX 12A as opposed to 1.79 for the baseline) is achieved at $\alpha \approx 34.5^\circ$ relative to $\alpha \approx 40^\circ$ for the baseline.

Variation of C_N and C_m with β at $\alpha = 35^\circ$ and 40° in Figure 64 reveal similar effects due to LEX 12A. The earlier stall due to LEX 12A is reflected in nose-down pitching moment increments. Thus, the premature bursting of the LEX vortices due to LEX 12A observed in the water tunnel is borne out in the wind tunnel data.

The wind tunnel data in Figure 65, which show rolling and yawing moment variation with sideslip at $\alpha = 35^\circ$ and 40° , indicate that LEX 12A promotes a more symmetric stall pattern in sideslip. Consequently, large, stable C_l -increments are achieved at these angles of attack. The unstable yawing moment increments associated with LEX 12A can be perceived from a qualitative standpoint by water tunnel test results. Dye entrained into the massive wake shed the wing surfaces traverses aft to the vertical tail region. The reduction in local "q" at the tails was evident by comparison with the free-stream flow.

The results discussed to this point serve to illustrate the significant influence of the LEX flow forward of the production break. Large improvements in lateral stability are achievable by judicious manipulation of the vortex feeding mechanism in this region. For example, LEX 12 and LEX 12A reduce the available lower surface vorticity which is shed at the LEX leading edge and

ORIGINAL AGE IS
OF POOR QUALITY.

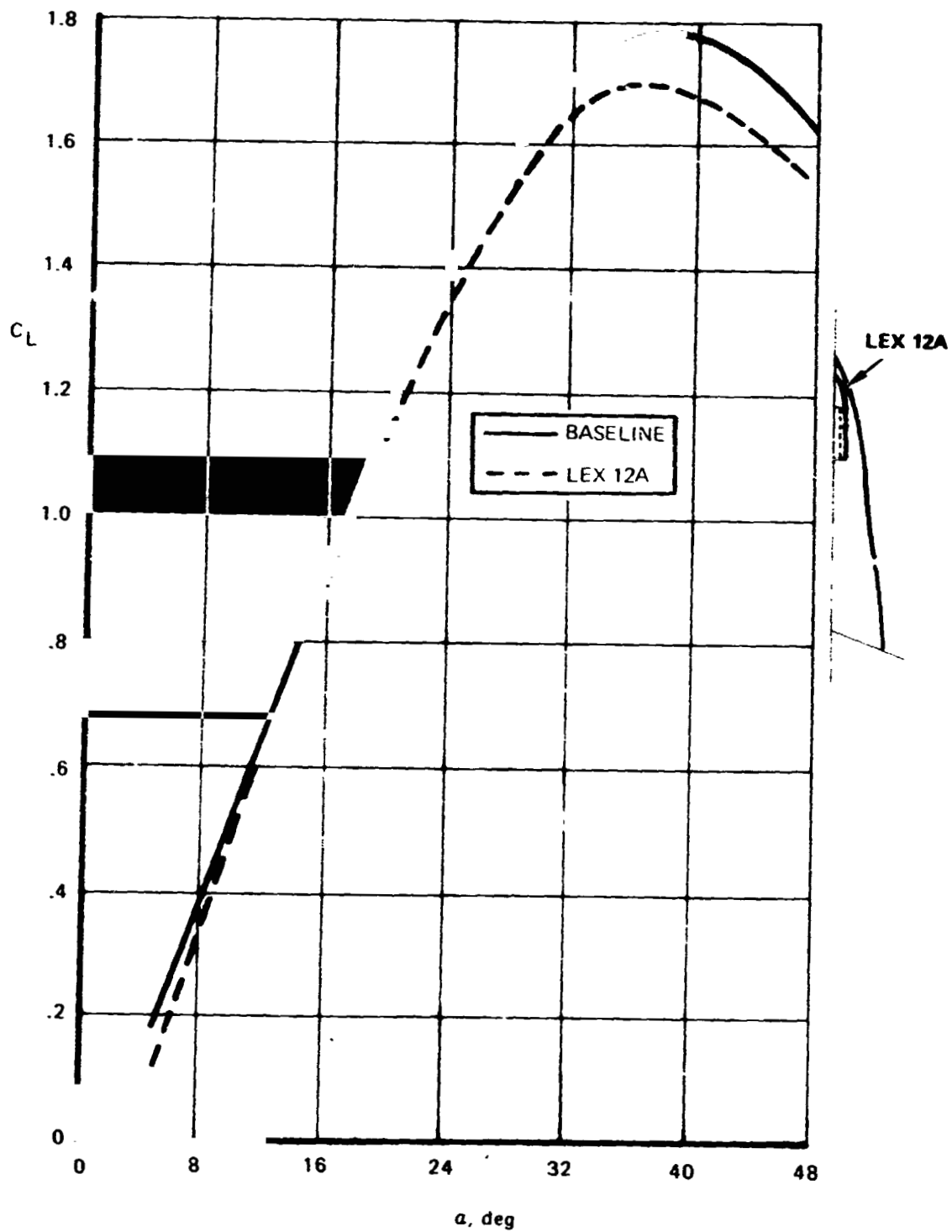


FIGURE 63. EFFECT OF LEX 12A ON LIFT COEFFICIENT;
 $\delta_n = 35^\circ$; $\delta_h = -12^\circ$; $Re_c = 1.1 (10^6)$.

ORIGINAL PAGE IS
OF POOR QUALITY

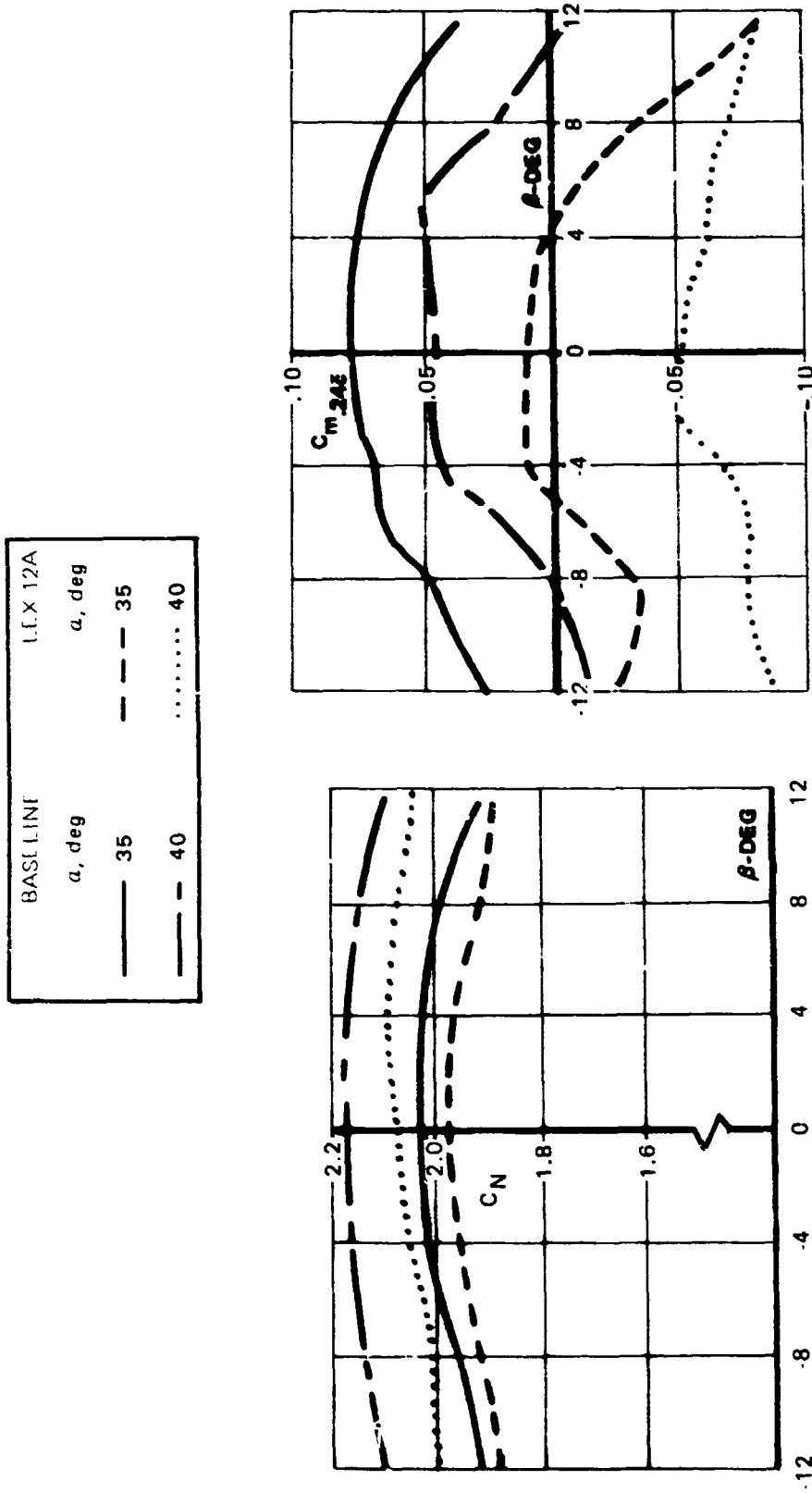
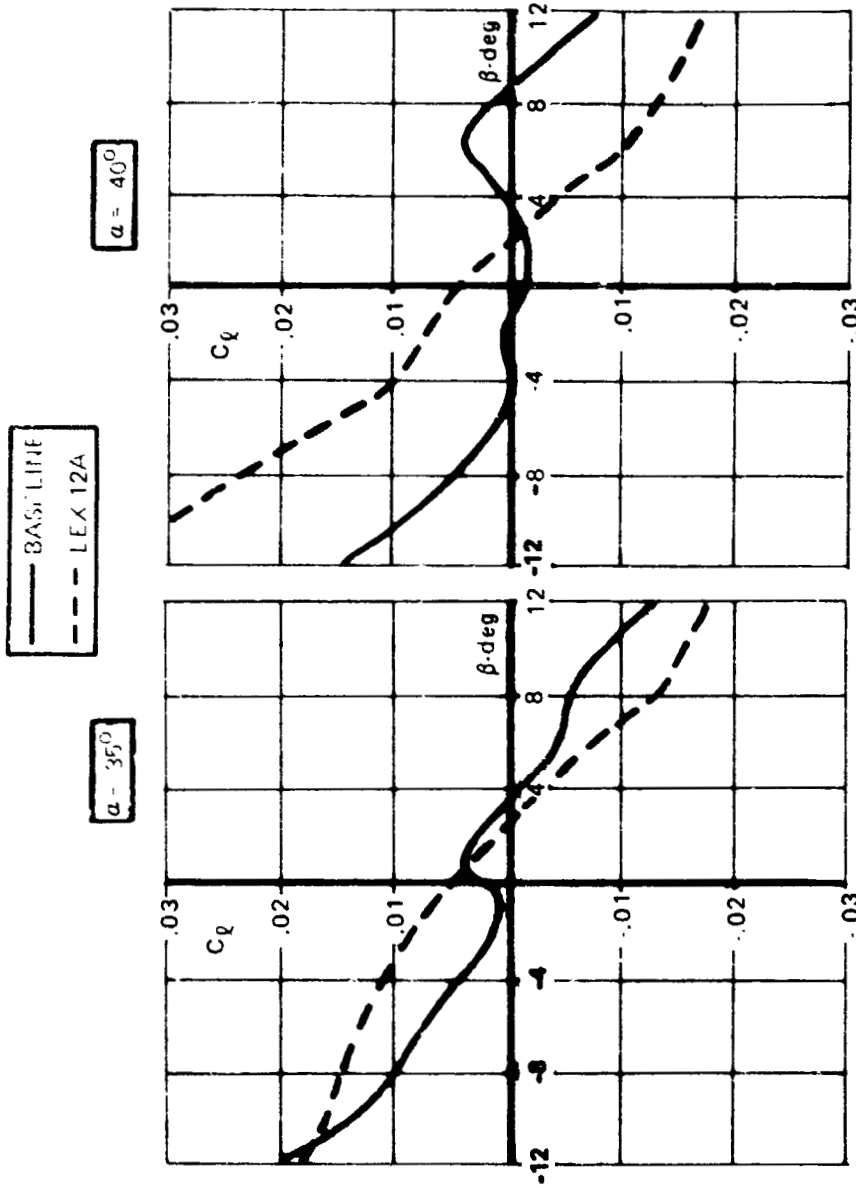


FIGURE 64. EFFECT OF LEX 12A ON NORMAL FORCE AND PITCHING MOMENT VARIATION WITH SIDESLIP; 0.16 -SCALE F/A -18; $\delta_n = 35^\circ$; $\delta_h = -12^\circ$; $Re_h = 1.1 (10^6)$.

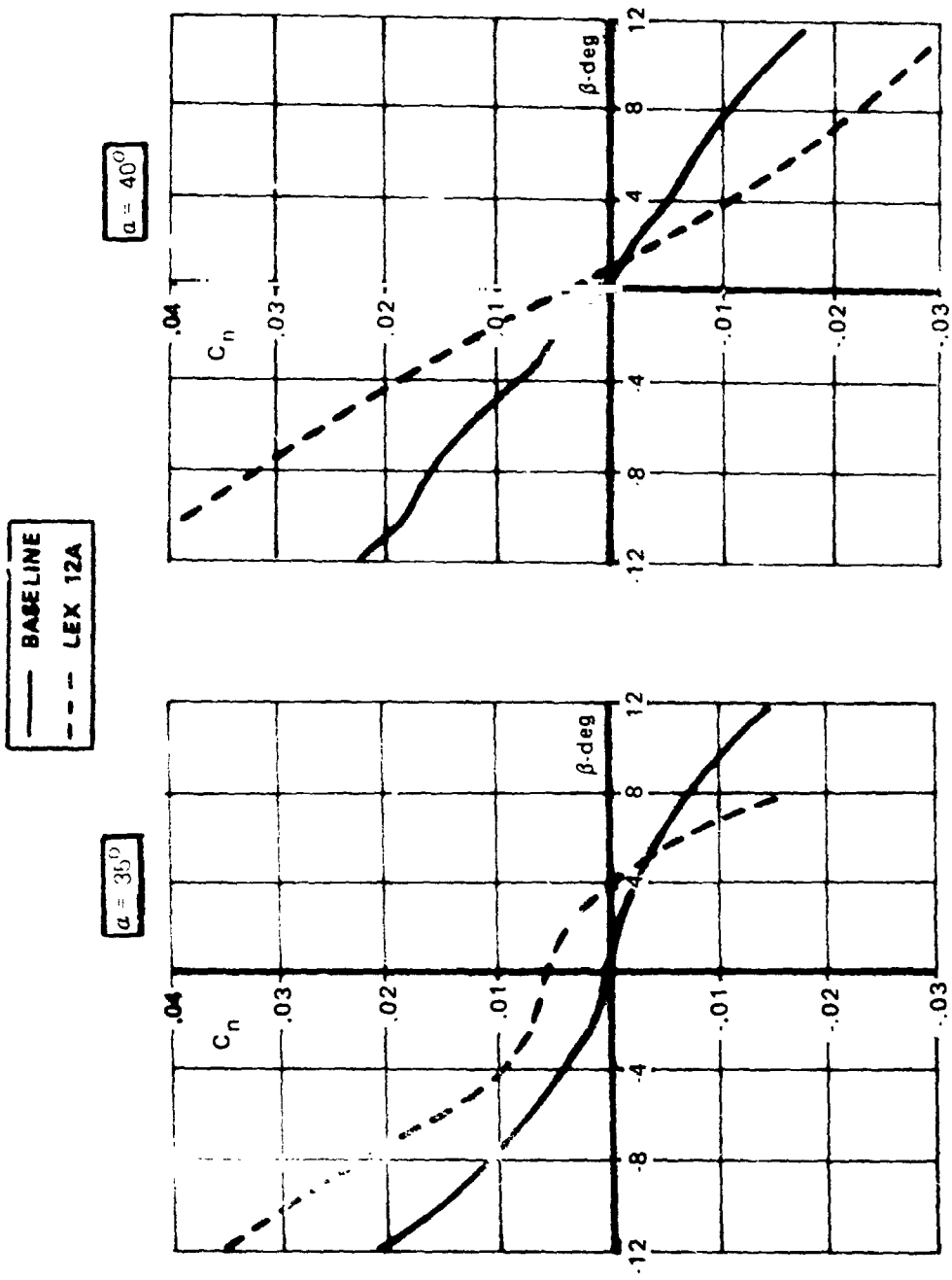
ORIGINAL PAGE IS
OF POOR QUALITY



(A) ROLLING MOMENT

FIGURE 65. EFFECT OF LEX 12A ON VARIATION OF ROLLING MOMENT WITH SIDESLIP;
 0.16 -SCALE F/A-18; $\delta_n = 35^\circ$; $\delta_h = -12^\circ$; $Re_c = 1.1 (10^6)$.

ORIGINAL PAGE IS
OF POOR QUALITY



(B) YAWING MOMENT

FIGURE 65. CONCLUDED.

feeds into the LEX vortex system. Concurrently, however, maximum lift capability is compromised depending on the extent to which the vortex feeding mechanism is restricted. It has also been observed in the water tunnel that the body vortex behavior is subject to perturbations due to LEX apex flow variations.

The following discussions pertain to wind tunnel data trends associated with alternate means of affecting the LEX apex flow field.

LEX Lower Surface Fence (Fence "B")

LEX Fence "B" is oriented oblique to the free-stream, terminating at the production break. This lower surface boundary layer fence limits the amount of shed vorticity along the LEX and, consequently, reduces the strength of the LEX vortex in the high angle-of-attack range. Examination of the lift characteristics in Figure 66 reveals a reduction in $C_{L_{MAX}}$ from 1.79 (baseline; $\delta_n = 35^\circ$) to 1.75 as well as a decrease in stall angle of attack to 37° from 40° . The water tunnel tests revealed the LEX vortex system with Fence "B" to be similar to the flow situation associated with LEX 12A. The latter, by way of flow entrainment into the forward slot, acts as a "fluid fence," diverting much of the lower surface spanwise flow in the region of interest to a chordwise direction. Similarly, the fence serves the same purpose, although with less lift loss since LEX surface area has not been removed and the LEX apex vortices are somewhat stronger.

The generating length of the LEX apex vortex is confined to the small region from the first point of intersection of the fence with the leading edge to the LEX apex. Interaction of the apex vortex with the aft primary vortex is limited and the former acts as a "free vortex." An analogous flow situation is leading-edge vortices shed from co-planar close-coupled canard-wing surfaces. The fences "fix" the point of origin of the aft primary vortices even in sideslip conditions. This is in contrast to the baseline configuration where, during water tunnel studies, it appeared that the leeward LEX vortex was fed by fluid from the LEX apex region which, at zero sideslip, was entrained into the apex vortex. This flow situation was not evident on the windward LEX.

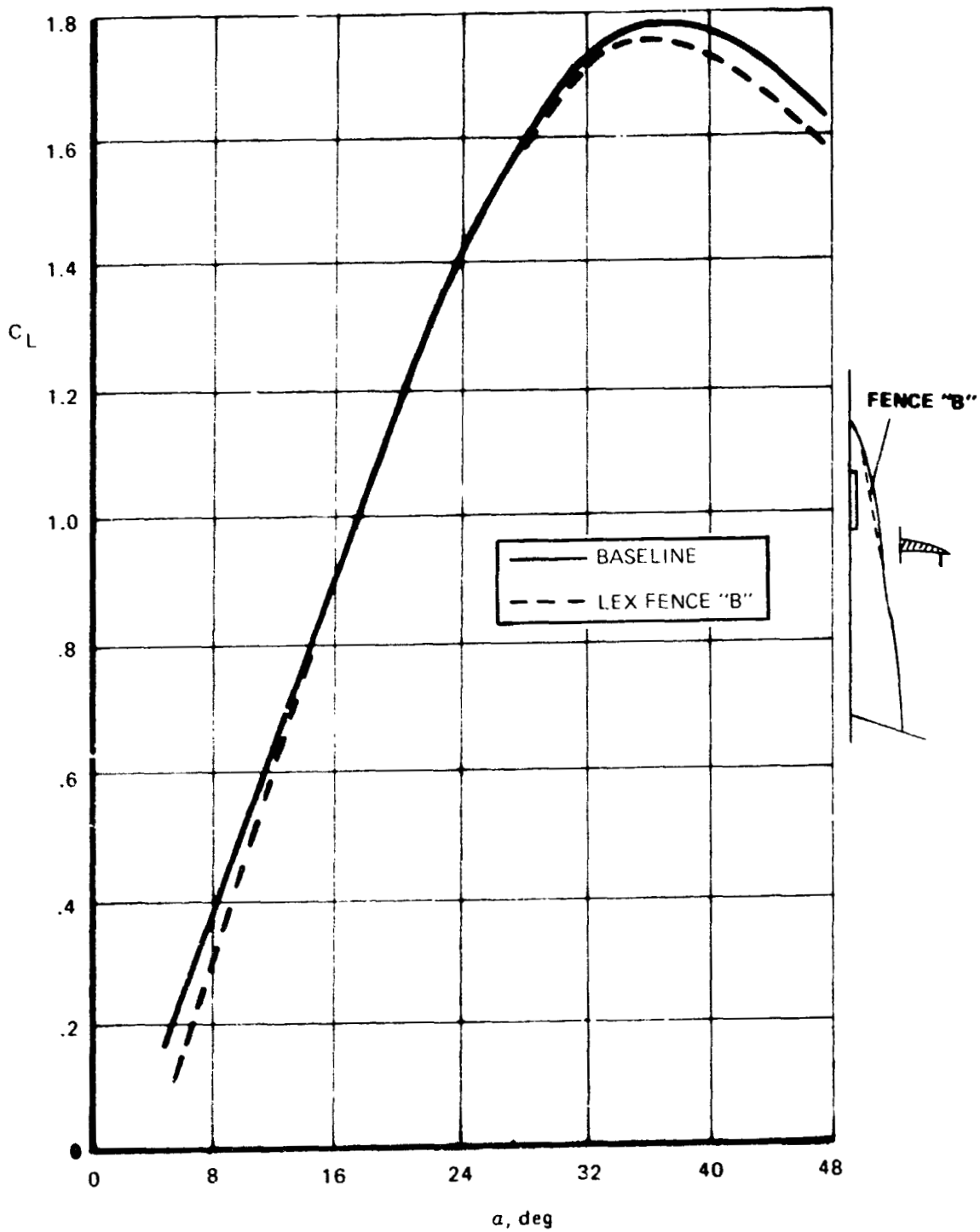


FIGURE 66. EFFECT OF LEX FENCE "B" ON LIFT COEFFICIENT; 0.16-SCALE F/A-18;
 $\delta_n = 35^\circ$; $\delta_h = -12^\circ$; $Re_c = 1.1 (10^6)$;

The LEX fences result in favorable rolling moment increments at $\alpha = 35^\circ$ and 40° as seen in Figure 67. The C_l -increments associated with Fence "B" are comparable to the LEX 12A results. However, wing stall is less pronounced with the fences and, accordingly, the unfavorable yawing moment increments in Figure 67 are less. Consequently, LEX Fence "B" appears more desirable in terms of an acceptable compromise between C_l improvements and $C_{L_{MAX}}$ reduction.

LEX Lower Surface Fence (Fence "A")

The effectiveness of LEX lower surface fences in improving lateral stability is sensitive to fence orientation. The data in Figure 68 indicate that fences oriented in a streamwise manner (Fence "A") are less favorable relative to Fence "B". A plausible explanation can be derived from water tunnel tests in terms of the effectiveness of the fence in decoupling the LEX aft primary vortex from the apex vortex. The streamwise fence does not provide a distinct break in the vorticity shed along the leading edge which will effectively isolate the aft primary vortex from the apex flow. The streamwise fence does, however, delineate the lower surface flow entrained into the forward slot from the fluid which proceeds spanwise to separate at the leading edge. Because the point of origin of the aft primary vortex is free to move with changes in angle of attack and sideslip, however, the streamwise fence is not as effective in promoting symmetric LEX vortex breakdown in sideslip.

LEX Planform Modifications

The LEX mods discussed up to this point - LEX 12, LEX 12A, Fence "A," Fence "B" - promote similar changes in the LEX vortex flow field at high angles of attack. Specifically, the LEX primary vortex developed in the presence of these mods exhibits stability characteristics similar to a vortex developed on a LEX with reduced generating length. To corroborate this conclusion, low-speed wind tunnel data are now presented that feature removal, to varying degrees, of LEX area near the apex. It will be shown that the effects on lateral stability at high angles of attack associated with LEX 12,

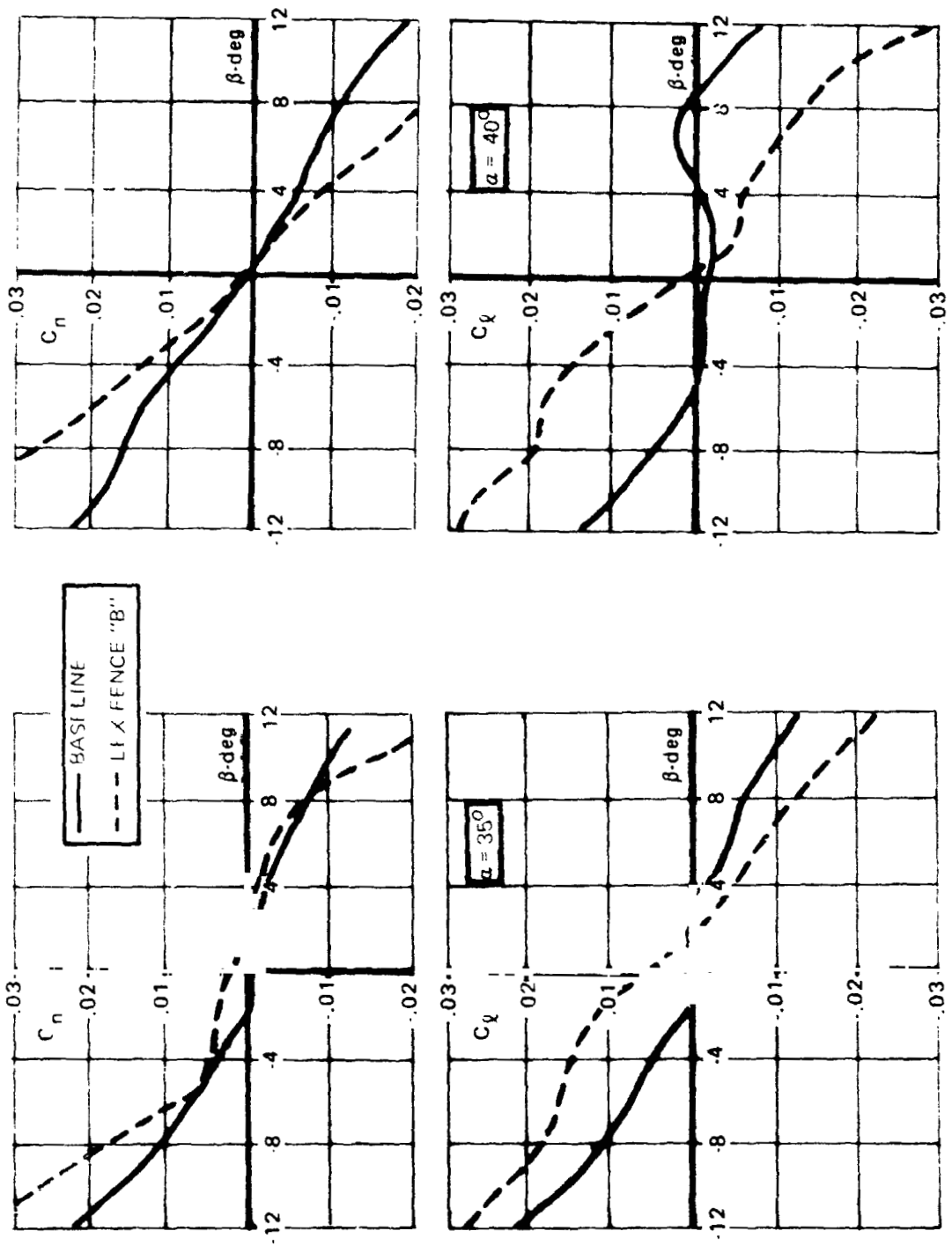


FIGURE 67. EFFECT OF LEX FENCE "B" ON ROLLING MOMENT AND YAWING MOMENT VARIATION WITH SIDESLIP; 0.1 -SCALE $F/A-18$; $\delta_h = -12^\circ$; $\delta_h = 35^\circ$; $\delta_h = -12^\circ$; $Re_c = 1.1 (10^6)$.

ORIGINAL PAGE IS
OF POOR QUALITY

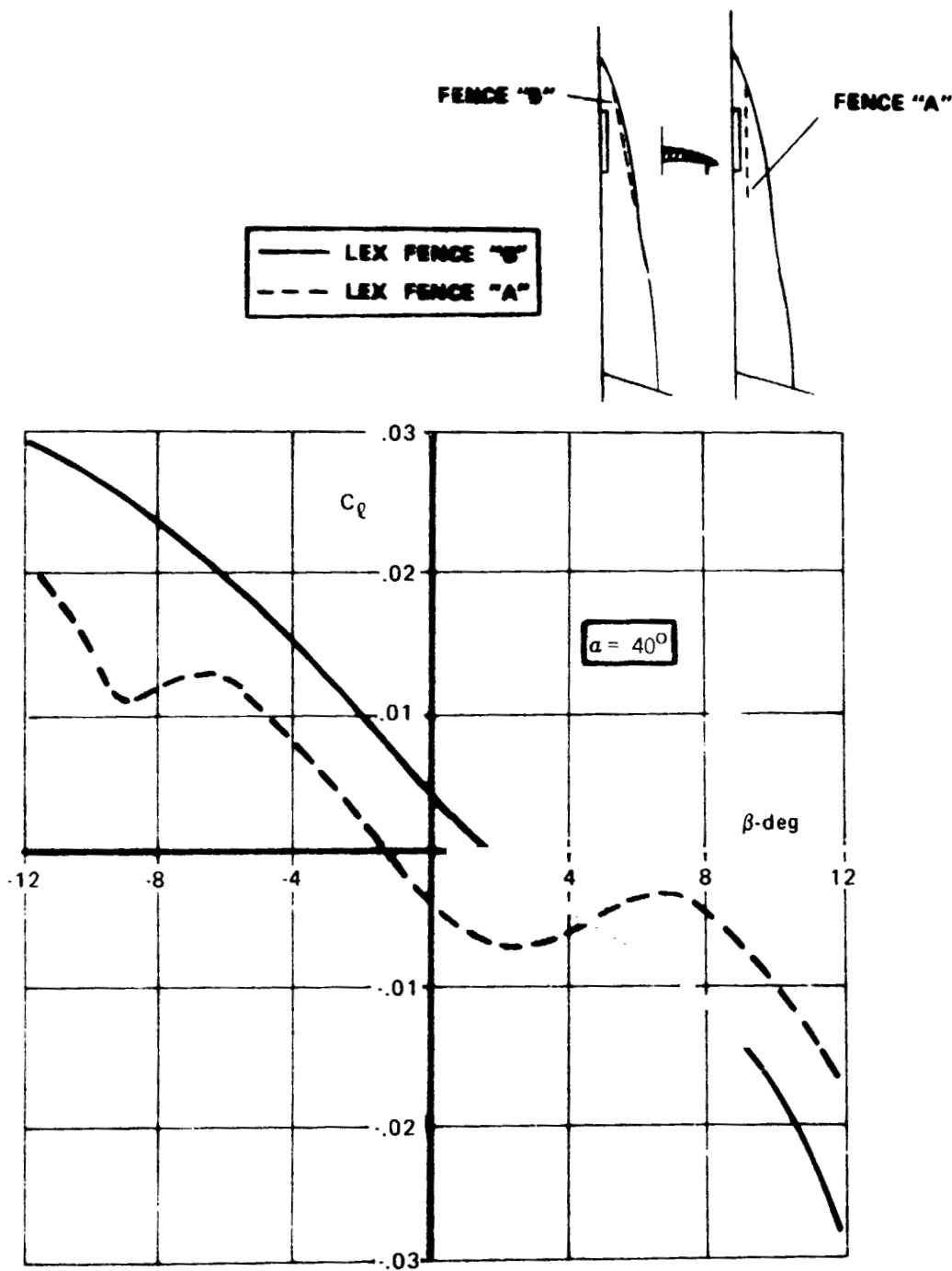


FIGURE 68. COMPARISON OF ROLLING MOMENT VARIATION WITH SIDESLIP FOR THE 0.16-SCALE F/A-18 WITH LEX FENCES "A" AND "B"; $\delta_n = 35^\circ$; $\delta_h = -12^\circ$; $Re_c = 1.1 (10^6)$.

LEX 12A, Fence "A," and Fence "B" are similar to the effects arising from removal of LEX area that corresponds approximately to the region of influence of LEX 12, etc. This is shown schematically in Figure 69.

Truncating approximately 88" (full-scale) of the LEX back to the production break as shown in Figure 69 greatly improves the rolling moment characteristics at $\alpha = 35^\circ$ and 40° as shown in Figure 70. At these angles of attack, the vortices shed from the smaller LEXs (designated LEX 2) are bursting over the LEX surfaces and vortex behavior is relatively insensitive to changes in sideslip. Both wings have passed through $C_{L_{MAX}}$ and the variation of rolling moment with sideslip in Figure 70 is highly stable.

Since the wings stall at lower α 's with LEX 2, the vertical tails are accordingly exposed to a larger wing wake relative to the baseline configuration. As a result, unstable yawing moment increments (data not shown) are developed at the higher angles of attack.

The trends associated with LEX 2 are quite similar to the effects observed with LEX 12, LEX 12A, Fence "A" and Fence "B." Since LEX 2 involves removal of lifting surface forward of the production break, the LEX modification which is expected to promote the most similar effects is LEX 12A. (The latter produced a significant lift loss at high α 's due to disruption of the LEX apex flow field.) A comparison of the rolling moment and yawing moment variations with sideslip at $\alpha = 35^\circ$ and 40° are shown in Figure 71. Note is made that the leading-edge flap deflection angles are not the same. The data trends are in good agreement, however. Consequently, the conclusion that LEX 12, LEX 12A, Fence "A," and Fence "B" are, in essence, different means (of varying effectiveness) of shortening the LEX "run length" appears substantiated.

Similar, but less favorable, effects are attained with LEX 7 and LEX 3 planforms, shown in Figures 72 and 73, respectively. LEX 7 features a 69-inch (full-scale) truncation of the LEX forward area and a 55° -swept-forward apex. LEX 3 reduces the baseline LEX area to a lesser extent and features a "gothic" or YF-17-type planform. Despite the planform differences, the effects on C_l and C_n variations with sideslip at $\alpha = 30^\circ$, 35° , and 40° are

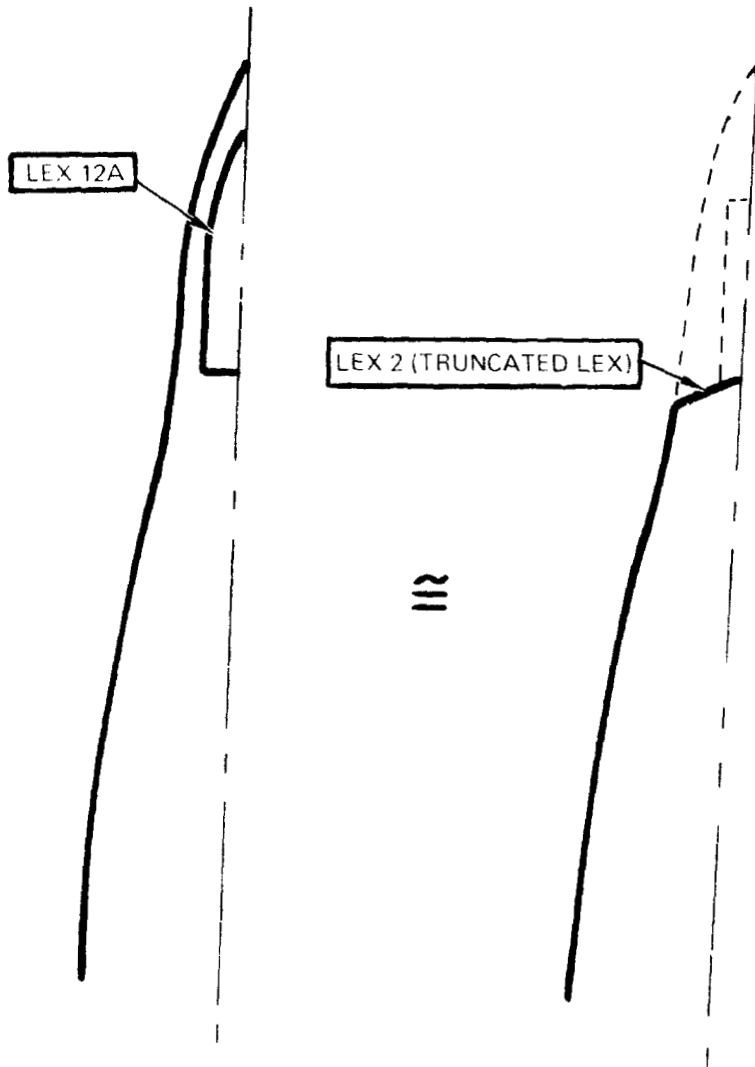


FIGURE 69. "EQUIVALENCE" OF LEX 12A AND TRUNCATED LEX (LEX 2).

ORIGINAL PAGE IS
OF POOR QUALITY

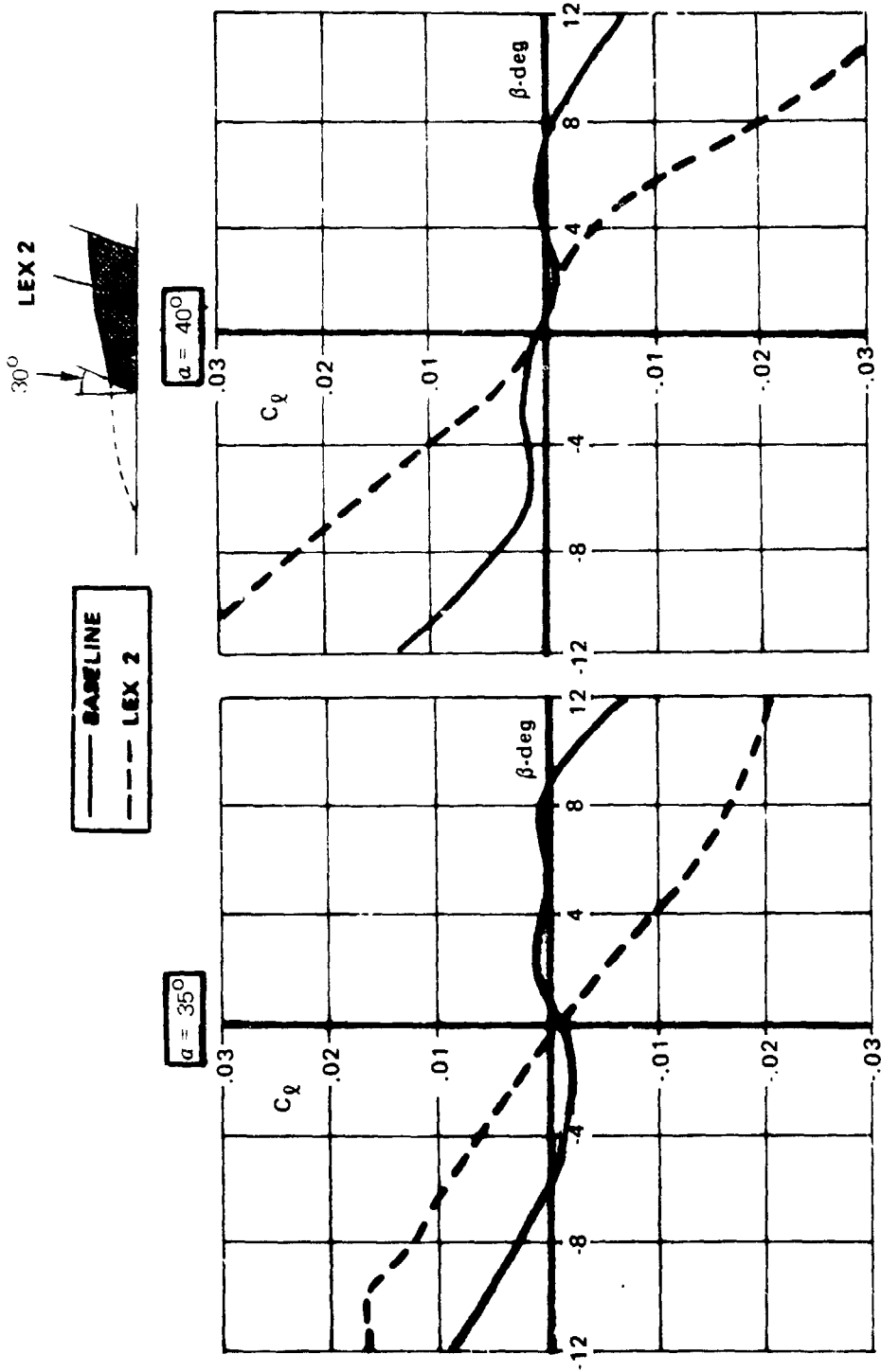


FIGURE 70. EFFECT OF LEX 2 ON ROLLING MOMENT VARIATION WITH SIDESLIP;
 0.16-SCALE F/A-18; $\delta_n = 25^\circ$; $\delta_h = -12^\circ$; $Re_c = 1.1 (10^6)$.

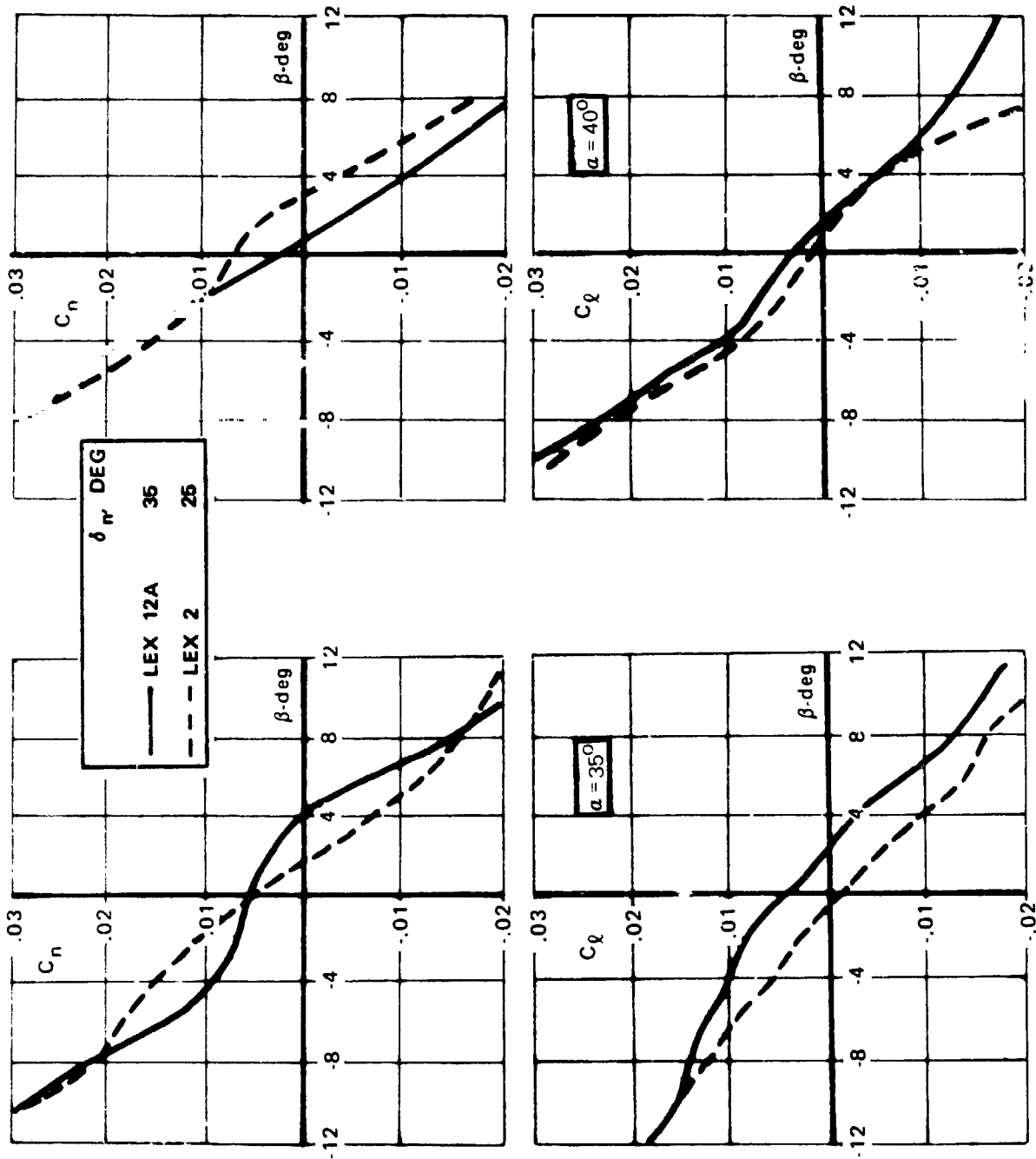


FIGURE 71. COMPARISON OF ROLLING MOMENT AND YAWING MOMENT
VARIATIONS WITH SIDESLIP FOR THE 0.16-SCALE F/A-18 WITH LEX 12A AND LEX 2;
 $\delta_h = -12^\circ$; $Re_c = 1.1 (10^6)$.

ORIGINAL PAGE IS
OF POOR QUALITY

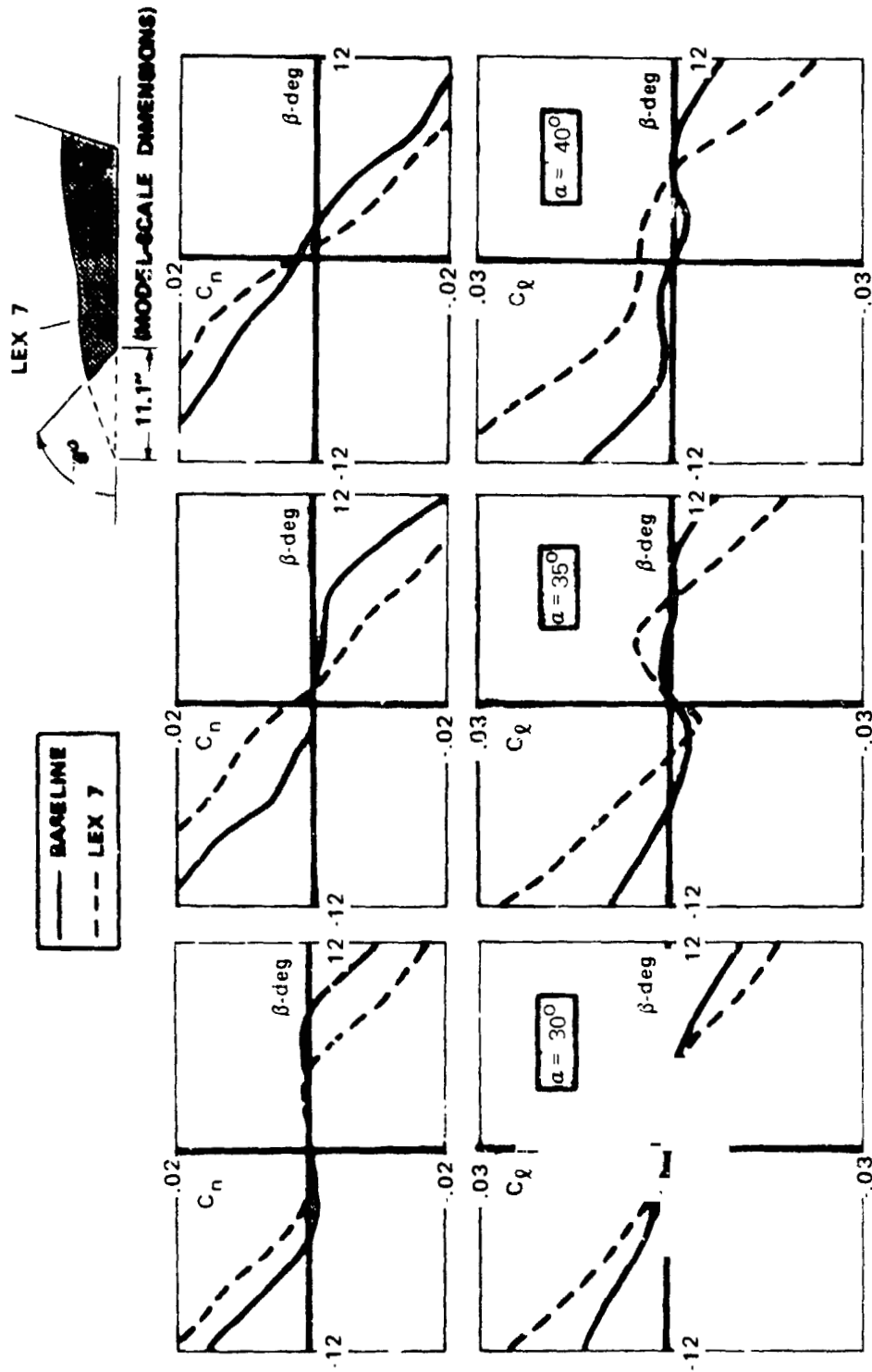


FIGURE 72. EFFECT OF LEX 7 ON ROLLING MOMENT AND YAWING MOMENT VARIATION WITH SIDESLIP; 0.16 -SCALE $F/A=18$; $\delta_n = 25^\circ$; $\delta_h = -12^\circ$; $Re_c = 1.1 (10^6)$.

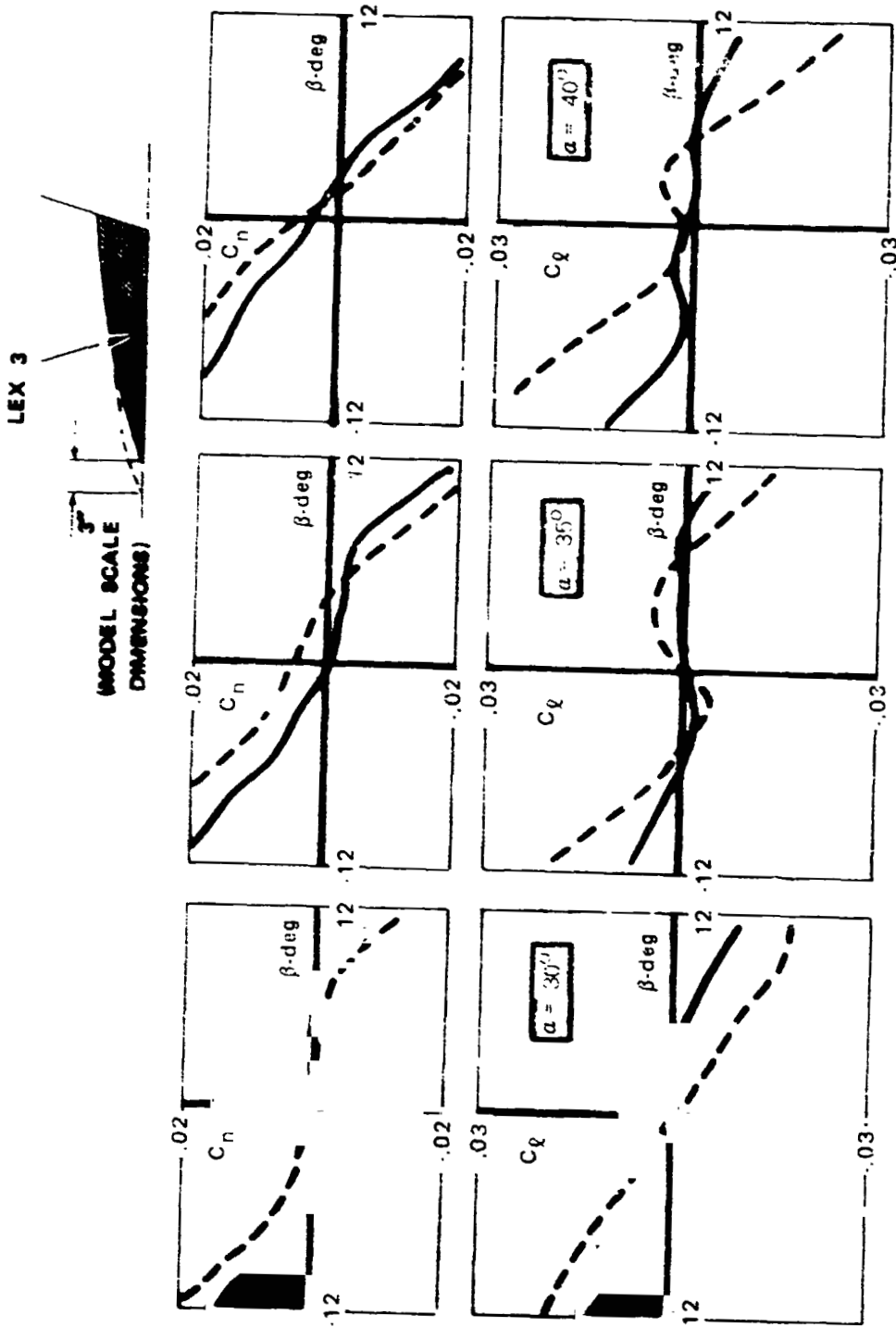


FIGURE 73. EFFECT OF LEX 3 ON ROLLING MOMENT AND YAWING MOMENT VARIATION WITH SIDESLIP; $\delta_n = 25^\circ$; $\delta_h = -12^\circ$; $Re_c = 1.1 (10^6)$.

very similar. These results are, thus, consistent with the trend that has emerged from the flow visualization studies and wind tunnel data analyses: shortening the LEX promotes a shed vortex system of reduced stability but greater resistance to asymmetric bursting in sideslip at $\alpha = 30^\circ$ - 40° .

By way of contrast, results obtained with LEX 10, which has a forward extension of the baseline LEX, are presented in Figure 74. The wind tunnel data show unstable rolling moment and stable yawing moment increments at $\alpha = 30^\circ$, 35° , and 40° for $|\beta| \leq 6^\circ$, approximately. Increasing the LEX generating length causes a more persistent vortex at high angles of attack. Vortex burst asymmetry due to sideslip is an undesirable fall-out, however. The more nonlinear variation of C_l and C_n with β appears due to the sensitivity of the longer LEX to vortex burst positions to small sideslip changes. At sideslip angles generally greater than $\pm 6^\circ$ the stable rolling moment coefficients can be attributed to the reduction in leeward LEX vortex stability, a characteristic inherent to slender planforms at high angles of attack and large sideslip.

The effects of LEX generating length on the aerodynamic characteristics can be summarized briefly in terms of the sketches in Figure 75. Maximum lift and stall angle of attack increase with increased LEX area. Although the trends associated with vortex breakdown asymmetry and rolling moment variation with sideslip are similar regardless of LEX size, the angles of attack at which major flow field changes occur are quite different. In the high angle of attack regime, the small LEX exhibits a recovery of lateral stability due to a reduction in vortex breakdown asymmetry. The curves for the large LEX, however, display a shift to higher angles of attack. Accordingly, significant vortex breakdown asymmetry and low levels of lateral stability prevail.

Wing Leading-Edge Snag and Upper Surface Fence

Results obtained with wing snag and fence combinations warrant discussion since the beneficial effects on lateral stability in certain cases are significant.

ORIGINAL PAGE IS
OF POOR QUALITY

LEX 10

(MODEL-SCALE
DIMENSIONS)

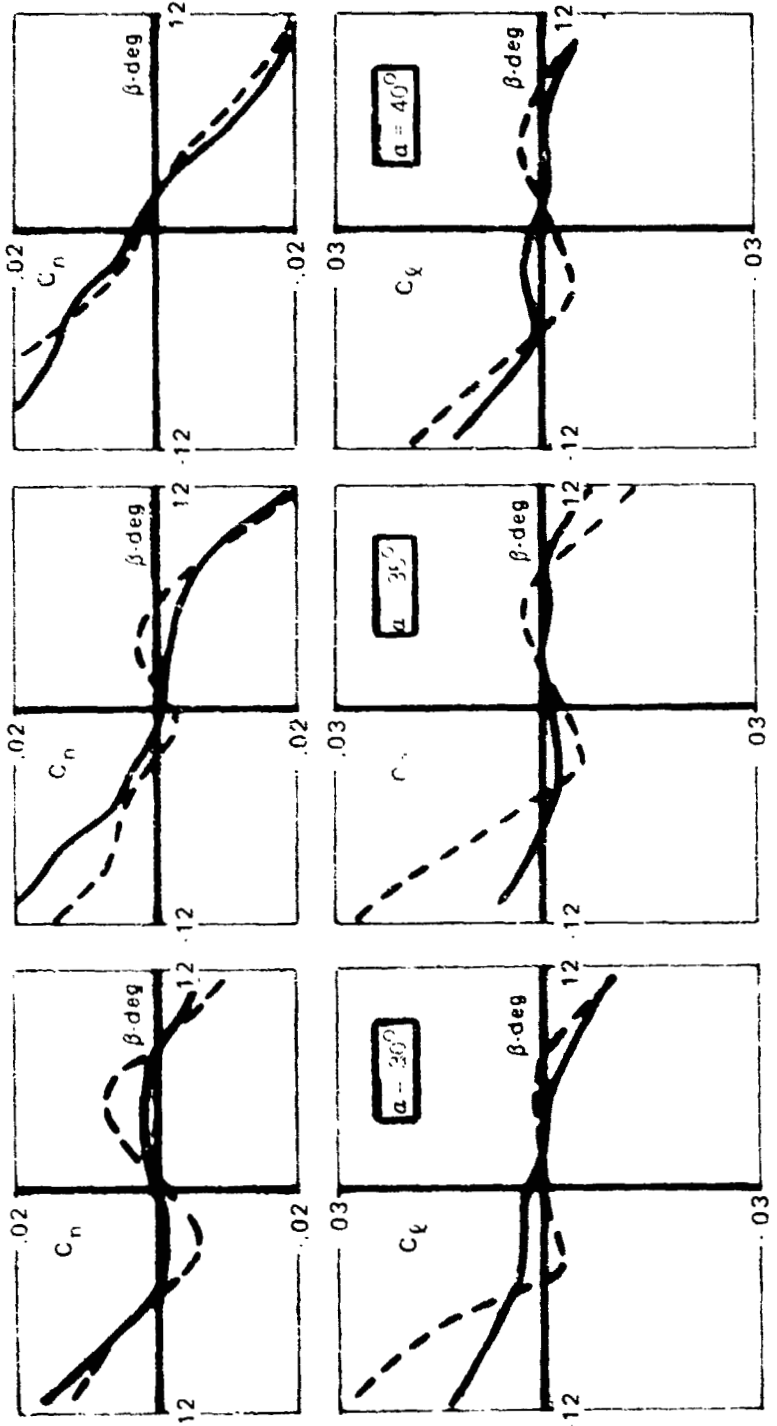


FIGURE 74. EFFECT OF LEX 10 ON ROLLING MOMENT AND YAWING MOMENT VARIATION WITH SIDESLIP; 0.16 -SCALE $F/A=18$; $b_h = 25^\circ$; $b_n = -12^\circ$; $Re_c = 1.1 (10^6)$.

ORIGINAL PAGE IS
OF POOR QUALITY

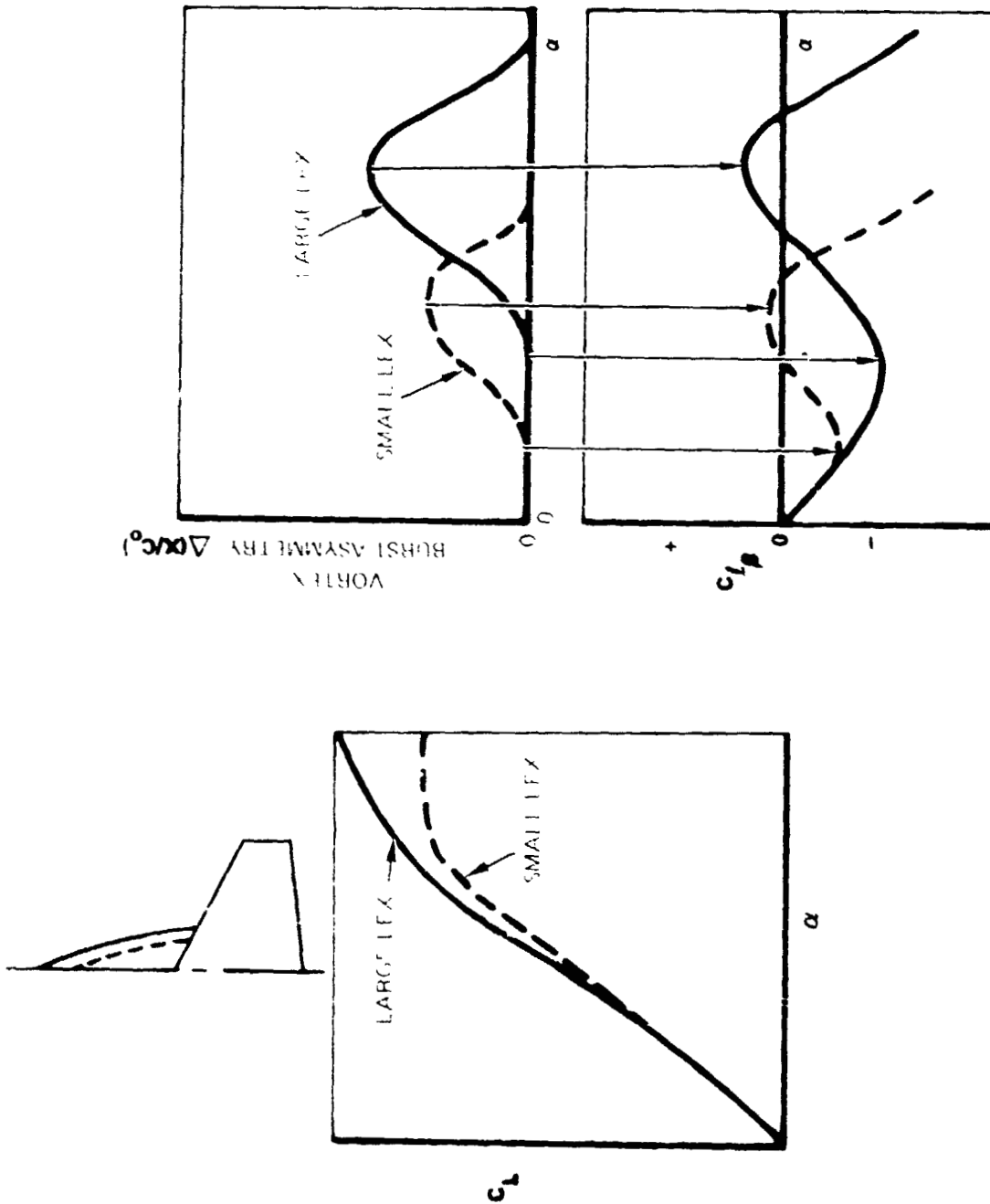


FIGURE 75. EFFECT OF LEX SIZE ON VARIATION OF LIFT, VORTEX BURST ASYMMETRY, AND LATERAL STABILITY WITH ANGLE OF ATTACK.

SN1 and SN3 snags shown in Figures 76 and 77 are flat-plate, 17% local chord extensions fairing linearly to 0% at the wing tips, positioned at 50% and 38% semi-span, respectively. The F1 and F3 upper surface fences, corresponding to the SN1 and SN3 snags, respectively, extend from the wing leading edge to the trailing-edge flap hingeline and are 8" (full-scale) in height. The favorable rolling moment increments in Figures 76 and 77 due to the snag-fence combinations can be attributed to (1) increased leading-edge camber due to the large snags extending along the deflected leading-edge flaps and (2) symmetry or LEX vortex behavior in sideslip. The latter factor is the result of the presence of upper surface fences, the greater effect of which is on the leeward LEX vortex. Water tunnel flow studies reveal a noticeable reduction in the stability of the leeward LEX vortex. The fence restricts the vortex-induced spanwise flow on the wing, shifts the vortex inboard, and promotes a forward movement of the burst position relative to the baseline configuration.

It is noted that the beneficial effects in roll of the snag (SN1) and fence (F1) combination are greater than the additive effects of a snag or fence in isolation. The data in Figure 78 indicate that the fence-alone is effective only at $\alpha = 30^\circ$. At $\alpha = 35^\circ$ and 40° the fence is submerged in the separated wing flow and, consequently, the favorable fence effects are lost. The large snag, analogous to increased leading-edge flap deflection, is favorable at all angles (see Figure 78) but with diminishing effectiveness with increased α . By reducing the separated flow region near the wing leading edge by addition of the snag, the fence is now able to effect a favorable flow field change at $\alpha = 35^\circ$ and 40° . These effects are similar to the trends associated with LEX mods (LEX 12, etc.). Extensive flow separation on the wings was shown to limit the effectiveness, in terms of improved $C_{l\beta}$, of the modifications. However, the combination of increased flap deflection and LEX mods was very effective, in general, up to and beyond stall angle of attack.

Forward LEX Slots Closed

Closure of the forward LEX boundary layer bleed slots alters the structure of the LEX vortex system but does not alter in any substantial manner the high- α characteristics. Closure of the slots produces a single primary vortex

ORIGINAL PAGE IS
OF POOR QUALITY.

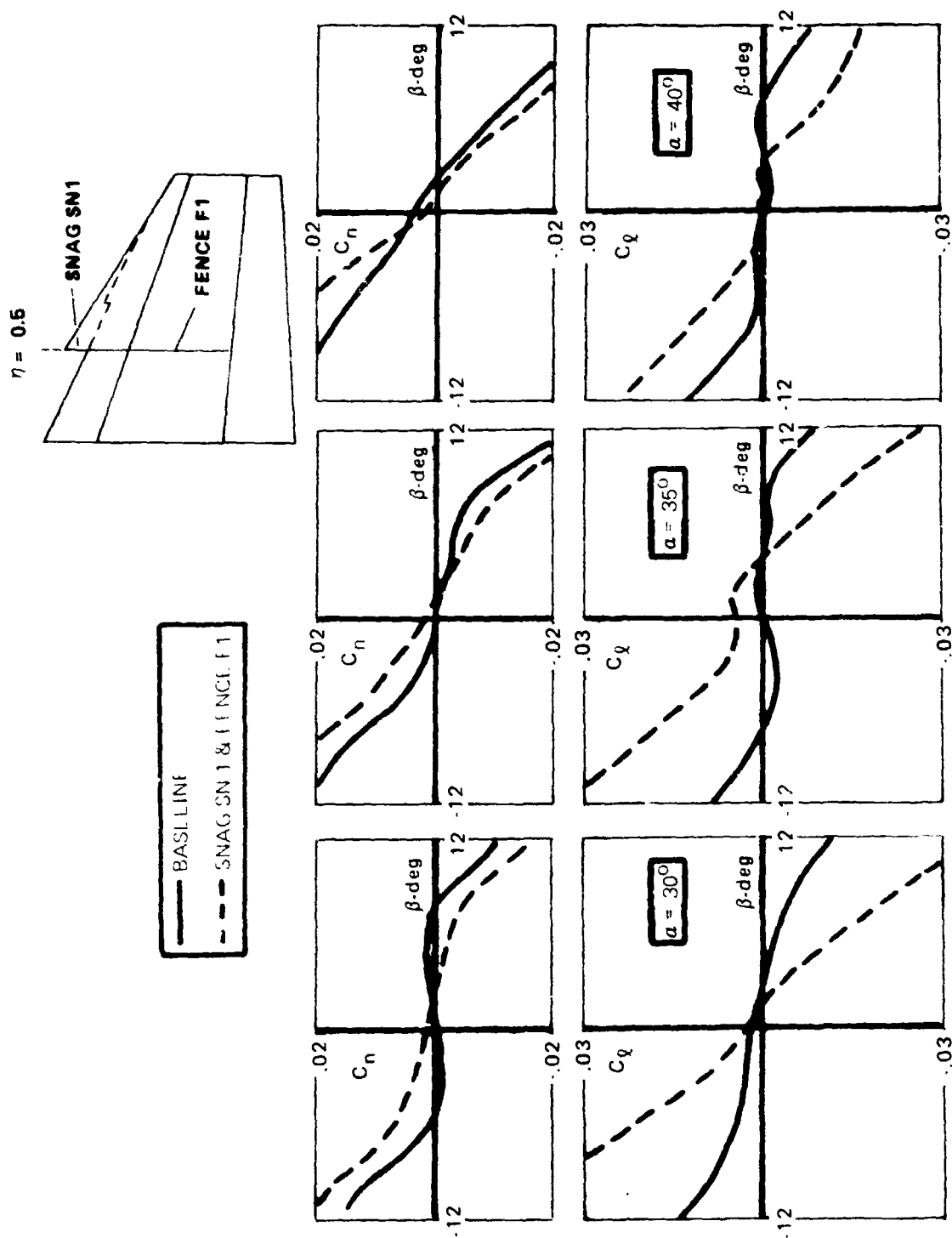


FIGURE 76. EFFECT OF SNAG AND FENCE COMBINATION ON ROLLING MOMENT
AND YAWING MOMENT VARIATION WITH SIDESLIP; 0.16-SCALE F/A-18;
 $\delta_n = 25^\circ$; $\delta_h = -12^\circ$; $Re_c = 1.1 (10^6)$.

ORIGINAL PAGE IS
OF POOR QUALITY.

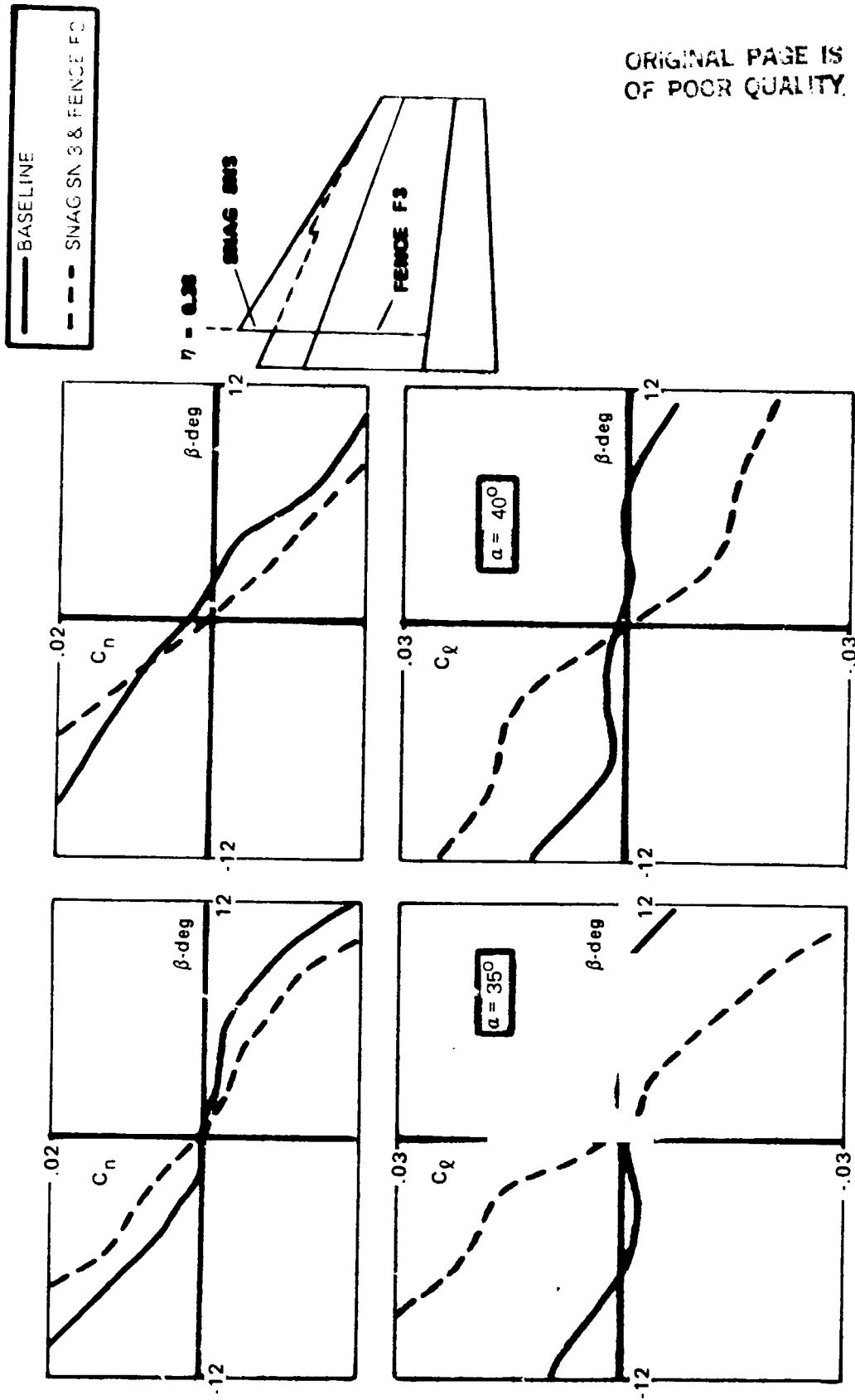


FIGURE 77. EFFECT OF SNAG AND FENCE COMBINATION ON ROLLING MOMENT
AND YAWING MOMENT VARIATION WITH SIDESLIP; 0.16-SCALE F/A-18;
 $\delta_n = 25^\circ$; $\delta_h = -12^\circ$; $Re_{\bar{c}} = 1.1 (10^6)$.

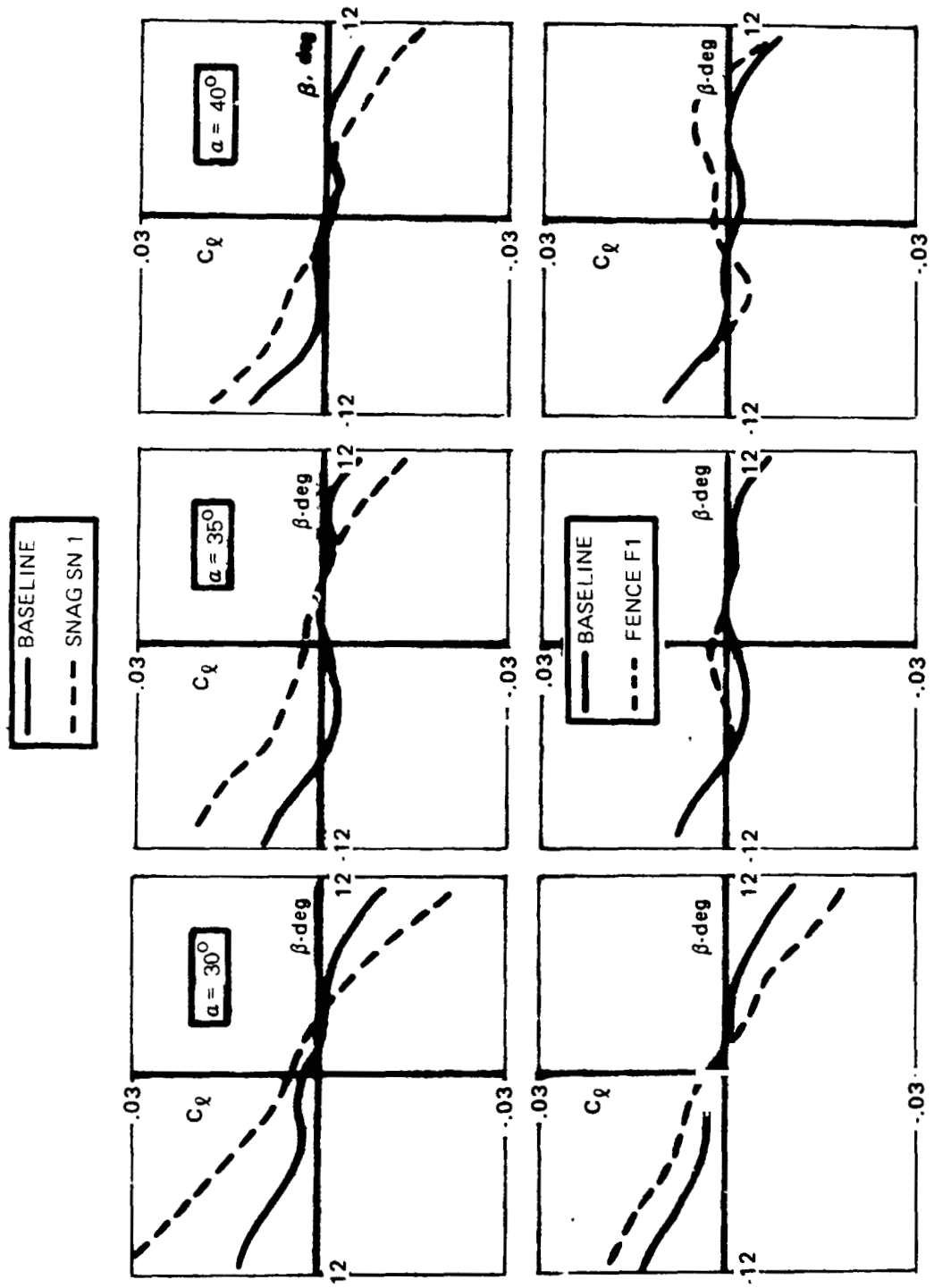


FIGURE 78. EFFECT OF SNAG AND FENCE ON ROLLING MOMENT VARIATION WITH SIDESLIP; 0.16 -SCALE $F/A-18$; $\delta_n = 25^\circ$; $\delta_h = -12^\circ$; $Re_{\bar{c}} = 1.1 (10^6)$.

rather than the two-vortex system characteristic of the slots-open case. At $\alpha = 25^\circ - 30^\circ$, slots closed actually results in a lift loss relative to the baseline as shown in Figure 79. This may be due to the greater local upwash along the LEX anex region with slots open, thereby promoting a stronger vortex system. At higher angles of attack, the slots-closed configuration exhibits more persistent vortices and, as a result, lift increases are evident at $\alpha = 35^\circ$ and 40° (with concurrent nose-up pitching moment increments (not shown)).

Water tunnel results indicated that the LEX vortices with slots closed burst in a slightly more asymmetric fashion at high α 's, thereby suggesting unfavorable rolling moment effects. The wind tunnel data shown in Figure 80 do not, in general, bear this out. Comparison with baseline results reveals little changes in C_L and C_n variation with β associated with slot closure at $\alpha = 30^\circ - 40^\circ$.

Forebody Strakes (Radial Location: $+40^\circ$)

F/A-18 modifications discussed to this point have featured changes to the LEX or wing geometry which directly affect the LEX vortex and wing flow behavior. The forebody vortex system is also affected in an indirect manner due to changes in LEX vortex path and stability characteristics and changes in the wing pressure field. The interaction of the forebody vortices with the LEX-wing flow field is a potential source of significant lateral stability effects. The strengths and trajectories of the body vortices can, under certain conditions, play a prominent role in the stall characteristics of the wings. The modifications to be discussed in the following sections describe the effects associated with thin, highly-swept surfaces positioned along the radome, i.e. forebody strakes. It will be shown that the forebody vortices can be a key to understanding the complex nature of the F/A-18 flow field at high α 's.

Strakes of approximately 55-inch length and 2.34-inch maximum height (full-scale dimensions) were mounted along the forebody at 40° above the maximum half breadth. Strakes mounted in this manner produce insignificant changes in the variation of normal force coefficient with sideslip at $\alpha = 30^\circ$ to 40° , as depicted in Figure 81. Water tunnel flow visualization

ORIGINAL PAGE IS
OF POOR QUALITY

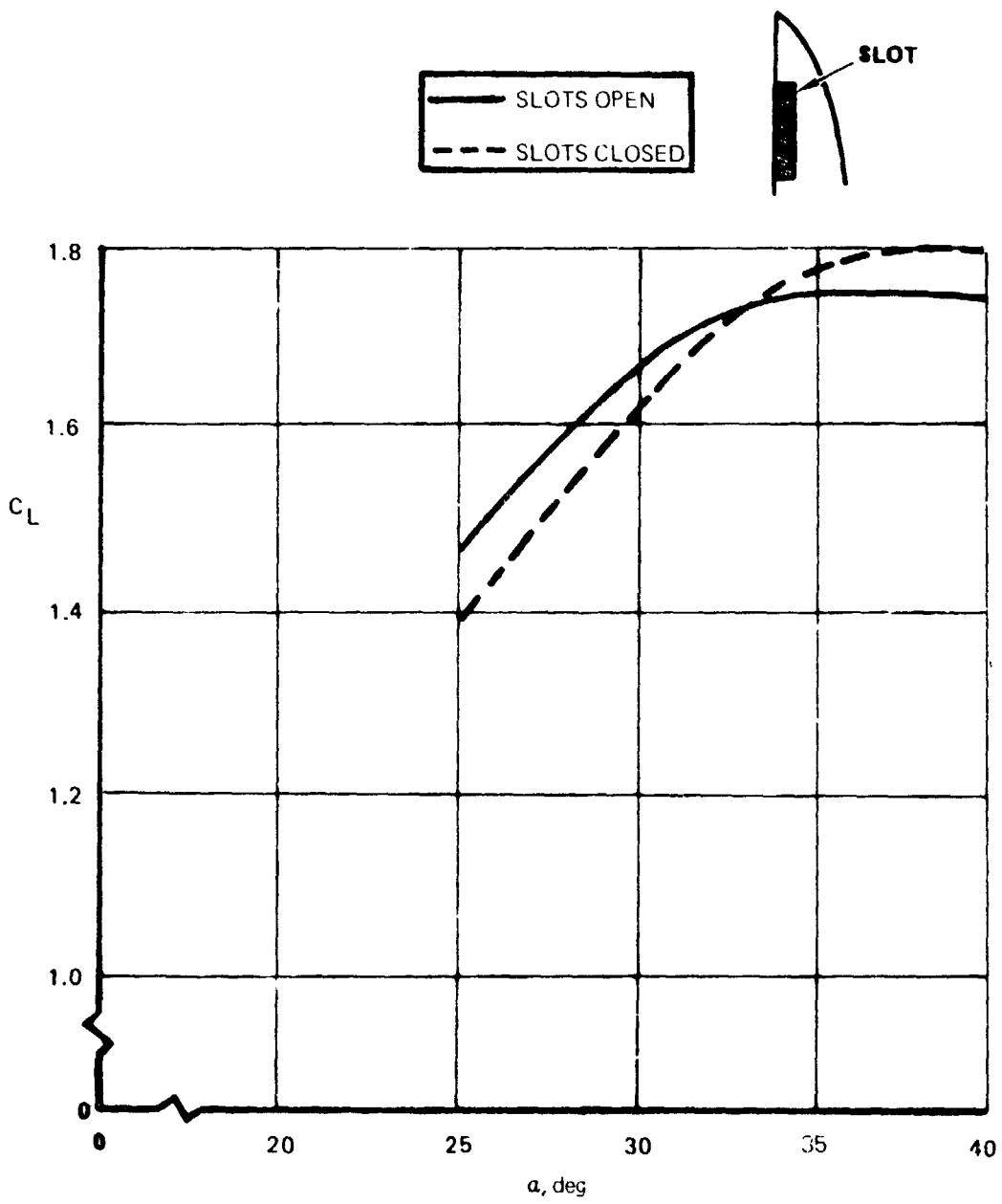


FIGURE 79. EFFECT OF FORWARD SLOT CLOSURE ON LIFT COEFFICIENT;
0.16-SCALE F/A-18; $\delta_n = 35^\circ$; $\delta_h = -12^\circ$; $Re_c = 1.1 (10^6)$.

ORIGINAL PAGE IS
OF POOR QUALITY

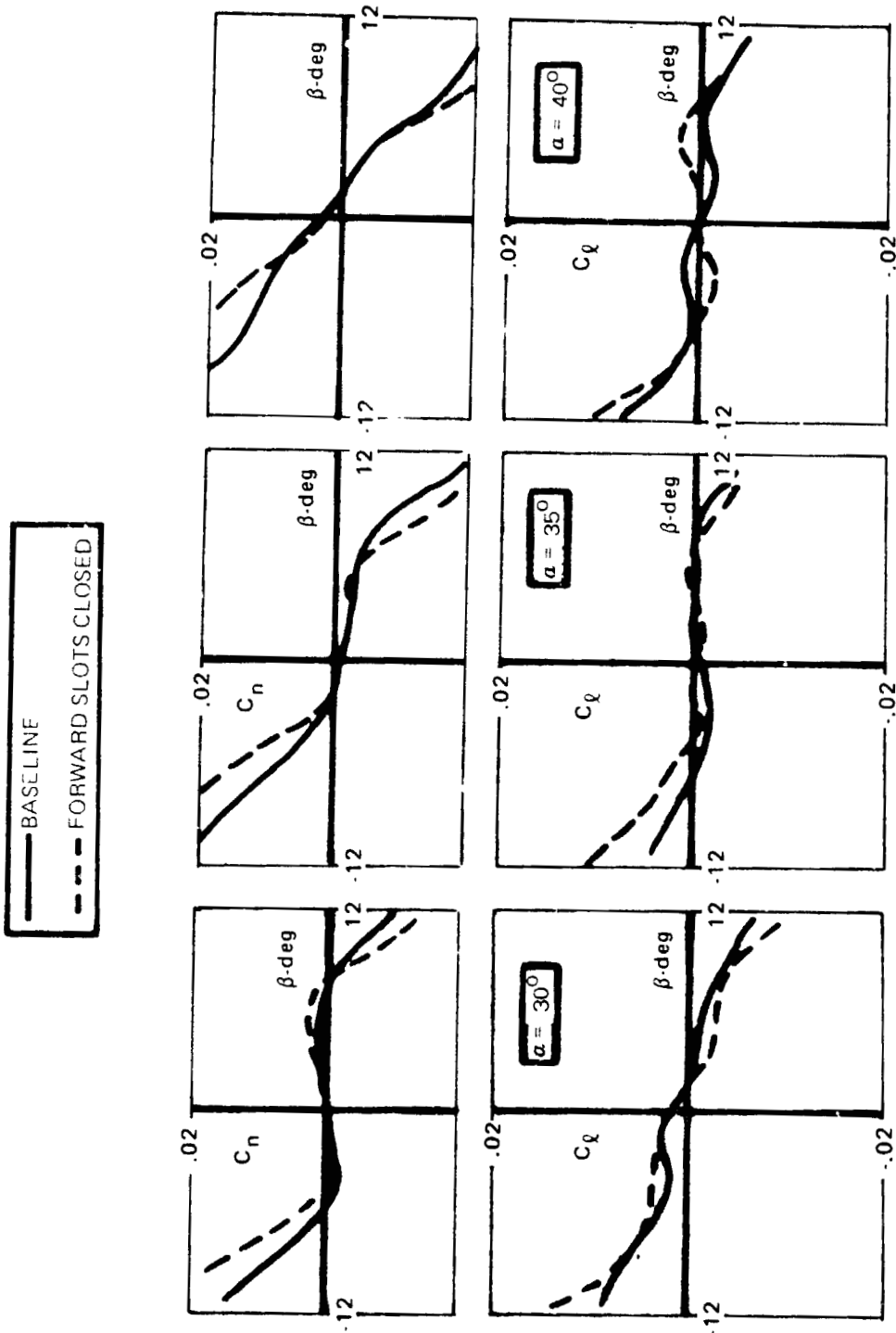


FIGURE 80. EFFECT OF FORWARD SLOT CLOSURE ON ROLLING MOMENT
AND YAWING MOMENT VARIATION WITH SIDESLIP; 0.16-SCALE F/A-18;
 $\delta_n = 25^\circ$; $\delta_h = -12^\circ$; $Re_{\bar{c}} = 1.1 (10^6)$.

BASELINE NOSE STRAKES	
α , DEG	α , DEG
—	35
- - -	35
.....	40

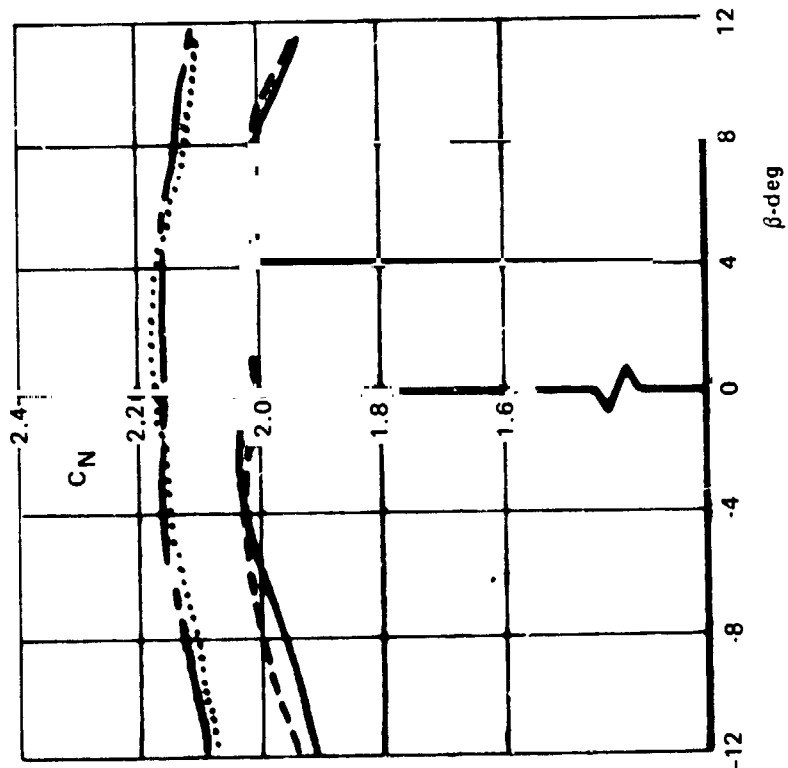
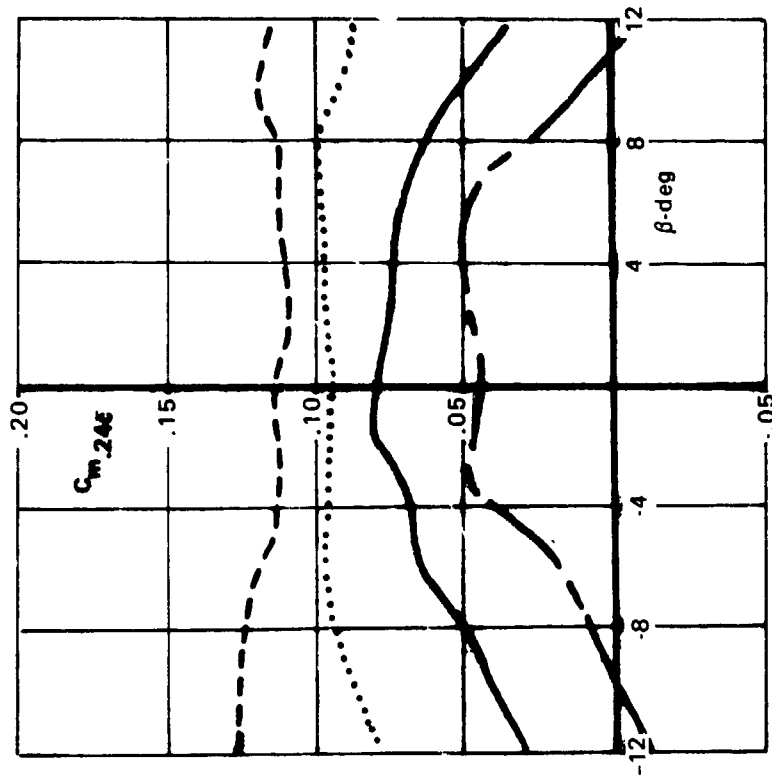


FIGURE 81. EFFECT OF FOREBODY STRAKES ($\phi = 40^\circ$) ON NORMAL FORCE AND PITCHING MOMENT VARIATIONS WITH SIDESLIP; 0.16-SCALE F/A-18; $\delta_n = 25^\circ$; $\delta_h = -12^\circ$; $Re_c = 1.1 (10^6)$.

results suggested that the strakes increased the body vortex strengths and, hence, body normal force. The incremental body vortex strength induces a corresponding downwash increment on the wings, however, thereby resulting in negligible effect on net normal force. Evident in Figure 81, however, are nose-up pitching moment increments, which reflect the long moment arm of the strake lift.

Examination of the baseline and nose strake C_L vs. α curves in Figure 82 indicates that maximum lift and stall angle of attack are essentially the same.

The wind tunnel results in Figure 83 indicate that the nose strakes induce large stable rolling moment increments at $\alpha = 35^\circ$ and 40° and promote a more linear variation of C_l with β . The F/A-18 baseline configuration is characterized by a strongly asymmetric forebody vortex orientation in sideslip: the leeward body vortex is entrained into the leeward LEX vortical flow while the windward body vortex is relatively uncoupled. The body primary vortex paths with nose strakes on, however, are extremely resistant to this asymmetric orientation in sideslip. Water tunnel and wind tunnel flow visualization have confirmed that the forebody vortices exhibit a mutual interaction such that the primary vortex-induced effects are experienced on the windward wing. As a consequence, stall of the latter is delayed while premature stall of the leeward wing is promoted. These results confirm that under certain flow conditions the forebody vortices can interact in a highly-favorable manner with the wing flow.

As sideslip angle is increased, test results in Figure 83 indicate reduced strake effectiveness. At the higher sideslip angles the water tunnel flow surveys revealed forebody primary boundary layer separation line rotation to such an extent that the strakes are less able to induce symmetric vortex shedding along the nose region. The wind tunnel data in Figure 83 exhibit a corresponding reduction in local slopes ($C_{l\beta}$) at the higher sideslip angles.

Increasing the length of the strakes produces a somewhat more stable variation of rolling moment with sideslip. Results at $\alpha = 40^\circ$ are shown

ORIGINAL PAGE IS
OF POOR QUALITY

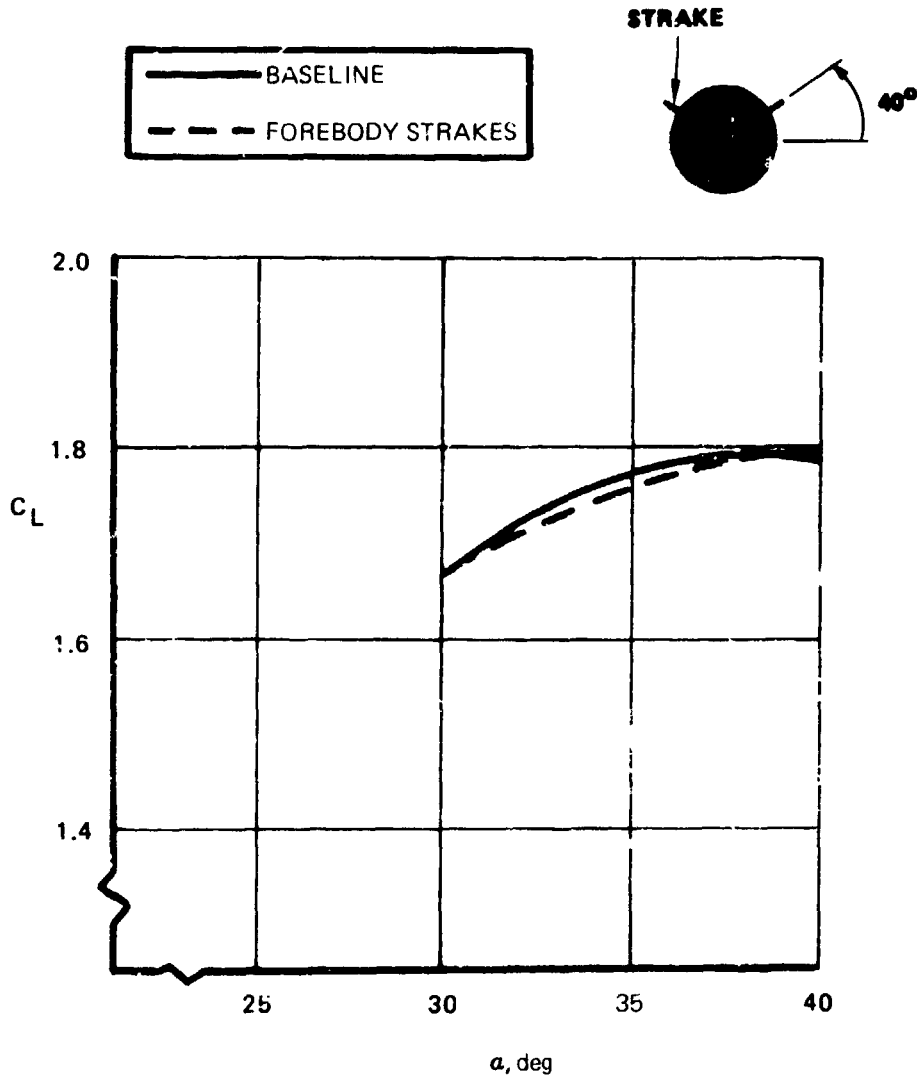
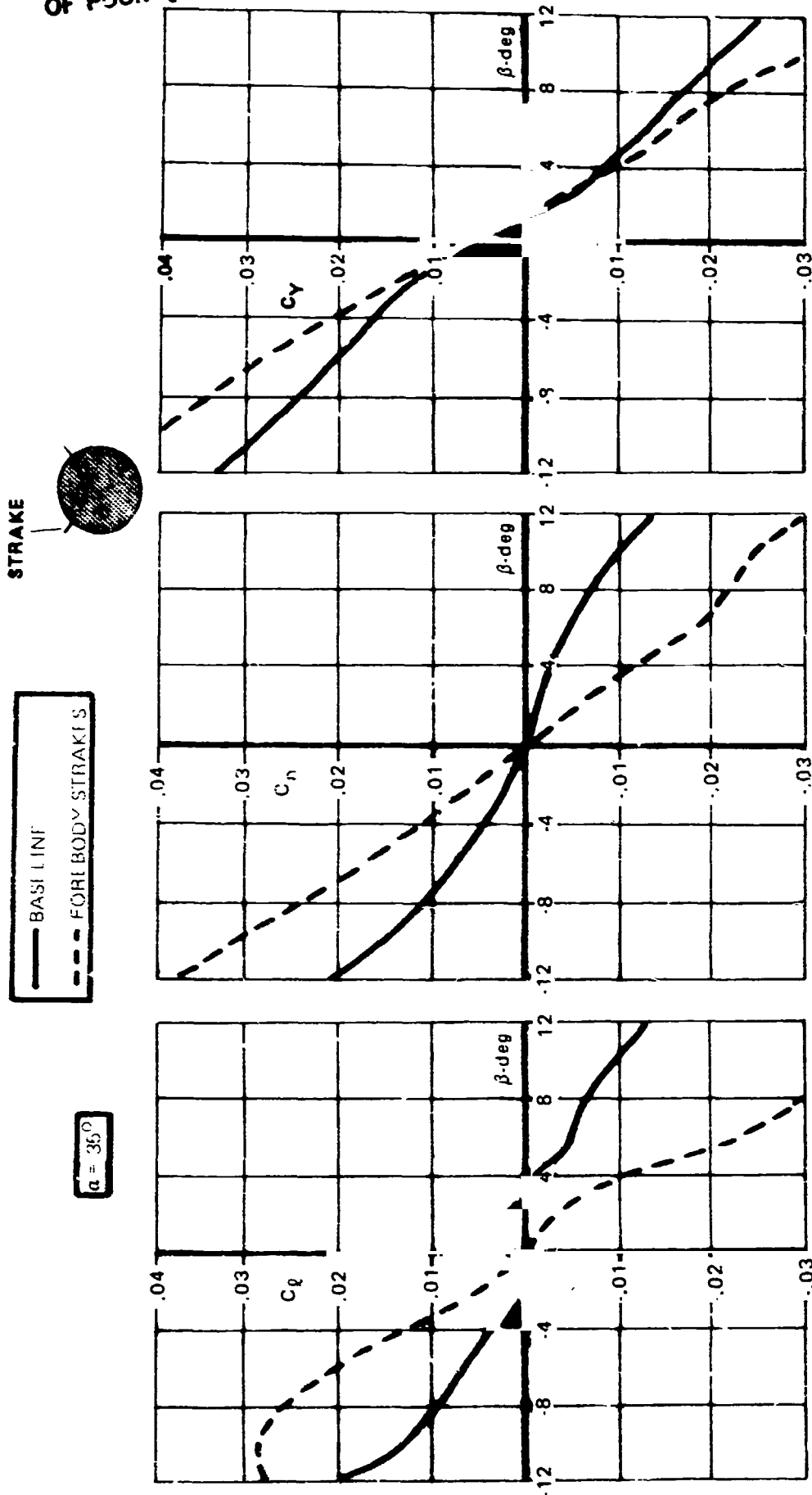


FIGURE 82. EFFECT OF FOREBODY STRAKES ($\phi = 40^\circ$) ON LIFT COEFFICIENT;
0.16-SCALE F/A-18; $\delta_n = 35^\circ$; $\delta_h = -12^\circ$; $Re_{\bar{c}} = 1.1 (10^6)$.

ORIGINAL PAGE IS
OF POOR QUALITY



(A) $\alpha = 35$ DEGREES

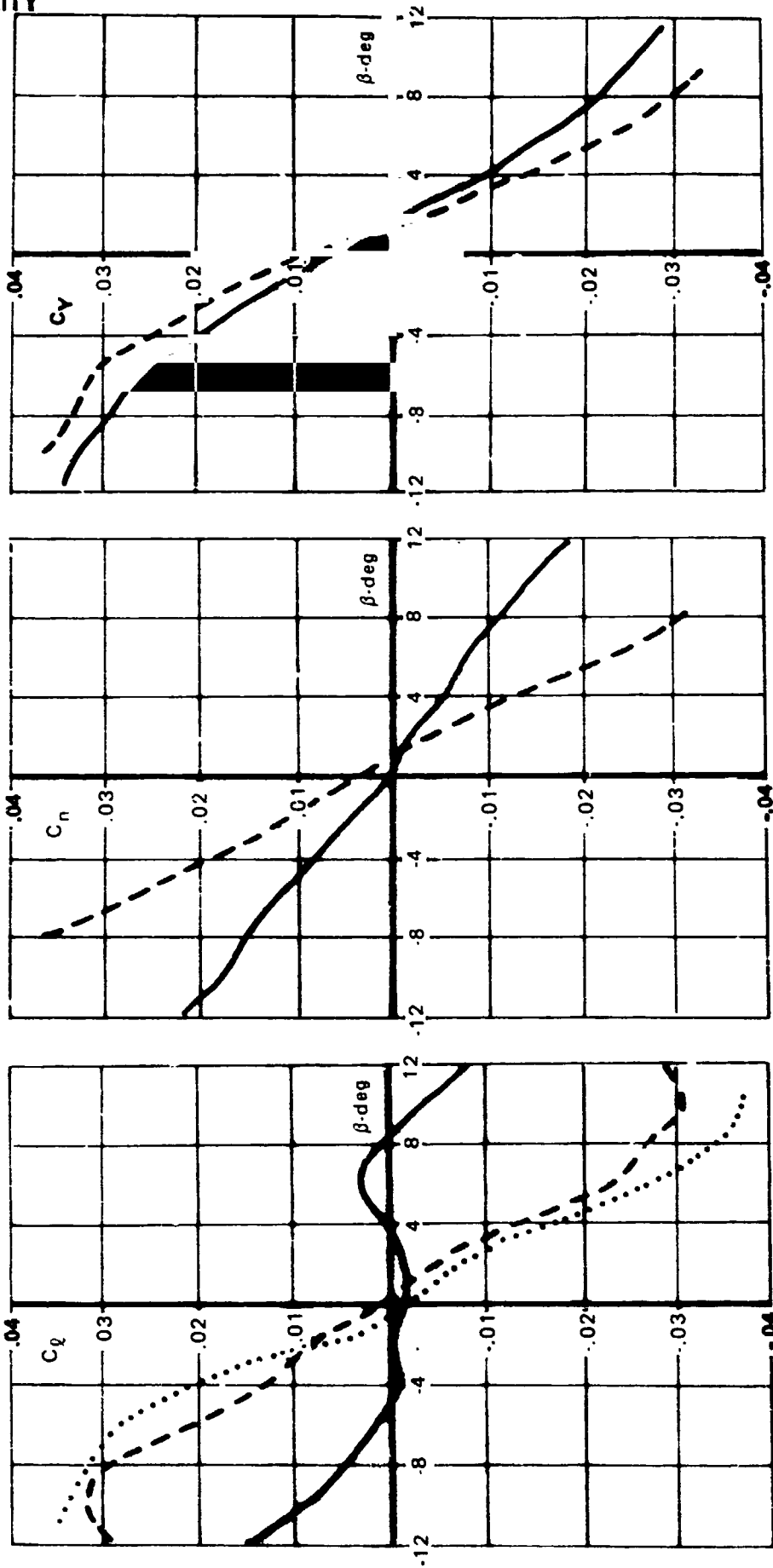
FIGURE 83. EFFECT OF FOREBODY STRAKES ($\psi = 40^\circ$) ON ROLLING MOMENT, YAWING MOMENT, AND SIDE FORCE COEFFICIENT WITH SIDESLIP; 0.16-SCALE F/A-18; $\delta_n = 35^\circ$; $\delta_h = -12^\circ$; $Re_c = 1.1 (10^6)$.

ORIGINAL PAGE IS
OF POOR QUALITY



——— BASELINE
 - - - FOREBODY STRAKES
 INCREASED STRAKE LENGTH

$\alpha = 40^\circ$



(B) $\alpha = 40$ DEGREES

FIGURE 83. CONCLUDED.

in Figure 83. Comparison of the long- and short-strake data indicate, however, the significance of the forward portion of the strakes. That is, affecting the initial body vortex development is a critical factor.

Concurrent with the beneficial strake effects on rolling moment are destabilizing yawing moment increments, shown also in Figure 83. The leeward strake vortex induces very low local pressures and can be perceived as a fluid boundary layer control device which delays boundary layer separation on the leeward fuselage side. This is depicted in the sketch in Figure 84. Without the strake, the primary boundary layer separates below the maximum half breadth. The increased suction pressures due to strake-induced attached flow along the leeward fuselage side result in unstable yawing moment increments. The sign of the side force coefficient increments in Figures 83 and 84 due to the strakes is consistent with increased suction pressures on the leeward forebody surface.

Forebody Strakes (Radial Location: $+60^\circ$)

The data in Figure 85 show that radome strakes located at $\phi = +60^\circ$ result in, relative to the $\phi = +40^\circ$ case, increasingly stable variation of rolling moment with sideslip at small sideslip angles. Within the approximate range $-4^\circ < \beta < 4^\circ$, the strakes increase the strong mutual interaction of the body vortices with a corresponding increase in the favorable vortex-induced effects on the windward wing panel. Strake effectiveness drops off rapidly, however, at higher sideslip angles due to rotation of the boundary layer separation lines. In brief, the higher strake position compresses the sideslip range within which symmetric (or nearly so) vortex development near the nose can be achieved.

Forebody Strakes (Radial Location: $+30^\circ$)

The effectiveness with which the strakes promote a discrete pair of body vortices which are less prone to asymmetry in sideslip is highly sensitive to strake radial position. With $\phi = +30^\circ$ much of the beneficial strake effect on lateral stability is lost, as shown in Figure 86 at $\alpha = 35^\circ$ and 40° . The results in Figure 86 suggest an approximate band of strake radial positions

ORIGINAL PAGE IS
OF POOR QUALITY

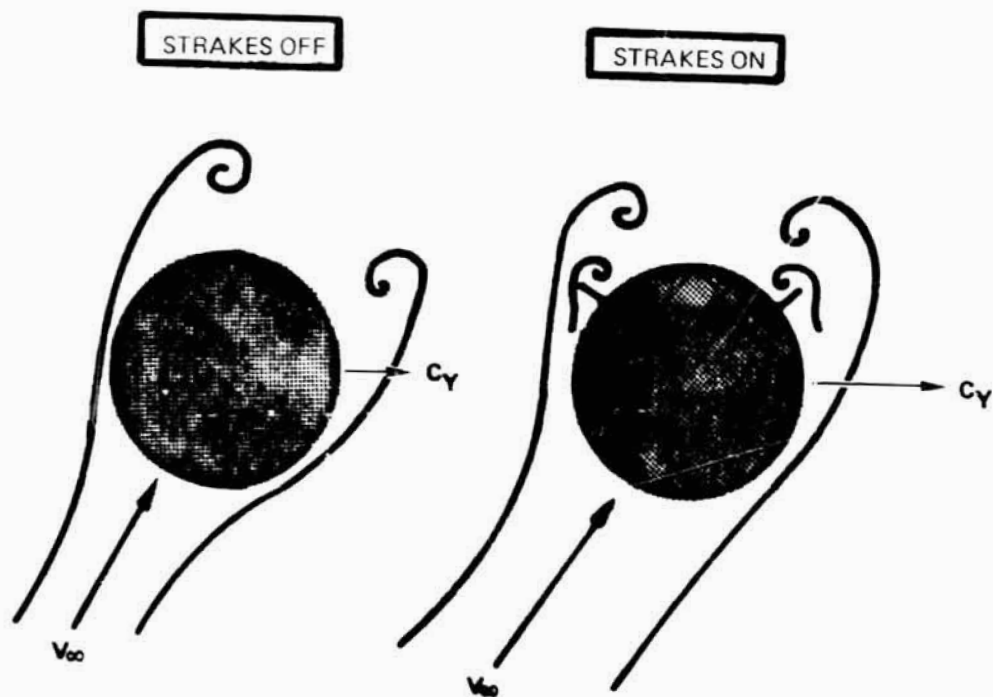


FIGURE 84. SKETCH OF FOREBODY STRAKE EFFECT ON BODY VORTEX BEHAVIOR.

ORIGINAL PAGE IS
OF POOR QUALITY

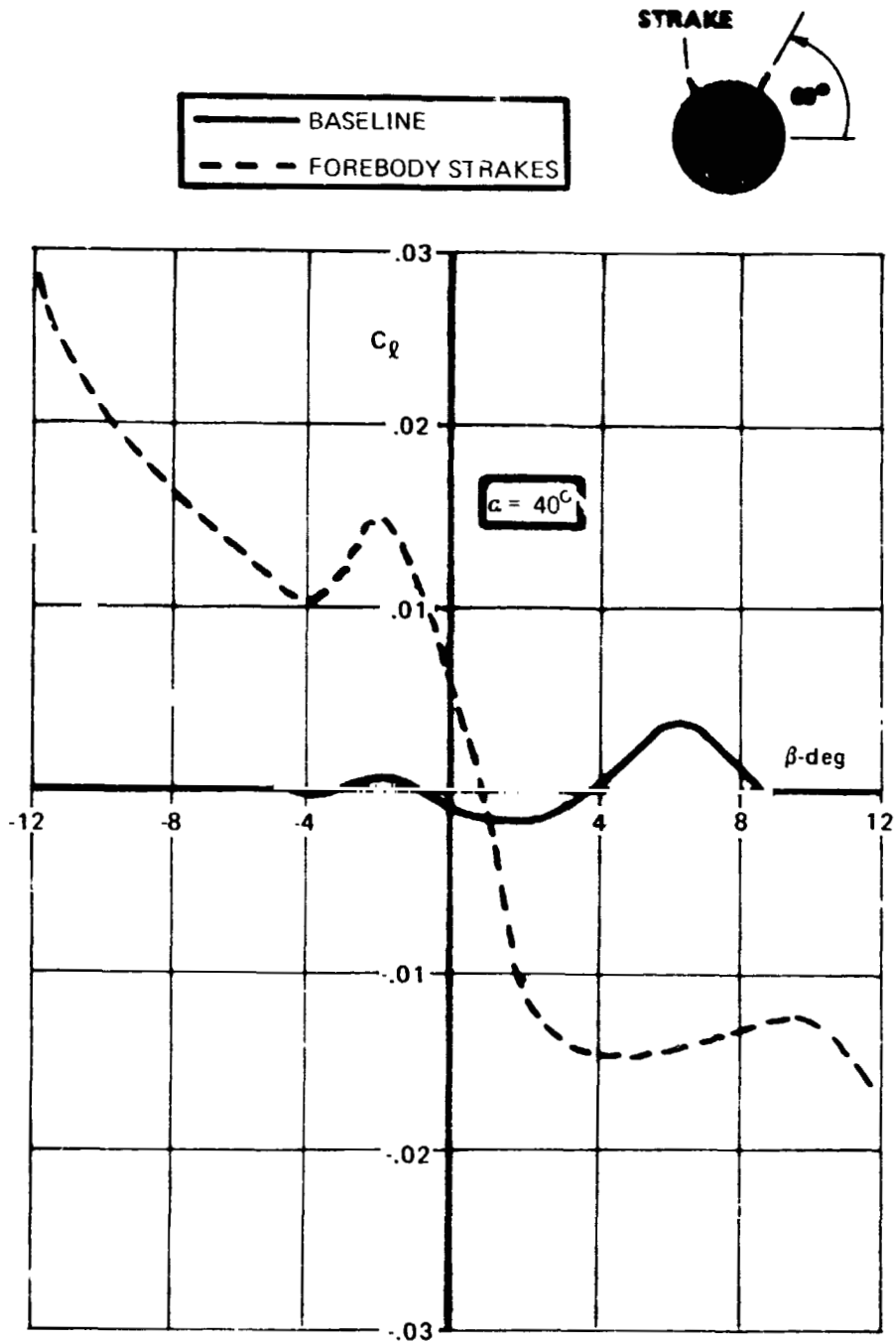
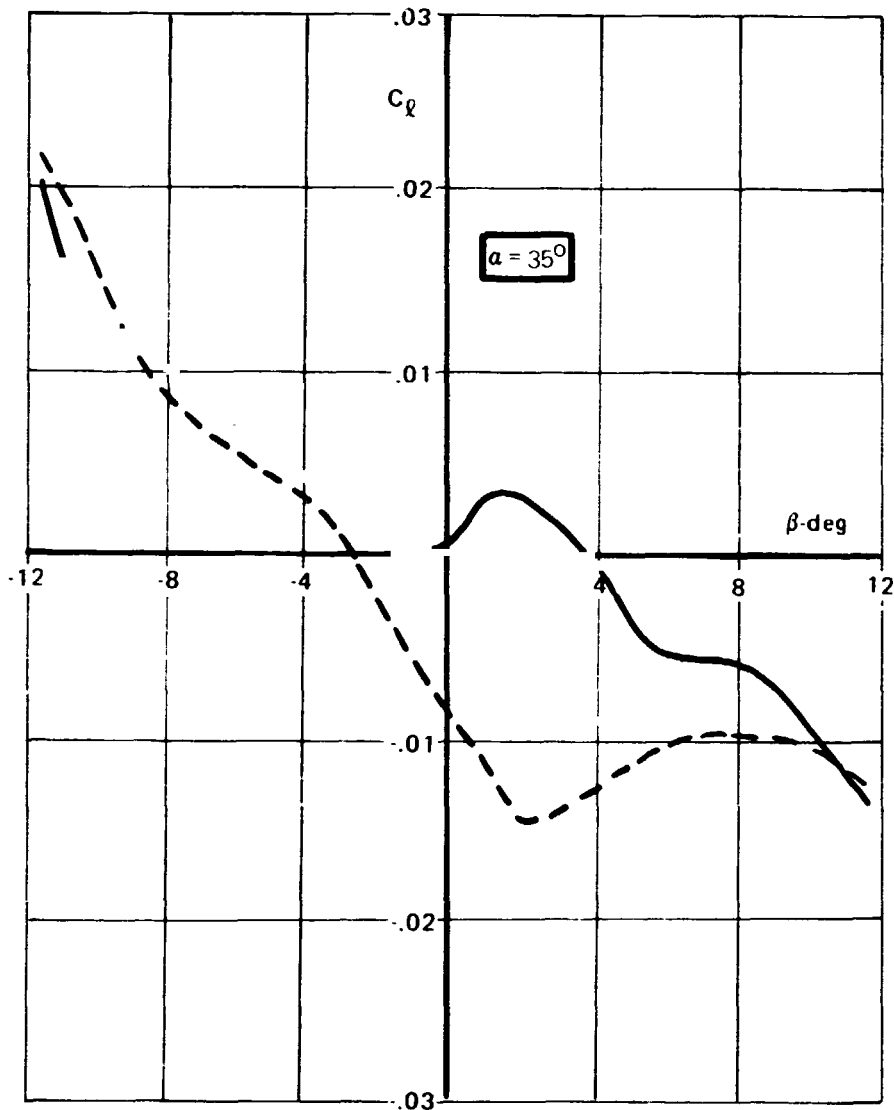
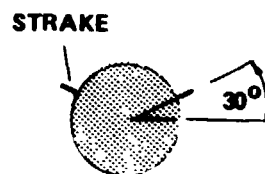
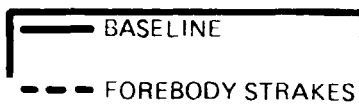


FIGURE 85. EFFECT OF FOREBODY STRAKES ($\phi = 60^\circ$) ON ROLLING MOMENT VARIATION WITH SIDESLIP; 0.16-SCALE F/A-18; $\delta_n = 35^\circ$; $\delta_h = -12^\circ$; $Re_c = 1.1 (10^6)$.

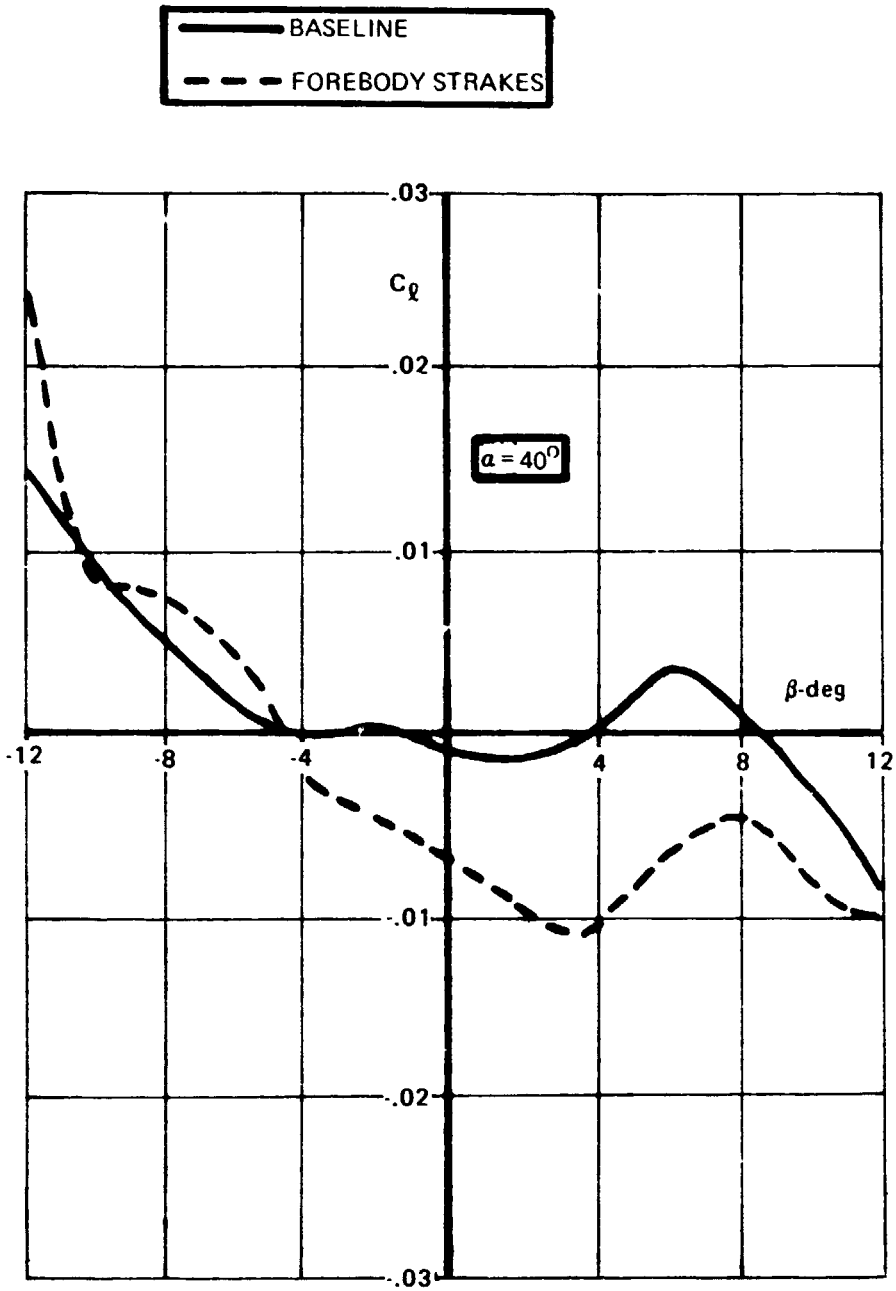
ORIGINAL POINTS
OF POOR QUALITY



(A) $\alpha = 35$ DEGREES

FIGURE 86. EFFECT OF FOREBODY STRAKES ($\phi = 30^\circ$) ON ROLLING MOMENT VARIATION WITH SIDESLIP; 0.16-SCALE F/A-18; $\delta_n = 35^\circ$; $\delta_h = -12^\circ$; $Re_c = 1.1 (10^6)$.

ORIGINAL PAGE IS
OF POOR QUALITY



(2) $\alpha = 40^\circ$

FIGURE 86. CONCLUDED.

above the maximum half breadth line within which favorable lateral stability effects are achieved: $30^\circ \leq \phi \leq 60^\circ$.

Forebody Strakes (Radial Location: 0°)

Strakes located along the MHB, approximately 80" in length and 3" maximum width (full-scale dimensions) are generally destabilizing in roll, as shown in Figure 87 at $\alpha = 35^\circ$ and 40° . Water tunnel flow visualization tests revealed a disruption of the forebody vortex flow field due to strakes mounted in this manner. The strakes presented a discontinuity in the body vortex-feeding mechanism and the strakes shed a wake-like, rather than vortex, flow which impeded the development of a body primary vortex pair.

The highly nonlinear rolling moment variation with sideslip in Figure 87 (unstable slope at small β 's; stable slope at higher β 's) is similar to the C_l vs. β variation at high angle of attack on a slender wing. Vortex burst asymmetry is the source of such variations on a cranked wing, for example. Water tunnel flow surveys of the $\phi = 0^\circ$ strake position were inconclusive however, due to the diffuse nature of the body flow field.

Nose strakes along the maximum half-breadth have generally been applied to improve directional stability, utilizing the windward strake flow to generate stable yawing moment increments. Accordingly, the wind tunnel test results in Figure 87 show a stabilizing nose-strake contribution to yawing moment at $\alpha = 35^\circ$ and 40° .

Forebody Strakes (Radial Locations: -15° and -30°)

Radome strakes positioned 15° below the MHB ($\phi = -15^\circ$) generally show no improvement in high angle-of-attack rolling moment characteristics. As shown in Figure 88, however, radome strakes at $\phi = -30^\circ$ provide a lateral stability increase at $\alpha = 40^\circ$, for example. Since the flow mechanism associated with strakes mounted in this manner is expected to differ from the top-mounted strake positions, a more detailed discussion is presented below.

ORIGINAL PAGE IS
OF POOR QUALITY

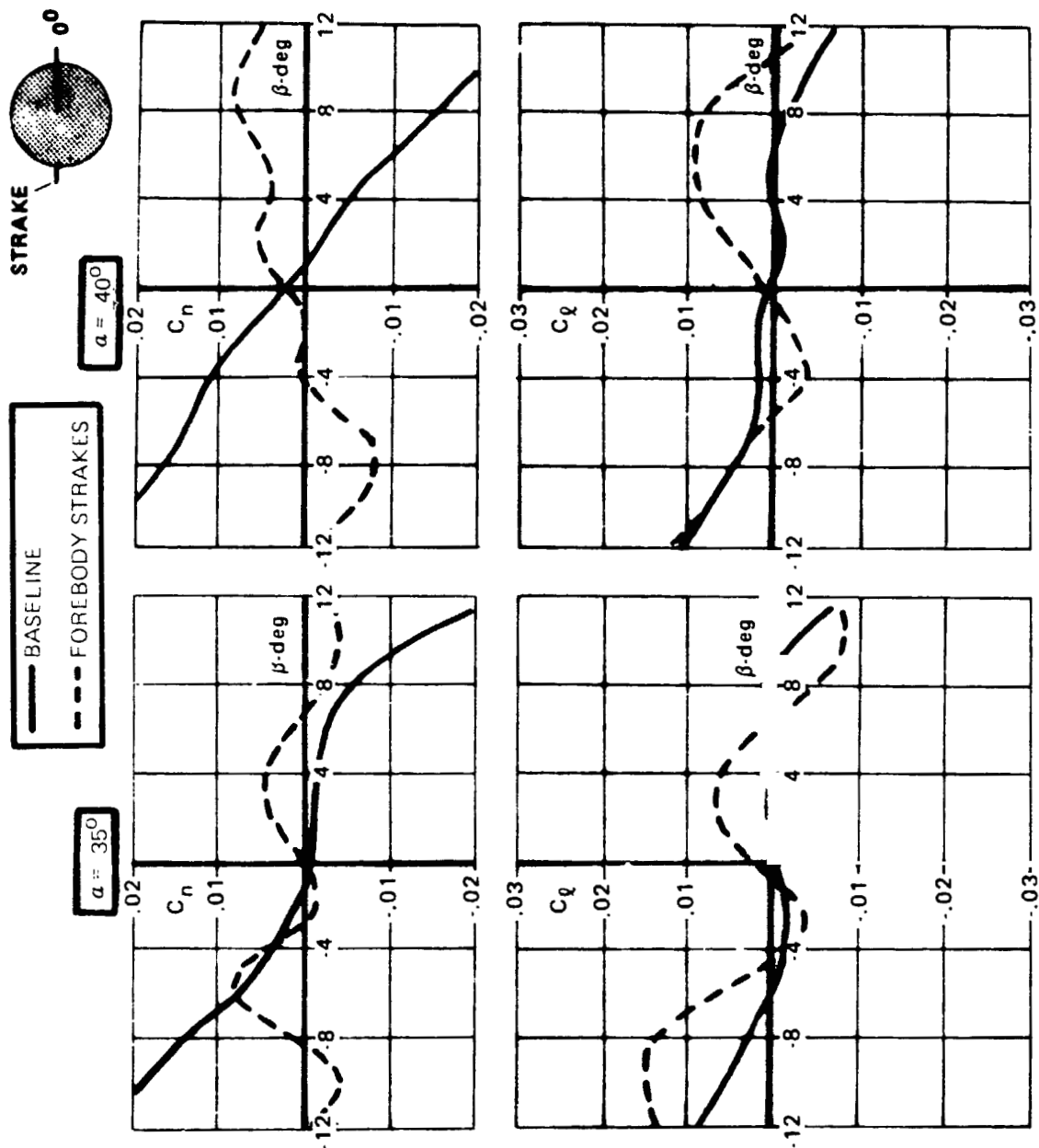
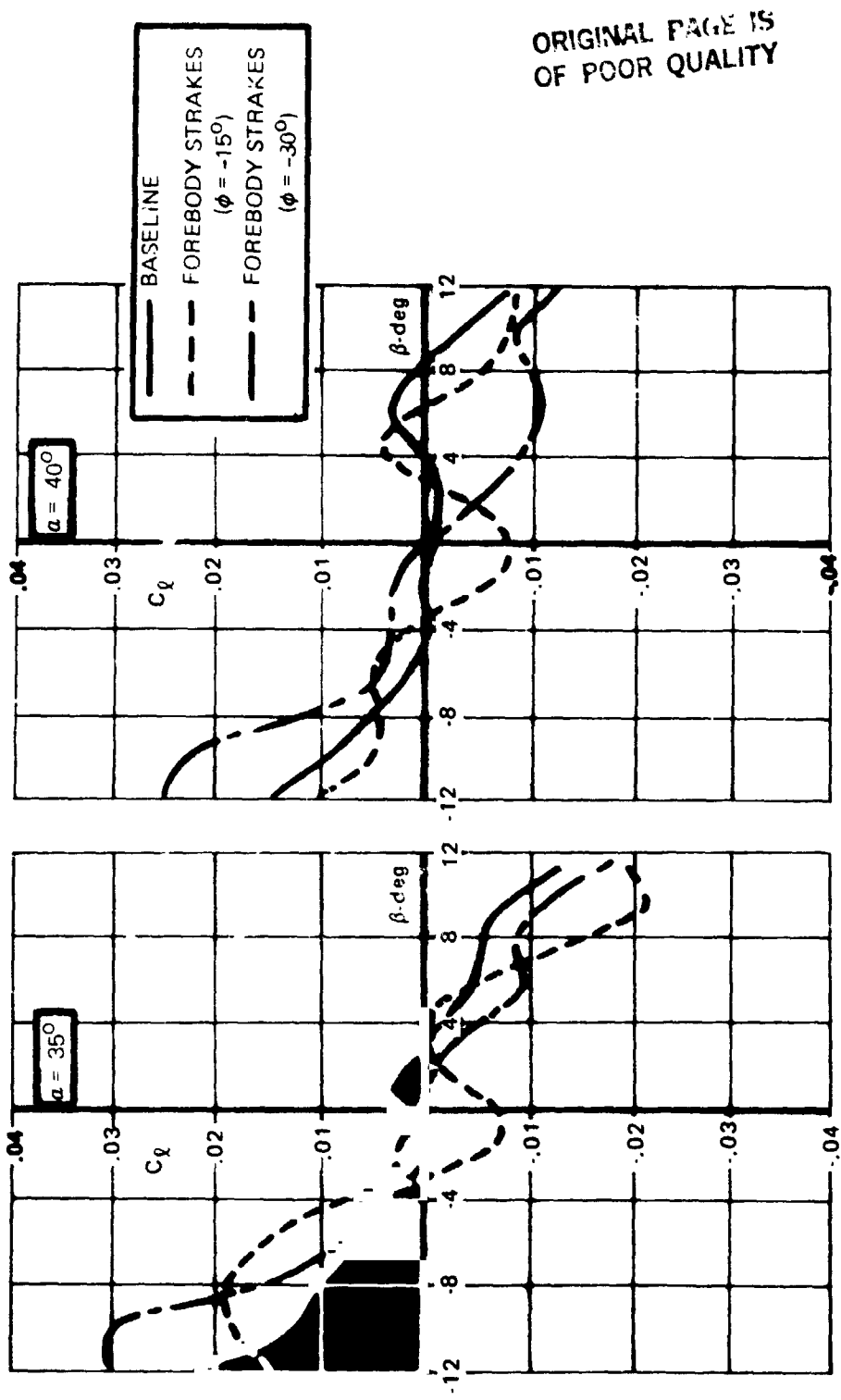


FIGURE 37. EFFECT OF FOREBODY STRAKES ($\phi = 0^\circ$) ON ROLLING MOMENT AND YAWING MOMENT VARIATION WITH SIDESLIP; 0.16-SCALE F/A-18; $\delta_n = 25^\circ$; $\delta_h = -12^\circ$; $Re_c = 1.1 (10^6)$.



ORIGINAL PAGE IS
OF POOR QUALITY

FIGURE 88. EFFECT OF FOREBODY STRAKES ($\phi = -15^\circ, -30^\circ$) ON ROLLING MOMENT VARIATION WITH SIDESLIP; 0.16 -SCALE $F/A-18$; $\delta_h = 35^\circ$; $\delta_n = -12^\circ$; $Re_{\bar{c}} = 1.1 (10^6)$.

Forebody Strakes (Radial Location: -45°)

Strakes S45, S47, and S48, characterized by lengths of approximately 164", 102", and 56" (full-scale), respectively, were mounted along the 0.16-scale model forebody at 45° below the MHB. Each strake was 3.13" (full-scale) maximum width tapering to zero at the nose.

The wind tunnel results in Figure 89 show large increases in lateral stability at high angle of attack (Note: $\alpha=40^\circ$, $\delta_n=40^\circ$), particularly for the longer strake lengths. Results at negative sideslip show little effect due to the S48 strake, yet at positive sideslip angles the same strakes induce a highly-stable variation of rolling moment with sideslip. Factors such as strake geometry and position asymmetries and different primary boundary layer separation characteristics aft of the short strakes are possible sources of the anomaly.

Visualization studies in the water tunnel suggested a plausible flow mechanism associated with the given strakes. The strake vortices are of sufficient strength to induce flow reattachment above the strakes. As a result, the body primary vortex pair tends to develop in a more symmetric manner in sideslip. The flow studies revealed a weakening of the body primary vortices relative to the $\phi = +40^\circ$ case since the strakes promote a discontinuous boundary layer separation line pattern. Although the strake vortices do not feed directly into the body primaries, the strakes serve much the same purpose in limiting the rotation of the separation lines in sideslip. At higher sideslip angles, the leeward strake appears to shed a wake instead of a discrete vortex. Consequently, the flow mechanism described above begins to break down with a resulting unstable variation of rolling moment with sideslip.

The increase in directional instability at high angles of attack is associated with the increased suction pressures along the leeward fuselage side, in much the same manner as the $\phi = +40^\circ$ case.

In summary, water tunnel flow visualization and wind tunnel test data analyses indicate that the flow mechanisms and effects on high- α lateral-

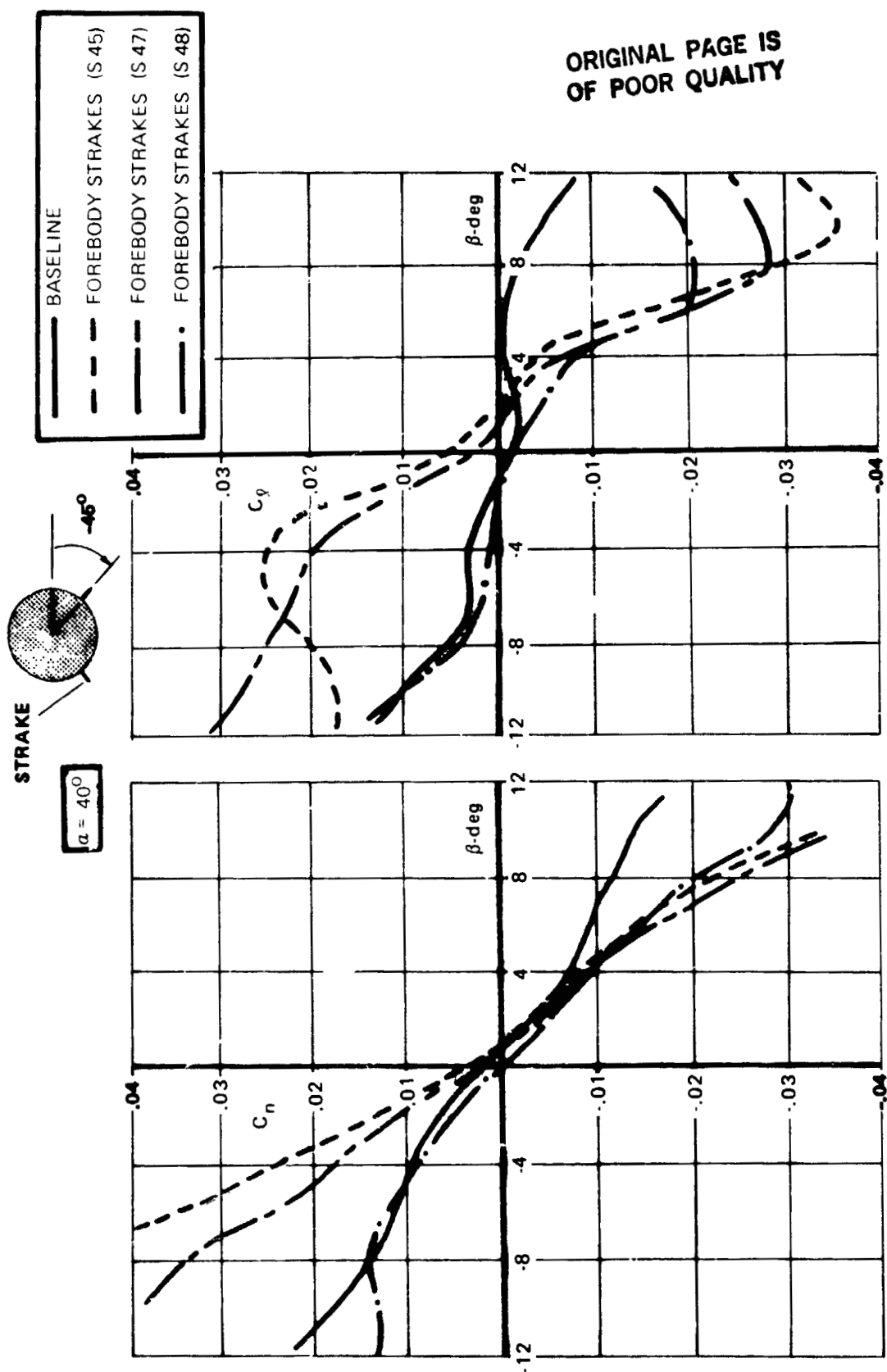


FIGURE 89. EFFECTS OF FOREBODY STRAKES ($\phi = -45^\circ$) AND STRAKE LENGTH ON ROLLING MOMENT AND YAWING MOMENT VARIATION WITH SIDESLIP;
 $\delta_n = 40^\circ$; $\delta_h = -12^\circ$; $Re_c = 1.1 (10^6)$.

directional stability of forebody strakes are dependent on strake radial location and, to a somewhat lesser degree, on strake length. In terms of lateral stability improvements, locating the radome strakes in a region of low local angle of attack, at $\phi = +40^\circ$ or $\phi = -45^\circ$, for example, is an effective means of generating discrete strake vortices which serve to enhance the body vortex strengths and/or limit the change in body vortex core paths due to sideslip. Strakes mounted at the MHB are immersed in a higher local angle of attack flow. The strake vortices are, therefore, less stable at high α 's and, in general, promote a less-defined forebody flow field.

It should be noted that, in an overall assessment, the strake-induced lateral stability improvements may be overridden by the concurrent yaw instability at high α 's. In addition, excessive lateral stability is undesirable since the aircraft will be sluggish to control input. Possible degradation of radar performance and ingestion of the strake vortices into engine inlets (at low α 's) are additional considerations.

Flight Test Nose Boom

Low-speed wind tunnel test results at $\alpha = 35^\circ$ obtained on the 0.16-scale F/A-18 model with flight test nose boom, shown in Figure 90, reveal small unstable effects in roll at small sideslip relative to the baseline. Water tunnel flow visualization indicated that the wake shed by the nose boom impeded the formation of the body primary vortices, although the vortex orientation relative to the baseline appeared not to be affected.

Flight Test Nose Boom and Forebody Strakes ($\phi = +40^\circ$)

Installation of the flight test nose boom in conjunction with radome strakes mounted at 40° above the MHB provides additional insight into the powerful forebody flow mechanism associated with this strake position. It was observed that the $\phi = +40^\circ$ strakes are extremely effective in enhancing the body vortices and, also, in dictating the body vortex interactive behavior with the wing flow. Despite the nose boom wake, the strake effects are essentially unchanged at $\alpha = 35^\circ$ and 40° within the sideslip angle range of about $-6^\circ \leq \beta \leq 6^\circ$, as shown in Figure 91. At higher sideslip angles the nose

ORIGINAL PAGE IS
OF POOR QUALITY

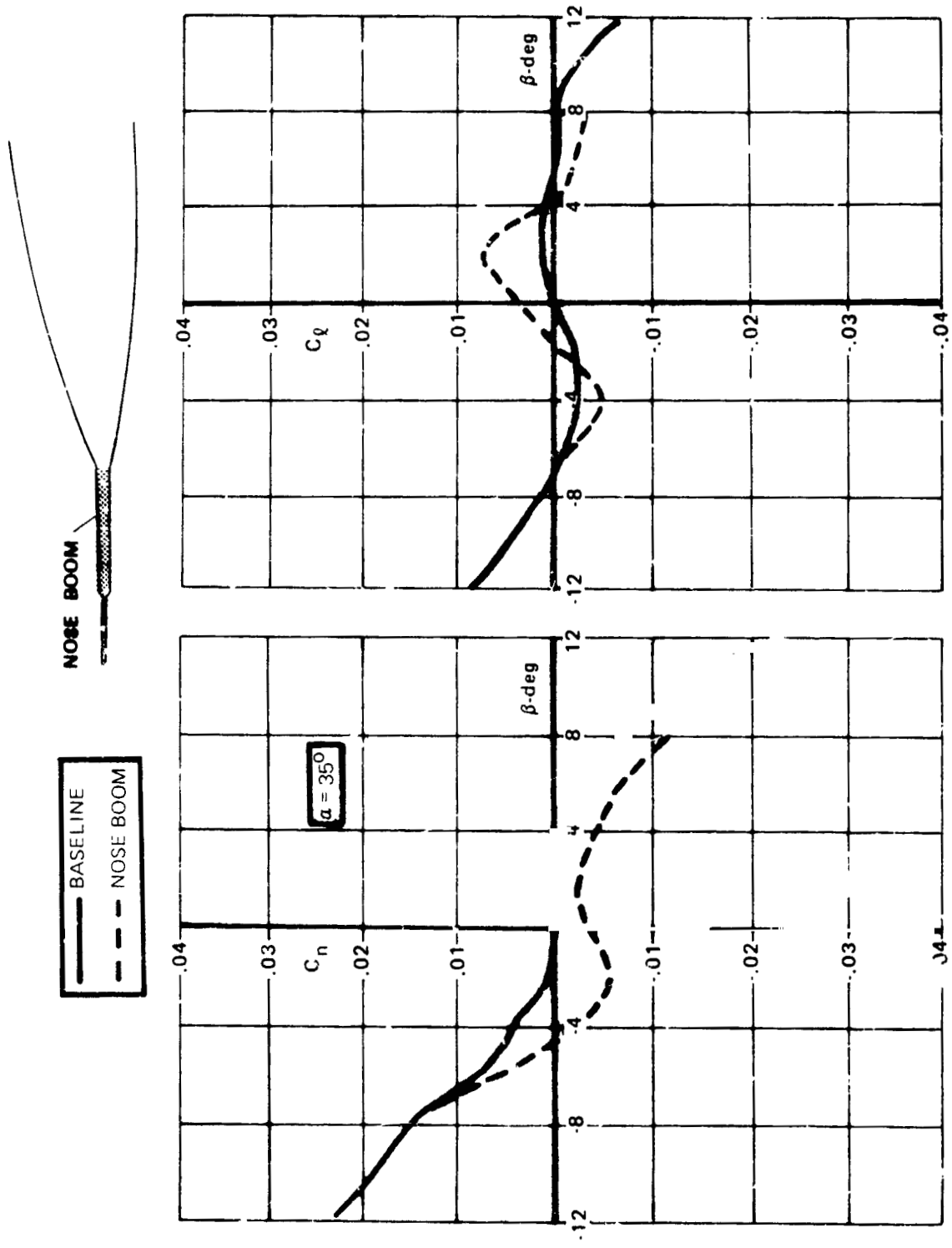


FIGURE 90. EFFECT OF FLIGHT TEST NOSE BOOM ON ROLLING MOMENT
AND YAWING MOMENT VARIATION WITH SIDESLIP: 0.16-SCALE F/A-18;
 $\delta_n = 25^\circ$; $\delta_h = -12^\circ$; $Re_c = 1.1 (10^6)$.

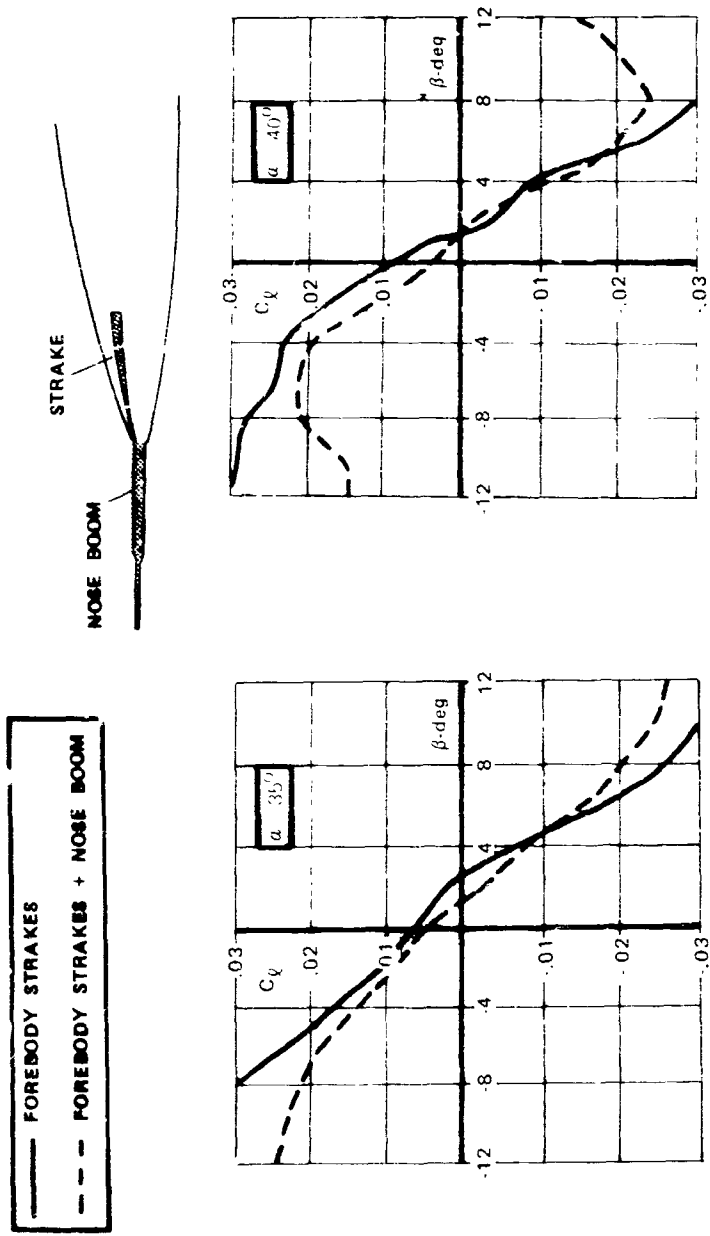


FIGURE 91. EFFECT OF FLIGHT TEST NOSE BOOM ON ROLLING MOMENT VARIATION WITH SIDESLIP; FOREBODY STRAKES ON ($\phi = 40^\circ$); 0.16-SCALE F/A-18; $\delta_n = 25^\circ$; $\delta_h = -12^\circ$; $Re_c = 1.1 (10^6)$.

boom flow field effects are evidenced by a reduction in body vortex stability and a corresponding unstable variation of rolling moment with sideslip.

"Wing Rock" Phenomena

Analysis of the water tunnel results obtained on the 0.025-scale F/A-18 model have revealed several correlations of the vortex flow behavior with the trends observed in low-speed wind tunnel tests. The water-to-air correlations have even extended to "wing rock" phenomena. Studies made at NASA Langley Research Center of the 0.16-scale F/A-18 model unconstrained in roll revealed the following: No "wing rock" was evident for the baseline ($\delta_n=25^\circ, 35^\circ$) or with LEX modifications (LEX fences, increased forward slot width and length, etc.). With nose strakes mounted 40 degrees above the MHB, however, modest "wing rock" was observed at $\alpha=35^\circ$ to 40° with a maximum amplitude of approximately $\pm 10^\circ$.

Northrop water tunnel studies of the 0.025-scale F/A-18 indicated that the nose strakes promoted a slightly oscillatory body vortex pattern at $\alpha=35-40$ degrees. This appeared due to a "hydrodynamic instability" phenomenon associated with two vortex cores in proximity to one another. As the body vortices traversed the wing flow field, the leeward body vortex showed a tendency to pass under the windward body vortex in a periodic manner. The baseline and LEX mods revealed only steady body vortex patterns.

ANALYSIS OF SCALE-MODEL F/A-18 WIND TUNNEL DATA

During the course of the low-speed wind tunnel tests commencing in 1979 in the NASA Langley Research Center 30x60-foot facility, comparisons of 0.06-, 0.07-, and 0.16-scale F/A-18 model data revealed large differences in lateral stability levels at high angles of attack ($\alpha=30^\circ-40^\circ$). Specifically, the 0.06- and 0.07-scale baseline models exhibited highly-stable variations of rolling moment with sideslip. Conversely, the 0.16-scale F/A-18 revealed a lateral sensitivity at stall and post-stall angles of attack. The discussions to follow will address this anomaly.

Baseline Configurations - Longitudinal Characteristics

Longitudinal aerodynamic data are available only for the 0.06- and 0.16-scale F/A-18 models. (The 0.07-scale model was originally fabricated for three-component (lateral-directional) tests at the Virginia Polytechnic Institute 6x6-foot wind tunnel.)

A comparison of lift characteristics of the 0.06- and 0.16-scale models obtained at approximately the same Reynolds number based on respective mean aerodynamic chords ($\sim 0.7(10^6)$) is presented in Figure 92. The results with flaps retracted ($\delta_n / \delta_f = 0^\circ / 0^\circ$) at $\beta = 0^\circ$ indicate an earlier stall of the large-scale model. This effect diminishes considerably, however, with leading-edge flaps deflected to 25° . Although the lift data in a sideslip condition ($\beta = -4^\circ$) are similar, the large model does exhibit a tendency to stall at a slightly lower angle of attack. This is reflected in the pitching moment data at $\beta = -4^\circ$ in Figure 93. The large model shows a stable stall at a lower lift coefficient relative to the small-scale F/A-18 model.

The results suggest that the LEX vortex burst progression on the 0.16-scale model is slightly more rapid relative to the 0.06-scale F/A-18. Comments by NASA Langley researchers involved in the F/A-18 test program indicated that during smoke flow visualization studies the small-scale model LEX vortices appeared slightly more concentrated at a given angle of attack. Although these observations are highly qualitative, they are consistent with the data trends.

The data differences are greatest in the stall angle-of-attack regime where small perturbations in the external flow field and slight differences in model contours can greatly affect stall behavior. As the analyses progress, a plausible flow mechanism will emerge which accounts for the model differences at high angles of attack.

Baseline Configurations - Lateral/Directional Characteristics

The variation of rolling moment with angle of attack at $\beta = -4^\circ$, shown in Figure 94, is similar for the 0.06- and 0.16-scale models. These results

ORIGINAL PAGE IS
OF POOR QUALITY

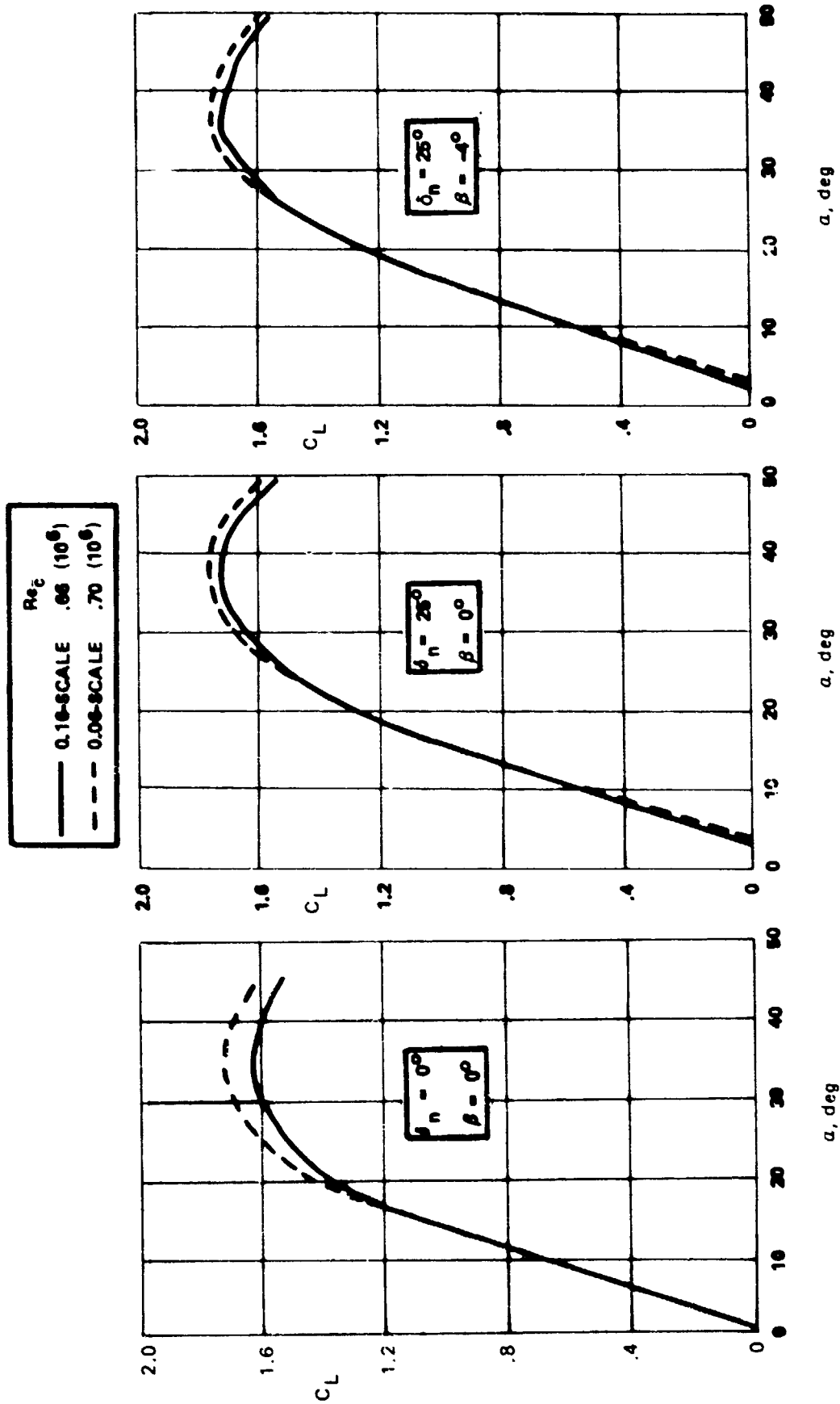


FIGURE 92. COMPARISON OF 0.06- AND 0.16-SCALE F/A-18 LIFT CHARACTERISTICS; $\delta_h = -12^\circ$

ORIGINAL PAGE IS
OF POOR QUALITY

	Re_E
——— 0.16-SCALE	.66 (10^6)
- - - 0.06-SCALE	.70 (10^6)

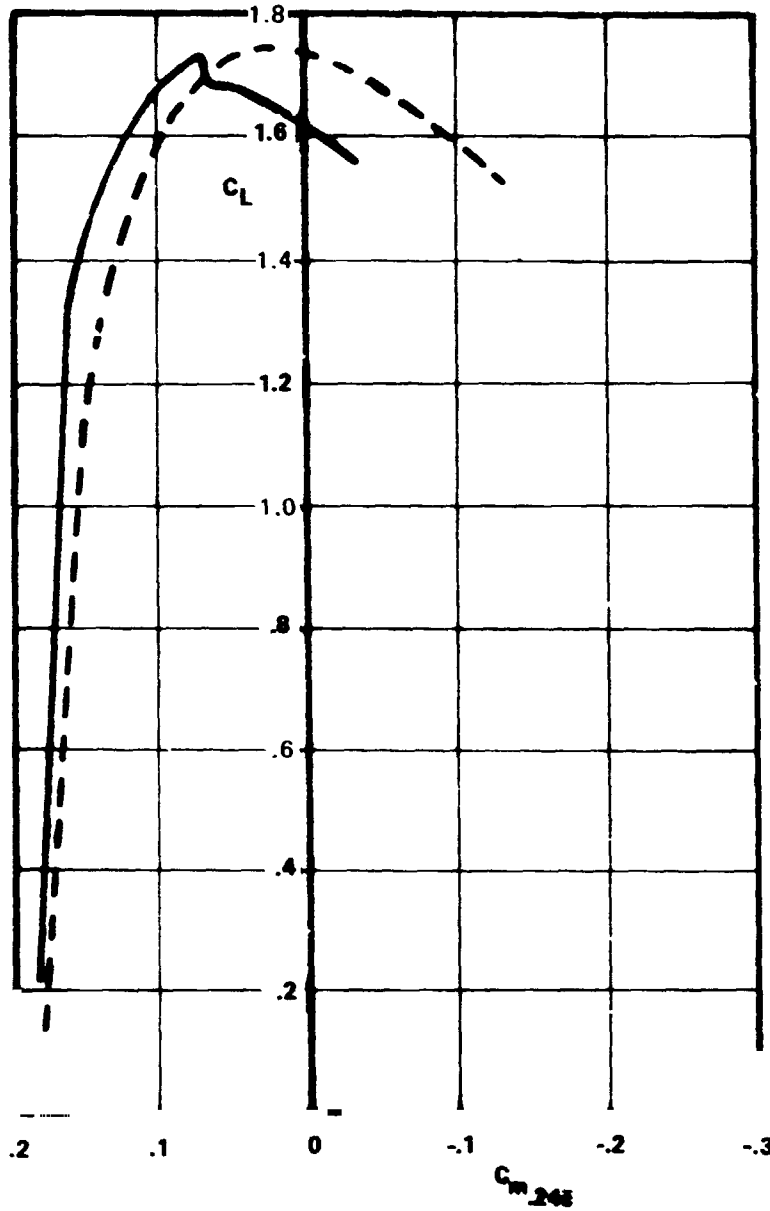


FIGURE 93. COMPARISON OF 0.06- AND 0.16-SCALE F/A-18 PITCHING
MOMENT CHARACTERISTICS; $\beta = -4^\circ$; $\delta_n = 25^\circ$; $\delta_h = -12^\circ$

ORIGINAL PAGE IS
OF POOR QUALITY.

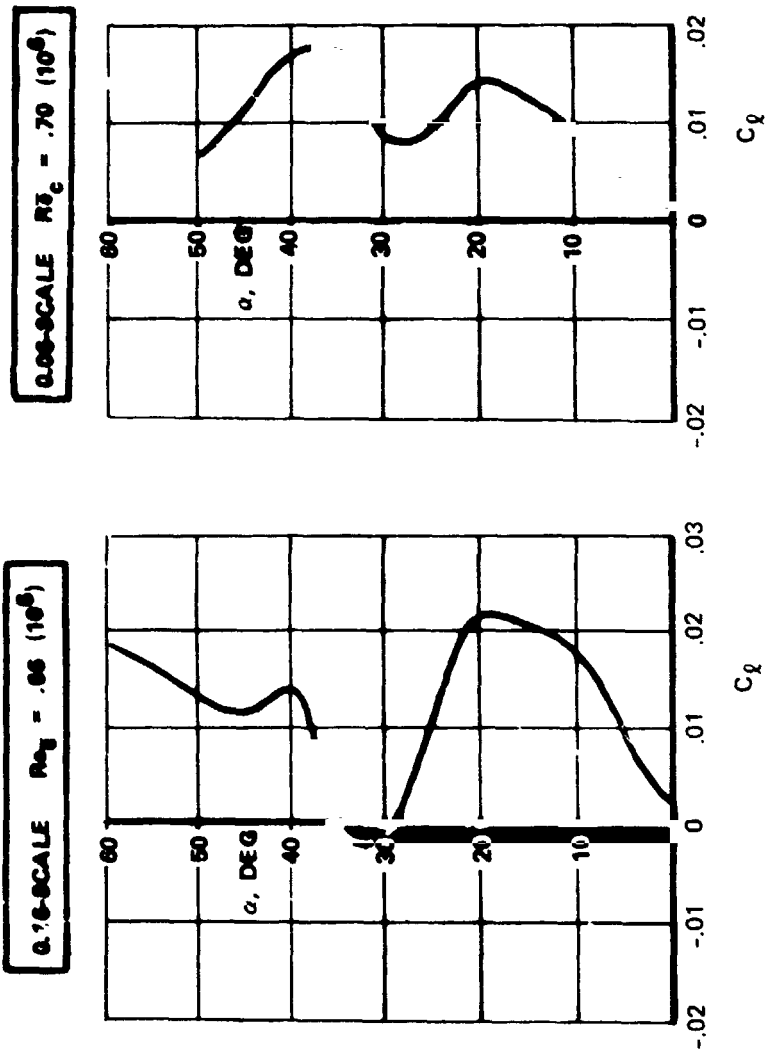


FIGURE 94. ROLLING MOMENT VARIATION WITH ANGLE OF ATTACK;
0.06- AND 0.16-SCALE F/A-18; $\delta_n = 25^\circ$; $\delta_h = -12^\circ$; $\beta = -4^\circ$

indicate that the aerodynamic flow phenomena are similar, although the degree to which flowfield changes occur and the angles of attack at which the latter are evident differ. An unstable "break" in rolling moment coefficient occurs at an angle of attack of about 20° for the 0.16- and 0.06-scale models. At angles of attack generally greater than 20 degrees, the rate at which rolling moment coefficient decreases with increased angle of attack is greater for the 0.16-scale model. Furthermore, the onset angle of attack at which rolling moment coefficient again exhibits a stable variation with angle of attack is approximately 5° higher ($\alpha \approx 35^\circ$) for the large model. These trends are indicative of a more pronounced and persistent LEX vortex breakdown asymmetry on the 0.16-scale F/A-18 in the angle of attack range of about 20° to 40° .

It should be noted that the difference in LEX vortex burst asymmetry between the models need not be great to promote significant variation in rolling moment characteristics. For example, a difference of windward vortex burst location of just a few per cent chord can greatly alter the wing stall behavior. Northrop low-speed wind tunnel tests of a 0.10-scale F-5E (Reference 9) provide a good example of this effect. Slightly below stall angle of attack ($\sim 26^\circ$) it is known from water tunnel tests and wind tunnel water vapor results that the LEX vortex core is distinguishable only near the LEX apex. Despite the fact that windward LEX vortex breakdown is so far forward on the LEX surface, the vortex-induced effects are sufficient to delay wing stall. Should the burst position shift forward slightly, the windward wing passes through $C_{L_{MAX}}$ and the abrupt wing stall promotes substantial reduction in lateral stability.

The violent nature of this lateral stability loss associated with asymmetric vortex breakdown has also been witnessed in Northrop wind tunnel tests during the development of the YF-17 (Reference 8). A sting-mounted model was observed to oscillate violently about the body axis under the influence of differential LEX vortex breakdown positions.

As angle of attack increases from 30° , the F/A-18 LEX vortex burst point at $\beta=0^\circ$ approaches the LEX-wing junction, a condition which can be interpreted

as approximating $C_{L_{MAX}}$. It is of interest to note that vortex breakdown at high angles of attack has been detected by F/A-18 pilots by an increase in noise level outside the cockpit. This is due to the highly turbulent nature of the burst vortex system. In sideslip, phenomena similar to that described for the F-5E can occur. Due to small perturbations in LEX vortex burst position the wings traverse $C_{L_{MAX}}$ at different angles of attack.

The "pitch sweeps" have been shown in order to reveal important force and moment data trends and to highlight areas of sensitivity. The fundamental question, however, concerns the scale-model data differences at angles of attack from approximately $30^\circ - 40^\circ$, where the full-scale aircraft during flight tests has experienced a lateral sensitivity. Consequently, emphasis will be made during this report of "sideslip-sweeps" at constant angle of attack.

It is noted that the analyses contained within this report are not intended to determine which model data are more credible. Indeed, the only model which has shown consistent agreement with the high- α lateral stability trends observed in flight is the 0.16-scale configuration. The intent of the analyses is to provide an understanding of potential fluid flow variations which will be of aid in future test programs designed to assess this problem in detail.

Rolling moment variation with sideslip on the 0.06-, 0.07-, and 0.16-scale models are presented in Figure 95 at $\alpha = 25^\circ, 30^\circ, \text{ and } 35^\circ$ with leading-edge flaps undeflected. Horizontal tail deflection angles vary from 0° to -12° , but the tail effects on rolling moment are small enough at these angles of attack that the comparisons are valid. At $\alpha = 25^\circ$, all models exhibit unstable rolling moment variations with sideslip at small sideslip angles, although the smaller models are characterized by less unstable values of rolling moment coefficient. For comparison, 0.08-scale Northrop F-18L data obtained in the Northrop 7x10-foot wind tunnel are shown, indicating reasonable agreement with the large F/A-18 model at $\alpha = 25^\circ$. At $\alpha = 30^\circ$, the small F/A-18 models (and the 0.08-scale F-18L) are in fair agreement, while the 0.16-scale model still exhibits an unstable variation of C_l with β at sideslip angles of about $-6^\circ \leq \beta \leq +6^\circ$. The trend continues at $\alpha = 35^\circ$ where the lateral

ORIGINAL PAGE IS
OF POOR QUALITY

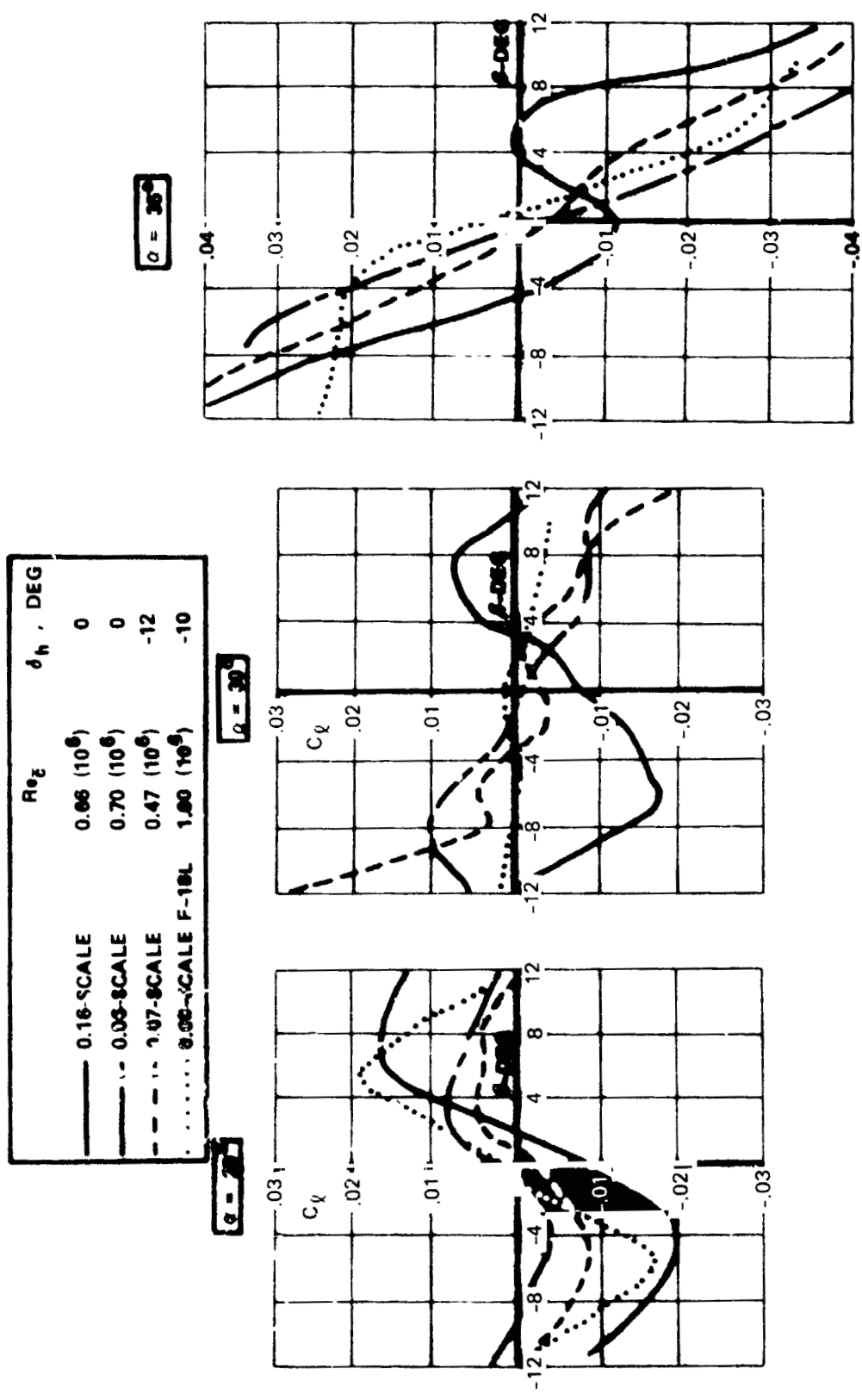


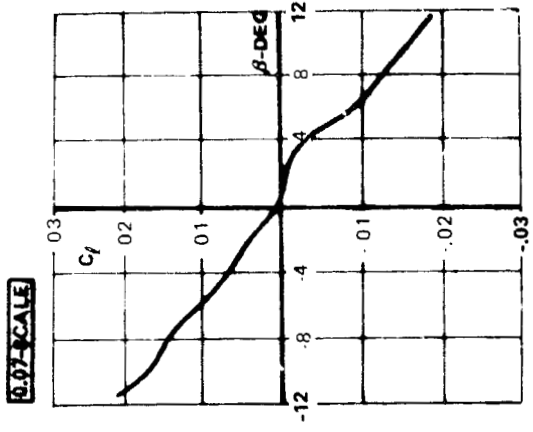
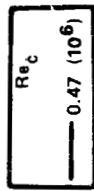
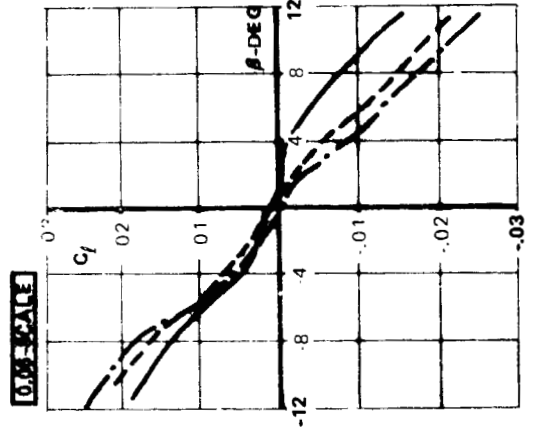
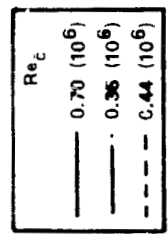
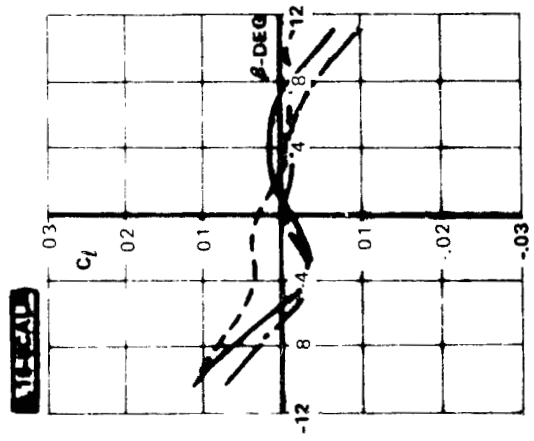
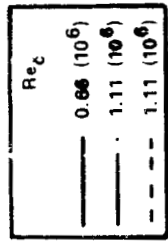
FIGURE 95. COMPARISON OF 0.06-, 0.07-, AND 0.16-SCALE F/A-18 ROLLING MOMENT VARIATION WITH SIDESLIP; $\delta_n = 0^\circ$

sensitivity at small sideslip of the 0.16-scale F/A-18 is in marked contrast to the highly-stable C_l vs. β variations exhibited by the small models.

Rolling moment characteristics at $\alpha=30^\circ$, 35° , and 40° with $\delta_n=25^\circ$ are presented in Figure 96 for the 0.06-, 0.07-, and 0.16-scale models. The data trends tend to be consistent with the $\delta_n=0^\circ$ results. Consequently, the model data differences cannot be attributed to leading-edge flap effects (although account must be made of possible slight leading-edge flap angle differences between each model and, also, on the same model). In general, the 0.06- and 0.07-scale F/A-18 models exhibit highly stable rolling moment variations at each angle of attack while the 0.16-scale F/A-18 generally shows a reduction in lateral stability to a near-neutral level. The wind tunnel data provide no indication that Reynolds number plays a prominent role in the apparent "model-scale" effect. It is noted, though, that the Reynolds numbers based on maximum body width all lie within the laminar range, according to the procedure defined in Reference 10. Consequently, without corresponding data in the transitional and fully-turbulent Reynolds number regimes, no conclusions can be made regarding Reynolds number effects on the high- α forebody-LEX vortex interactions.

The lateral sensitivity at high angles of attack is not confined to the F/A-18, however. For comparison, Northrop 0.12-scale P-530 and 0.08-scale F-18L data are presented in Figure 97. (The P-530 was a precursor of the Northrop YF-17.) Any advanced fighter configuration which develops large amounts of vortex lift is prone to nonlinear behavior near stall. For example, results from Reference 11 show similar levels of lateral stability at high α 's on a 3-surface canard-derivative of the F-15 and, also, on an F-16 fighter model, both of which were characterized by powerful vortex flows and vortex interactions.

The nature of vortices is such that their behavior may not necessarily be consistent from model-to-model or even on the same model during repeat runs. For example, wind tunnel data from Reference 12 shown in Figure 98 reveal "model-scale" effects, independent of Reynolds number, on the YF-17. The 0.03- and 0.08-scale models, both of which were built for high-speed testing

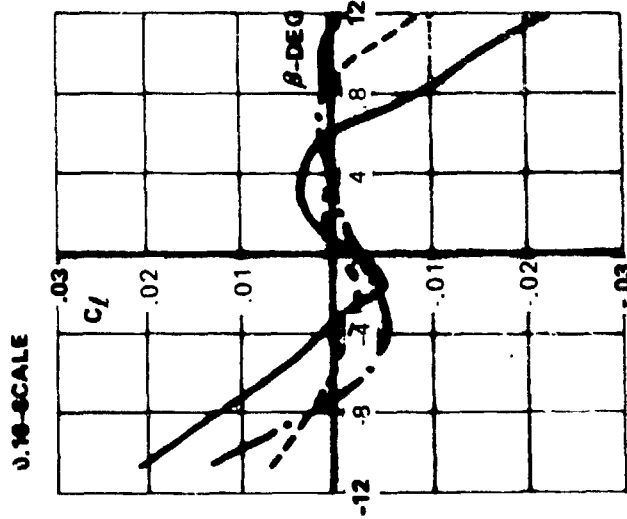
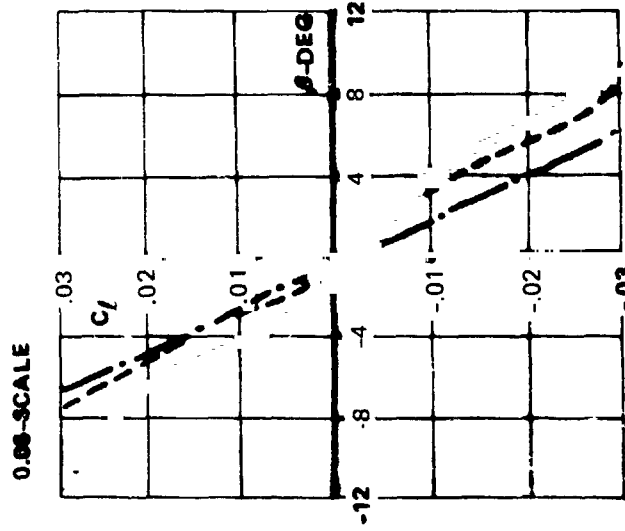
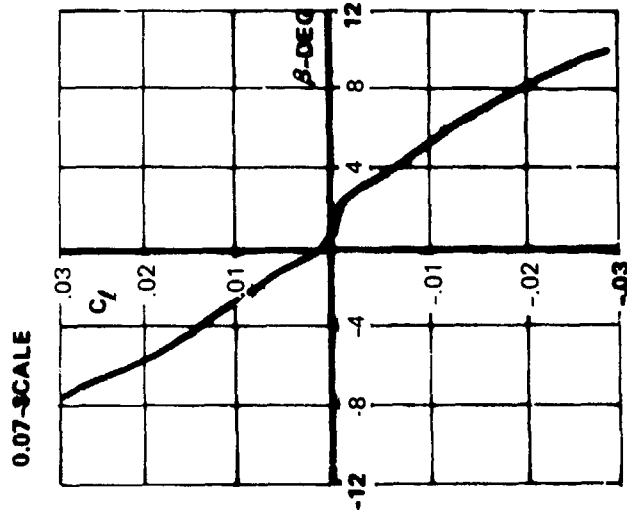


(A) $\alpha = 30$ DEGREES

ORIGINAL PAGE IS
OF POOR QUALITY

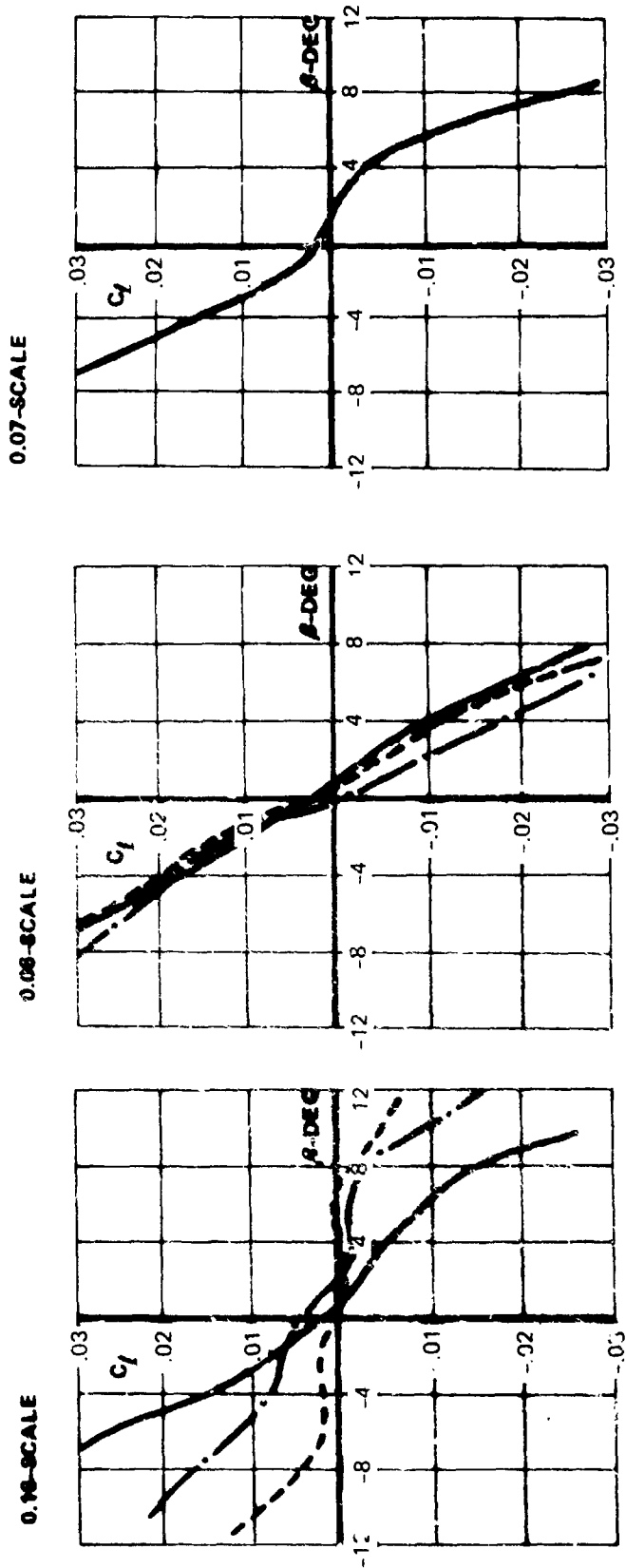
FIGURE 96. COMPARISON OF 0.06 -, 0.07 -, AND 0.16-SCALE F/A-18 ROLLING MOMENT VARIATION WITH SIDESLIP; $\delta_n = 25^\circ$; $\delta_h = -12^\circ$

ORIGINAL PAGE IS
OF POOR QUALITY



(B) $\alpha = 35$ DEGREES

FIGURE 96. CONTINUED



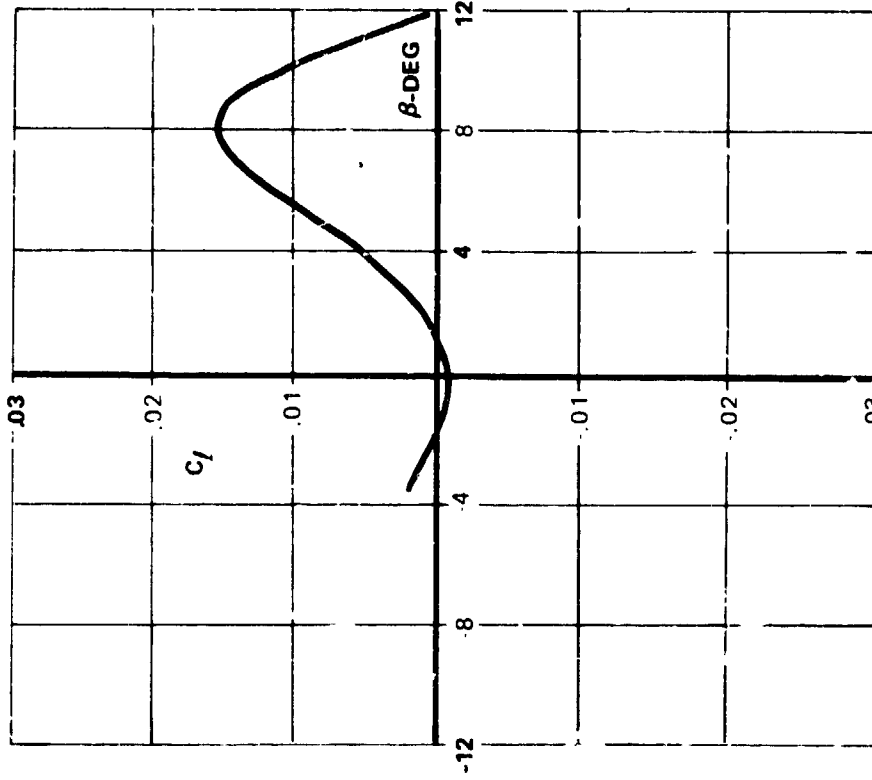
ORIGINAL PAGE IS
OF POOR QUALITY

(C) $\nu = 40$ DEGREES

FIGURE 96. CONCLUDED

ORIGINAL PAGE IS
OF POOR QUALITY

0.12-SCALE P-530 $Re_{\bar{c}} = 1.1 (10^6)$ $\alpha = 35^\circ$



0.08-SCALE F-18L $Re_{\bar{c}} = 1.6 (10^6)$ $\alpha = 30^\circ$

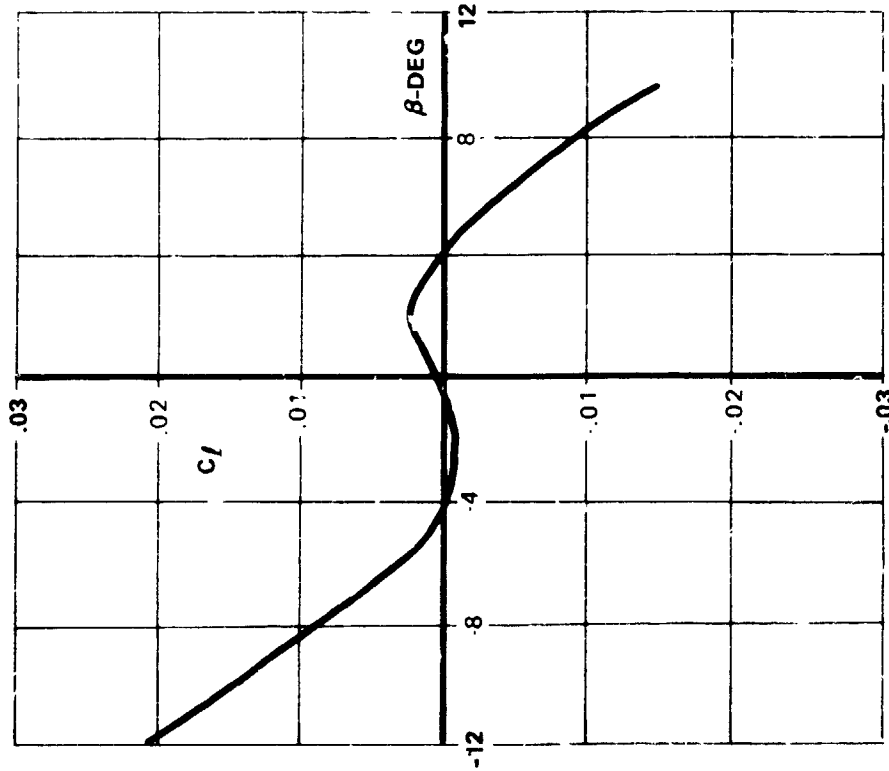


FIGURE 97. ROLLING MOMENT VARIATION WITH SIDESLIP FOR 0.08-SCALE
F-18L AND 0.12-SCALE F-530; $\delta_n = 25^\circ$

ORIGINAL PAGE IS
OF POOR QUALITY.

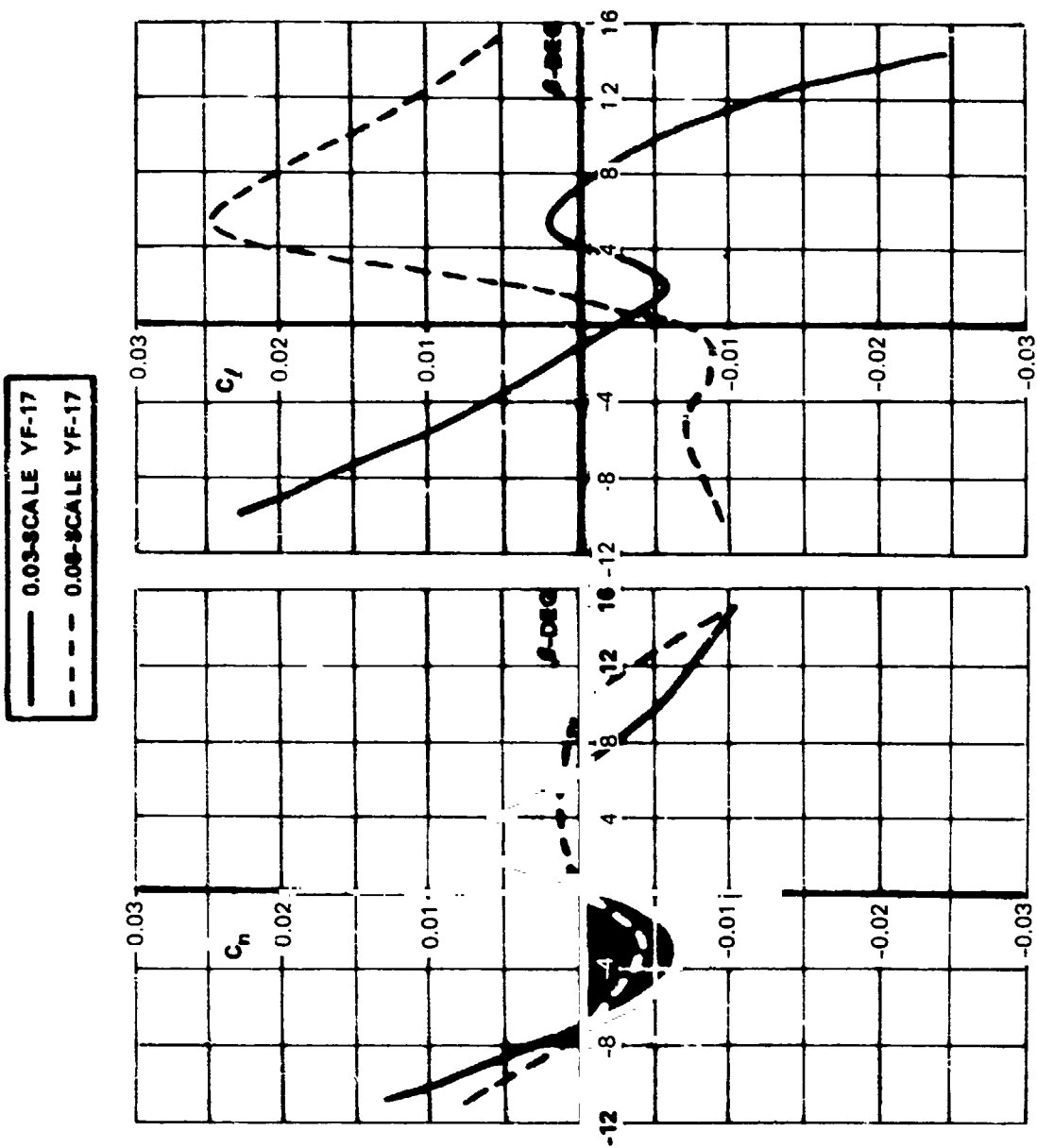


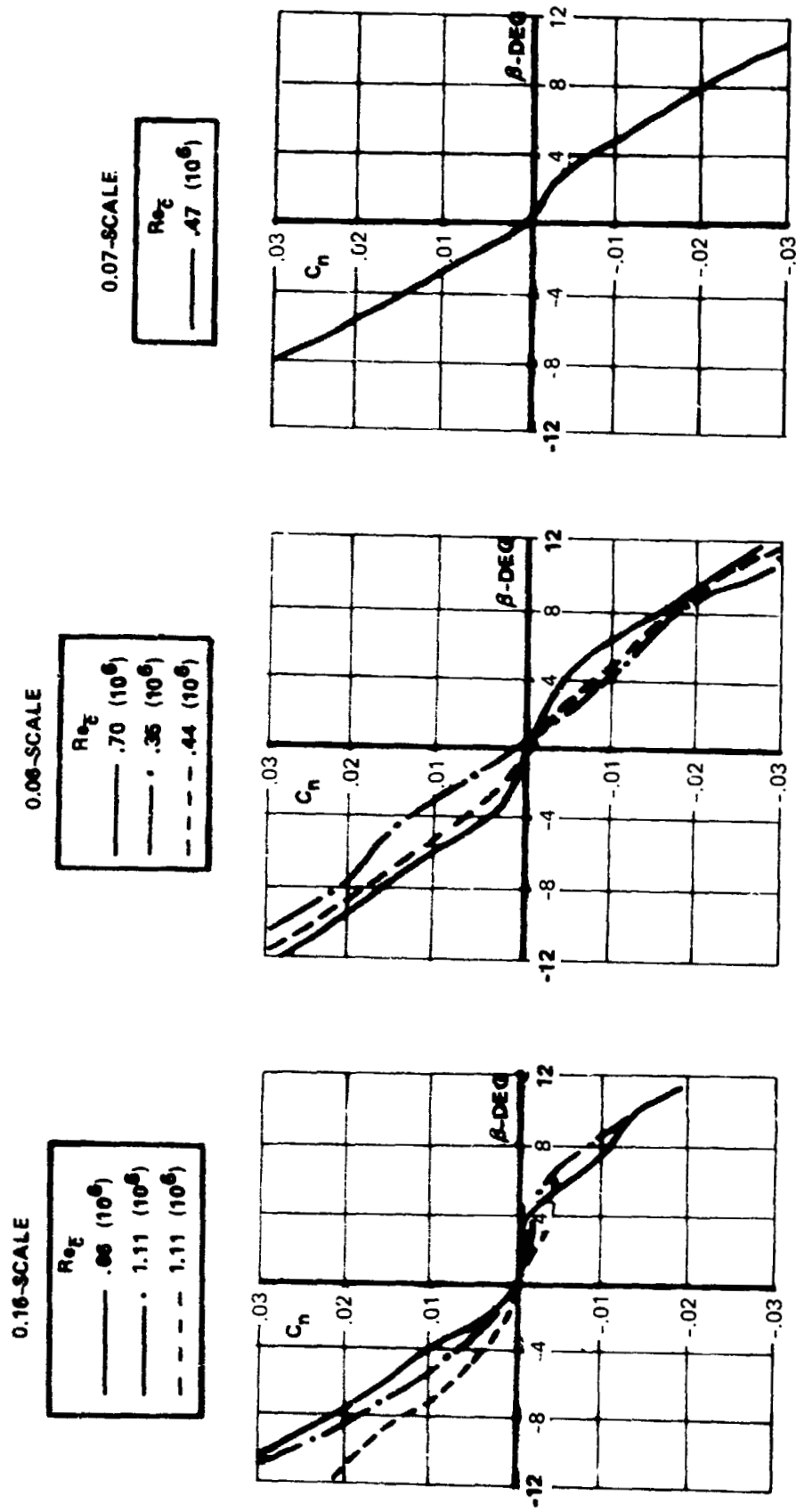
FIGURE 98. COMPARISON OF 0.03- AND 0.08-SCALE YF-17 ROLLING MOMENT AND YAWING MOMENT VARIATION WITH SIDESLIP; $\alpha = 30^\circ$; $Re_{\bar{c}} = 0.7 (10^6)$

in the Northrop 2x2-foot transonic tunnel, develop different stall patterns near $\alpha=30^\circ$. Consequently, the rolling moment variations with sideslip are quite different.

It is interesting to note that fighter pilots will often refer to a specific airplane within a fighter squadron since its behavior is distinguishable from that exhibited by identical aircraft operating under the same flight conditions. This phenomenon appears similar to the "model-scale" effect and may be attributable to subtle differences in aircraft geometry. For example, it has been established in flight tests of the Northrop F-5F that minute geometry differences in the nose region can, at very high angles of attack, cause one aircraft to nose slice right while another will slice left on a consistent basis. Furthermore, comments in Reference 13 indicate that a 0.10-inch "nick" (full-scale dimensions) in the LEX leading edge on an F-5E was the apparent source of large differences in lateral stability near stall angle of attack in flight relative to the behavior of another F-5E. These examples reveal the sensitivity of the forebody and LEX vortices at high angles of attack to seemingly innocuous geometry differences.

The F/A-18 yawing moment characteristics at $\alpha=35^\circ$ presented in Figure 99 generally show reasonable agreement of all model data. In addition, the side force coefficient variations with sideslip at $\alpha=35^\circ$ in Figure 99 are similar.

The wind tunnel data comparisons show the "model-scale" sensitivity is isolated to the rolling moment behavior with sideslip. The primary airframe contributor to static lateral stability is the wing. A check of the F/A-18 models at the NASA Langley model shop using standard procedures revealed no discernible differences in LEX-wing positions and geometries. The remaining sections will provide evidence to support the conjecture that very subtle differences in the forebody geometries are the source of model data disparity due to the potentially-strong coupling of the F/A-18 forebody and LEX vortices. The model inspection cited above included an assessment of the forebody contours. However, the inspection was not geared towards the identification of extremely small model differences.

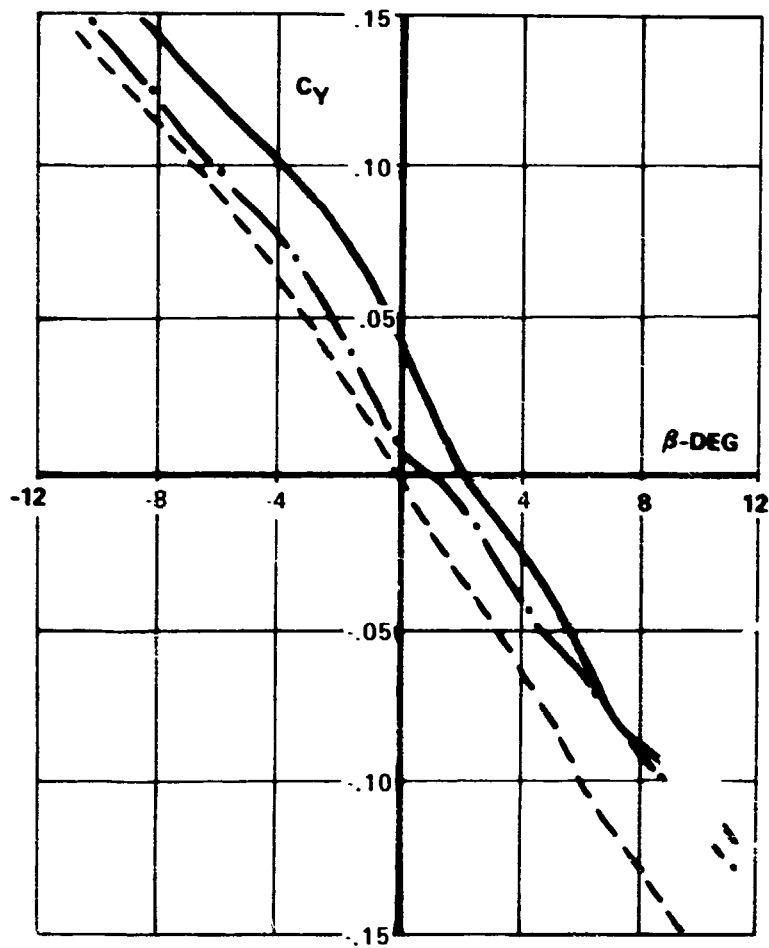


(A) YAWING MOMENT

FIGURE 99. COMPARISON OF 0.06-, 0.07-, AND 0.16-SCALE F/A-18 YAWING
MOMENT AND SIDE FORCE COEFFICIENT VARIATION WITH SIDESLIP;
 $\delta_n = 25^\circ$; $\delta_h = -12^\circ$; $\alpha = 35^\circ$

ORIGINAL PAGE IS
OF POOR QUALITY

	R_{eq}
—— 0.16-SCALE	.86 (10^6)
- - - 0.08-SCALE	.70 (10^6)
- - - 0.07-SCALE	.47 (10^6)



(B) SID FORCE

FIGURE 99. CONCLUDED

The discussions to follow pertain to the effects of removing the twin vertical tails, the wing leading-edge extensions (LEXs), the fuselage forebody, and addition of forebody strakes. Since the 0.07-scale F/A-18 was in consistent agreement with the 0.06-scale model, the former was tested along with the 0.16-scale F/A-18 to provide comparative results to address the "model-scale" effect.

Vertical Tail Effects

For illustrative purposes, 0.07-scale F/A-18 rolling moment variation with angle of attack at $\beta = -5^\circ$ is presented in Figure 100. 0.16-scale data were not available at the same sideslip angle. The trends, however, were similar. Figure 100 indicates that removal of the vertical tails generally promotes large unstable rolling moment increments at high α 's. The tail contribution to rolling moment at low angles of attack is of a direct nature. The tail resultant lift acts at a point above the moment reference center and, hence, contributes stable, rolling moment increments. The C_l decrements at high α 's are associated primarily with an upstream influence on the wing flow behavior due to removal of the verticals. In the absence of the tails, the LEX vortices are somewhat more stable, although the vortices burst more asymmetrically in sideslip. Removal of the vertical tails removes the adverse pressure gradient imposed on the flow field by these downstream obstacles. As a result, the potential for vortex burst asymmetry in sideslip increases. Although the vertical tails are not the source of model data differences, the results nonetheless reveal the sensitivity of the F/A-18 LEX vortex behavior to downstream flow variations.

Because the twin vertical tails impose a positive pressure gradient in the flow field, the F/A-18 vortex flow behavior may be somewhat more resistant to support interference effects. The results in Reference 14 have shown after vortex breakdown had been established over a delta wing by installing a flat-plate obstacle downstream, vortex stability was insensitive to the introduction of a pressure probe into the vortex core. Indeed, 0.16-scale F/A-18 tests conducted in the Langley 30x60-foot tunnel using two very different support arrangements suggest such effects are, at most, second order on the F/A-18.

ORIGINAL PAGE IS
OF POOR QUALITY

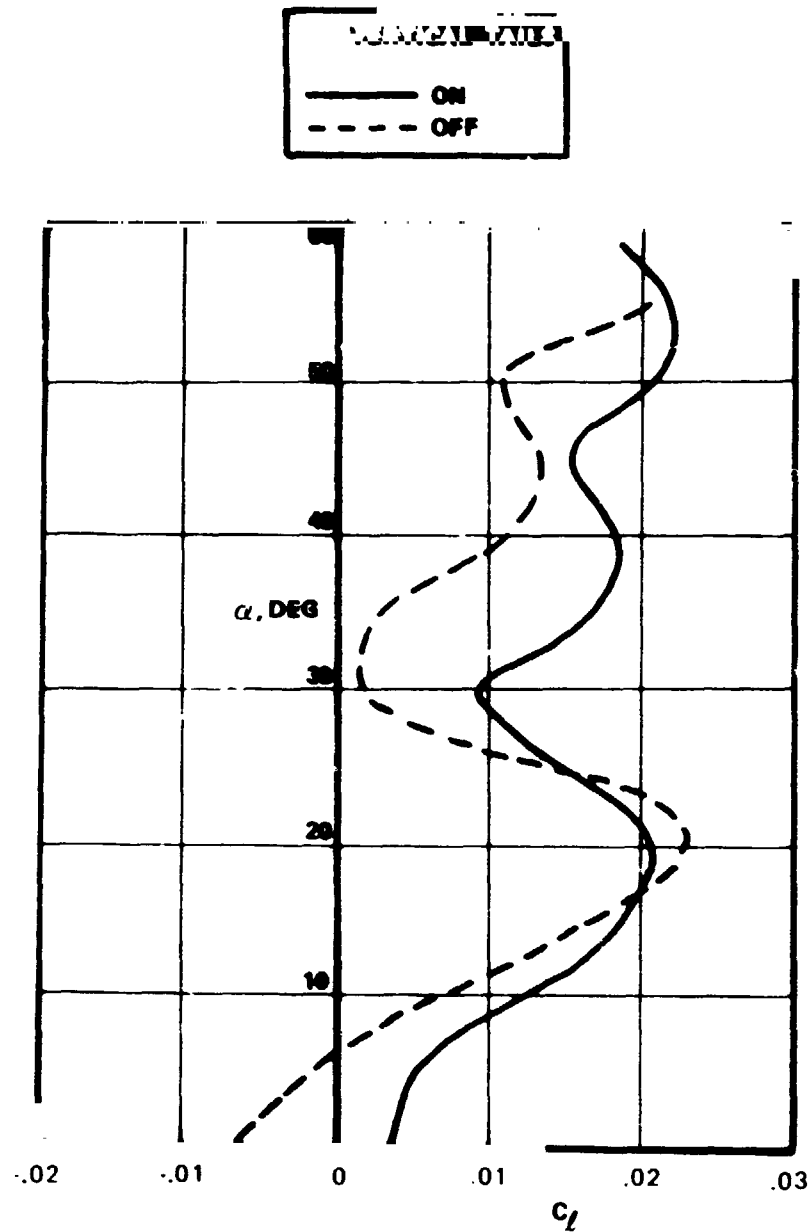


FIGURE 100. ROLLING MOMENT VARIATION WITH ANGLE OF ATTACK; VERTICAL TAILS ON AND OFF; 0.07-SCALE F/A-18; $\delta_n = 25^\circ$; $\delta_h = -12^\circ$; $Re_c = 0.47 (10^6)$; $\beta = -5^\circ$

Variations of rolling moment with sideslip were not available for the large model without vertical tails. The available 0.07-scale model results shown in Figure 101, however, provide interesting trends. At $\alpha=30^\circ$, 35° , and 40° the model with tails removed is characterized by an unstable variation of rolling moment with sideslip at small sideslip angles. Indeed, the levels of lateral stability are remarkably similar to the baseline 0.16-scale model behavior. These results support in an indirect manner the conjecture that the baseline 0.16-scale model develops slightly more asymmetric vortex bursting in sideslip relative to the baseline 0.06- and 0.07-scale F/A-18 models.

It will be shown that the differences in LEX vortex burst asymmetry in sideslip can be attributed not to downstream flow variations but, instead, to different forebody-LEX vortex coupling mechanisms.

Wing Leading-Edge Extension (LEX) Effects

Removal of the wing leading-edge extensions results in large lift reductions, particularly at the higher angles of attack where the wings without LEX have stalled. This effect is illustrated for the 0.16-scale model in Figure 102. Even though LEX vortex bursting at $\alpha=30^\circ$ - 40° has advanced far upstream on the wing, the LEX vortex-induced lift increments are very large. The LEX vortex flow field greatly alters the wing spanwise lift distribution. Consequently, disturbances in the vortex behavior due, say, to sideslip can promote potentially-large changes in the spanwise lift distribution and, hence, rolling moment characteristics.

The wind tunnel results suggest, again in an indirect fashion, that the 0.16-scale model with LEXs on develops a more asymmetric LEX vortex burst pattern relative to the 0.07-scale F/A-18. Figures 103 and 104 present rolling moment and yawing moment coefficient variations with sideslip for the 0.16- and 0.07-scale models, respectively, at $\alpha=30^\circ$, 35° , and 40° . Large stable rolling moment increments arise due to LEX removal on the large-scale F/A-18 (see Figure 103). However, as shown in Figure 104, the 0.07-scale model shows only a small variation with LEXs off. Furthermore, very good data agreement is obtained for the 0.07- and 0.16-scale models with LEXs off.

ORIGINAL PAGE IS
OF POOR QUALITY

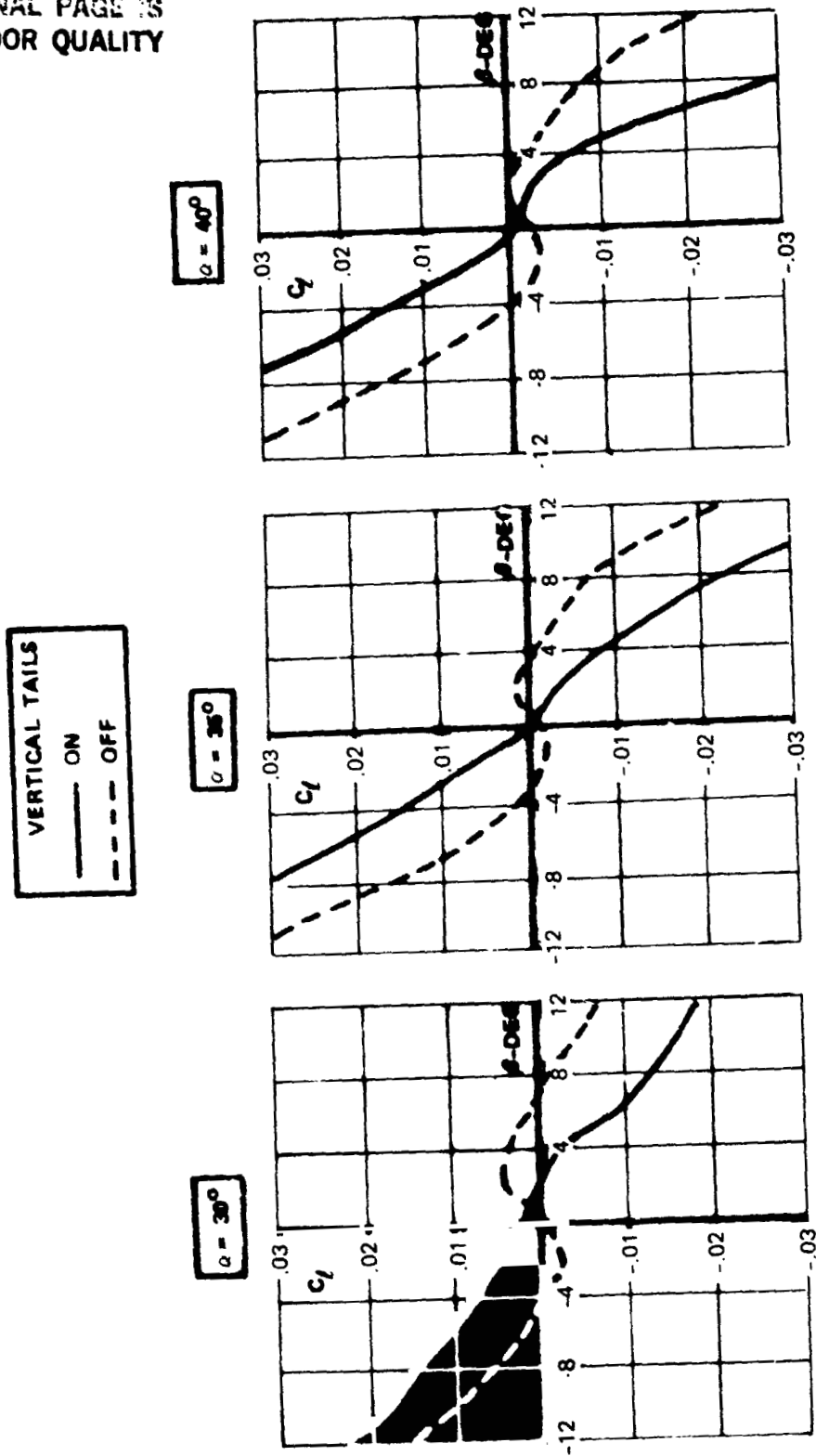


FIGURE 1J1. EFFECT OF TWIN VERTICAL TAIL REMOVAL ON 0.07-SCALE F/A-18
ROLLING MOMENT VARIATION WITH SIDESLIP; $\delta_n = 25^\circ$; $\delta_h = -12^\circ$; $Re_\xi = 0.47 (10^6)$

ORIGINAL PAGE IS
OF POOR QUALITY

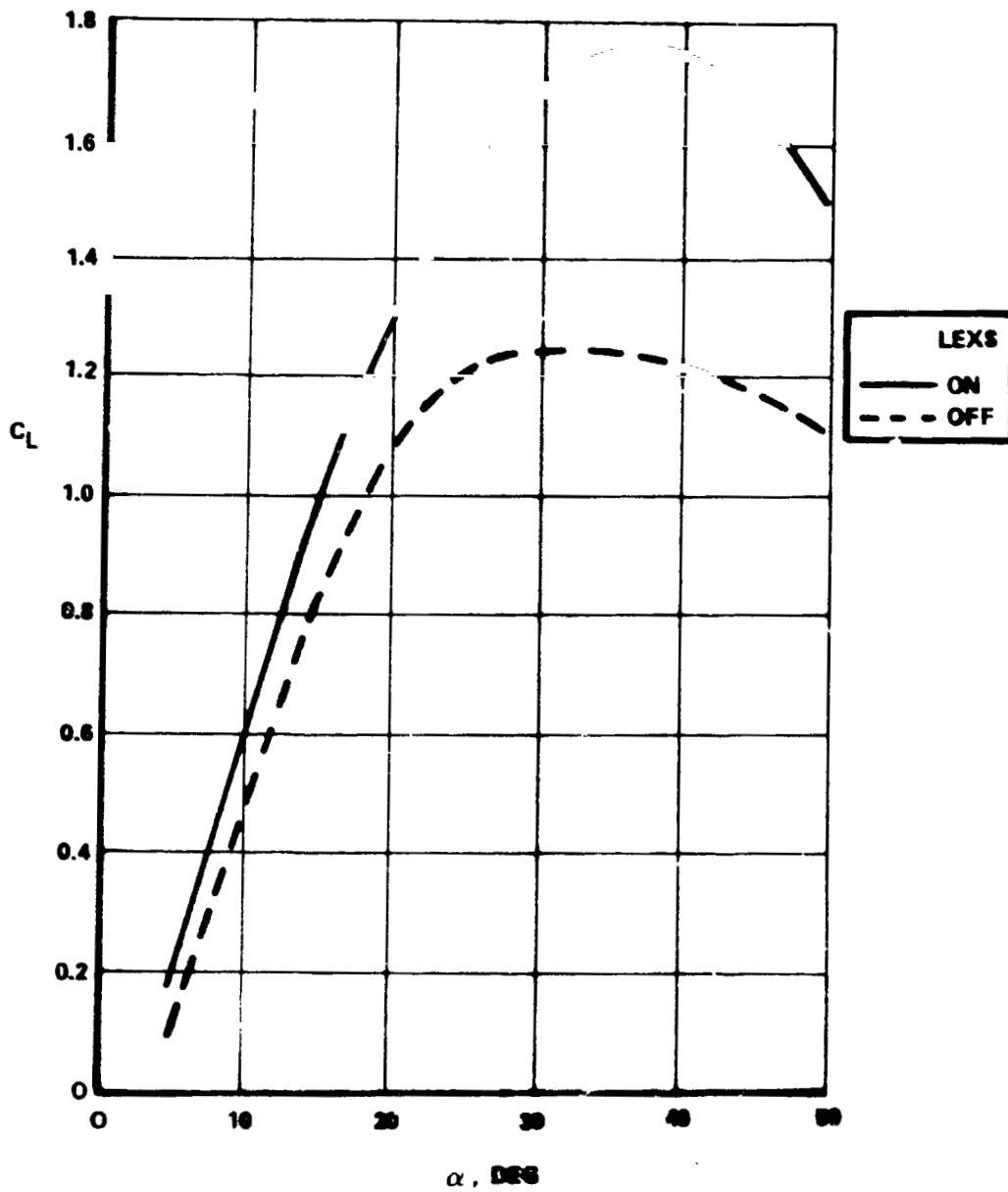
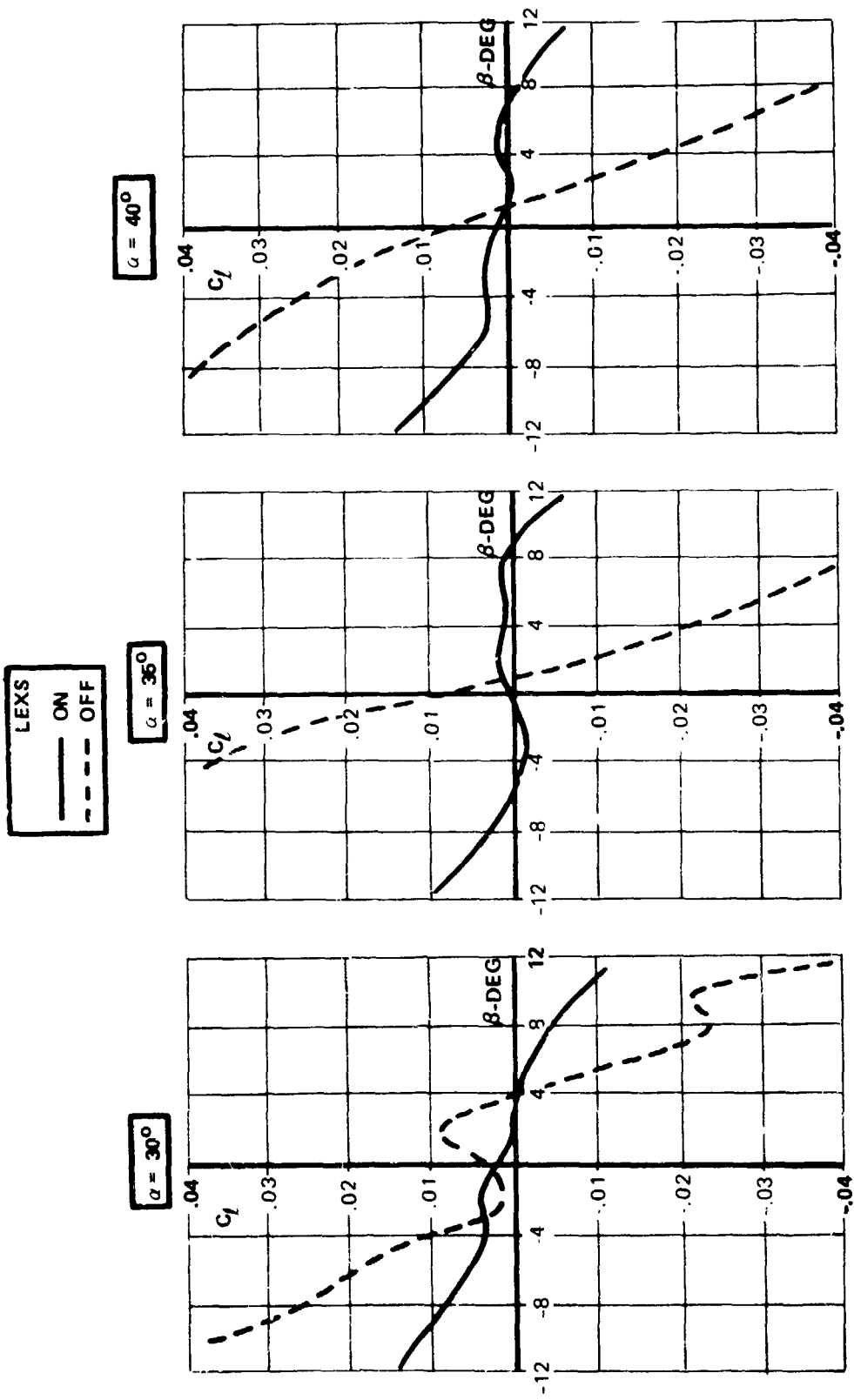


FIGURE 102. EFFECT OF LEX REMOVAL ON 0.16-SCALE F/A-18 LIFT CHARACTERISTICS; $\delta_n = 25^\circ$; $\delta_h = -12^\circ$; $Re_c = 1.1 (10^6)$

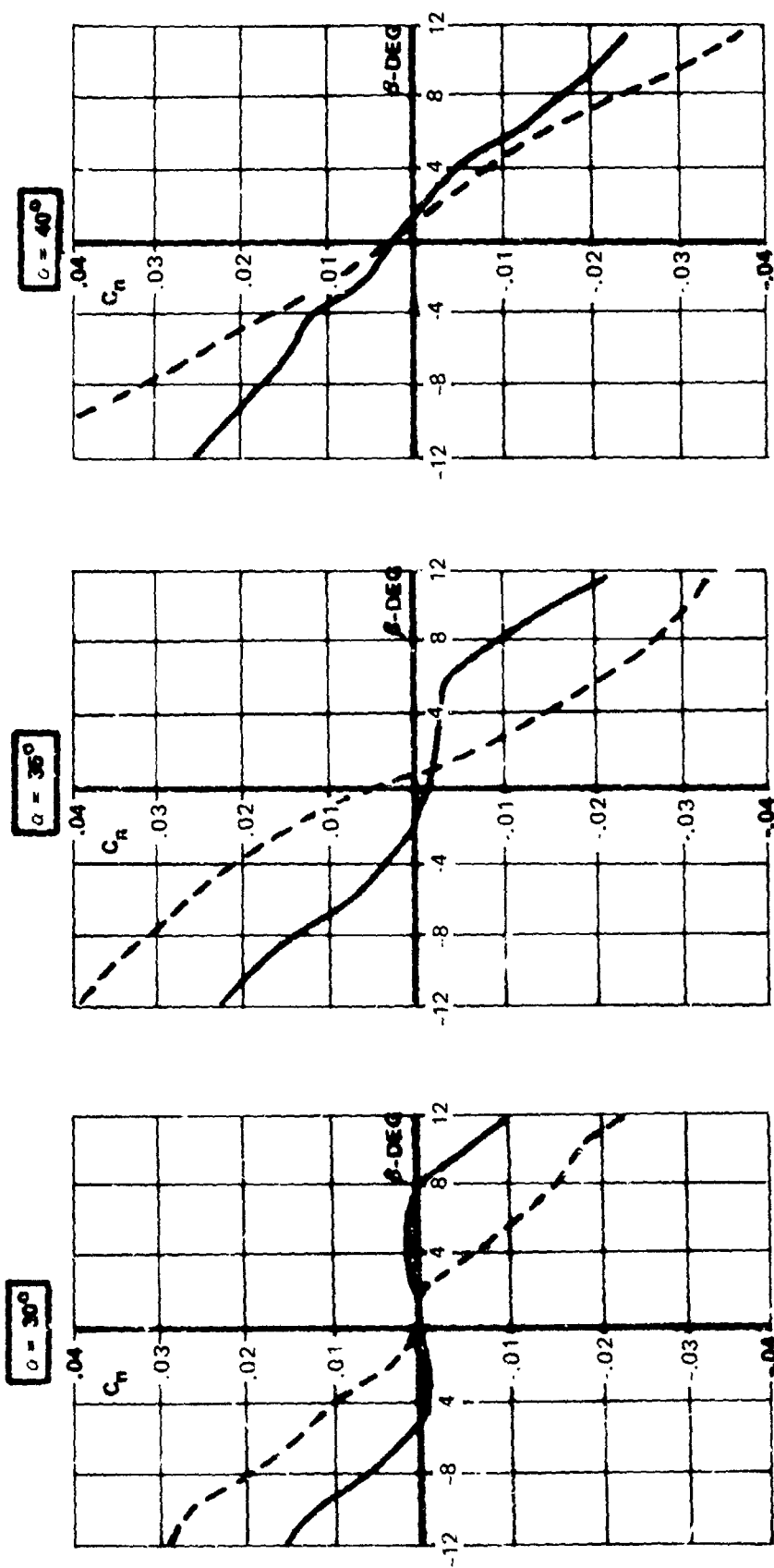
ORIGINAL PAGE IS
OF POOR QUALITY



(A) ROLLING MOMENT

FIGURE 103. EFFECT OF LEX REMOVAL ON 0.16-SCALE F/A-18 ROLLING MOMENT AND YAWING MOMENT VARIATION WITH SIDESLIP; $\delta_h = -12^\circ$; $\delta_n = 25^\circ$; $Re_c = 1.1 (10^6)$

ORIGINAL PAGE IS
OF POOR QUALITY

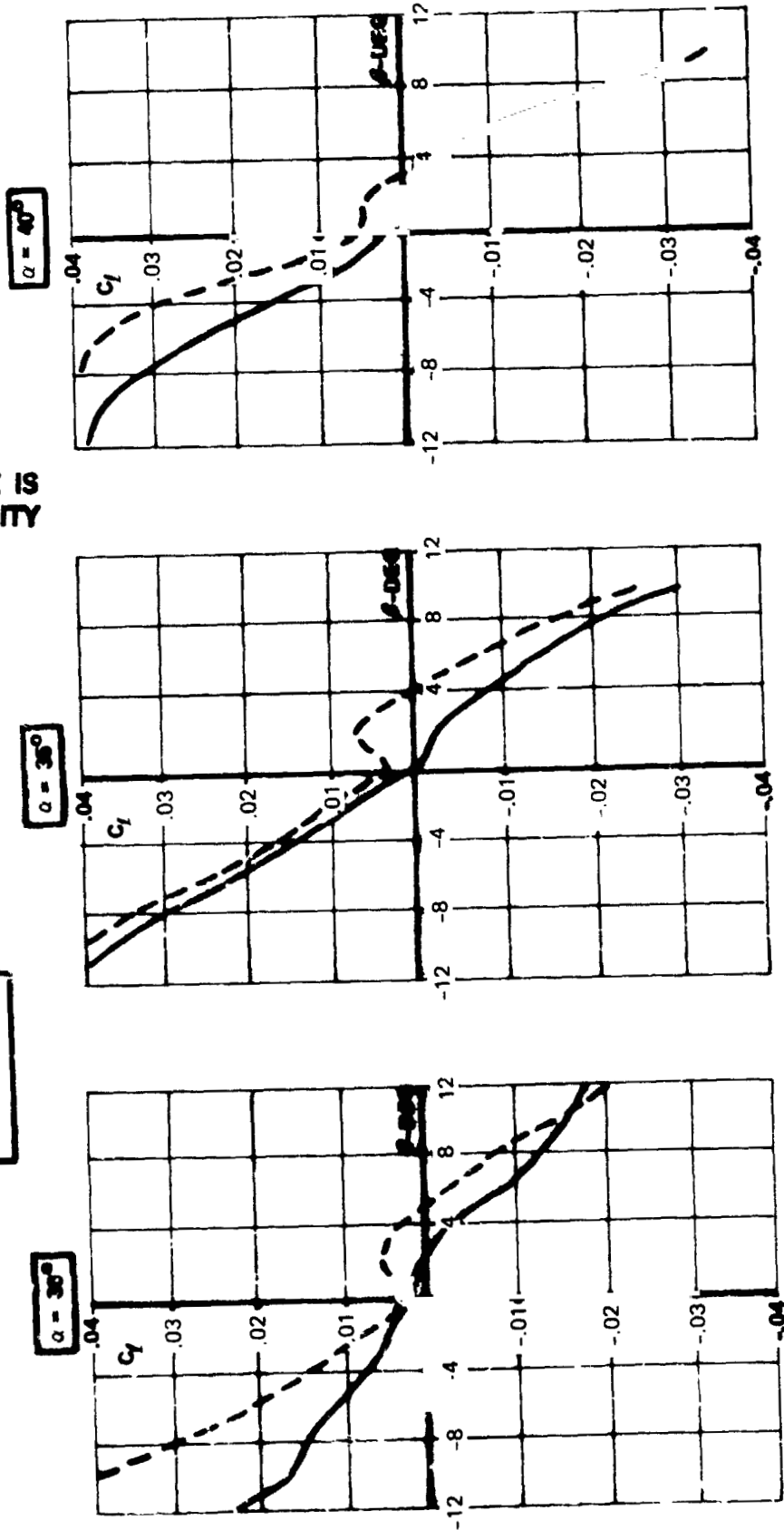


(B) YAWING MOMENT

FIGURE 103. CONCLUDED.

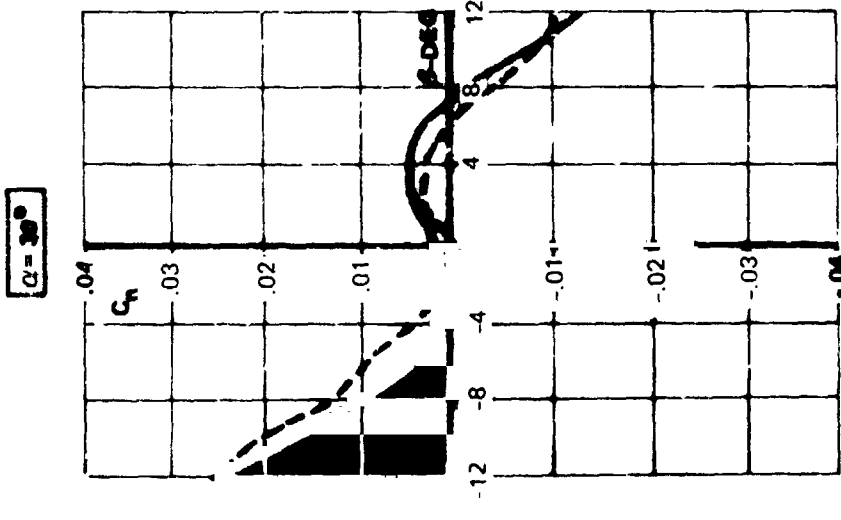
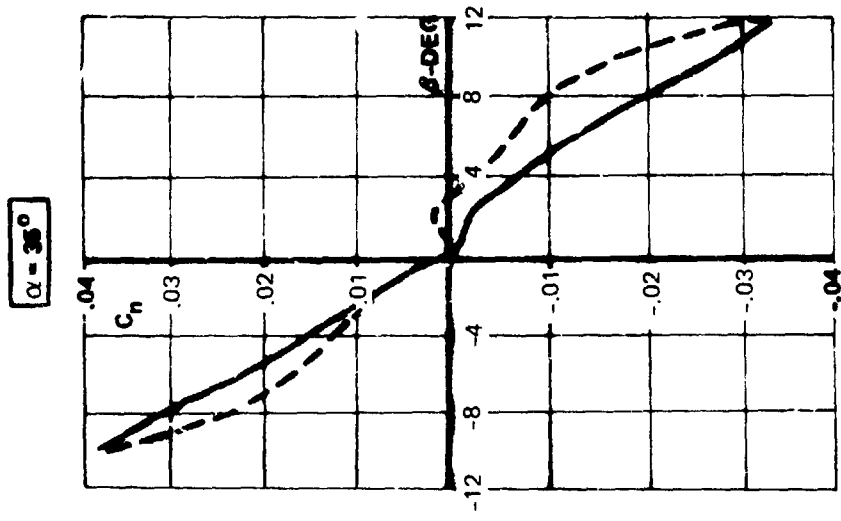
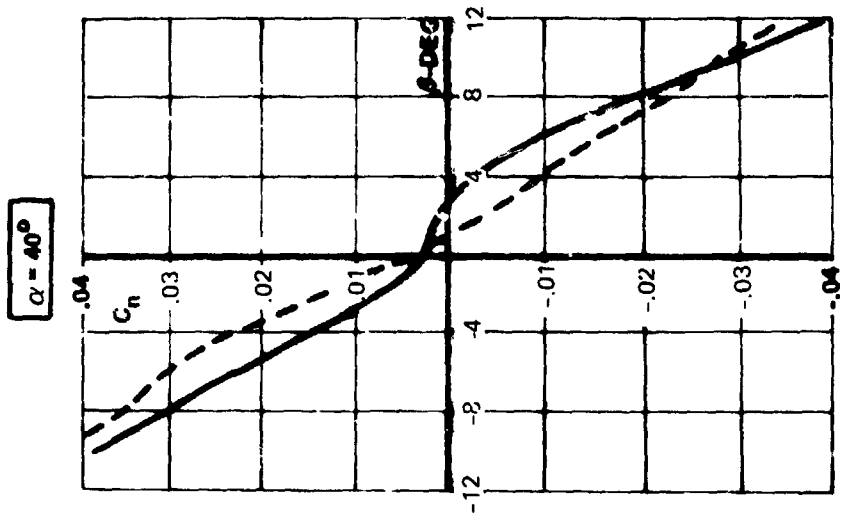
ORIGINAL PAGE IS
OF POOR QUALITY

LEXS
— ON
- - OFF



(A) ROLLING MOMENT

FIGURE 104. EFFECT OF LEX REMOVAL ON 0.07-SCALE F/A-18 ROLLING MOMENT AND YAWING MOMENT VARIATION WITH SIDESLIP; $\delta_h = 25^\circ$; $\delta_h = -12^\circ$; $Re_{\bar{c}} = 0.47$ (10^6)



ORIGINAL PAGE IS
OF POOR QUALITY

(B) YAWING MOMENT

FIGURE 104. CONCLUDED

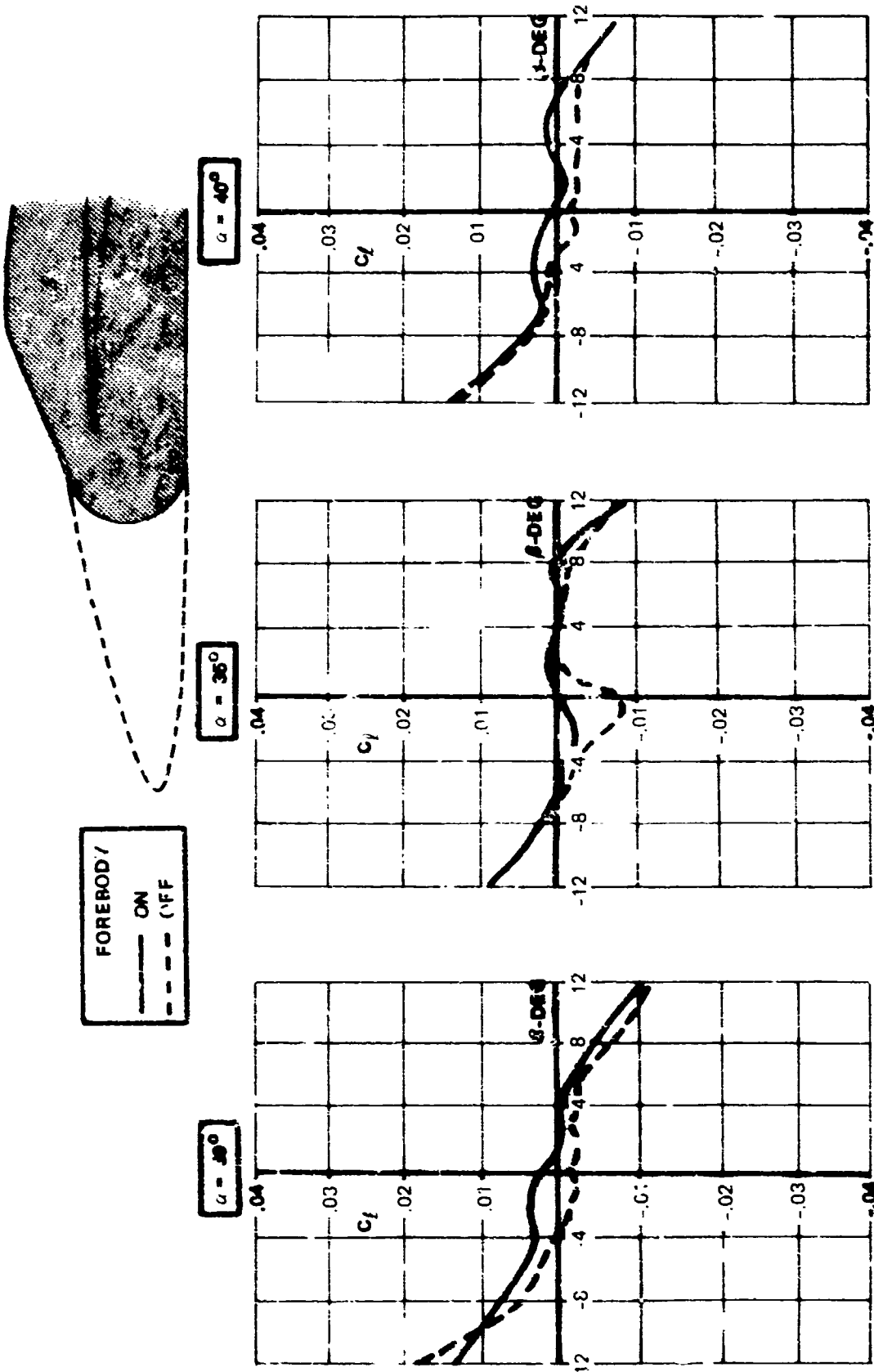
Therefore, removal of the LEX vortices from the flow field and, hence, elimination of forebody-LEX vortex interaction, promotes scale-model data correlation.

Forebody Effects

To this point in the analyses, it has become evident that a fundamental flow field difference exists between the small (0.06- and 0.07-scale) and large (0.16-scale) models causing a substantial variation in lateral stability levels near stall angle of attack.

Removal of the fuselage forebody is expected to provide a realistic assessment of the incremental forebody effects on lateral stability at high angles of attack (30° - 40°). The F/A-18 forebody geometry (cross-sectional shape, fineness ratio, etc.) is such that at high α 's the contribution to yawing moment is small (destabilizing). Furthermore, forebody vortex interactions with the vertical tail surfaces are minimal according to flow visualization studies in the water tunnel. Absence of the fuselage forebody boundary layer should not affect the LFV vortex behavior to any significant extent. For example, Northrop water tunnel studies of full-span and half-span delta wings have indicated that the reflection plane boundary layer on the half-span wing model had no observable effect on the vortex stability characteristics when compared to the full-span wing vortex behavior. The primary effect to be revealed by removal of the forebody, then, is the degree of coupling between the forebody and LEX-wing flow fields and, hence, the contribution of the forebody vortices to lateral stability.

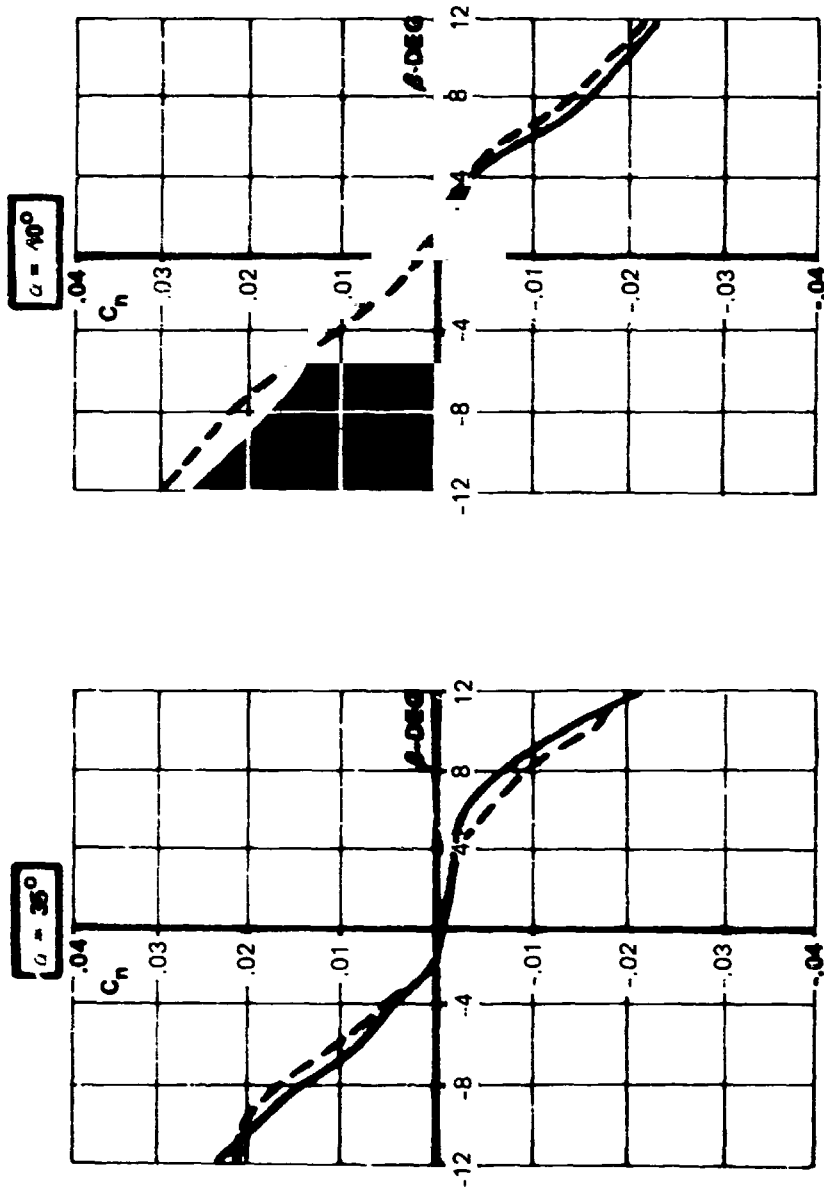
Rolling moment and yawing moment variations with sideslip at $\alpha=30^\circ$ to 40° are presented in Figure 105 for the 0.16-scale F/A-18. Minimal effects are evident due to absence of the forebody. From these results it can be concluded that the forebody vortex interactions with the wing flow field high angles of attack are not significant on the large-scale model. These trends are consistent with the initial water tunnel studies of the 0.025-scale baseline model which did not exhibit discernible, strong body-LEX vortex interactions.



(A) ROLLING MOMENT

FIGURE 105. EFFECT OF FOREBODY REMOVAL ON 0.16-SCALE F/A-18 ROLLING
MOMENT AND YAWING MOMENT VARIATION WITH SIDESLIP; $\delta_n = 25^\circ$; $\delta_h = -12^\circ$;
 $Re_\sigma = 1.1 (10^6)$

ORIGINAL PAGE IS
OF POOR QUALITY

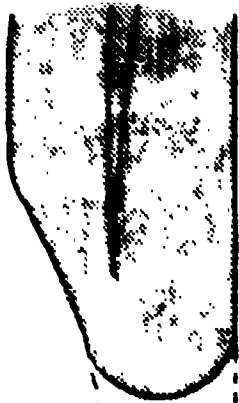


(B) YAWING MOMENT

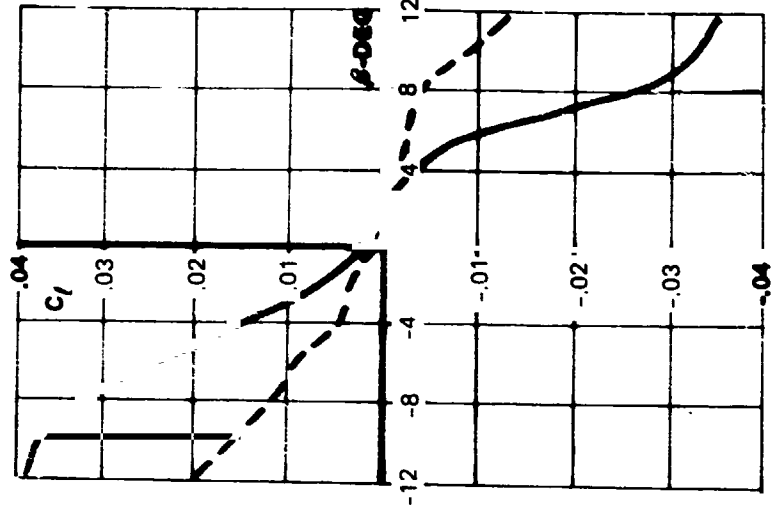
FIGURE 105. CONCLUDED

Data obtained on the 0.07-scale model with forebody on and off indicate a measurable difference in lateral stability levels at $\alpha=30^\circ$ to 40° , as shown in Figure 106. Removal of the forebody promotes large unstable rolling moment increments. These data strongly suggest that the 0.07-scale model with forebody on develops a favorable flow interaction between the body and LEX vortices similar to the flow characteristics observed during repeat flow visualization runs of the baseline water tunnel model (after reinstallation of the LEXs). The latter low surveys showed significant flow field changes, particularly in regards to the windward wing stall behavior, associated with a small change in the forebody vortex pair orientation. Furthermore, when the forebody was removed, it was observed that the vortex-induced effects on the windward wing with forebody on were noticeably absent. This is consistent with the results obtained on the 0.07-scale model. In addition, it is conjectured that similar flow phenomena are developed on the 0.06-scale F/A-18 model, since the small-scale wind tunnel data were in consistent agreement.

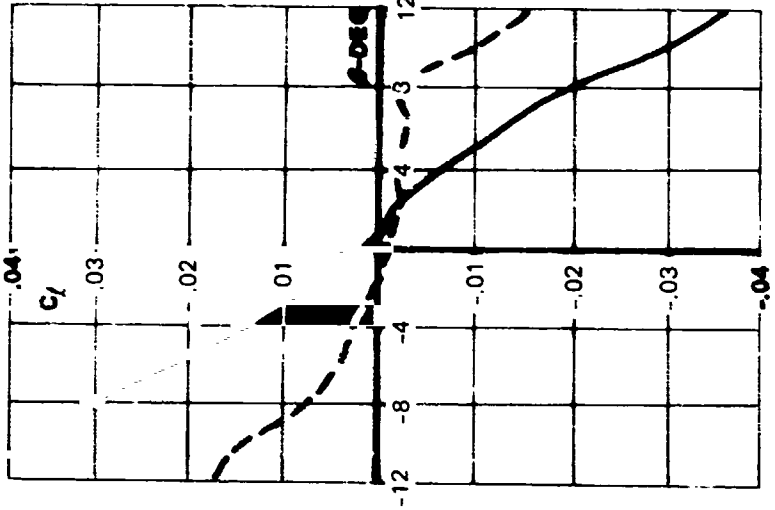
The results shown in Figures 105 and 106 support the hypothesis that the vortices developed on the forebody are a key to understanding the high- α "scale" effects. For example, comparison of the forebody-off rolling moment and yawing moment variations with sideslip at $\alpha=30^\circ$, 35° , and 40° indicates very good agreement of the 0.07- and 0.16-scale model data. In a manner similar to the LEXs-off case, elimination of forebody-LEX vortex coupling at high angles of attack promotes good correlation of the sub-scale wind tunnel model data. This agreement is an indication of different body vortex behavior on the baseline F/A-18 models resulting from such factors as slight forebody misalignment, subtle forebody cross-sectional shape variations, model support rigidity, etc. Plausible flow mechanisms are sketched in Figure 107. The different forebody vortex patterns may be due to a slight difference in leeward and windward primary boundary layer separation line locations along the respective fuselage forebody sides. The 0.07-scale model may feature a rotation of the forebody vortex system towards the windward side as sketched in Figure 107. This rotation of the vortex pair results in increased interaction with the windward wing and, consequently, stable rolling moment increments. In contrast, the 0.16-scale F/A-18 develops a relatively uncoupled windward and leeward body vortex pair, the former shearing away from the



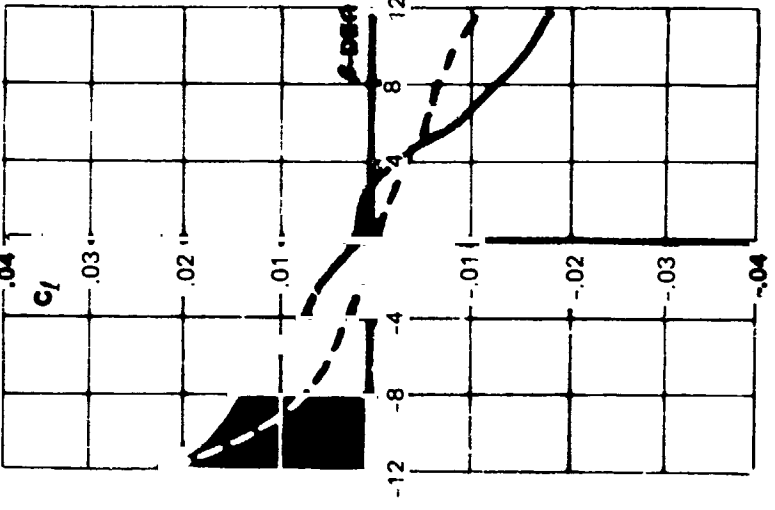
$\alpha = 40^\circ$



$\alpha = 35^\circ$



$\alpha = 30^\circ$



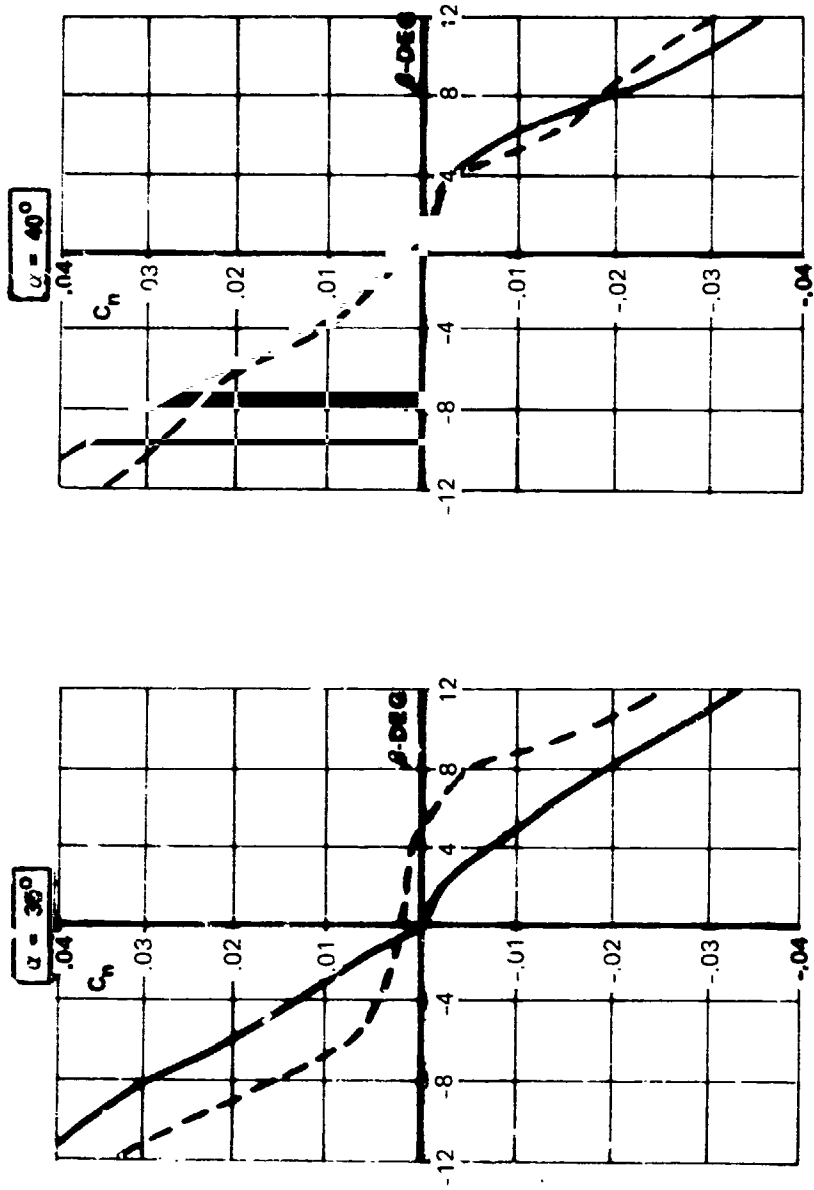
FOREBODY
 — ON
 - - - OFF

ORIGINAL PAGE IS
 OF POOR QUALITY

(A) ROLLING MOMENT

FIGURE 106. EFFECT OF FOREBODY REMOVAL ON 0.07-SCALE F/A-18 ROLLING MOMENT AND YAWING MOMENT VARIATION WITH SIDESLIP; $\delta_n = 25^\circ$; $\delta_h = -12^\circ$; $Re_g = 0.47 (10^6)$

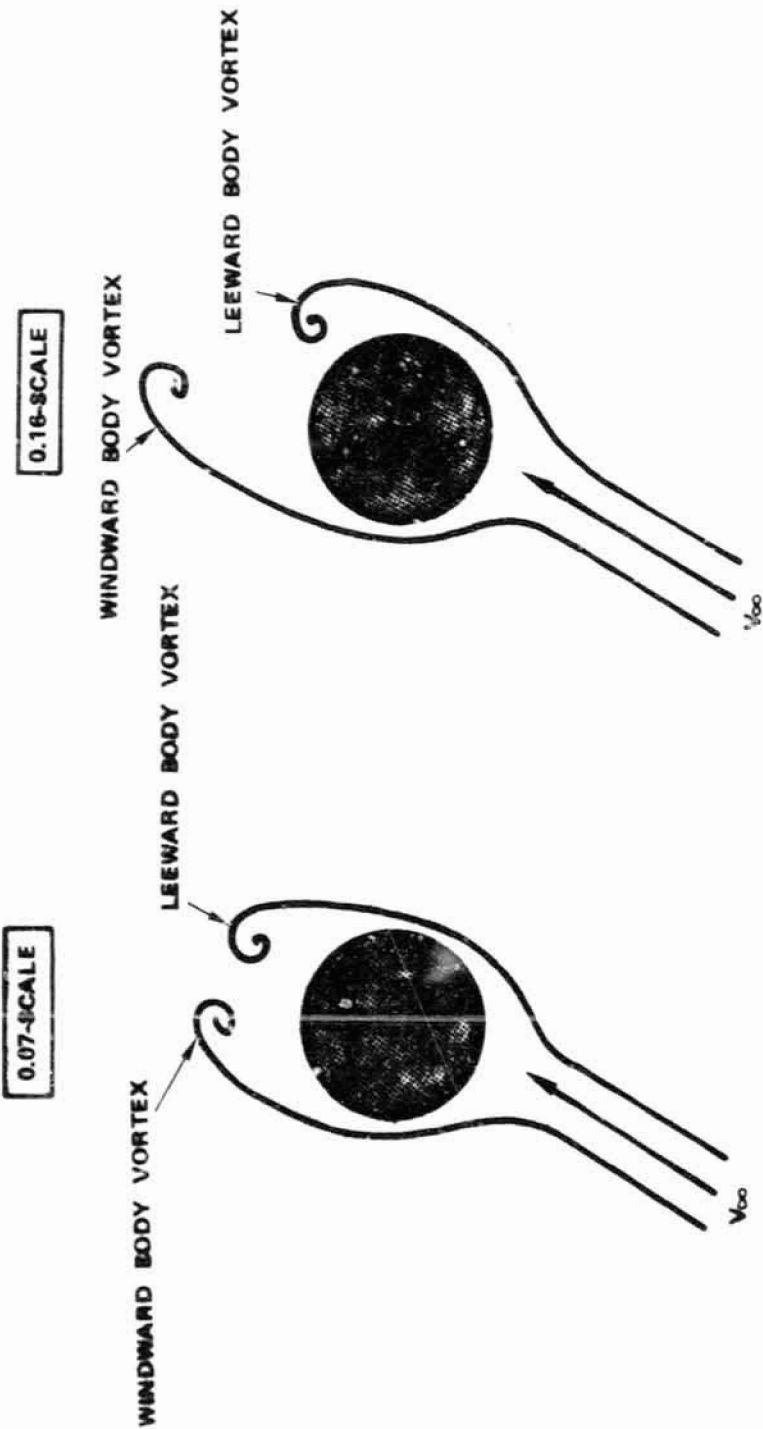
ORIGINAL PAGE IS
OF POOR QUALITY



(B) YAWING MOMENT

FIGURE 106. CONCLUDED

ORIGINAL PAGE IS
OF POOR QUALITY



(SKETCHES ARE EXAGGERATED FOR CLARITY)

FIGURE 107. COMPARISON OF FOREBODY VORTEX LOCATIONS IN SIDESLIP
ON LARGE AND SMALL F/A-18 MODELS

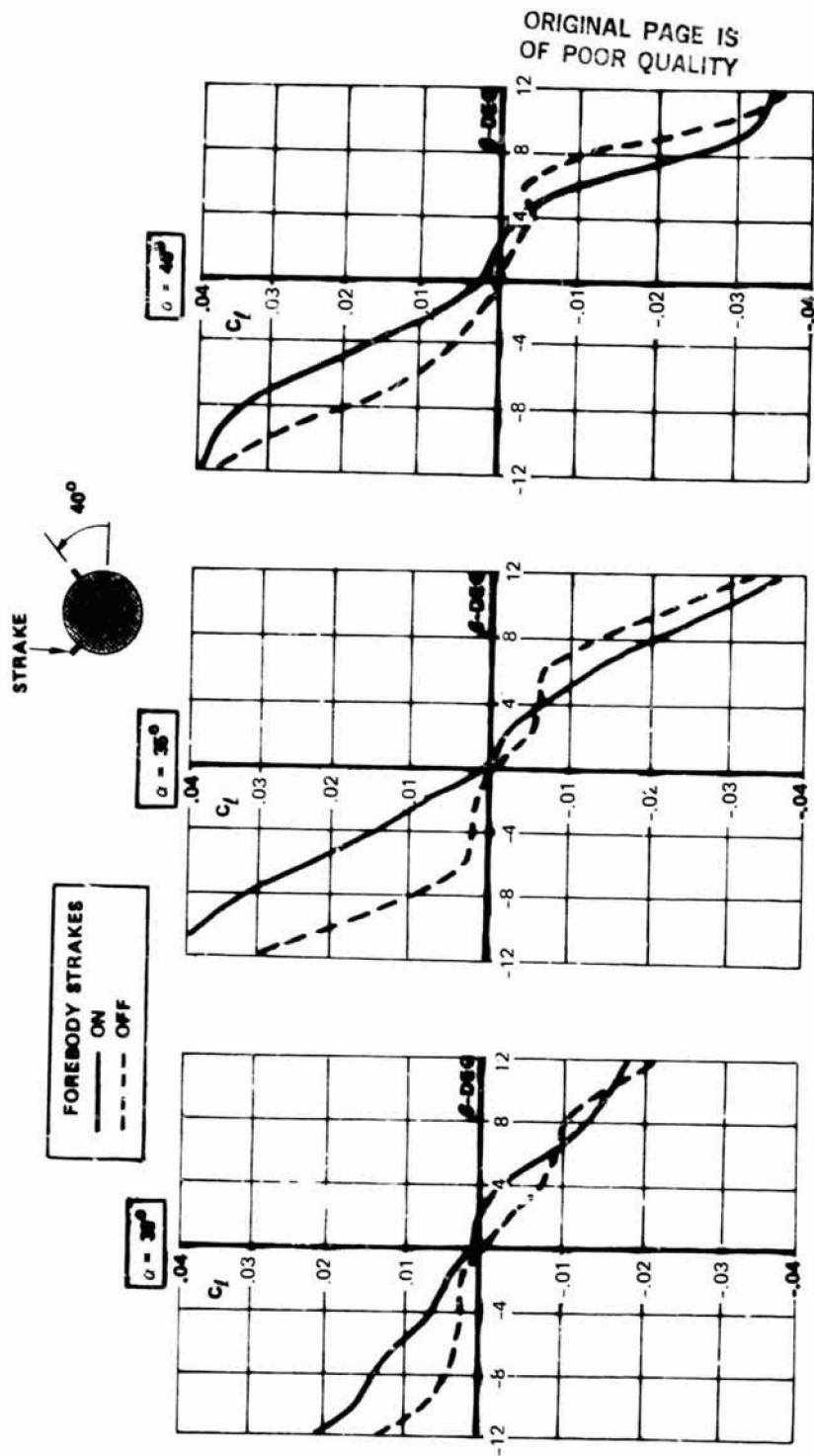
fuselage. As a result, no flow mechanism exists that would provide favorable spanwise flow components on the windward wing.

Forebody Strake Effects

Further corroboration of the significance of the forebody vortex flow field in influencing the high angle-of-attack lateral stability characteristics is provided by comparisons of nose strake effects on the 0.06-, 0.07-, and 0.16-scale F/A-18 models. Direct comparisons are generally not possible due to, for example, different leading-edge flap deflection angles. Conclusions can still be made, however, regarding the relative effects of radome strakes mounted at varying radial positions.

Addition of nose strakes at $\phi = +40^\circ$ to the 0.07-scale model ($\delta_n = 25^\circ$) promotes unstable rolling moment increments at $\alpha = 30^\circ$, 35° , and 40° , as shown in Figure 108. The adverse effect of the strakes mounted in this position at high α 's is indicative of a disturbance of the favorable forebody vortex interactions with the wing flow field. With strakes off, the body primary vortices assume an orientation in sideslip which results in strong vortex-induced effects on the windward wing panel. The vortices shed by the nose strakes are not optimally positioned, and as a result, tend to oppose the vortices formed by flow separation along the fuselage sides. The stability and trajectories of the body vortices are altered such that the windward wing exhibits more pronounced flow separation.

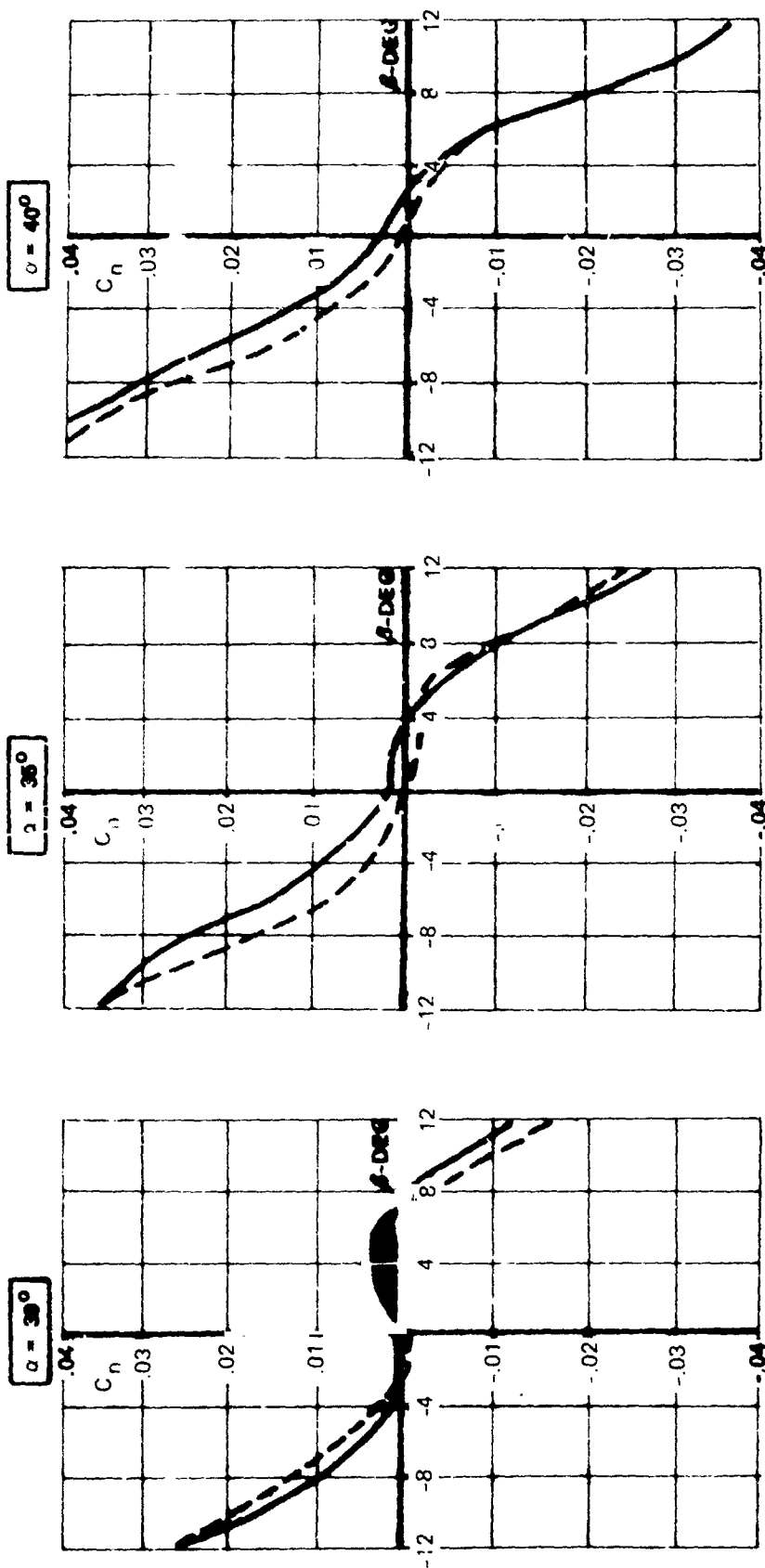
Differences in the primary boundary layer separation line locations on the 0.07- and 0.16-scale models are evidenced by the highly-favorable effects shown in Figure 109 on the 0.16-scale model rolling moment variation with sideslip associated with strakes mounted at $\phi = +40^\circ$. The radome strakes are more nearly-aligned with the separation lines in this region of the large model and tend to enhance, rather than disrupt, the forebody vortices. The vortex behavior with strakes on becomes comparable to the flow about the small model without strakes. This is apparent in the respective variations of rolling moment with sideslip at high angles of attack. Conversely, the variations of rolling moment with sideslip for the small model with strakes and the large model with strakes off are similar, which also suggests similar forebody vortex flow field characteristics.



(A) ROLLING MOMENT

FIGURE 108. EFFECT OF FOREBODY STRAKES ($\phi = 40^\circ$) ON 0.07-SCALE F/A-18 ROLLING MOMENT AND YAWING MOMENT VARIATION WITH SIDESLIP;
 $\delta_n = 25^\circ$; $\delta_h = -12^\circ$; $Re_g = 0.47 (10^6)$

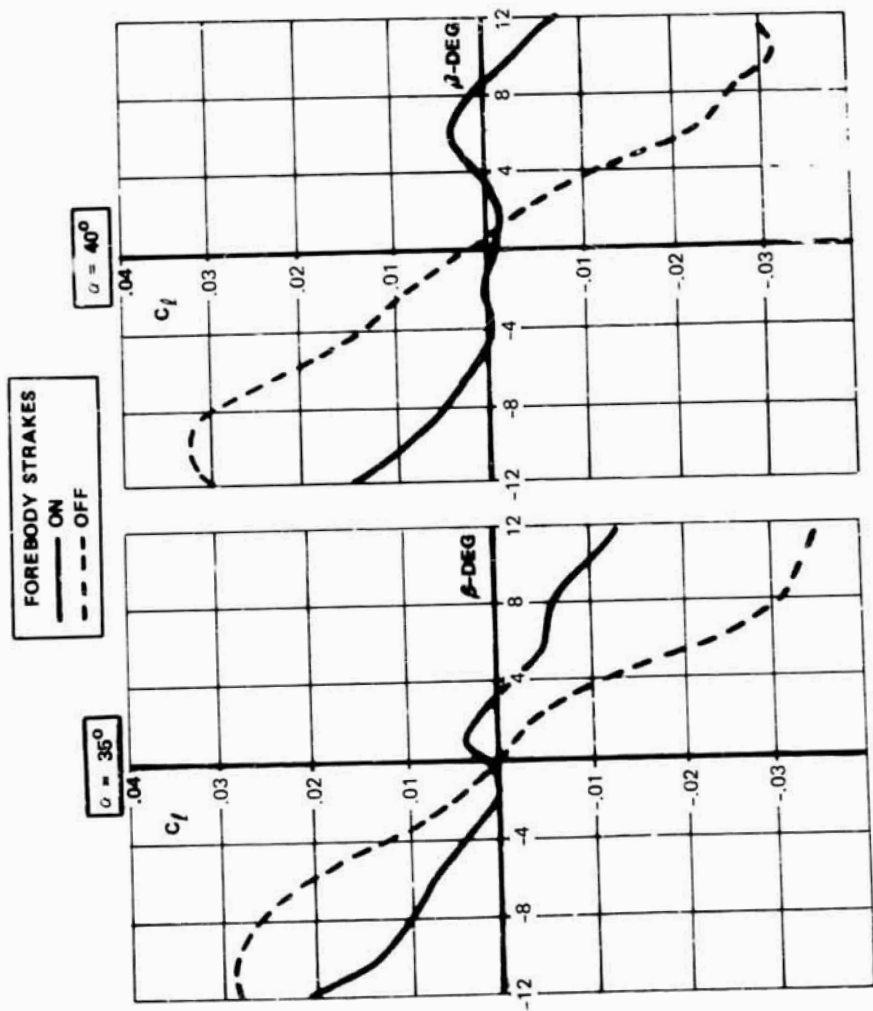
ORIGINAL PAGE IS
OF POOR QUALITY



(B) YAWING MOMENT

FIGURE 108. CONCLUDED

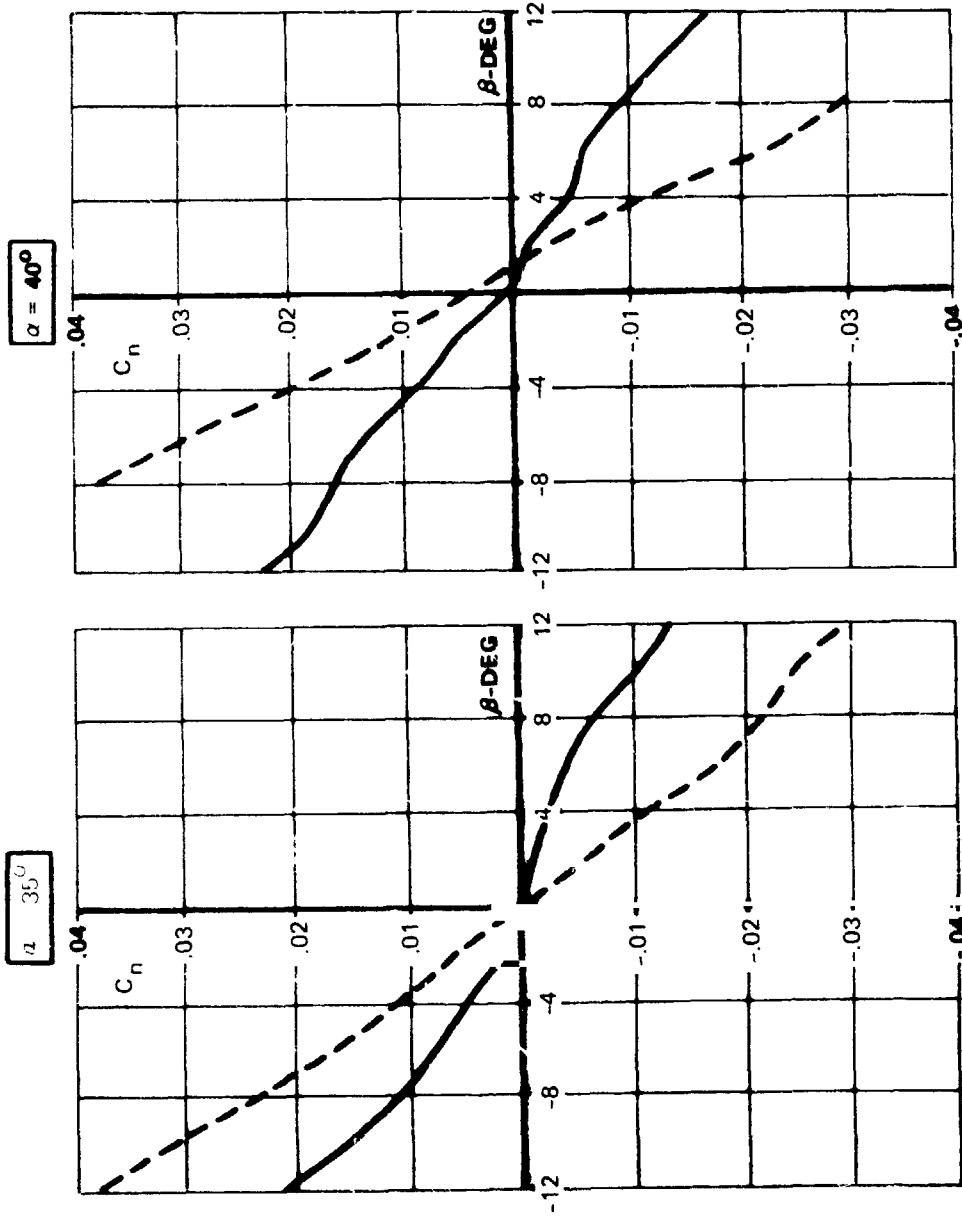
ORIGINAL PAGE IS
OF POOR QUALITY



(A) ROLLING MOMENT

FIGURE 109. EFFECTS OF FOREBODY STRAKES ($\phi = 40^\circ$) ON 0.16-SCALE F/A-18
ROLLING MOMENT AND YAWING MOMENT VARIATION WITH SIDESLIP;
 $\delta_n = 25^\circ$; $\delta_h = -12^\circ$; $Re_c = 1.1 (10^6)$

ORIGINAL PAGE IS
OF POOR QUALITY.



(B) YAWING MOMENT

FIGURE 109. CONCLUDED

Another example to support the contention of dissimilar boundary layer separation characteristics on the small and large models is provided by data obtained on the 0.06-scale F/A-18 (tested in the NASA Ames Research Center 12-foot tunnel) and 0.16-scale model (tested at NASA Langley) with YF-17-type nose strakes mounted along the maximum half breadth. Recall that water tunnel flow visualization results revealed a disruption of the body vortices due to strakes mounted at the MHB. Hence, if differences exist in the body vortex structure on the sub-scale baseline models, strakes at the MHB should reduce the flow anomalies. This, in turn will decrease the differences in body-LEX-wing flow interactions and, consequently, the rolling moment characteristics. Rolling moment and yawing moment variation with sideslip at $\alpha=35^\circ$ in Figure 110 shows excellent agreement between the 0.06-scale Ames data and the 0.16-scale Langley results.

As a final example of the forebody flow sensitivity to disturbances along the radome, 0.08-scale Northrop F-18L data are presented in Figure 111 which show the effects of nose grit (#45 corborundum grit) and wire trips (0.0625" diameter (model-scale)) mounted at 20° above the maximum half breadth. At $\alpha=35^\circ$, for example, nose grit promotes a significant increase in stable rolling moment coefficient at all sideslip angles, whereas wire trips are highly-destabilizing. The respective flow mechanisms are dissimilar, the former tending to enhance the forebody-wing interactions by promoting a more symmetric body vortex pair in sideslip and the latter causing a decoupling of the forebody and wing flow fields by disrupting the forebody vortex flows.

— 0.16-SCALE (LANGLEY 30 x 60 FT TUNNEL)
- - - 0.06-SCALE (AMES 12 FT TUNNEL)

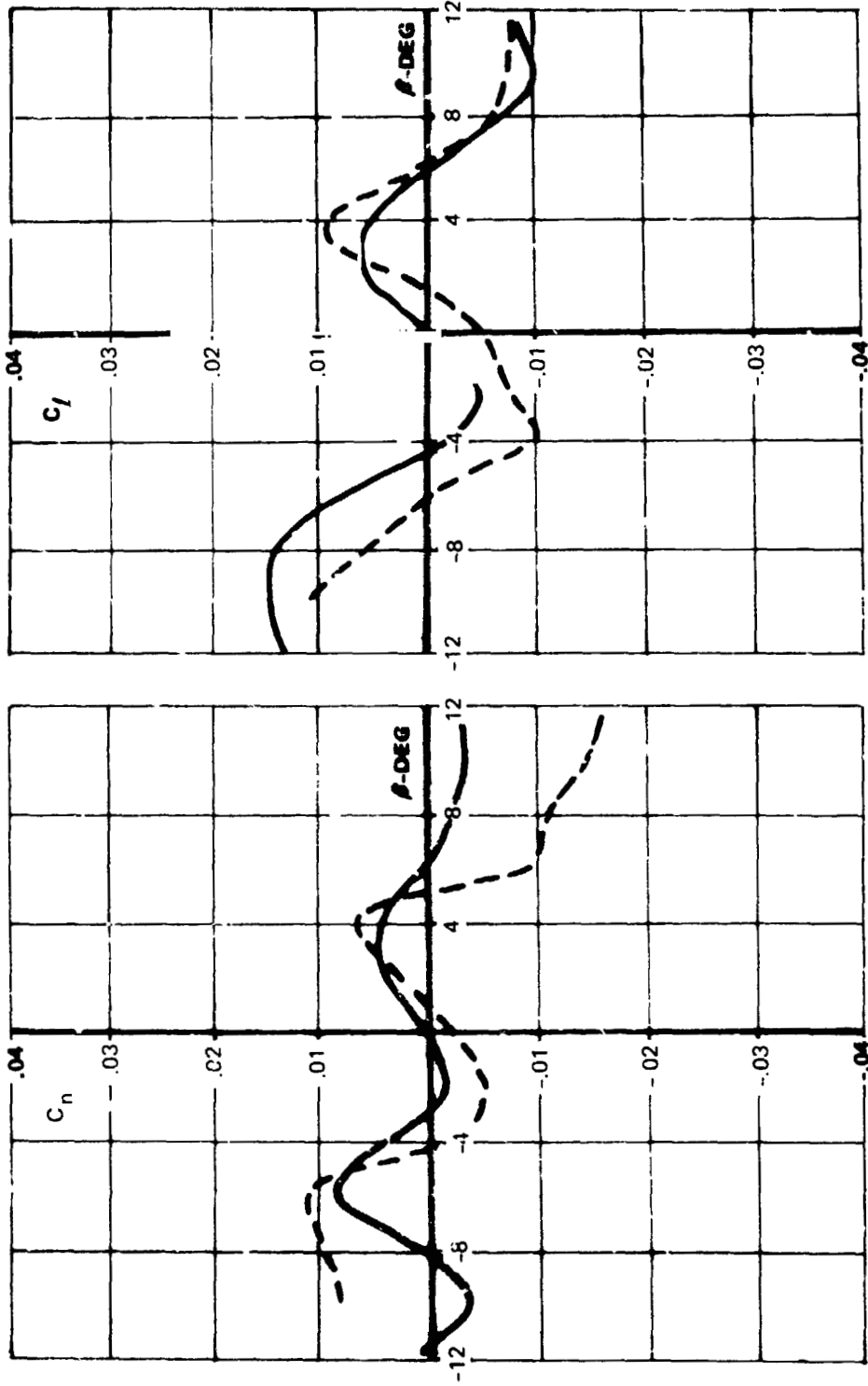
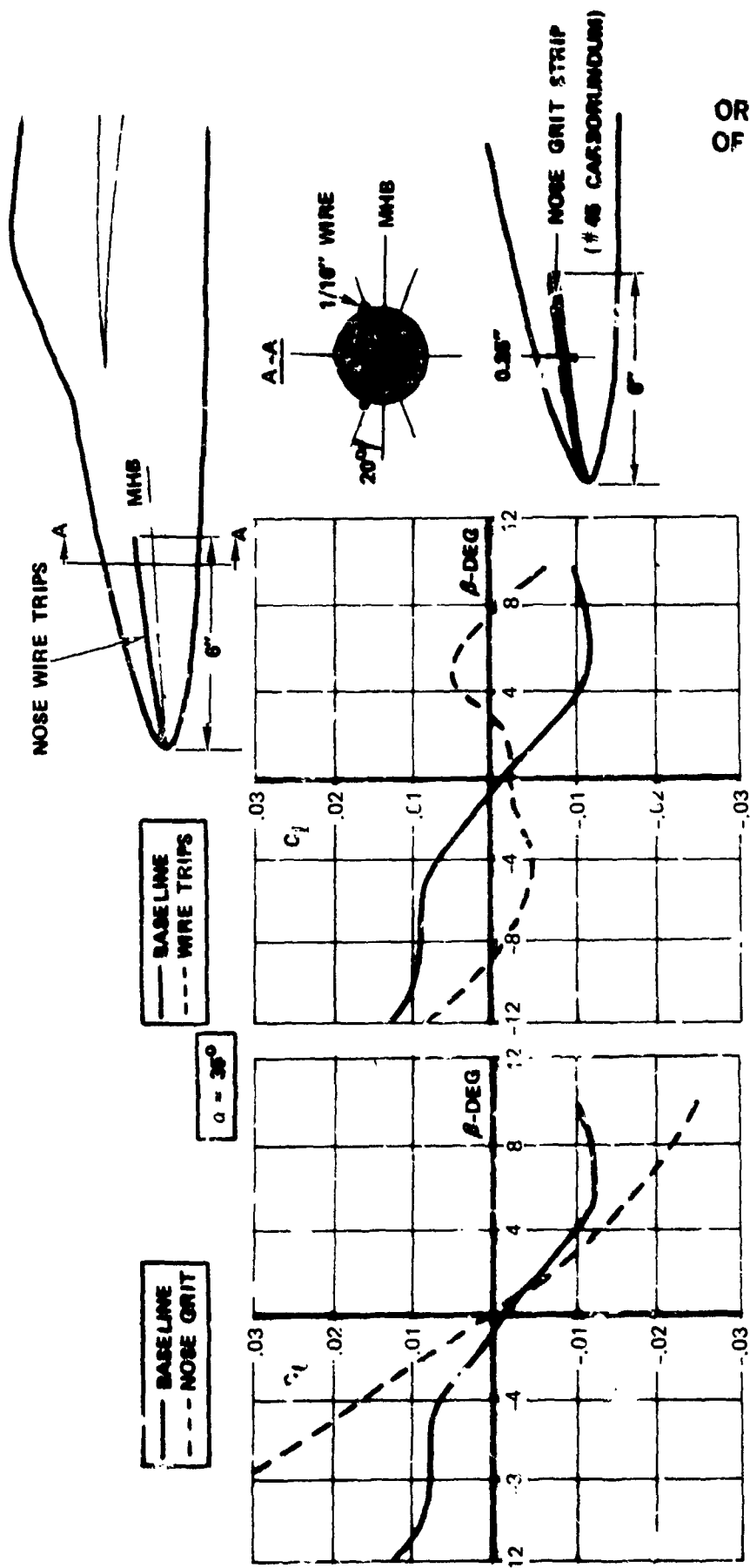


FIGURE 110. COMPARISON OF YAWING MOMENT AND ROLLING MOMENT VARIATION
WITH SIDESLIP WITH FOREBODY STRAKES ($\phi = 0^\circ$); 0.06- AND 0.16-SCALE F/1-18
MODELS; $\alpha = 35^\circ$; $\delta_n = 25^\circ$; $\delta_h = -12^\circ$



ORIGINAL PAGE IS
OF POOR QUALITY

FIGURE 111. EFFECTS OF NOSE GRIT AND NOSE WIRE TRIPS ON 0.08-SCALE F-10L ROLLING MOMENT VARIATION WITH SIDESLIP; $\delta_n = 25^\circ$; $\delta_h = -10^\circ$; $Re_{\bar{c}} = 1.6 \times 10^6$

CONCLUSIONS

The F/A-18 operating at high angles of attack develops powerful vortices shed from the fuselage forebody and wing leading-edge extensions (LEXs). Because of the close-coupling of the forebody and LEX surfaces the flow field is characterized by strong interactions between the multiple vortices and the occurrence of vortex breakdown. Furthermore, the global flow field becomes more complex in sideslip due to the asymmetric manner in which the forebody vortices interact with the LEX vortical motions.

Results obtained in this study contract have revealed the sensitivity of the F/A-18 forebody-LEX vortex interactions and vortex breakdown characteristics at high angles of attack to relatively small variations in model geometry.

LEX geometry changes near the apex have been shown in the water tunnel flow visualization studies of a 0.025-scale F/A-18 model to promote differences in LEX vortex behavior sufficient to alter the wing stall patterns, in some cases, and the manner in which the forebody vortices interact with the lifting surfaces. Specifically, the primary LEX modifications considered in this investigation were, in every case, means by which the available vorticity shed at the LEX leading edge was reduced at high angles of attack. As a consequence, LEX vortex stability and vortex breakdown asymmetry in sideslip were decreased.

The flow field observations in the hydrodynamic facility were consistent with the premature wing stall and increased levels of lateral stability near stall associated with the LEX mods determined in low-speed wind tunnel tests in the NASA Langley Research Center 30x60-foot facility. A compromise appears required in terms of maximum attainable lift and lateral stability at high angles of attack. The former varies directly with LEX area whereas the latter appears to vary inversely with LEX size.

The sensitivity of vortices shed from slender forebodies at high attitudes to virtually undetectable model distortions, Reynolds number, Mach

C-3

number, freestream conditions, model support interference and support rigidity, among other factors, has been investigated in detail by many researchers. In wind tunnel tests of axisymmetric bodies where the above factors were carefully controlled, virtually imperceptible model distortions near the nose tip promote large variations in forces and moments.

Consistent with these studies, results obtained in the present research effort have revealed the vortices shed from the F/A-18 forebody to be sensitive to small model distortions. As a consequence of the highly-coupled nature of the forebody and LEX vortices on the F/A-18, slight changes in body vortex orientation can dictate the manner in which the wing panels stall at high angles of attack and in sideslip conditions.

Corroborative evidence of the powerful mechanism associated with forebody-LEX vortex interactions was provided in water tunnel flow visualization tests of the baseline F/A-18 which indicated that the extent to which flow separation occurs on the windward wing panel is directly related to the manner in which the forebody vortices orient themselves in sideslip and, particularly, to the proximity of the windward forebody vortex. The F/A-18 forebody-LEX geometry is such that the windward body vortex is not as strongly-coupled with the LEX-wing flow field as its leeward counterpart. However, small forebody contour distortions can promote a windward body vortex that is considerably more coupled with the wing flow. In the latter situation, a greatly-magnified response can be triggered in the downstream flow field characteristics.

Additional supportive data was obtained in flow visualization studies of small strakes symmetrically-deployed along the radome. A direct relationship was observed between the strength and orientation of the body vortex flows (dependent on strake radial position) and the degree of flow separation from the wing surfaces.

The qualitative data obtained on forebody vortex behavior in the hydrodynamic facility are in consistent agreement with smoke flow visualization and low-speed wind tunnel data trends obtained in the Langley 30x60-foot facility using the 0.16-scale F/A-18 model. Furthermore, the water tunnel



results used in parallel with analyses of 0.06-, 0.07-, and 0.16-scale F/A-18 data, provide a better understanding of the nonlinear behavior of the static aerodynamic characteristics at high angles of attack. Results indicate that generation of forebody vortex flows resistant to asymmetric orientation in sideslip is conducive to high levels of lateral stability near $C_{L_{MAX}}$.

Previous Northrop and NASA studies of the F-5 have shown that the manner in which the forebody vortices orient themselves in sideslip can be correlated with the high level of directional stability exhibited by the aircraft at high angles of attack. The vortex flow situation is illustrated in the water tunnel photograph in Figure 112. Results from the present investigation indicate that the F/A-18 forebody vortex orientation at high α 's is consistent with the lateral stability behavior due to the coupled nature of the F-18 forebody and wing flow fields. The flow phenomenon is depicted in Figure 113. The increased complexity of the F-18 vortex flow field relative to the F-5 is also evident from a comparison of Figures 112 and 113.

Evidence compiled within this report strongly suggests that the apparent model-scale sensitivity encountered in the Langley F/A-18 wind tunnel tests is associated with different primary boundary layer separation line locations along the fuselage forebody sides resulting from small variations in forebody cross-sectional shape. As a consequence, the manner in which the forebody primary vortices interact with the LEX-wing flow field at high angles of attack is different on the small and large models. An as yet unresolved and conflicting anomaly is that the 0.06- and 0.07-scale F/A-18 models, which were fabricated at different sites and using different materials, yielded consistent agreement throughout the test program.

The low-speed wind tunnel data suggest that the body vortex-induced effects on the windward wing panels of the 0.06- and 0.07-scale F/A-18 models are greater than the corresponding effects on the 0.16-scale model. The small-scale wind tunnel models are characterized by windward body vortices less prone to "shearing away" from the fuselage. As a result, the windward wing experiences favorable vortex-induced sidewash near stall angle of attack.

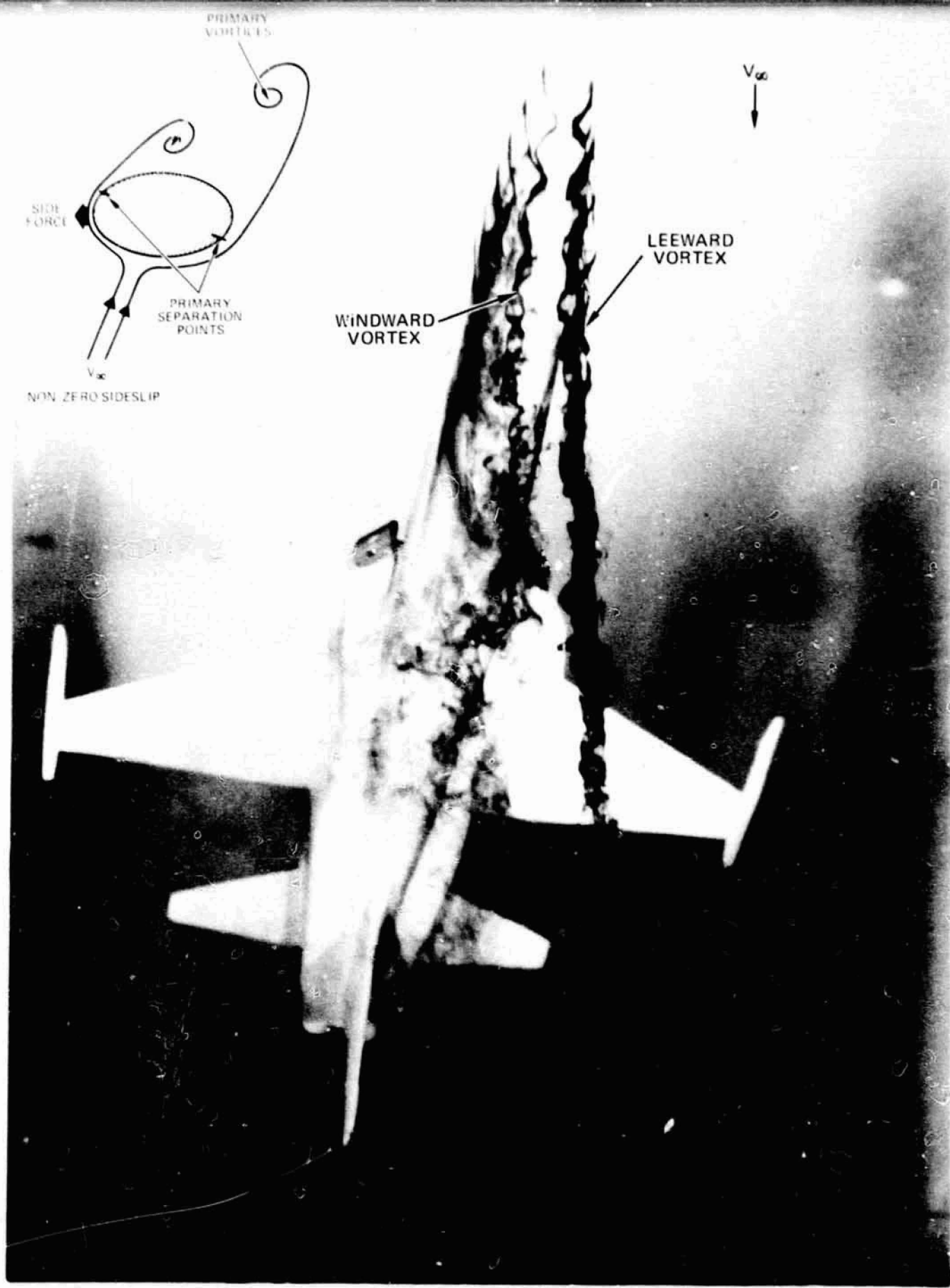


FIGURE 112. F-5F FOREBODY VORTEX ORIENTATION IN SIDESLIP
 $\alpha = 40^\circ$; $\beta = -10^\circ$. (NORTHROP WATER TUNNEL)

ORIGINAL PAGE
 COLOR PHOTOGRAPH

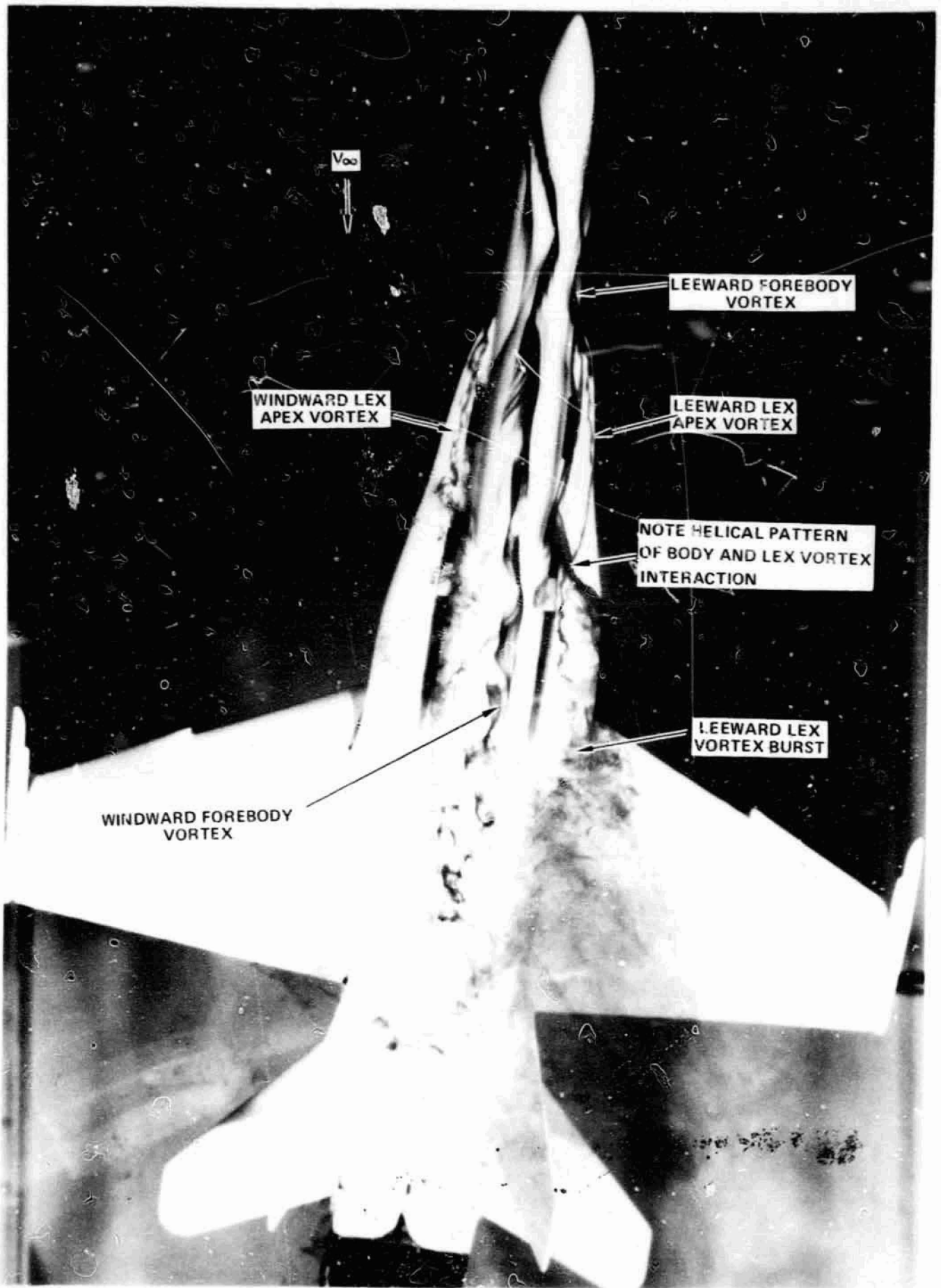


FIGURE 113. VORTEX PATTERNS ON THE F/A-18 IN SIDESLIP; $\alpha = 32^\circ$; $\beta = -10^\circ$
(NORTHROP WATER TUNNEL).

ORIGINAL PAGE
COLOR PHOTOGRAPH

PRECEDING PAGE BLANK NOT FILLED

PRECEDING PAGE BLANK NOT FILLED

Detailed examination of the flow field about the 0.025-scale water tunnel model indicates that removal of the forebody provides a realistic assessment of the direct forebody vortex-induced effects on the LEX-wing flow characteristics. This is significant in that superfluous flow changes are not introduced that would, otherwise, preclude such an assessment. The same logic was applied to analysis of the low-speed wind tunnel data which revealed an excellent match of small- and large-scale F/A-18 model rolling moment variation with sideslip with forebodies removed. This correlation supports the hypothesis that a key to understanding the apparent model-scale effect is the forebody vortex behavior. Furthermore, addition of YF-17-type nose strakes also promoted an excellent match. Flow field surveys indicate that this strake arrangement impedes development of the body vortices and, consequently, will significantly reduce any differences that exist in the scale-model body vortex behavior.

Based on the present results, it appears necessary to reduce the model tolerances on F/A-18-type configurations for high angle-of-attack testing due to the sensitivity of closely-coupled forebody and LEX vortex flows. A large model is then more desirable for such testing since model tolerances can be more easily satisfied. Until experiments are conducted in a systematic manner, however, one cannot define what a reasonable tolerance level is or, indeed, whether this is the pivotal problem in the apparent scale-effect.

ORIGINAL PAGE IS
OF POOR QUALITY

RECOMMENDATIONS FOR FUTURE WIND TUNNEL TESTS

It is recommended that, prior to further testing of the F/A-18 models, a very detailed inspection be made of the 0.05-, 0.07-, and 0.16-scale models. Specifically, inspection is recommended of: LEX, wing, horizontal and vertical tail locations on the fuselage to assure that symmetry exists and, also, that LEX incidence angle, wing dihedral, vertical tail cant angles, etc. are correct; wing leading-edge radius, wing camber and thickness, and wing flap deflection angles are consistent; LEX boundary layer bleed slot geometry, LEX thickness and camber, and leading-edge sharpness are the same on all models. Particular attention should be paid to the fuselage forebody contours, surface finish, and forebody alignment.

Emphasis should be placed on identifying even very subtle variations in model lines since such differences can trigger greatly magnified effects on body vortex behavior. Any discrepancies in model geometries uncovered during the model inspection should be resolved before conducting further wind tunnel tests.

Contingent on determination of even small model distortions and their subsequent elimination, it is recommended that the baseline F/A-18 models be retested in the Langley 30x60-foot wind tunnel. Agreement of the 0.06-, 0.07-, and 0.16-scale model rolling moment variations with sideslip would confirm that very small model tolerances are necessary for high angle-of-attack testing of aircraft models which develop powerful vortex flows.

If the apparent model-scale effect persists, however, then the following discussion applies.

To address the sensitivity of high angle-of-attack lateral stability characteristics to model scale, a suitable alternate wind tunnel facility must be identified. This facility must feature: accommodation of the small- and large-scale F/A-18 models without prohibitive blockage; operation at a sufficient range of free-stream dynamic pressure to enable force and moment

ORIGINAL PAGE IS
OF POOR QUALITY

data to be obtained on each model at the same Reynold number; flow visualization capabilities enabling a qualitative determination of forebody and LEX vortex core stability and trajectory characteristics and surface flow patterns; and capability, as required, of investigating more subtle flow details involving the behavior of the boundary layer flow.

The proposed facility is the NASA Langley Research Center VSTOL wind tunnel. Force and moment data should be obtained on the 0.06-, 0.07-, and 0.16-scale F/A-18 models with which to compare the existing data obtained in the Langley 30x60-foot facility. Should the 0.06-scale model not be available from McDonnell-Douglas, then it is mandatory that the 0.07-scale Langley model be capable of accommodating a six-component balance. A proper assessment of the high- α characteristics necessitates acquisition of all six force and moment components on the 0.07- and 0.06-scale F/A-18 models.

Baseline data trends obtained in the VSTOL tunnel consistent with existing results would require assessment of the effects of forebody geometry changes on rolling moment variations with sideslip to confirm that the source of data discrepancies lies in the forebody region. It is recommended that studies be made of the effects of radome strakes (including asymmetric strake deployment) and removal of the fuselage forebody on the high- α characteristics, augmented by flow visualization. Fuselage forebody and wing surface pressure instrumentation would be helpful in assessing pressure distributions along the forebody, boundary layer separation on the forebody, and wing spanwise lift distributions associated with the presence of the forebody and LEX vortex flows. Alternate forebody geometries are desirable, particularly forebody shapes which limit the primary boundary layer separation degree of freedom. Nose and aft strain gage balances are recommended in order to assess the influence of the forebody on vertical tail loads.

Flow visualization techniques involving helium-filled bubbles, tuft grids, laser vapor screen, and surface oil flow visualization would provide valuable information regarding the overall flow characteristics. The helium-bubble method, tuft grids suspended above the models, or laser vapor screen would enable an assessment of forebody and LEX vortex positions. Detailed

surface oil or naphthalene flow visualization along the fuselage forebodies will provide information on primary boundary layer separation line locations, regions of boundary layer transition (characterized by a "kink" in the separation line), areas of vortex-induced reattached flow, and positions of secondary boundary layer separation lines. Any differences in the surface flow characteristics on each model would be indicative of variations in the body vortex paths.

Detailed forebody boundary layer measurements are required if the data differences are yet unresolved. The extensive data base on slender missile configurations has shown that subtleties in the boundary layer separation characteristics are the source of large global flow field variations. Determination of such differences on the small and large F/A-18 models does not bode well for future testing of such configurations since extremely small model tolerances are, in general, unrealistic in wind tunnel investigations. Only when a salient edge of separation exists along the forebody will the confidence level with which sub-scale model data are correlated increase.

Should the VSTOL facility baseline data do not concur with previous test results but, instead, exhibit scale-model correlation, it is recommended that investigation be made of the effects of such factors as free-stream turbulence, model support rigidity, and support interference. It is noted, however, that parameters which have been shown to be of major import to the behavior of slender body vortices at high angles of attack may not be so on the F/A-18. The reason for this being the F/A-18 forebody vortex behavior is influenced in large part by the powerful LEX vortices. The latter are shed from relatively thin, slender, sharp-edged surfaces and are less sensitive relative to vortices developed on surfaces with boundary layer separation line degree of freedom.

The National Transonic Facility (NTF) at Langley Research Center is a suitable facility in which to assess Reynolds number and Mach number effects on the behavior of highly-coupled body and wing vortex flows.

A fundamental study of forebody and wing vortex interactions is desirable. Results from the present study indicate that knowledge of the proper integration of forebody and wing geometries to ensure desirable high angle-of-attack stability and control characteristics remains lacking. A definitive data base on the effects of forebody length, cross-sectional shape, wing planform, aspect ratio, location, etc. on vortex development and interactive behavior at high α 's would assist in the design process of highly-maneuverable fighter aircraft. The advent of supersonic-cruise fighter designs, inherent to which are more slender wing planforms, requires a knowledge of the flow behavior at off-design conditions where flow separation in the form of concentrated vortices occurs. Use of diagnostic hydrodynamic flow visualization and low-speed wind tunnel facilities (featuring six-component force and moment capability and high-quality smoke flow visualization to complement the dye-tracer method in water) prior to more sophisticated and costly wind tunnel testing is one means of enhancing the understanding of effective utilization of organized separated flows (vortex flows).

REFERENCES

1. Aviation Week and Space Technology, Vol. 114, No. 25, 22 June 1981, p. 18.
2. Werle, Henri: Flow Visualization Techniques for the Study of High-Incidence Aerodynamics. AGARD Lecture Series No. 121 on High Angle-of-Attack Aerodynamics, presented at the von Karman Institute, Brussels, Belgium, 22-23 March 1982.
3. Erickson, Gary.: Vortex Flow Correlation. AFWAL-TR-80-3143, January 1981.
4. Lamar, John E.; and Frink, Neal T.: Experimental and Analytical Study of the Longitudinal Aerodynamic Characteristics of Analytically and Empirically Designed Strake-Wing Configurations at Subcritical Speeds. NASA TP-1803, June 1981.
5. Erickson, Gary E.: Water Tunnel Flow Visualization: Insight to Complex Three-Dimensional Flow Fields. AIAA Paper No. 79-1530 presented at the 12th Fluid and Plasma Dynamics Conference, Williamsburg, Virginia, July 10-12, 1979.
6. Erickson, Gary E.: Water Tunnel Studies of Leading-Edge Vortices. Journal of Aircraft, Vol. 19, No. 6, June 1982.
7. Johnson, Joseph L., Jr.; Grafton, Sue B.; and Yip, Jong P.: Exploratory Investigation of the Effects of Vortex Bursting on High Angle-of-Attack Lateral-Directional Stability Characteristics of Highly-Swept Wings. AIAA Paper No. 80-0463, March 1980.
8. Gerhardt, Heinz. A.: The Aerodynamic Development of the Wing Root Leading Edge Extension of the P530 Airplane Configuration. NOR 73-71, Northrop Corp., Aircraft Division, 1972.

REFERENCES (Continued)

9. Headley, Jack W.: Analysis of Wind Tunnel Data Pertaining to High Angle of Attack Aerodynamics. Vol. I, AFFDL-TR-78-14, 1978.
10. Lamont, Peter J.: The Complex Asymmetric Flow Over a 3.5D Ogive Nose and Cylindrical Afterbody at High Angles of Attack. AIAA Paper No. 82-0053, January 1982.
11. Agnew, J. W.; Lyster, G. W.; and Grafton, S. B.: Linear and Nonlinear Aerodynamics of Three-Surface Aircraft Concepts. Journal of Aircraft, Vol. 18, No. 11, November 1981, pp. 956-962.
12. Pietzman, F. W.: Low-Speed Wind Tunnel Investigation to Develop High Attitude Wall Corrections in the Northrop 7 x 10-Foot Low-Speed Wind Tunnel. NOR-78-20, Northrop Corp., Aircraft Div., May 1978.
13. Skow, Andrew M.: Panel Discussion. AGARD Symposium on High Angle of Attack Aerodynamics, AGARD-CP-247, October 1978.
14. Hummel, D.: Experimental Investigation of the Flow on the Suction Side of a Thin Delta Wing. Z. Flugwiss., Jahrg. 13, Heft 7, July 1965, pp. 247-252.